KfK 3768
März 1987

Post Test Investigation of the Single Rod Tests ESSI 1-11 on Temperature Escalation in PWR Fuel Rod Simulators due to the Zircaloy/Steam Reaction

S. Hagen, H. Kapulla, H. Malauschek, S. Katanishi
Hauptabteilung Ingenieurtechnik
Projekt Nukleare Sicherheit

Kernforschungszentrum Karlsruhe

KERNFORSCHUNGSZENTRUM KARLSRUHE
HAUPTABTEILUNG INGENIEURTECHNIK
PROJEKT NUKLEARE SICHERHEIT

KfK 3768

Post Test Investigation of the Single Rod Tests ESSI 1-11 on Temperature Escalation in PWR Fuel Rod Simulators due to the Zircaloy/Steam Reaction

S. Hagen, H. Kapulla, H. Malauschek, S. Katanishi*)

*) Delegate to Kernforschungszentrum Karlsruhe from
Japan Atomic Energy Research Institute

KERNFORSCHUNGSZENTRUM KARLSRUHE GMBH,
KARLSRUHE

Kernforschungszentrum Karlsruhe GmbH
Postfach 3640, 7500 Karlsruhe 1

ISSN 0303-4003

Nachuntersuchungen der Einzelstabexperimente ESSI-1 bis ESSI-11 zur Temperatureskalation an DWR Brennstabsimulatoren infolge der Zirkaloy/Dampf Wechselwirkung.

Kurzfassung

Es werden die metallographischen Nachuntersuchungen der Einzelstabversuche ESSI-1 bis ESSI-11 diskutiert. Die Experimente dienten der Untersuchung des Eskalationsverhaltens der Temperatur von zirkaloy-umhüllten Brennstäben im Wasserdampf. Die Betrachtung des Eskalationsverhaltens in den out-of-pile Experimenten ist Teil des Severe Fuel Damage Programms des PNS.

Der Brennstabsimulator bestand aus einem zentralen Wolframheizer, den UO_2-Ringpellets und dem Zirkaloy-Hüllrohr. Das den Simulator umgebende Dampfführungsrohr bestand ebenfalls aus Zirkaloy und war wiederum von einer Keramikfaser-Isolationsschicht umgeben.

Die drei einführenden Experimente sollten erste Informationen über die Temperatureskalation liefern. Die Versuche ESSI-4 bis ESSI-8 wurden mit zunehmender Temperaturanstiegsrate gefahren, um die Abhängigkeit der Eskalation von der Oxid-Schichtdicke beim Eskalationsbeginn zu erfassen. In den Versuchen ESSI-9 bis ESSI-11 wurde der Einfluß der Isolationsschichtdicke auf das Eskalationsverhalten untersucht. Die Experimente zeigten, daß auch der Spalt zwischen Shroud und Isolation einen merklichen Einfluß auf die Eskalation besitzen kann.

Nach dem Versuch wurde der Brennstabsimulator in Epoxidharz eingebettet und geschnitten. Die Schnitte wurden zunächst photographiert und anschließend mit dem Metallmikroskop, dem Rasterelektronenmikroskop und der Mikrosonde untersucht.

Das Schadensverhalten wird im wesentlichen durch den Oxidationsgrad bestimmt, der wiederum vom Temperaturanstieg abhängt. Die Oxidation des Zirkaloys tritt in Konkurrenz zur Auflösung des UO_2 durch das beim Erreichen seines Schmelzpunktes verflüssigte Zirkaloy. Je steiler der Temperaturanstieg, desto dünner ist die beim Erreichen der Zirkaloy-Schmelztemperatur vorhandene Oxidschicht und desto stärker ist die Auflösung des UO_2. Bei schnellem Anstieg kann es zum vollkommenen

Auflösen des UO_2-Ringpellets kommen (ESSI-8), während beim langsamen Anstieg mit voll durchoxidierter Hülle die Auflösung vermieden wird (ESSI-4).

Die Auflösung des UO_2 durch Zirkaloy erfolgt durch Sauerstoffentzug, wenn beim Schmelzen des Zirkaloys ein enger Kontakt zwischen den Materialien hergestellt wird. Aus der entstehenden (U, Zr, O)-Schmelze bilden sich in Abhängigkeit vom Sauerstoffgehalt beim Erstarren bis zu drei der folgenden Phasen: eine uranreiche metallische (U, Zr) Legierung, metallisches α-Zr(O) und ein (U, Zr)O_2-Mischoxid.

Summary

This KfK-report describes the posttest investigation of the single rod tests ESSI-1 to ESSI-11. The objective of these tests was to investigate the temperature escalation behaviour of zircaloy clad PWR-fuel rods in steam. The investigation of the temperature escalation is part of the program of out-of-pile experiments (CORA) performed within the frame work of the PNS Severe Fuel Damage Program.

The experimental arrangement consisted of fuel rod simulator (central tungsten heater, UO_2 ring pellets and zircloy cladding), zircaloy shroud and fiber ceramic insulation.

The introductory test ESSI-1 to ESSI-3 were scoping tests designed to obtain information on the temperature escalation of zircaloy in steam. ESSI-4 to ESSI-8 were run with increasing heating rates to investigate the influence of the oxide layer thickness at the start of the escalation. ESSI-9 to ESSI-11 were performed to investigate the influence of the insulation thickness on the escalation behaviour. In these tests we also learned that the gap between removed shroud and insulation has a remarkable influence due to heat removal by convection in the gap. After the test the fuel rod simulator was embedded into epoxy and cut by a diamond saw. The cross sections were photographed and investigated by metalograph microscope, SEM and EMP examinations.

The damage behaviour is determined by the degree of oxidation, which itself is dependent on the imposed heating rate. The oxidation of the zircaloy cladding with the dissolution of the UO_2 by the molten zircaloy, when the melting point of zircaloy is reached. The faster the temperature increase, the thinner is the oxide layer of the cladding, with the consequence of a higher dissolution. For the fast temperature increase of ESSI-8 we get the complete dissolution of the UO_2 -annular pellet and for the slow heatup of ESSI-4 with the fully oxidized cladding the dissolution is avoided.

The dissolution of the UO_2 by zircaloy results from the extraction of the oxygen from the UO_2, when molten zircaloy comes into close contact with the UO_2 pellet. Depending on the overall oxygen content, the resulting (U,Zr, O)-melt forms up to three of the following phases upon refrezing:

an uranium rich metallic (U, Zr)-alloy, α-Zr(O) and a (U, Zr)O_2 mixed oxide.

Contents

1. Introduction

Within the Project Nuclear Safety (PNS) at the Kernforschugnszentrum Karlsruhe (KfK), a comprehensive programm /1/ for the investigation of Severe Fuel Damage (SFD) is scheduled. As part of this programm, out-of-pile experiments are being conducted at the Hauptabteilung Ingenieurtechnik (IT) (CORA Programm /2/). The mechanisms causing damage to PWR fuel rods for temperatures up to 2200°C are to be investigated. The experiments are designed to give information on the integral behaviour of the processes, which are investigated in detail and under well defined conditions in the separate effect tests of the SFD-programm. In the first group of these tests /3-9/ the interaction of the solid and liquid Zry with UO_2 and the phases formed from the resulting Zr-U-O-System are determined.

The second group of tests /10-16/ was done to investigate the oxidation behaviour of Zry. The out-of-pile experiments will also be used for the assesment of the SFD computer codes to simulate the integral behaviour of the fuel rods under Severe Fuel Damage condition. In addition, these experiments directly complement integral inpile bundle tests being conducted at PBF,ACRR, NRU and PHEBUS.

Earlier experiments have shown that the behaviour of fuel rods at high temperatures is strongly dependent on the degree of cladding oxidation. Highly oxidized rods are very brittle and can fragment during operation or during quenching, whereas relatively unoxidized cladding melts, dissolves UO_2, and runs down the rod. The extent of oxidation depends, in part, on the temperature heating rate, which in turn is influenced by the exothermic oxidation process. If the heat of reaction is not removed fast enough, the exponential increase of the reaction with temperature can give rise to a rapid temperature escalation. Therefore, oxidation-induced temperature escalation plays an important role in determining fuel behaviour. To investigate the temperature escalation and the processes leading to a turnaround of the escalation, a series of single rod and bundle experiments with fuel rod simulators are being performed.

The results of single rod tests are given in the KfK-report 3507, 3557 and 3567 /17-19/. The bundle tests ESBU-1 and ESBU-2a are described in the KfK-reports 3508 and 3509 /20, 21/. The posttest investigations of ESBU-1 and ESBU-2A are given in the KfK-reports 3769 and 3789 /22, 23/.

This paper reports on the posttest investigations of the single rod tests ESSI-1 to ESSI-11.

The single rod test ESSI 1 to 11 were run to get information on the temperature escalation of zircaloy in steam. Details of these tests are given in the test results reports of tests ESSI 1 to 3 (KfK-report 3507) and the test results report for tests ESSI 4 to 11 (KfK-report 3557). In the following section an overview of the test is given .

The tests can be grouped in three sections. The introductory tests ESSI 1 to 3 were done to obtain initial information on the temperature escalation behaviour of zircaloy in steam. The second group ESSI 4 to 8 were run with increasing initial temperatures to investigate the influence of the oxide layer at the start of escalation. The last group ESSI 9 to 11 was performed to investigate the influence of the insulation thickness on the escalation behaviour. In these tests we also learned that the gap between shroud and insulation has an important influence.

The number of the figures are given as a double-number, separated by a dash. The first number always corresponds to the test number. So we have 12 groups of Figures from 1-1 to 11-5. Following after this eleven groupes are then Figures 22 to 26.

The difference in the test arrangement of these groups can be seen from Figures 22 to 26 which can be found at the end of this report. The length of the fuel rod simulator in the first group was 25 cm. In the second and third group the fuel rod simulator has a length of 37 cm. The insulation was identical in group 1 and group 2, (i.e., tests 1-8). The thickness of the insulation at these tests was about 100 mm. In the third group the insulation thickness of test 9 was only 12.7 mm, in test 10 and 11 it was 6.35 mm. In test 9 a small gap was left between shroud and insulation, and in test 10 and 11 the insulation was directly wrapped onto the shroud.

2. Experimental Arrangement

The tests were performed in the NIELS facility located in the Hauptabteilung Ingenieurtechnik at KfK. Figures 22 and 23 show side and

top cross sections of the fuel rod simulators, shroud, and insulation for tests ESSI 1 to 3. The fuel rod simulators conformed as nearly as possible to German PWR dimensions, using zircaloy cladding of 10.75 mm outer and 9.29 mm inner diameter, UO_2 ring pellets of 9.2 mm outer and 6.1 mm inner diameter, and tungsten heater rods of 6.0 mm diameter. The overall length of the simulators was 250 mm in tests ESSI 1 to 3. For tests ESSI 4 to 11 the simulators had a length of 370 mm.

To simulate the exothermal reaction energy of neighbouring rods a zircaloy shroud was installed around the fuel rod simulators. The shroud had an inner diameter of 26.5 mm and a 0.5 mm wall thickness for ESSI 1-3. For tests ESSI 4-11 the shroud had a wall thickness of 1 mm.

To inhibit radial heat losses the simulator and shroud were surrounded by about 100 mm of fiber ceramic insulation for tests ESSI 1-8. The inner 25.4 mm was made from ZrO_2 and the outer 76.2 mm from an Al_2O_3/SiO_2 mixture. the ZrO_2 fiberboard is 92% porous and has a thermal conductivity of 0.24 W/m-K at 1650°C. The Al_2O_3/SiO_2 mixture has a conductivity of 0.20 W/m-K at 1100°C.

ESSI 9 was insulated by a cylinder of 12.7 mm thick ZrO_2 machined from zirconia fiberboard. In the tests ESSI 4 to 9 there was a gap between the insulation and the zircaloy shroud. This resulted in a direct heat loss from the shroud to the surrounding atmosphere by natural convection. For tests ESSI 10 to 11, an insulating blanket of zirconia felt was wrapped around the zircaloy flow shroud. Consequently, for these last two tests, there wass no gap between the insulator and the flow shroud, eliminating the direct heat loss from the shroud to the outer atmosphere.

Steam was injected into the shroud through a double tube system. The four holes in this system ensured a uniform supply of steam to the surface of the rod. Rod and Shroud surface temperatures were measured by two color pyrometers. Holes for these measurements were cut into the shroud and insulation 140 mm above the lower end of the rod. Temperatures in the insulation were measured by NiCrNi-thermocoples with inconel sheaths.

3. Test Conduct

3.1 ESSI-1 to ESSI-3

A major parameter of the three scoping tests was to determine initial information on the magnitude of the temperature escalation for different initial oxide layers. Test ESSI-1 was intended to have a minimum initial oxide thickness and thus the rod was heated in argon until the surface temperatue reached about 1700°C before steam was introduced. During the same time the shroud had reached a temperature of about 1200°C by radiant heating from the rod. At about 32 minutes 32 g/min steam was introduced. The rod temperature increased due to the zircaloy/steam reaction to about 2250°C. After the reaction stopped, steam cooling significantly lowered the rod temperature.

The objective of test ESSI-2 was an initial heatup rate of roughly 4°C/s in a continuous steam flow (23 g/min). The voltage was increased linearly.

The objective of text ESSI-3 was a slow initial heatup rate of 0.5°C/s in a steam atmosphere (17 g/min) in order to produce a thick oxide layer before the escalation began. The voltage was increased linearly throughout the test.

3.2 ESSI-4 to ESSI-11

The single rod tests, ESSI-4 to ESSI-11 were all run in a flowing steam atmosphere. The steam supply for all of these tests was high enough to preclude steam starvation during the transient. The steam flow was set to a constant rate during each of the tests, and the pressure in the NIELS facility was controlled by adjusting the outlet flow of steam from the test chamber. The pressure was maintained at about 1 bar for each of these tests. To prevent condensation in the test chamber during the tests, the outer walls of the test chamber were heated to 150°C before beginning each of the test runs. The general test conditions for tests ESSI-4 to ESSI-11 are given in Table 2. The test rods were heated by resistance heating of the tungsten heater rods. The heatup was performed by applying a linear voltage ramp to the heater rods. Once a sufficiently high temperature was reached, the reaction between the

zircaloy and steam caused a rapid temperature escalation. Then a constant voltage was maintained until the heating from the metal water reaction decreased substantially.

The tests ESSI-4 to ESSI-8 investigated the influence of the oxide thickness on the temperature escalation behaviour. In these tests, the oxide layer thickness on the zircaloy was varied by changing the initial heatup rate. Starting with ESSI-4, the initial heatup rate was 0.3°C/min. The initial heating rate was then increased with each succeeding test through test ESSI-8, which had an initial heating rate of 3.6°C/min. The different heating rates were achieved by applying different linear voltage ramps to the tungsten heaters in the test rods.

Test ESSI-4/5 was run at a heating rate which fell between ESSI-4 and ESSI-5. This test investigated directly how strongly the metal water reaction affected the temperature escalation. In this test the same voltage ramp was run two times in steam (the zircaloy was oxidized during the first heatup, therefore the reaction energy was strongly reduced during the second run) and then repeated a third time in argon, and a fourth time in an evacuated vessel. Between the two steam tests the test rod was cooled to 1200°C, the measuring lower limit of the two color pyrometer. The first heatup in steam showed the escalation peak, the second did not. The heatup in argon and in the empty vessel gave the influence of the test atmosphere.

The influence of the insulation on the thermal response of the system was investigated in tests ESSI-9, ESSI-10 and ESSI-11. In test ESSI-9, a 12.7 mm thick cylinder of insulation was used instead of the 100 mm block of insulation used in the earlier tests. In ESSI-10 and ESSI-11, the insulation thickness was only 6.35 mm. In these last two tests however, the insulation is wrapped directly on the zircaloy flow shroud, eliminating heat losses by convection from the outside of the shroud.

4. Posttest Examination

After the test the insulation and the shroud were removed from the fuel rod simulator. After visual inspection in general the rods were photographed from four different directions. Special areas were registered in close up views. Then the rods were encapsulated in epoxy,

for preperation of cross sections. The cross section were photographed and also investigated with the optical microscope, scanning electron microscope (SEM) and with the electron mciroprobe (EMP). In the following the results of these examinations are discussed for each experiment.

4.1 Test ESSI-1

Figure 1-1 gives the posttest appearance of the fuel rod simulator of test ESSI-1 from four directions. The axial temperature profile can be recognized from the metallic appearance of the lower 6 cm and the increasing oxidized appearance of the upper rod. This unsymmetrical temperature distribution was produced by the input of relatively cold steam of about 130°C at the lower end of the fuel rod.

At about 120 mm above the bottom of the rod, molten material through the cladding and ran down the outside. Most of the material refroze on the rod. Also some drops ran down and refroze on the copper electrode and steam supply system. Appearantly a significant amount of zircaloy inside the zirconium oxide layer melted and drained downwards. This relocation may have limited the reaction energy.

The breaking of the thin oxide layer at the upper end of the fuel rod simulator at an elevation of about 200 mm is assumed to have happened during the cooldown. As one can see from the structure of the survived oxide layers, the zirconium oxide at the temperature of the test was quite flexible. The missing pieces of UO_2 in the area of the breakage were dislodged during the dismantling of the test arrangement. To remove the shroud it was necessary to remove the upper electrode. This caused mechanical stresses on the fuel rod which broke some of the UO_2 pieces.

Figures 1-2 and 1-3 gives the cross sections of test ESSI-1. The deviation from the circular shape of the oxide layer above 75 mm shows that above this height the zircaloy inside the oxidized outer layer must have been molten. As described above the cross sections show an increasing deformation of the oxidized outer skin with increasing elevation. With the exception of some holes up to an elevation of 105 mm

the oxidized outer layer is filled with refrozen material. Above 125 mm most of the metallic zircaloy is missing. The whole material has run away at the time of high temperatures and is refrozen on the outside of the rod as one can see in Figure 1-1.

At the elevation 75 mm the inner region of the oxidized skin is filled with refrozen melt. One can recognize two types of refrozen layer. There is a black area of the refrozen material close to the outside of the white zirconium oxide layer. As we will discuss later, this black seam on the outside of the fuel rod corresponds to molten material which is oxidized during the test due to oxygen diffusing through the outer zirconium oxide layer. Due to the increase of the melting point in this oxidized region this area is solidified during the test at the high temperature. The inner area between the skin and the UO_2 pellets is refrozen during cooldown.

The elevations 35 mm to 93 mm also show refrozen material on the outside of the fuel rod. One can recognize that for elevations above 75 mm an outer crust was formed with empty space in the inside.

In Figure 1-4 enlarged views of the cladding area are given. The microphotographs show at 35 and 50 mm elevation a thin oxide layer with the rest of the unmolten cladding. A sharp boundary between the zirconium oxide and the metallic cladding can be seen. At the elevations 75 mm and higher the microphotographs were taken from areas where refrozen melt has formed between the outside of the cladding and the UO_2 pellet. One can recognize a relatively thin layer of large grains of zirconium oxide which is followed by a relatively homogeneous area. This darker area corresponds to the black seam of the cross section. As a later discussion will show, this region is formed by a mixed zirconium/uranium oxide. In the remaining region towards the UO_2 pellet metallic α-zircaloy and mixed zirconium/uranium oxide are found.

The liquid Zry in contact to the UO_2 pellet started to dissolve the UO_2. At test temperature a homogenous (U, Zr, O) melt is formed. From this melt a mixed oxide starts to precipitate in contact to the ZrO_2 layer.

This is due to the oxygen diffusing through the oxide layer, delivered by the steam outside the rod.

The measurement of the outer oxide layer formed by oxidation of the original cladding is given in Fig. 1-A. At each cross section four measurements were made. The solid line gives the mean value of these measurements. The dashed lines connect the maximum and minimum measured values. In the region of cross sections with internal molten zircaloy (75 mm to about 180 mm) we find practically the same oxide thickness of 0.2 mm.

The decrease of the UO_2 annular pellet wall thickness due to the dissolution is given in Figure 1-B. The original UO_2 annular thickness is 1.55 mm. Also here at each cross section four measurements are made. The solid line gives the mean value and the dashed lines the maximum and minimum measured value. The largest attack is found in the region between 100 and 150 mm elevation. 0.35 mm is the mean value of lost thickness. The ratio of the UO_2-pellet cross section change to the original pellet cross section is given in fig. 1-C. At the elevation of maximum temperature less than 1/3 of the cross section is dissolved.

Figures 1-5 to 1-9 show cross sections of special regions from 50 to 188 mm. Figure 1-5 gives an overview showing the axial location for each close up view.

Figure 1-5a gives micrographs from the cross sections at 50 mm elevation in the region of the refrozen material at the outside of the fuel rod simulator. Photo 2 gives an cross section through the outside refrozen material. One can clearly recognize the outside oxidized area compared to the inner region. Photo 4 gives an enlarged presentation of the transition region from the inside material to the outside oxidized layer. The inside area is given by photo 6 in a magnification of 1000. Here one can recognize the typical two phases. The black areas are the mixed uranium/zirconium oxide and the white area consists of α-zircaloy. Photo 5 shows in large magnification the outer oxidized area. Here we

have one homogeneous phase, it consists of the mixed zirconium/uranium oxide. Photo 3 gives an enlarged presentation in the direct transition area in the lower region. One can see the oxidized single phase region in the lower portion of the photo and in the upper portion the two phase region is seen (as discussed before). Photo 1 finally shows the area of the refrozen melt in contact to the fuel rod simulator. Also here one can recognize the outer oxidized area. Note that the enlarged picture is upside down with respect to the marked region in photo 2.

In Figure 1-5b photo-micrographs of the cross sections at 105 mm are given. These figures show mainly the cladding area, and one can clearly recognize the inner regions where the original cladding remains. On the outside we have the zirconium oxide layer. It follows the layer of mixed zirconium/uranium oxide. The remaining region (towards the UO_2 pellets) is filled with the two phase area formed by the mixed oxide and the α-zircaloy. The same behaviour is seen in the following figures 1-5c to 1-9 at different elevations.

Figure 1-10 shows a scanning electron microscope (element distribution) photo in the outer region of the refrozen melt at elevation 50 mm. The areas of these pictures are marked in the photograph of the cross section on the left side of figure 1-10. This area extends from the outer oxidized skin to the inside of the refrozen droplet.

In all three pictures one can recognize two different regions: An area of one homogeneous phase on the outside and a two phase region on the inside. In the bottom scanning electron picture the two phases appear as black and grey structures. The white lines and dots, which appear black in the element distribution pictures are cracks or areas of missing material.The comparison of the electron scanning picture with the Zr + U distribution pictures shows, that the grey phase consists preferential of Zr: The grey structures in the electron scanning picture correspond to the bright areas of the Zr-distribution and to the dark areas of the U-distribution. The dark phase also contains Zry and Uranium. In the outer seam of the refrozen droplet Zry and uranium is homogenously distributed.

Figure 1-11 gives for the same area of investigation microprobe results. These results show that in the outer seam only one phase is found: a mixed $(U,Zr)O_2$-oxide. The two phases in the inner region are again a mixed $(U, Zr)O_2$-oxide and a α-Zry with a small amount of Uranium.

Figure 1-12 gives the scanning electron microscope and element distribution pictures in the region of the original cladding from outside refrozen material to the UO_2-pellet on the inside. The uranium distribution picture shows (by the Uranium in the region of the original cladding), that the inner region of the cladding must have been molten. This conclusion is confirmed by the microprobe analysis (see figure 1-13) since Uranium can also be found in the region of the original cladding. The microprobe analysis show the mixed oxide and the α-Zircaloy (Pos. 10 + 11) in the refrozen melt on the outside of the cladding. The ZrO_2 of position 12 indicates that the outer skin of the cladding was oxidized. In agreement with the element distribution picture, the microprobe results show the strong variation of the Uranium in the inner region of the former cladding.

Figure 1-14 shows the element distribution in the area of the gap between the tungsten rod and the UO_2 pellet at 50 mm elevation: Element distribution pictures and microprobe results are given. The lower left side of this figure also shows the scanning electron microscope photo. In these figure the upper part shows the UO_2 pellet. The gap is filled with refrozen material which has run down from upper regions. In the lower area of this picture the tungsten is seen.

This relocation is confirmed by the element distribution pictures. The tungsten can be seen as little white dots only in the region of the central heater. The UO_2 can be recognized in the upper part of the pellets but it is contained also in the gap. Here the refrozen melt, which consists of zircaloy which has dissolved some uranium, is refrozen. The zircaloy distribution picture shows that the zircaloy can be found only in the area of the gap as refrozen material. The microprobe analysis shows that the white phase in the gap consists of α-zircaloy containing a small amount of uranium as given in measuring point 24. The dark phase contains a large amount of uranium.

Figures 1-15 to 1-16a give results for microprobe investigations at the 188 mm elevation. The overview for the different measurement positions is given in Figure 1-16a. It is an area in which molten zircaloy has remained between the oxidized cladding and the UO_2 pellets. Contacting the oxidized zircaloy skin one can recognize the black area from which four regions were examined in detail: regions A-D. Region A is the transition from the zirconium oxide to the mixed oxide. Region B is the transition area from the mixed oxide to material refrozen during cooldown. Region C is taken from the material frozen during cooldown. Region D gives the transition from the region refrozen during cooldown to the UO_2 pellets. Finally region E is the area of gap between the UO_2 pellet and the tungsten heater.

On Figure 1-15 the scanning electron microscope picture is given on the lower part of the left side for region A. The upper white area corresponds to the zirconium oxide skin. The black area on the lower part of the picture corresponds to the black seam. Position 1 shows that the outer white area is pure zirconium oxide. Measuring position 2 shows that in this oxide there are some α-zirconium inclusions. Measuring position 3 in the lower dark area indicates that this region is a mixed oxide containing a relative small amount of uranium.The molten zircaloy has interacted with the UO_2 and dissolved some material of the uranium oxide pellet.

Area B in Figure 1-15 gives the transition region from the mixed oxide area to the region refrozen during cooldown . Due to different exposures of the pictures for region A and B the dark appearing lower portion of picture A appears much brighter in the upper region of picture B. The measuring position 4 in this brighter upper region shows that this area corresponds to a mixed uranium zirconium oxide, with a relatively small amount of uranium. It is due to the short reaction time between the UO_2 and the melt in this test. Measuring position 5 and 6 in the lower region of this area show that there we have two phases. The first phase in the measuring position 5 is the α-zircaloy containing a small amount of uranium. The second phase is the $(U, Zr)O_2$ mixed oxide.

Measuring area C is in the region of melt refrozen during cooldown. Here we find two phases. First the α-zirconium in measuring position 7 and the mixed oxide in measuring position 8. We see that closer to the uranium oxide pellet we have a higher concentration of uranium.

Measuring area D is in the transition from the refrozen melt to the UO_2 pellet. Position 9 and 10 in the refrozen melt again give the two phases: α-zircaloy on measuring position 9 and the mixed oxide in position 10. In this position we have a higher uranium concentration than concentration in zircaloy. Measuring position 11 inside the UO_2 pellet gives as expected the uranium oxide .

Measuring area E is in the gap between the UO_2 pellet and the tungsten heater. Inside the gap we find two phases . The darker phase consisting of the mixed uranium/zirconium oxide. The brighter phase is formed by α-zircaloy containing a small amount of uranium. The measuring position 16 which is not given in this figure contained only tungsten.

Figure 1-17 to 1-18a contain the results of microprobe investigations at the 105 mm elevation. Again region A corresponds to the transition from the zirconium oxide to the mixed oxide. Region B is the transition area from the mixed oxide to the two phase area. Region C is inside the two phase area . Measuring region D is in the transition from the two phase area to the UO_2 pellet and finally measuring region E is in the gap between the UO_2 pellet and tungsten heater.

Measuring area A shows in the three measuring points 1 to 3 the transition from a pure zirconium oxide to a mixed zirconium/uranium oxide with increasing uranium content. One can recognize a clear boundary between the two areas of mixed oxide. This means that precepitation may have taken place from melts of different uranium concentrations. We again find nearly the same uranium concentration in measuring positions 3 and 4 in the area of the mixed oxides. Also here at 105 mm elevation we find an increase in the uranium concentration of the mixed oxide as one approaches the UO_2 pellet. This was also seen at measuring positions 6,8 and 10.

In the measuring region E in the scanning electron microscope picture one can recognize that in addition to the white α-zircaloy (measuring point 14) there are two additional other phases: The dominant grey phase which consist of the mixed oxide and a deep dark phase which is measured in position 15. This phase has a high concentration of uranium. This corresponds the third possible phase: an uranium/zirconium alloy. The relatively high oxygen concentration of this phase is probably caused by oxygen contamination. (When polishing cross sections the metallic uranium always has the tendency to oxidize on the surface.)

In Figure 1-19 a summary of the compositions are given which are found in the microprobe measurements from the various cross sections of ESSI-1. The results of the analysis are represented in a ternary phase diagram. In general this summary show that materials can be categorized into 3 groups. The first group is an α-zircaloy material with about 35% oxygen concentration. The second group of materials are mixed oxides which lie near the connection line between the UO_2 and the ZrO_2. The third group of materials have high uranium concentration with a relatively small oxygen content. For these values the measured value for the oxygen may be to high due to oxygen contamination after the preparation.

Figure 1-20 to 1-22 show enlarged photographs of the upper region of the fuel rod simualtor ESSI-1. In this area the molten zircaloy inside the zirconium oxide skin has run down inside the skin and has left the cladding in the lower region of the rod. At the time taking the photograph the oxide layer has partly broken away. Now the remaining pellets can be seen over a larger region than in Figure 1-1. The left picture Figure 1-20 shows that the gaps between the pellets is glued together by the refrozen melt. The melt running into the gaps may also have filled the gap between the inside of the pellets and the tungsten heater as we have seen in Figure 1-16 an 1-18. The former smooth surface of the pellets becomes rough due to the dissolution of the pellet surface by the liquid zircaloy.

4.2 Test ESSI-2

The posttest appearance of the rod from test ESSI-2 seen from four different directions is given in Figure 2-1. The metallic appearance of the lower 4 cm of the rod which changes to severely oxidized cladding higher up shows the effect of the axial temperature profile. From 7.5 to 10.5 cm above the bottom of the rod the oxide has broken away, presenting the smooth surface of refrozen material. This smooth surface shows that the oxide layer must have covered the rod during the high temperature portion of the transient and then have broken away during cool down. At the upper end of the fuel rod a strong deformation of the oxide layer can be recognized.

As discussed in the test results report, the fuel rod temperature escalation of test ESSI-2 began around 1100°C and reached a peak temperature of about 2100°C. The shroud escalation began a little later and reached a peak temperature of about 2050°C. The steam flow was continuous throughout the test at 23 g/min. The maximum steam consumption rate as estimated by the MULTRAN Code was 2.5 g H_2O/min on the rod and 10 g H_2O/min on the shroud. Steam starvation therefore did not occur.

Figures 2-2 and 2-3 gives the cross sections of test ESSI-2. As in ESSI-1 the partly missing oxide layer and the strong deformation at about 200 mm can be recognized. Also here, the outer ZrO_2 oxide layer, the precipitated mixed oxide, and the refrozen metalic melt is found. The micrographs of the cladding area are given in Figure 2-4. The distinct boundary between the oxidized and unoxidized region in Figure 2-4 shows that in the area below 50 mm no melting occured. The zirconium oxide layer has nearly the same size in the cross setions from 100 and 162 mm. At 168 mm the outside oxide layer of large crystals has a definately larger thickness. From 180 to 210 mm the thickness of the outside oxide layer decreases. The molten cladding inside this outer oxide layer is oxidized by the oxygen diffusing through the zirconium oxide layer. At 225 mm we can recognize the sharp boundary of the oxide layer in unmolten zircaloy.

The measured values of the zirconium oxide layer thickness are given in figure 2-A. These values do not include the oxidized layer of prior molten material. As already seen in the micrographs, the oxide thickness at the elevation of unmolten cladding at 50 mm and 225 mm is larger than the thickness at the next cross section with internal molten cladding (at 100 and 210 mm elevation). At these elevations the melting temperature was reached before thicker layers were developed. The locally larger thickness at 168 mm seems to be connected with azimuthal asymetric behaviour of the cladding. The oxide layer in the region of molten Zry has a mean value of about 0.3 mm.

The molten zircaloy has interacted with the pellet and dissolved its outer layer. The remaining diameter of the pellets are given in fig.2-B. From the measured 4 values the minimum, the maximum and the mean value are display. The decrease of the UO_2-thickness due to the dissolution is given in Fig. 2-B. The main attack in this test is found from 135 to 165 mm elevation. The region of maximum atttack has moved to higher elevations. About 0.65 mm is the mean value of the lost thickness in this region. This is nearly twice as much as in test ESSI-1. The maximum attack in this region is about the half pellet thickness. The measured UO_2 diameters are used to calculate the dissolved part of the cross section. The ratio of the dissolved area of the cross section to the original pellet cross section are given in fig. 2-C. The high value at 210 mm elevation is due to strong local effects.

Figures 2-10 to 2-12 give enlarged views of the fuel rod simulator ESSI-2. The oxidized cladding is partly broken away. The frozen melt inside the oxide shell can be recognized. At the lower end of the picture on the right hand side of Figure 2-10 at the hight of 0.10 to 0.11 one can recognize the rest of the pellets. Here the area between pellets and oxidized shell was not filled with molten material. The pictures of the cladding region on Figures 2-11 and 2-12 show the varying thickness of the oxide layer for different elevations.

4.3 Test ESSI-3

Figure 3-1 shows the posttest appearance of the fuel rod simulator from test ESSI- 3. The objective of test ESSI-3 was a slow initial heat up rate in steam atmosphere in order to produce a thick oxide layer before the escalation begins. Figure 3-1 shows that this aim was reached. One can recognize a smooth undestroyed surface.

Figures 3-2 and 3-3 show the cross sections of test ESSI-3. The micrographs of the cladding region are given in Figure 3-4. Up to 60 mm one can recognize a sharp boundary between the oxidized and unoxidized region of the cladding. This means that at these elevations the melting temperature of the zircaloy was not reached. The strong increase in temperature with elevation is reflected in the steep increase of the oxide thickness from 50 to 60 mm elevation. At the 60 mm elevation a thickness of 0.6 mm was reached. From 140 to 190 mm the zircaloy cladding was almost entirely oxidized before the melting temperature of the zircaloy was reached. This can also be seen from Figure 3-A giving the thickness of the zirconium oxide layer. In the cross sections betwen 60 to 140 mm and 205 and 220 mm the cladding was only partly oxidized when the melting temperature of the zircaloy was reached and consequently some of the inner zircaloy has melted.

Fig. 3-B gives the thickness of the annular pellet. The original thickness of the annular pellet wall was 1.55 mm. The contact area between UO_2 and oxidized cladding is so strongly embrittled (Fig. 3.5), that the measurement is influenced by increase of the surface and break away of UO_2 particals. Thus, in figure 3-C the missing UO_2-area is due to the embrittlement and break away, and not due to dissolution.

Figure 3-7 shows the cross section at the 90 mm elevation and some enlarged photo-graphs of the cladding region in contact to the UO_2 pellet. One can recognize that at this elevation the zirconium oxide layer is only about half the thickness of the original cladding. Inside this white oxide layer a black layer has formed. In comparison to the earlier given results it is assumed that this black layer consists of an uranium/zirconium mixed oxide.

Figure 3-8 shows the cross section and two close up views of the cross section at an elevation of 205 mm. At this elevation less than half of

the cladding was oxidized when the melting temperature was reached. Consequently the internal zircaloy melted and some of the molten zircaloy ran into the lower area of the fuel rod bundle to fill the space in this region. Molten material which stuck between the oxide layer and the pellet was oxidized by the oxygen diffusing through the outside layer. Figure 3-9 shows variations of the oxide layer thickness at the elevation of 205 mm. Figure 3-10 gives the cross section at 230 mm elevation.

4.4 Test ESSI-4

Figure 4-1 gives the posttest appearance of the fuel rod simulator of test ESSI-4. ESSI-4 was a test with slow initial heat up rate, so that the behaviour should be similar to test ESSI-3. The bulging of the oxidized cladding at 150 mm is assumed to be due to the different shrinking of the tungsten rod and the oxide shell. The cladding is glued to the tungsten rod at the upper and lower end by the material molten in this region. The black thin layer in the region between 150 and 250 mm elevation is refrozen melt which must have penetrated through cracks in the oxide shell.

The cross sections of ESSI-4 are given in Figures 4-2 to 4-4. The micrographs can be found in Figures 4-5 to 4-6. The cross sections below 97 mm and above 325 mm show the straight boundary between unmolten Zry and oxide layer. In the middle region we find the fully oxidized cladding. At the upper end in the region of about 300 mm we find the partly oxidized cladding area with an additional layer of oxidized melt. Fig. 4-A gives the measured zirconium oxide layer. Between 200 and 310 mm elevation the cladding is fully oxidized. The variation of the oxide layer thickness with elevation reflects the temperature/time history at different elevations.

Fig. 4-B gives the UO_2 pellet wall thickness as function of elevation. The decrease of the pellet wall thickness between 170 and 270 mm is caused by embrittlement and break away and not by dissolution. The percentage of the broken away area is given in fig. 4-C.

Figure 4-7 shows the cross section at 310 mm and micrographs with different enlargement in the boundary area between UO_2 and cladding.

One can recognize that between the outer zirconium oxide shell and the UO_2 pellet a small layer has melted which was then subsequently oxidized by the oxygen diffusing to this region.

Figure 4-8 shows the cross section of an unheated fuel rod simulator. The appearance of the annular UO_2 pellet and the zircaloy cladding is given at an enlargement of 50. The UO_2 pellet is also shown at the much higher enlargement of 1000.

Figure 4-9 to 4-11 show enlarged representations of the bulged area of the fuel rod cladding and the upper end of the same fuel rod simulator. The close up views in Figure 4-10 show the lift of the cladding with the break at the largest elevation. The break at this position gives the hint that the rupture occured during the cool down of the fuel rod simulator. The surface of the fuel rod pellet in the lower left picture in Figure 4-10 shows some refrozen liquid material. It is not clear if this liquid material is due to interaction between zircaloy and cladding at this elevation, or if molten material from higher elevations has run down into this region.

Position 1 on Figure 4-11 shows how molten material refroze inside the outer oxidized layer. The two lower pictures of Figure 4-11 shows the area where the thermocouple touched the cladding. One can recognize the interaction between the Inconel and the zircaloy.

4.5 Test ESSI-4/5

Figure 4/5-1 shows the posttest appearance of the fuel rod simulator from test ESSI-4/5. The initial heat up rate in this test was 0.5 °C/sec. The power was then reduced to lower the temperature to about 1000 degree and then heated a second time in steam with the same electric power input. This heatup was repeated in argon and in vacuum. A thick oxide layer with a smooth surface has developed.

The cross section of this fuel rod simulator are given in Figures 4/5-2 and 4/5-3. The micrographs of the cladding region are given in Figure 4/5-4. Also this test shows practically the same behaviour as ESSI-3 and

ESSI-4. In the middle region the oxide layer is completely oxidized. At the upper and lower end one can recognize the partly oxidized unmolten cladding. The straight boundaries between oxide and metal in the cross sections at 65 mm and 325 mm show, that below and above these elevations there was no melting of the zircaloy.

The mesured thickness of the oxide layer is given in figure 4/5-A . The comparison against fig. 4-A shows, that in the additional heating (page 11) also in lower areas between 100 and 200 mm elevation a complete oxidation of the cladding was reached. The oxidation starts at the upper elevation with the highest temperature and moves than downwards.

Fig. 4/5-B gives the wall thickness of the annular UO_2-pellet. Again here the measured losses are due to embrittlement and breakaway. Fig. 4/5-C gives the percentage of area broken away.

4.6 Test ESSI-5

The test ESSI-5 was run with an initial heat up rate of 0.8°C/sec. The posttest appearance is given in Figure 5-1. The figure shows that between 150 and 175 mm elevations the oxidized cladding is broken away. The smooth surface of the material appearing in this region indicates that it must be refrozen material. The existance of molten material inside the oxide layer also means that the break away of the oxide layer must have happened after refreezing of the molten material. In the region between 215 and 300 mm, we recognize that a much thinner oxide layer has formed. One also can recognize a strong deformation of the oxide layer in this region.

The cross sections of this fuel rod simulator are given in Figures 5-2 and 5-3 and the micrographs of the cladding region in Figure 5-4. Also the cross sections and the micrographs show the refrozen melt inside the oxide layer. The strong deformation of the cladding above 200 mm can be seen in the cross sections above 200 mm elevation. The cross sections at 115 mm and 325 mm show the straight boundary between oxide and metal for the unmolten cladding.

Fig. 5-A gives the measured values of the oxide layer as function of elevation. A large spread for the values at the same elevation can be

recognized. Due to the faster initial temperature increase complete oxidation was not reached. The attack of the liquid zircaloy on the UO_2 pellet resulting in dissolution of UO_2 is given in fig. 5-B and 5-C.

Figures 5-5 to 5-8 show details of the refrozen melt inside the oxide layer and the deformed oxide layer in the upper region of the fuel rod simulator.

4.7 Test ESSI-6

The test ESSI-6 was run with an initial heat up rate of 1.1 °C/sec. The posttest appearance is given in figure 6-1. A smooth oxide layer has formed. At about 300 mm elevation part of the oxide layer has swept away and the molten material has run down to refreeze at an elevation between 200 mm to 250 mm

At 150 mm elevation the oxide layer is broken away after the test. The smooth surface of the underlying material without pellet structure is evidence, that molten material must have formed here, which refroze during cooldown.

The cross sections are given in fig. 6-2 and fig. 6-3. Above 200 mm elevation the strong deformation of the cladding and the location of the refrozen melt can be recognized. The micrographs in fig. 6-4 show that as low as 115 mm molten material is refrozen inside the cladding.

Fig. 6-A gives the measured values of the ZrO_2-layer. The thickness increases from about 0.35 to 0.6 mm from 115 mm to 280 mm elevation. The large spread of the measured values for the thickness at 280 mm is due to the loss of the cladding on one side of the rod.

The interaction between pellet and liquid zircaloy resulting in the thinning of the pellet is represented in fig. 6-B and 6-C. The maximum attack is found at 250 mm with about 30% of annular cross section area.

Details of surface structure are given in fig. 6-5 and 6-6.

4.8 Test ESSI-7

Test ESSI-7 was run with an initial increse of 2.3 °C/sec. The posttest appearance is given in fig. 7-1. Due to the fast initial heat up rate a strong temperature escalation is develloped. Consequently the molten zircaloy dissolved in the region between 180 and 270 mm elevation nearly the whole annular pellet. The molten material refroze between 120 mm and 180 mm elevation.

The cross sections are given in fig. 7-2 and fig. 7-B . They clearly show the strong dissolution in the upper area. Also the deformation of oxidized part of the cladding can be recognized. At 265 mm elevation the typical "flowering" effect can be seen. Flowering means the stretching away of oxidized cladding from the original circular form. This behaviour shows the deformability of the oxide layer at high temperatures.

Fig. 7-A gives the measured oxide layer. Between about 150 mm and 300 mm the values represent the layers left only on one side of the rod. Fig. 7-B and fig. 7-C represent the attack on the UO_2 pellet by the liquid zircaloy. Details of the surface structure after the test are given in figures 7-5 and 7-6.

4.9 Test ESSI-8

Test ESSI-8 was run with an initial heat up rate of 3.6 °C/sec. The posttest appearance is given in fig. 8-1. The fast heatup and the consequently interaction between the liquid zircaloy and the UO_2 pellet has brought about the melt away of the complete fuel rod simulator between 130 mm and 300 mm elevation. The melt refroze in the gap between rod and shroud and broke away during dismantling of the shroud. The cross sections and micrographs are given in fig. 8-2 and fig. 8-3. The fuel rod simulator survived below 85 mm elevation. But the influence of interaction can be seen as low as 65 mm elevation. Fig. 8-A, fig. 8-B and fig. 8-C can only give values in the region, where the fuel rod simulator has survived.

4.10 Test ESSI-9

Test ESSI-9 was run with the same power input as test ESSI-6 (1.1°C/sec), but a 12.7 mm thick cylinder of insulation was used instead of the 100 mm insulation in the earlier test. The internal diameter of this insulation cylinder was 51 mm, compared to the inner free space inside insulation of 43 mm in square. The escalation of temperature started somewhat later but the initial temperature increase was the same in ESSI-9 as in ESSI-6 (fig. 25, KfK report 3557). In the following period of about 10 min with constant power input, however the temperature in ESSI-9 was about 200 degree lower, with a maximum value at 1900°C. This is due to the higher losses for the smaller insulation.

The posttest appearance of the fuel rod simulator ESSI-9 is given in fig. 9-1. Compared to the appearance of ESSI-6 less molten matrial has flown down on the outside of the rod. This is due to the lower maximum temperature. Also for ESSI-9 we find no remarkable breakaway of the oxide layer, though also here small pieces have broken away at the same elevation of 150 mm.

The cross sections and the micrographs are given in fig. 9-2 to fig. 9-4. One can recognize the refrozen melt inside the oxide layer. Above 200 mm elevation strong deformation of the cladding and attack on the pellets can be recognized.

The measured values of the oxide layer thickness are given in fig. 9-A. The values are in general lower than in test ESSI-6. The attack of the melt on the UO_2 ring pellet (fig. 9-B and fig. 9-C) is found to be higher, especial at the lower elevations between 150 mm and 200 mm. For ESSI-9 more of the molten zircaloy was kept inside the oxide layer.

4.11 Test ESSI-10

Test ESSI-10 was run again with the same power input as test ESSI-6 (1.1°C/sec), but in ESSI-10 the insulation was wrapped directly on the zircaloy flow shroud. The insulation thickness was only 6 mm. This insulation technique prevented significant heat losses by convection from the outside of the shroud. As consequence the escalation of the temperature started earlier (lower temperature about 1100 °C) and

reached a steeper gradient. The maximum temperature and the length of the temperature peak are smaller (fig. 23, KfK report 3557).

The posttest appearance is given in fig. 10-1. Compared to ESSI-6 a much larger region of the cladding has broken away. This is probablly due to the faster temperature increase, which resulted in a thinner oxide layer.

The cross sections and the micrographs are given in fig. 10-3 and fig. 10-4. At 115 mm only about 1/5 of the cladding is oxidized, with no melting at this elevation. For higher elevations molten material is refrozen inside the cladding. Here remarkable attack on the pellet and deformation of the cladding can be recognized.

The measured values of the oxide layer thickness are given in fig. 10-A. The thickness is smaller than in ESSI-6 due to the faster heat up and lower maximum temperature and time at temperature.

The attack on the UO_2 pellet is represented in 10-B and 10-C. There is more dissolution in ESSI-10 than in ESSI-6 especial at the elevations of above 250 mm.

Details of surface structure are given in fig. 10-5 and 10-6.

4.12 Test ESSI-11

Test ESSI-11 was heated up with the same power input of test ESSI-5 (0.8°C/s), but in the same way as in ESSI-10. The insulation of 6 mm thickness was wrapped directly on the shroud. Again in ESSI-11 the temperature escalation occured at a lower temperature (1100 °C) and with a steeper temperature gradient. The maximum temperature reached (1900 °C) which was nearly the same as in ESSI-10.

The posttest appearance of ESSI-11 is given in fig. 11-1. A large amount of molten material has flown out of the cladding and refrozen on the outside. In test ESSI-5 no molten material had flown to the outside. In contrary no oxide layer has broken away from the fuel rod during cooldown in test ESSI-11.

The cross sections and the micrographs are given in fig. 11-2 to fig. 11-4. A strong deformation of the oxidized cladding is found at the upper elevations.

The measured values of the oxidized layers are given in fig. 11-A. The values are lower than in test ESSI-5 in the lower and upper region of the rod with nearly the same thickness between 150 mm and 210 mm elevation.

The measurements on the behaviour of the UO_2 pellets are given in fig. 11-B and 11-C. Above 250 mm elevation we get a larger dissolution of the UO_2 by the molten zircaloy for ESSI-11 in comparison to ESSI-11.

5. Conclusions

The tests ESSI-1 to ESSI-11 were performed to investigate the temperature escalation of zircaloy clad PWR-fuel rods in steam and its consequences on the damage behaviour. In all tests uncontrolled temperature escalation due to the exothermal zircaloy/steam reaction is observed. The maximum cladding surface temperature measured was about 2200°C. The starting temperature of the escalation increases with decreasing initial heating rate. The test with different insulation geometry show that for higher heat losses the escalation again starts at a higher temperature. For fast heating rates, the run away of the molten zircaloy is the rate limiting process in the temperature escalation. For low heating rates, the formation of a thick protective ZrO_2 oxide layer limits the reaction energy.

For fast heatup rates, a large amount of the UO_2 pellet is dissolved by liquid Zircaloy. The ZrO_2 layer formed during heatup is quite flexible at high temperatures. Depending on the amount of steam available on the outside of this UO_2 shell, the oxide layer is partly dissolved by the metallic alloy for absence of steam or an $(U, Zr)O_2$ precipitate is formed on the inner surface for oxygen present by the steam on the outside.

For low heatup rates a thick protective oxide layer is formed. If the heatup rate is slow enough to oxide the whole thickness of the Zry-

cladding, than there is no remarkable chemical interaction between the oxidized cladding and the UO_2 pellet.

The results discussed show that there is quite a dependancy of the damage behaviour on the heatup rate. The slower heatup rates seems to produce the more favourable damage. The geometry of the fuel rods is kept to higher temperatures and the formation of lumps at high temperatures is reduced. Also the fragmentation of the rods embrittled by the strong oxidic during cooldown, produces a geometry which is much favourable for cooling, compared to a refrozen lump of molten material.

6. Acknowledgements

The authors would like to thank Dr. P. Hofmann (KfK, IMF I) and Dr. S. Wright (SNL, Albuquerque) for their thorough technical and editorial review of the manuscript, Mr. Brand for the picture taking, Mr. Seibert and Mr. Barth for the preparation of the microscopic pictures and Mrs. Ivanitsch for her careful typing of the manuscript.

7. References

1. A. Fiege, Severe Fuel Damage Investigations of KfK/PNS, KfK 3431B, 1983

2. S. Hagen et.al., CORA-Program, KfK 3677, 1986

3. P. Hofmann et.al.; Temperaturtransiente UO_2/Zircaloy-Reaktionsexperimente unter oxidierenden Bedingungen, PNS-Jahresbericht 1984, KfK 3550 (1985) p. 4200/76

4. P. Hofmann, H.J. Neitzel; Experimental and Theoretical Results of Cladding Oxidation Under Severe Fuel Damage Conditons. 7th Intern. Conf. on "Zirconium in the Nuclear Industry", 24-27 June 1985, Strasbourg, France

5. P. Hofmann, D.K. Kerwin-Peck; Chemical interaction of Zircaloy-4 with UO_2 above 1700°C under Nonoxidizing Conditions, Intern. Meeting on "LWR Severe Accident Evaluation", August 28 - September 1, 1983, Cambridge, Massachusetts, USA

6. P. Hofmann, et.al.; Chemische Auflösung von festem UO_2-Brennstoff durch geschmolzenes Zircaloy-Hüllmaterial, PNS Jahresbericht 1985, KfK 4000 (1986), p. 4200/56 - 4200/86

7. P. Hofmann, S. Hagen; Untersuchugen zu schweren Kernschäden, insbesondere die chemischen Wechselwirkungen zwischen Brennstoff und Hüllmaterial, KfK 4170 (1986) 251-319

8. W. Dienst, P. Hofmann, D.K. Kerwin-Peck; Chemical Interaction between UO_2 and Zircaloy-4 from 1000 to 2000°C, Nuclear Technology, Vol. 65 (1984) 109-124

9. P. Hofmann, H. Uetsuka; UO_2 Dissolution by Molten Zircaloy Cladding, to be published as KfK report

10. S. Leistikow, G. Schanz; The oxidation behavior of Zircaloy-4 in steam between 600 and 1600°C, Werkstoff und Korrosion 36, (1985), p. 105 - 116

11. S. Leistikow, G. Schanz, H. v. Berg; Kinetik und Morphologie der isothermen Dampf-Oxidation von Zircaloy-4 bei 700-1300°C, KfK 2587 (1978)

12. S. Leistikow, G. Schanz, H. v. Berg, A.E. Aly; Comprehensive Presentation of Extended Zircaloy-4/Steam Oxidation Results 600-1600°C, Proc. OECD-NEA-CSNI/IAEA Spec. Meeting on "Water Reactor Fuel Safety and Fission Product Release in Off-Normal and Accident Conditions", Riso (Denmark) May 16-20, 1983 IAEA-Summary Report IWGFPT/16 (1983) 188-199

13. G. Schanz, S. Leistikow; Microstructural Reasons for Mechanical Oxide Degradation (Breakaway Effect) and Resulting Kinetic Anomalies of Zircaloy-4/Steam-HT-Oxidation, Proc. 8th Intern. Congress Metallic Corrosion, Mainz, Sept. 6-11, 1981, Vol. II, 1712-1717

14. G. Schanz, S. Leistikow; ZrO_2-Scale Degradation during Zircaloy-4 High Temperature Steam Exposure, Microstructural Mechanisms and Consequences for PWR Safety Analysis, Proc. ANS/ENS Top. Meeting on "Reactor Safety Aspects of Fuel Behavior", August 2-6, 1981, Sun Valley; Idaho, USA, Vol. II, 342-353

15. G. Schanz, S. Leistikow; Zur konkurrierenden Sauerstoff- und Wasserstoffaufnahme des Zircaloy-4 bei hohen Temperaturen, Ber. DGM-Tagung "Gase in Metallen", Darmstadt, 28-30 März 1984, 413-426

16. S. Leistikow, G. Schanz, H. v. Berg; Untersuchungen zur temperatur-transienten Dampfoxidation von Zircaloy-4 Hüllrohrmaterial unter hypothetischen DWR-Kühlmittelverlust.Störfallbedingungen, KfK 2810 (1979)

17. S.Hagen et.al., Temperature Escalation in PWR Fuel Rod Simulators due to the Zircaloy/Steam Reaction: Tests ESSI 1-3, Test Results Report, KfK 3507, 1983

18. S.Hagen et.al. Temperature Escalation in PWR Fuel Rod Simulators due to the Zircaloy/Steam Reaction: Tests ESSI 4-11, Test Results Report, KfK 3557, 1984

19. S.Hagen, Out-of-pile Experiments on the High Temperature Behaviour of Zry-4 Clad Fuel Rods, KfK 3567, 1983

20. S. Hagen et.al., Temperature Escalation in PWR Fuel Rod Bundles due to the Zircaloy/Steam Reaction: Bundle Test ESBU-1, Test Results Report, KfK 3508, 1983

21. S. Hagen et.al., Temperature Escalation in PWR Fuel Rod Bundles due to the Zircaloy/Steam Reaction: Bundle Test ESBU-2A, Test Results Report,KfK 3509, 1984

22. S. Hagen et.al.; Post Test Investigations for Bundle Test ESBU-1, KfK 3769, 1986

23. S. Hagen et.al.; Post Test Investigations for Bundle Test ESBU-2A, KfK 3789, 1986

Table 1: TEST ASSEMBLY DESIGN CHARACTERISTICS

Parameter	Value
Fuel Rod Simulator	
Length 1-3	250 mm
Length 4-11	370 mm
Tungsten Heater O.D.	6.0 mm
Fuel Material	Annular UO2-pellets
Pellet I.D.	6.1 mm
Pellet O.D.	9.2 mm
Cladding Material	Zircaloy-4
Cladding I.D.	9.29 mm
Cladding O.D.	10.75 mm
Shroud	
Material	Zircaloy-4
Shroud I.D.	26.5 mm
Wall Thickness 1-3	0.5 mm
Wall Thickness 4-8	1.0 mm
Insulator	
ZrO2 Thickness 1-8	25.4 mm
Al2O3/SiO2 Thickness 1-8	76.2 mm
ZrO2 Thickness Test 9	12.7 mm
ZrO2 Thickness Test 10-11	6.35 mm

Table 2: Test Conditions for Tests ESSI-1 to ESSI-11

Test	Initial Heatup Rate (°C/s)	Steam Flow (g/min)	Insulation Thickness (mm)	Flow Shroud/ Insulation Gap	Peak Temperature (°C)
ESSI-1	in Argon	35	100	yes	2200
ESSI-2	2.0	23	100	yes	2100
ESSI-3	0.5	17	100	yes	----
ESSI-4	0.3	21	100	yes	2050
ESSI-4A,5	0.5	20	100	yes	1970
ESSI-5	0.8	20	100	yes	1900
ESSI-6	1.1	20	100	yes	2100
ESSI-7	2.3	22	100	yes	1925
ESSI-8	3.6	25	100	yes	1970
ESSI-9	E-6	25	12.5	yes	1950
ESSI-10	E-6	25	6.2	no	2025
ESSI-11	E-5	25	6.2	no	1900

List of Figures

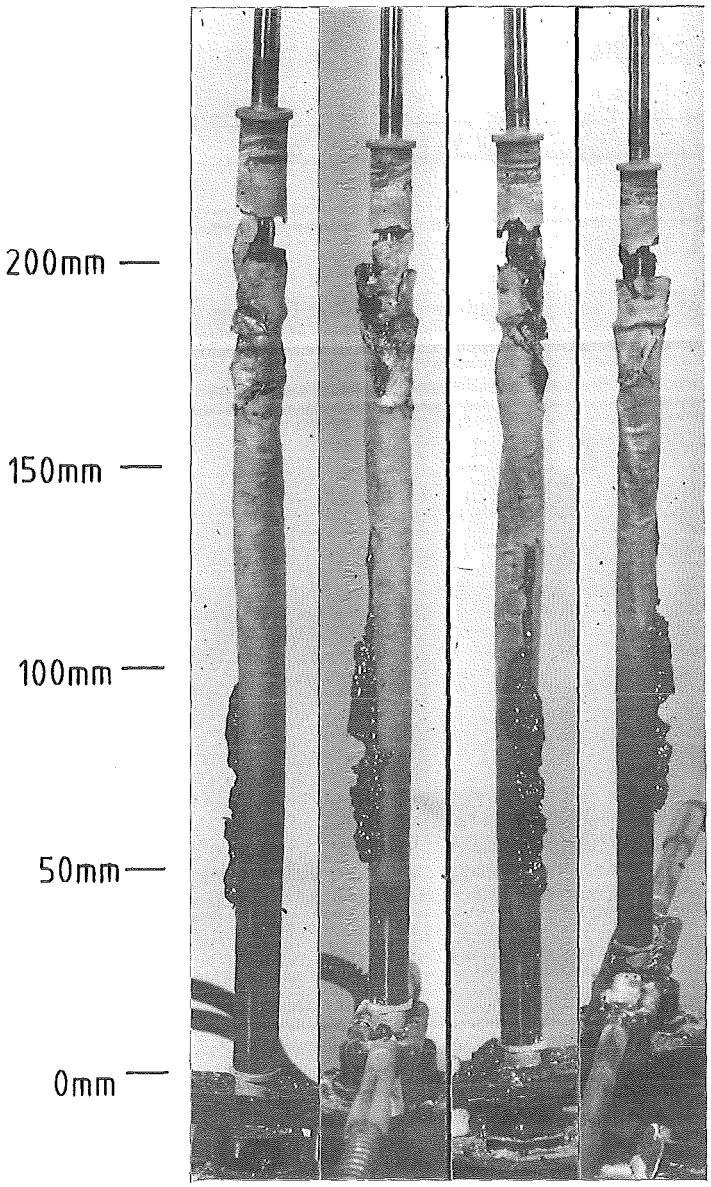

FIG. 1-1: POSTTEST APPEARANCE OF THE FUEL ROD SIMULATOR AND SCALE OF THE CROSS SECTION ELEVATIONS FOR ESSI-1

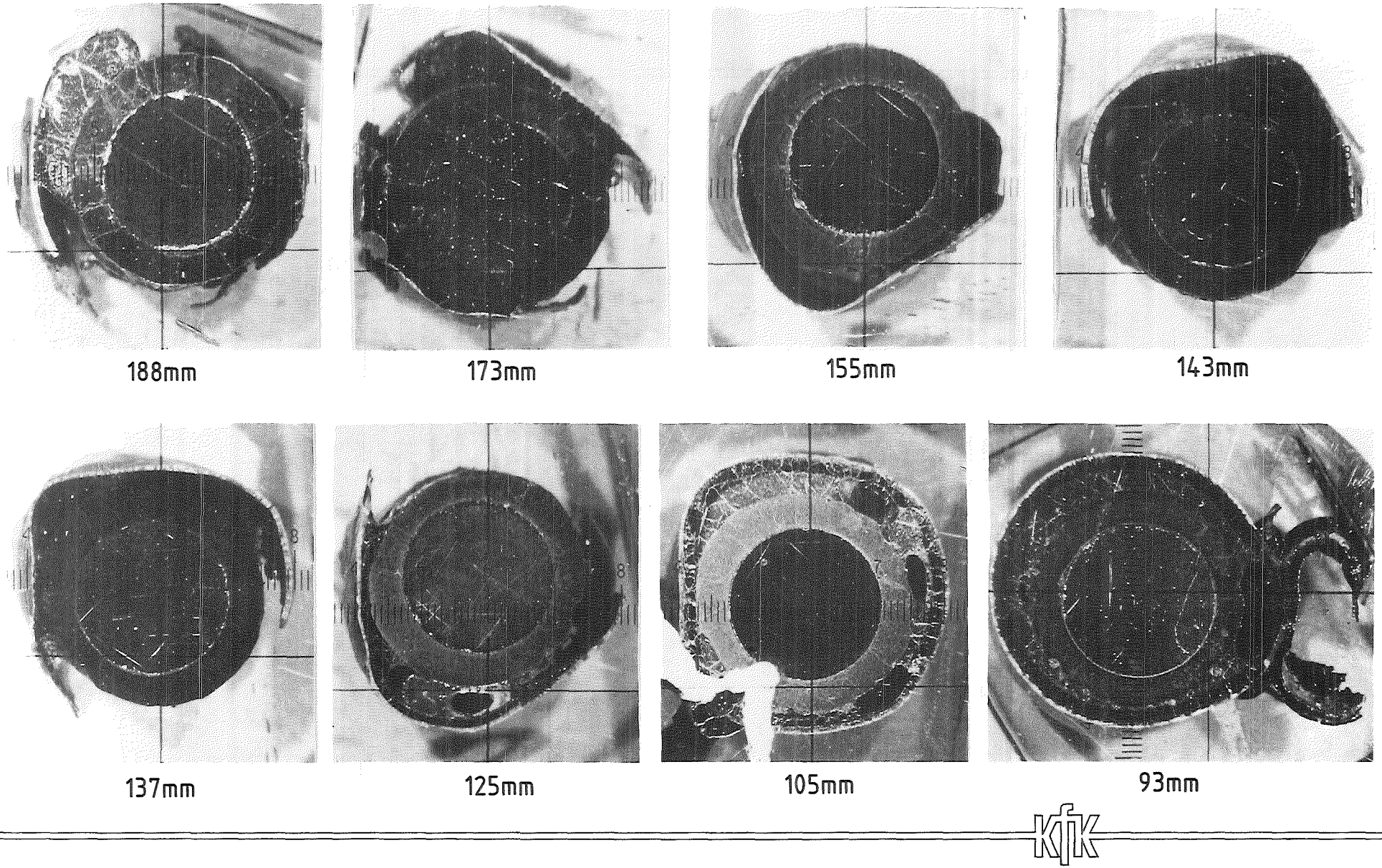

Fig.1-2: Cross Sections of Test ESSI-1

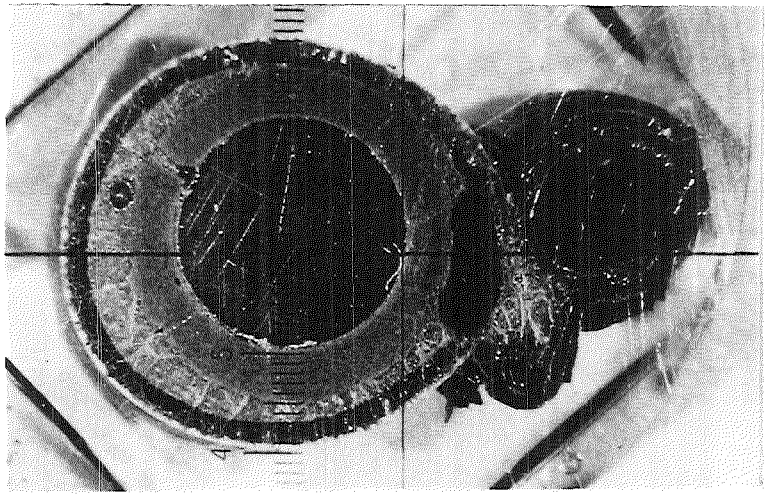

87mm

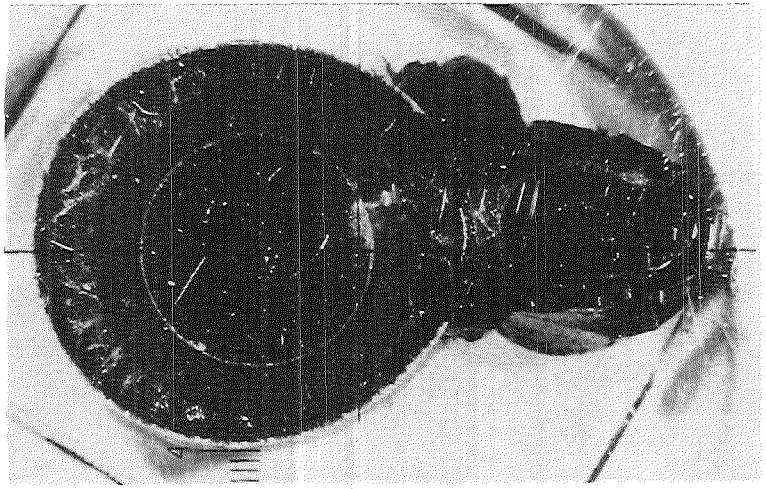

75mm

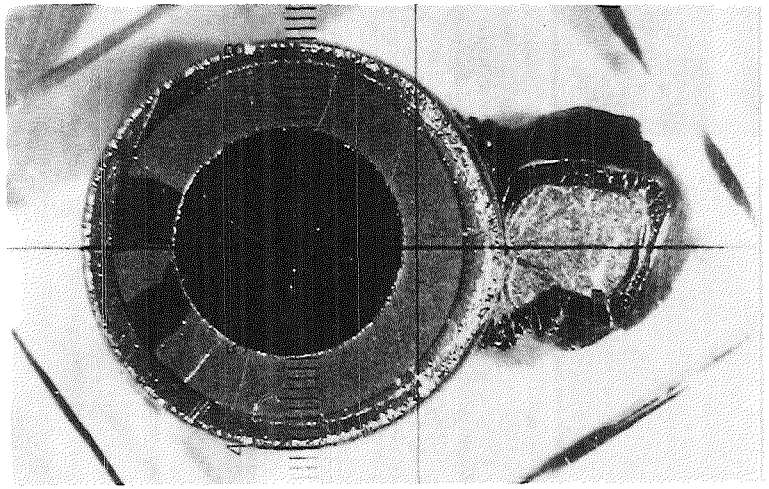

50mm

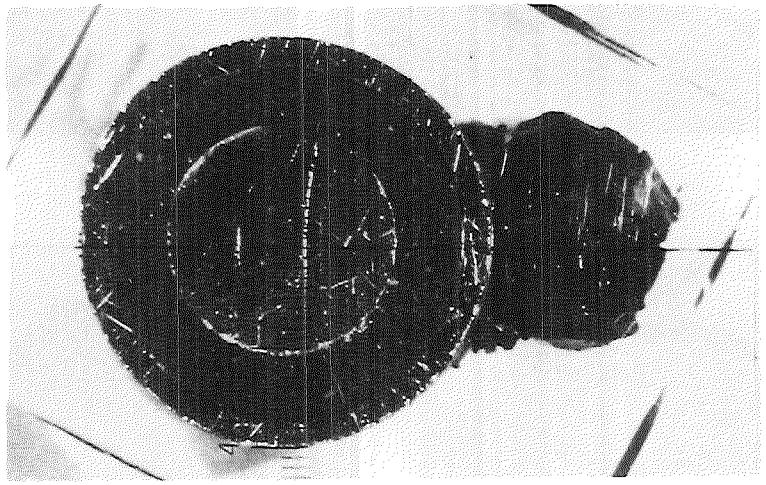

35mm

KfK

Fig.1-3: Cross Sections of Test ESSI-1

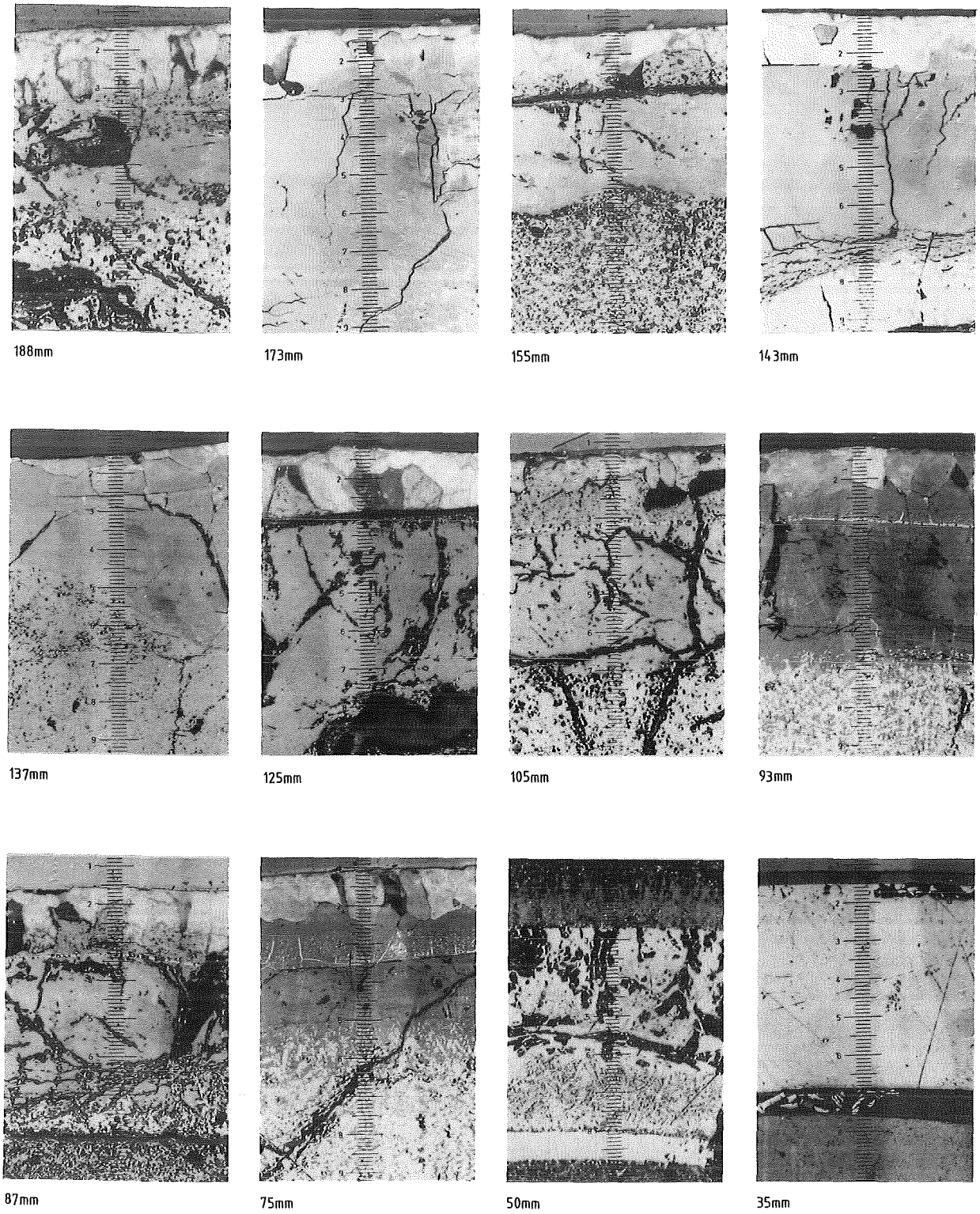

Fig. 1-4: Enlarged View (100x) of Cross Sections From ESSI-1

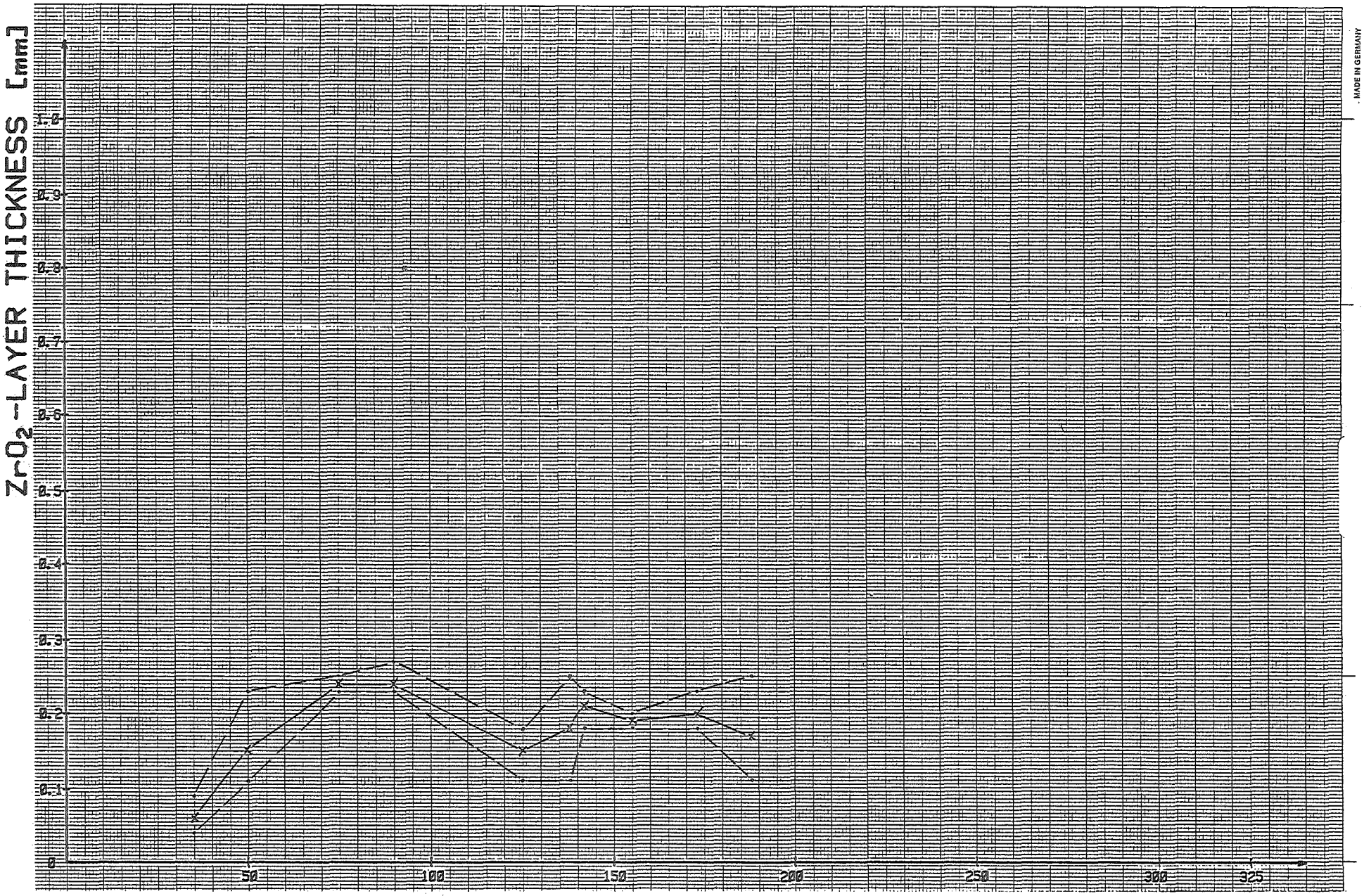

Fig. 1-A: Zirconoxid layer thickness for test ESSI-1 (– – – maximum or minimum value; —— mean value)

Fig. 1-B : Uranium oxide layer thickness for test ESSI-1 (---maximum or minimum value;——mean value)

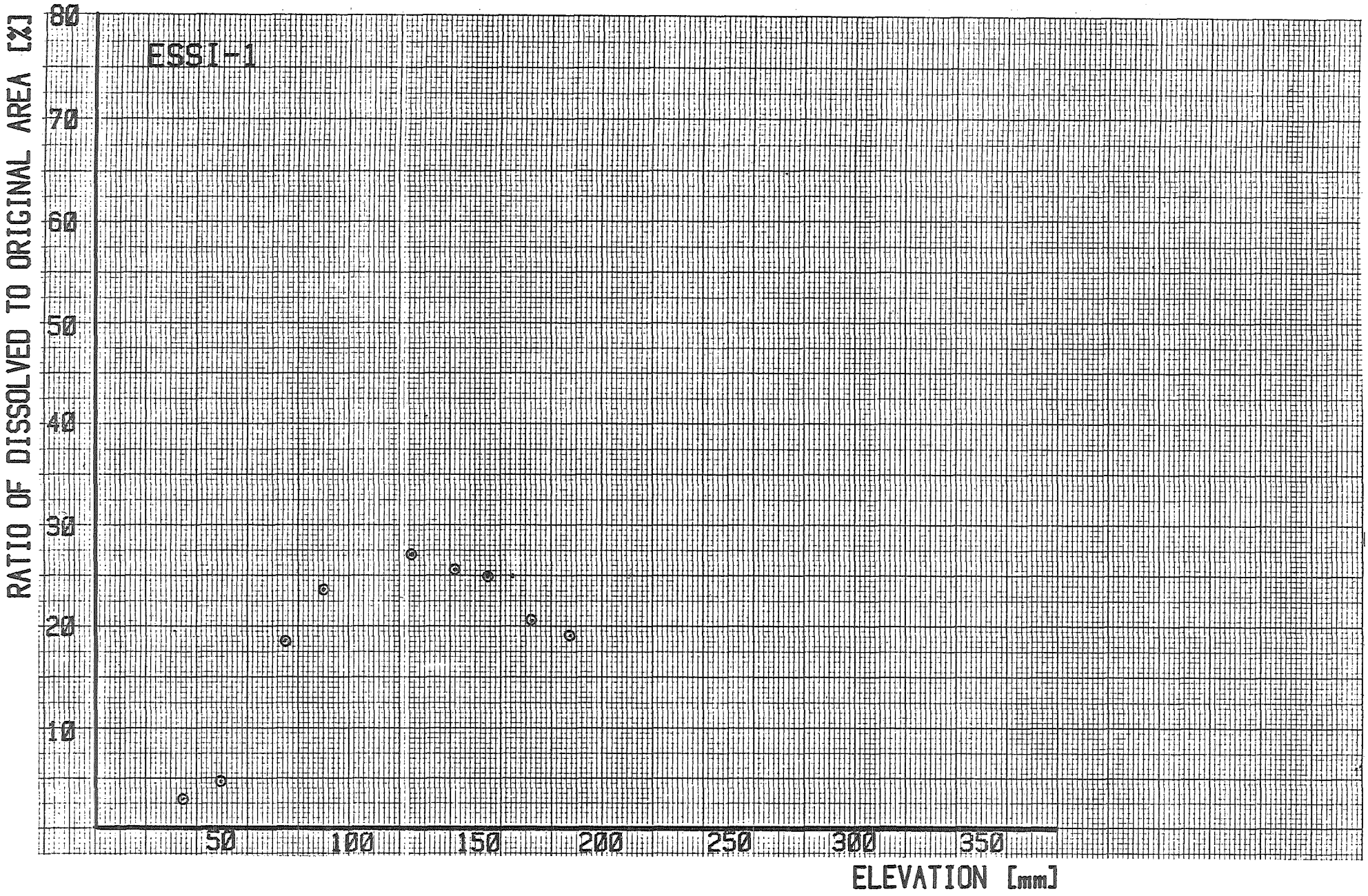

Fig.: 1-C
Dissolution of the UO_2-pellet at different elevations (ESSI-1)

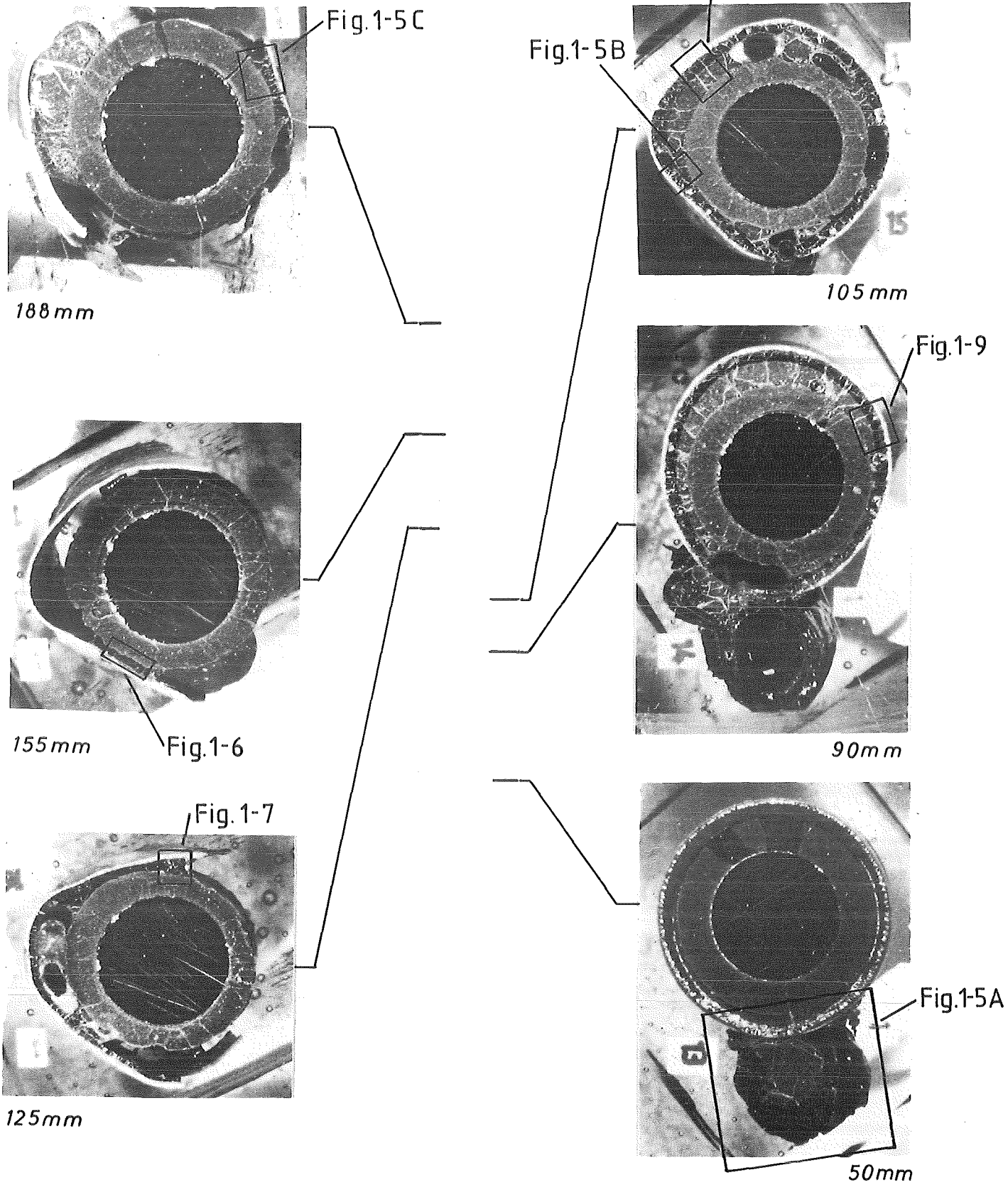

FIG.1-5: LOCATIONS OF ENLARGED VIEWS FROM CROSS SECTIONS OF THE FUEL ROD SIMULATOR ESSI-1 GIVEN IN THE FOLLOWING FIGURES

100x 1

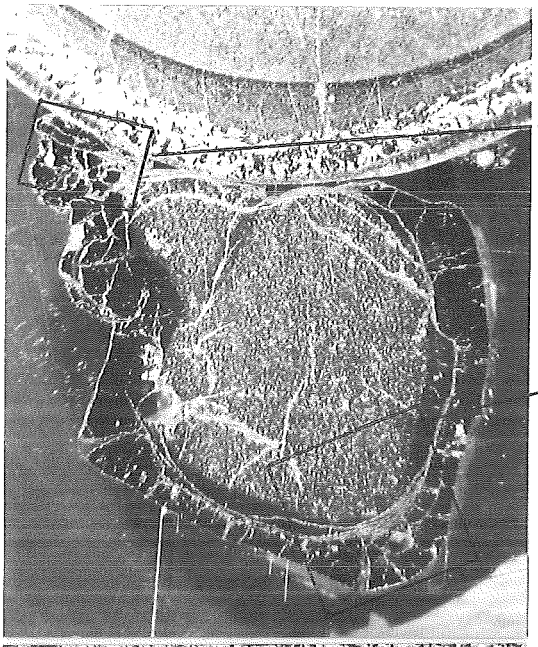

12x 4

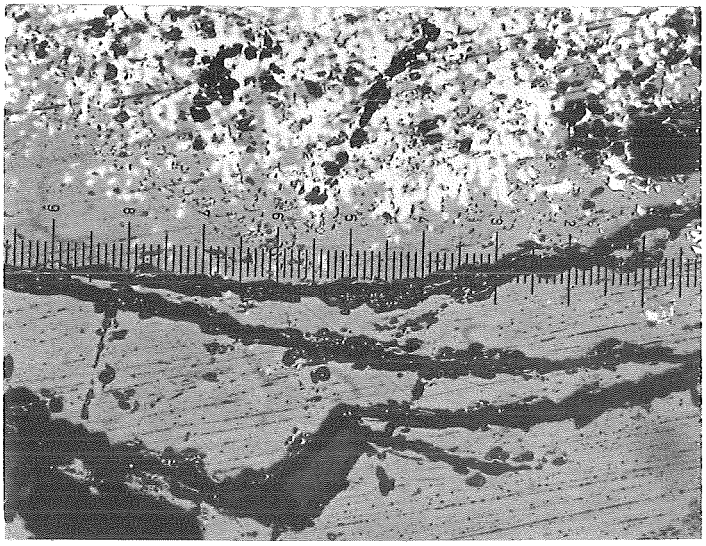

200x 3

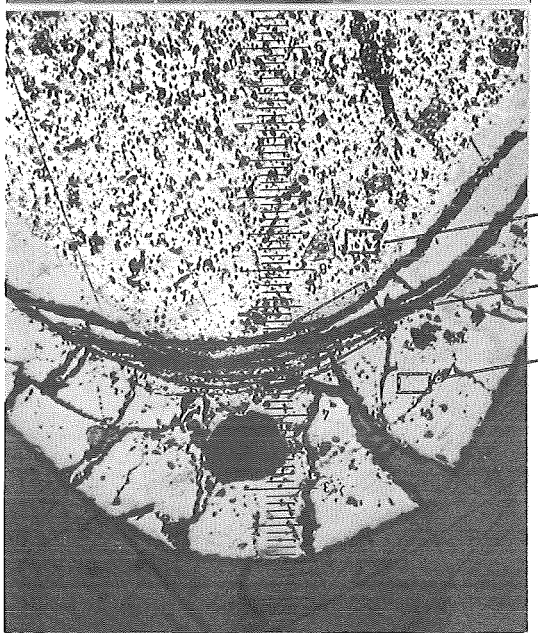

50x

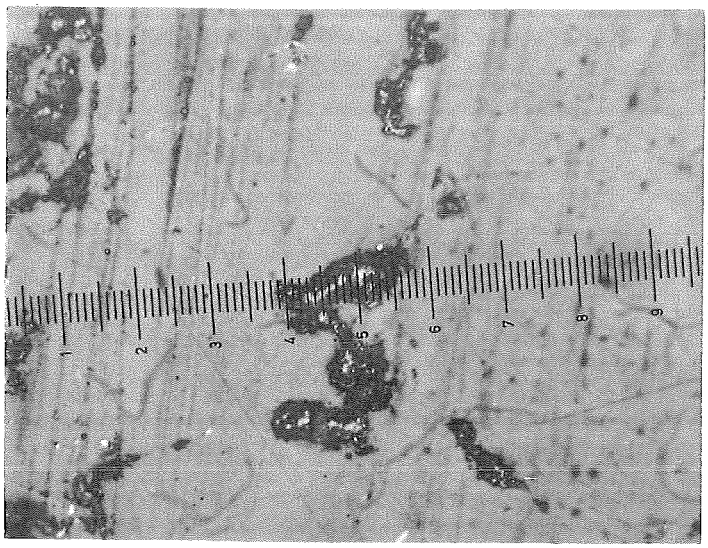

1000x 5

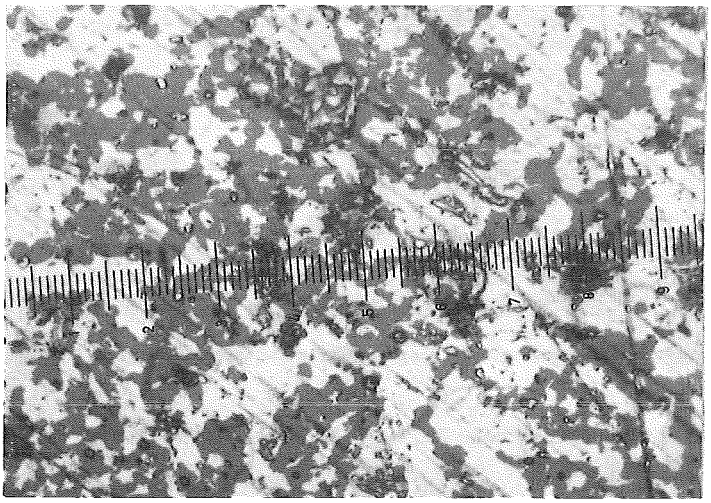

1000x 6

FIG.1-5A: DETAILS OF THE CROSS SECTION AT THE 50 MM ELEVATION OF ESSI-1 IN THE REGION OF REFROZEN MATERIAL

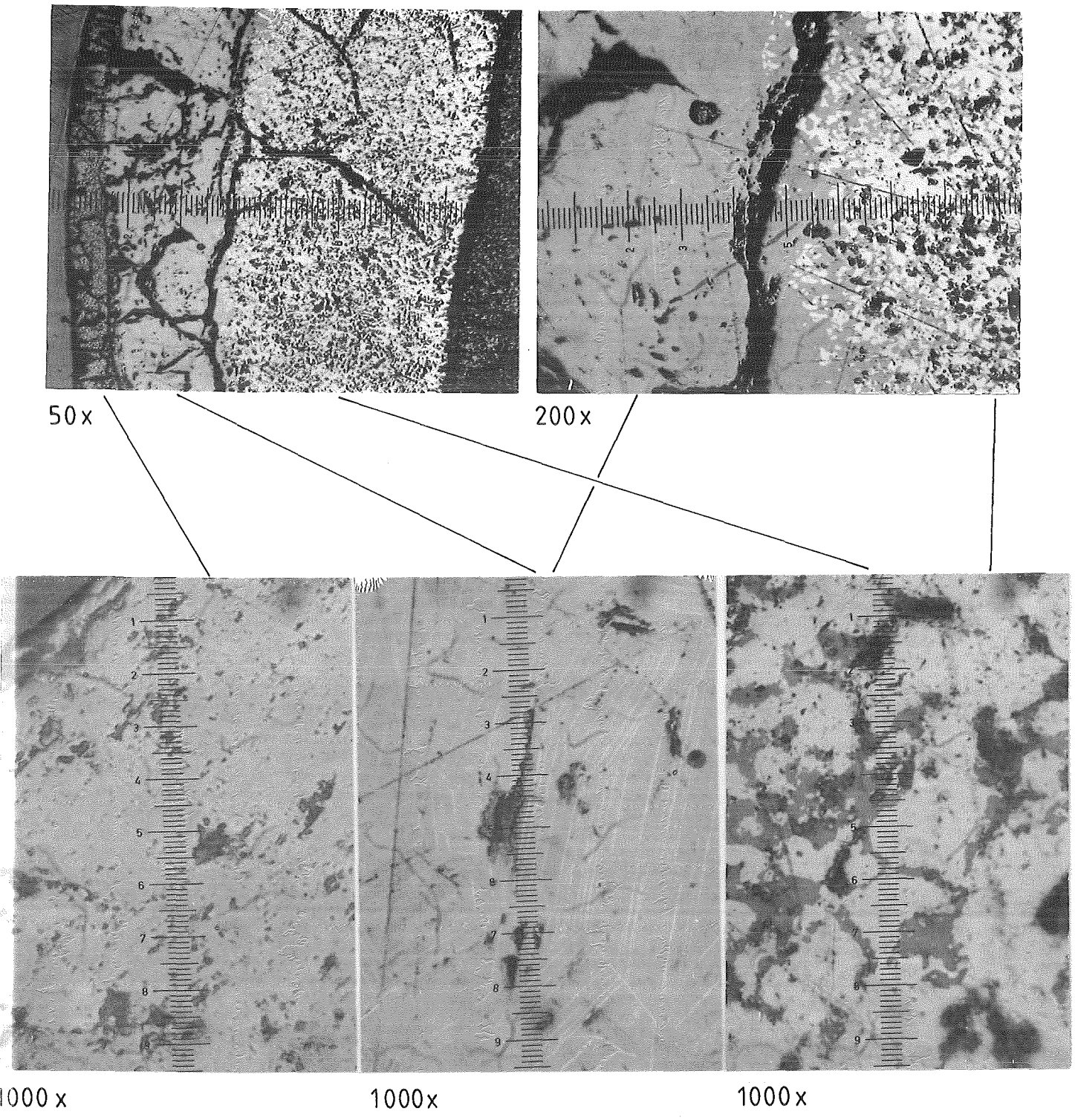

FIG.1-5B: DETAILS OF THE CROSS SECTION AT THE 105 MM ELEVATION OF ESSI-1 IN THE REGION OF FORMER CLADDING

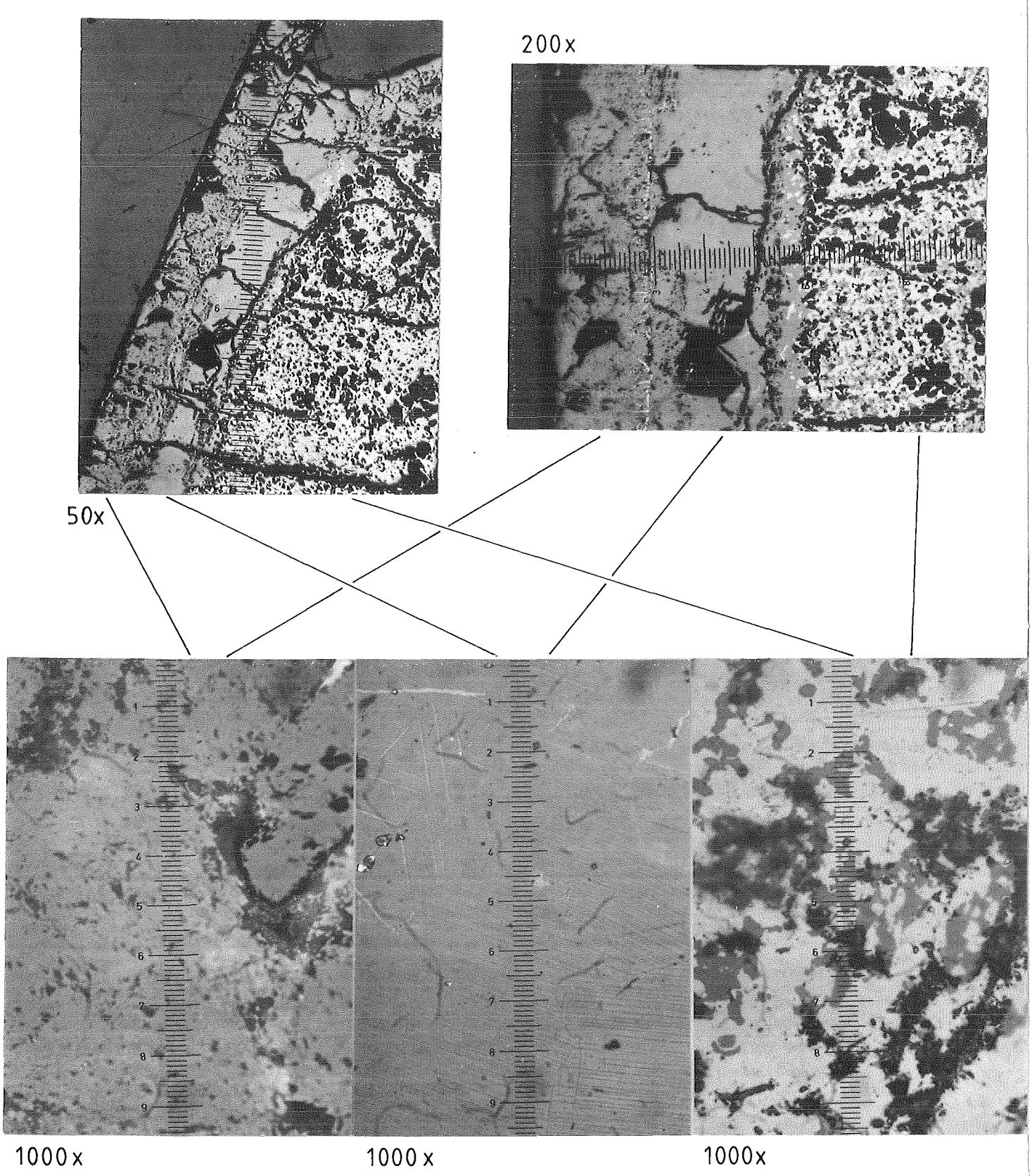

FIG.1-5C: DETAILS OF THE CROSS SECTION AT THE 188 MM ELEVATION OF ESSI-1 IN THE REGION OF FORMER CLADDING

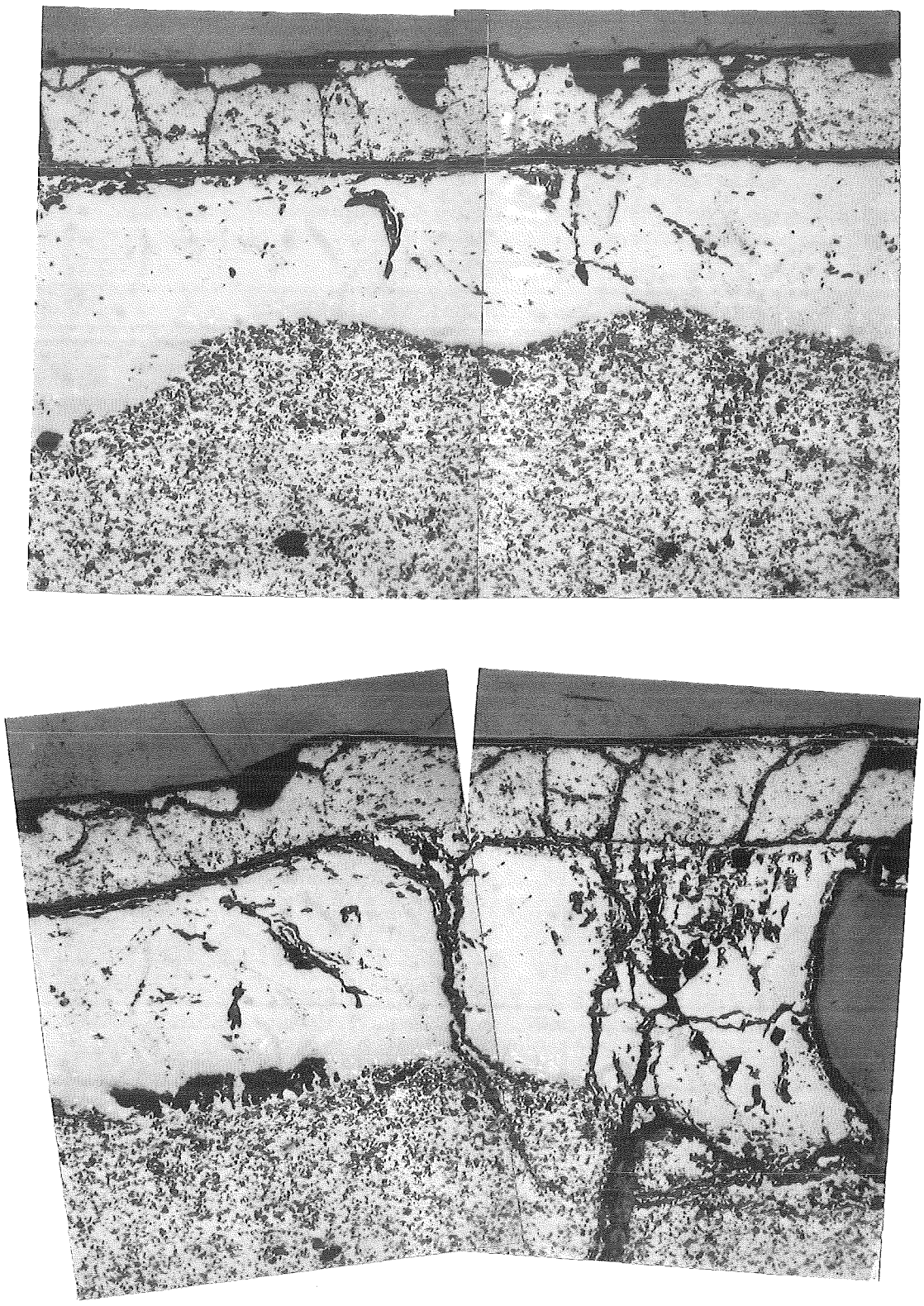

100x

FIG.1-6: ENLARGED VIEW OF A REGION OF FORMER CLADDING FROM THE CROSS SECTION AT THE 155 MM ELEVATION ESSI-1 (FIG.1-5)

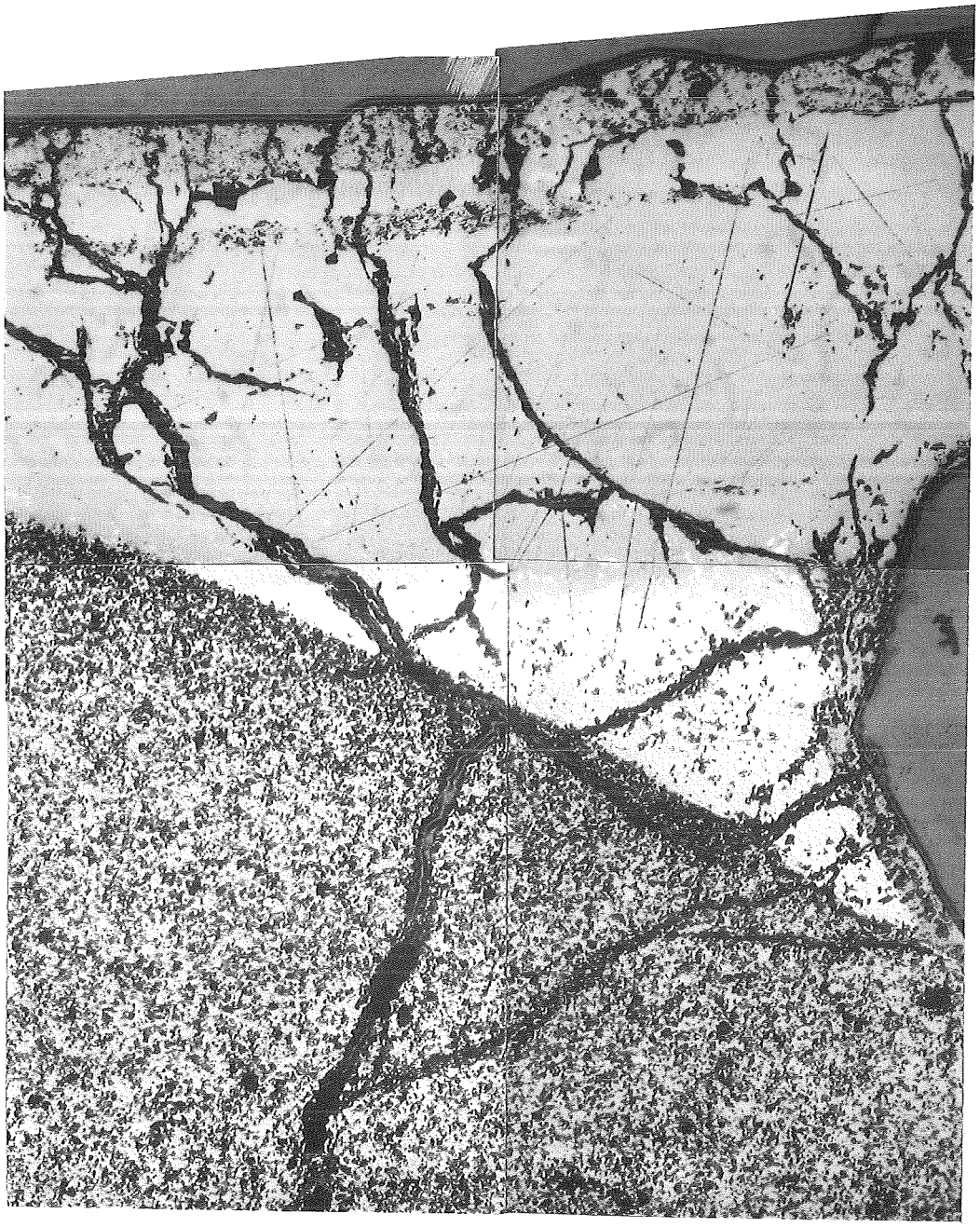

100 x

FIG.1-7: ENLARGED VIEW OF A REGION OF FORMER CLADDING FROM THE CROSS SECTION AT THE 125 MM ELEVATION ESSI-1 (FIG.1-5)

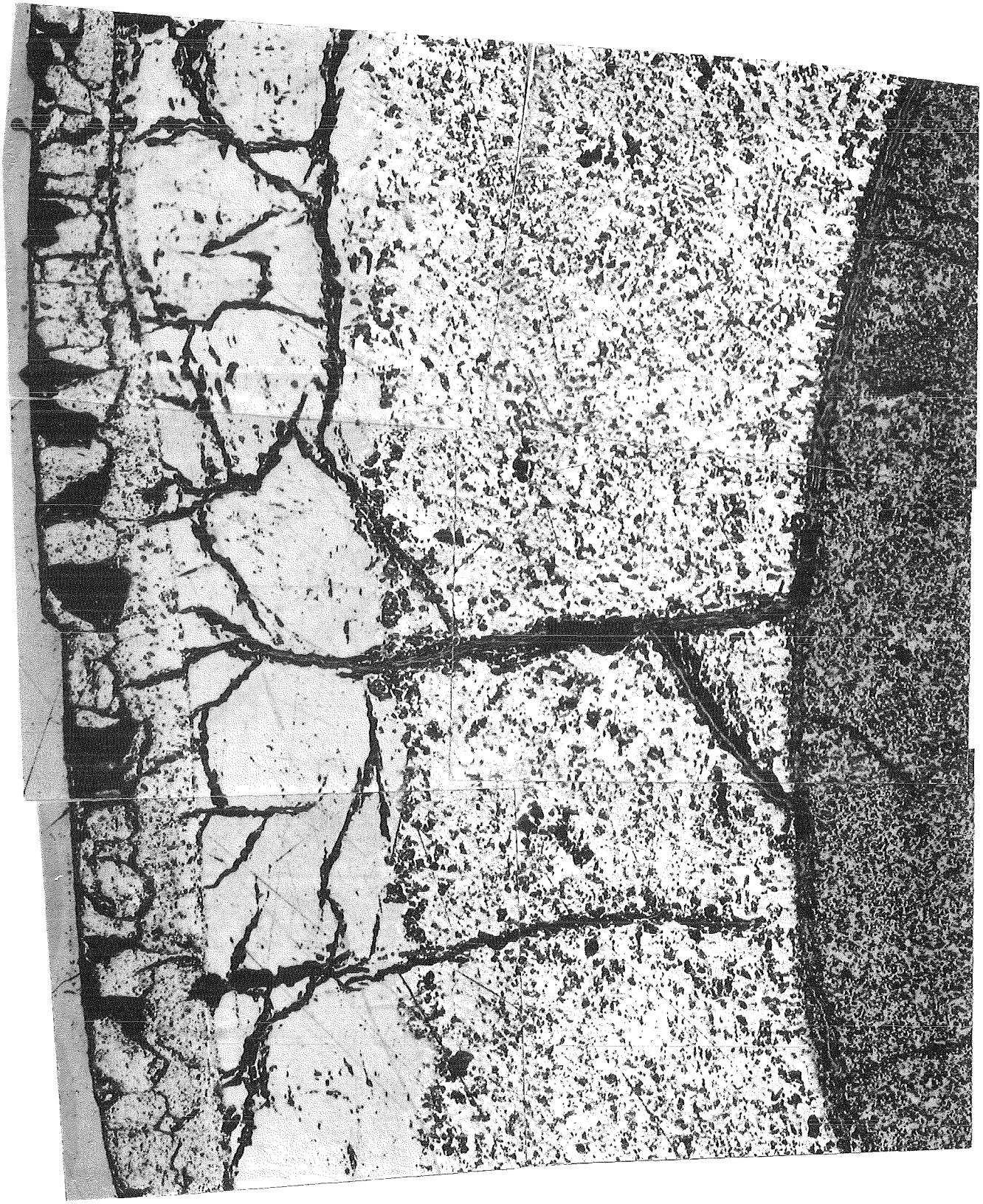

100 x

FIG.1-8: ENLARGED VIEW OF A REGION OF FORMER CLADDING FROM THE CROSS SECTION AT THE 105 MM ELEVATION ESSI-1 (FIG.1-5)

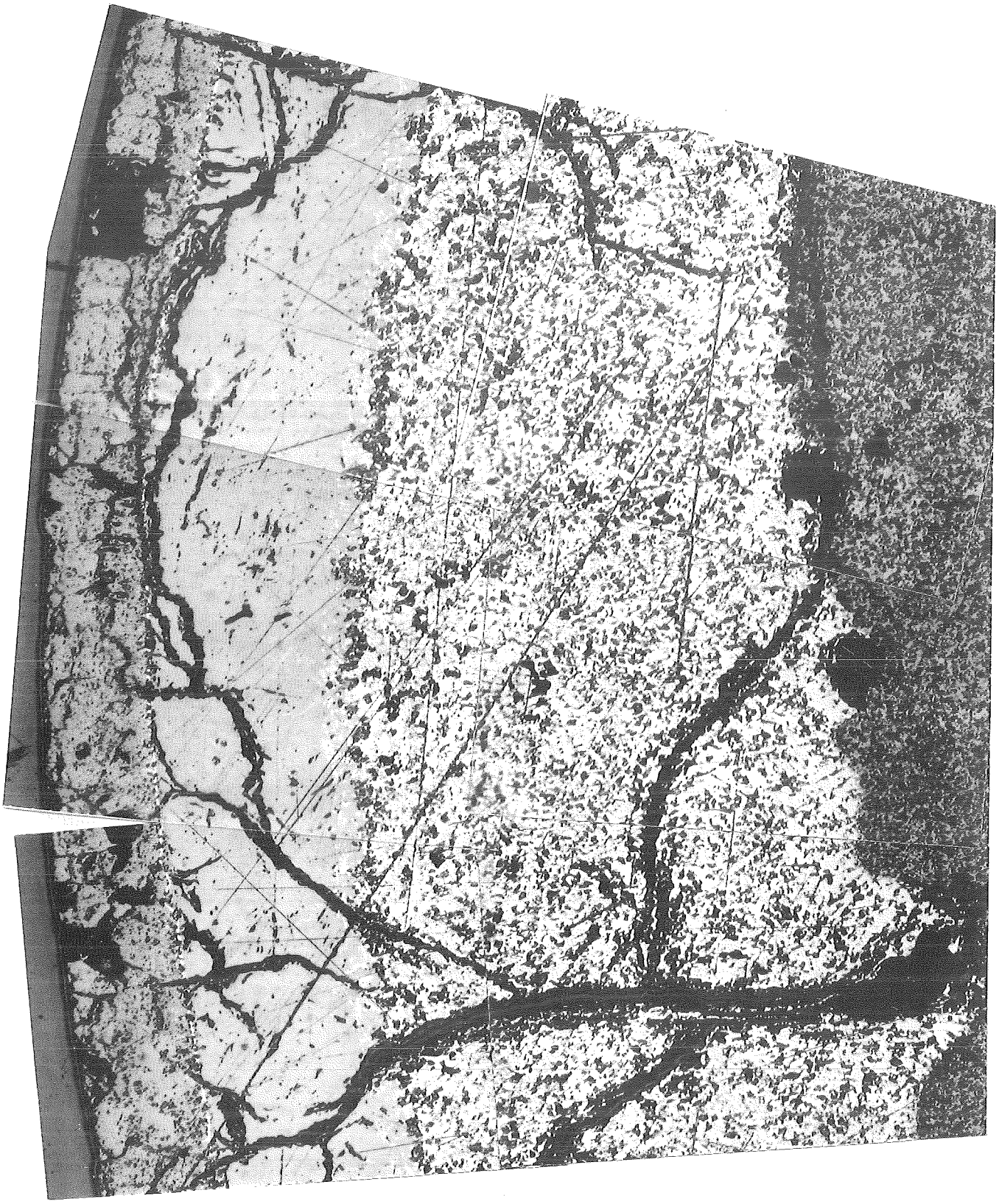

100x

FIG.1-9: ENLARGED VIEW OF A REGION OF FORMER CLADDING FROM THE CROSS SECTION AT THE 90 MM ELEVATION ESSI-1 (FIG.1-5)

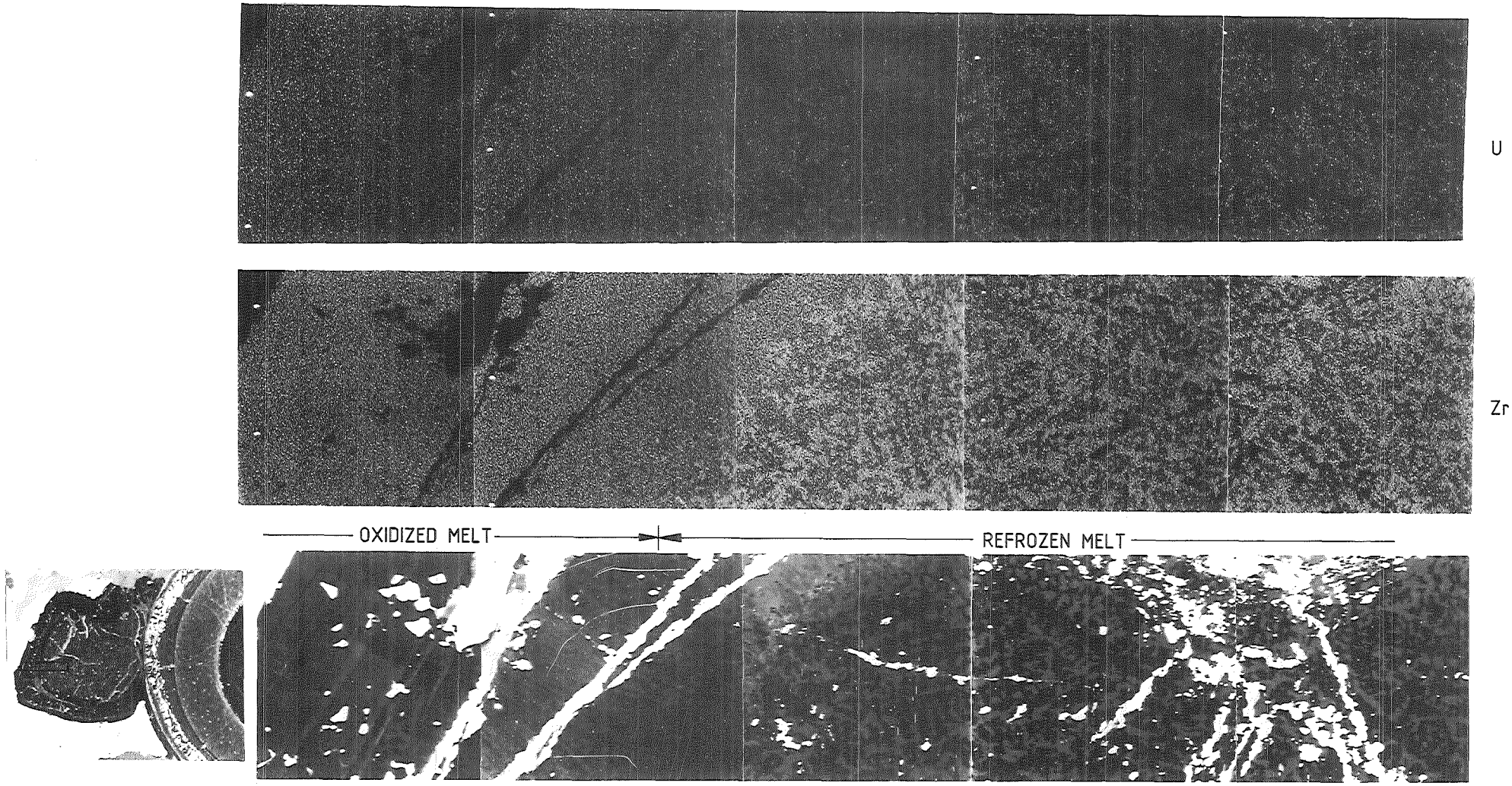

FIG.1-10: SCANNING ELECTRON MICROSCOPE PICTURE FROM THE OUTER REGION OF THE REFROZEN MELT AND THE ELEMENT DISTRIBUTIONS FOR ZR AND U (CROSS SECTION AT 50 MM FOR ESSI-1)

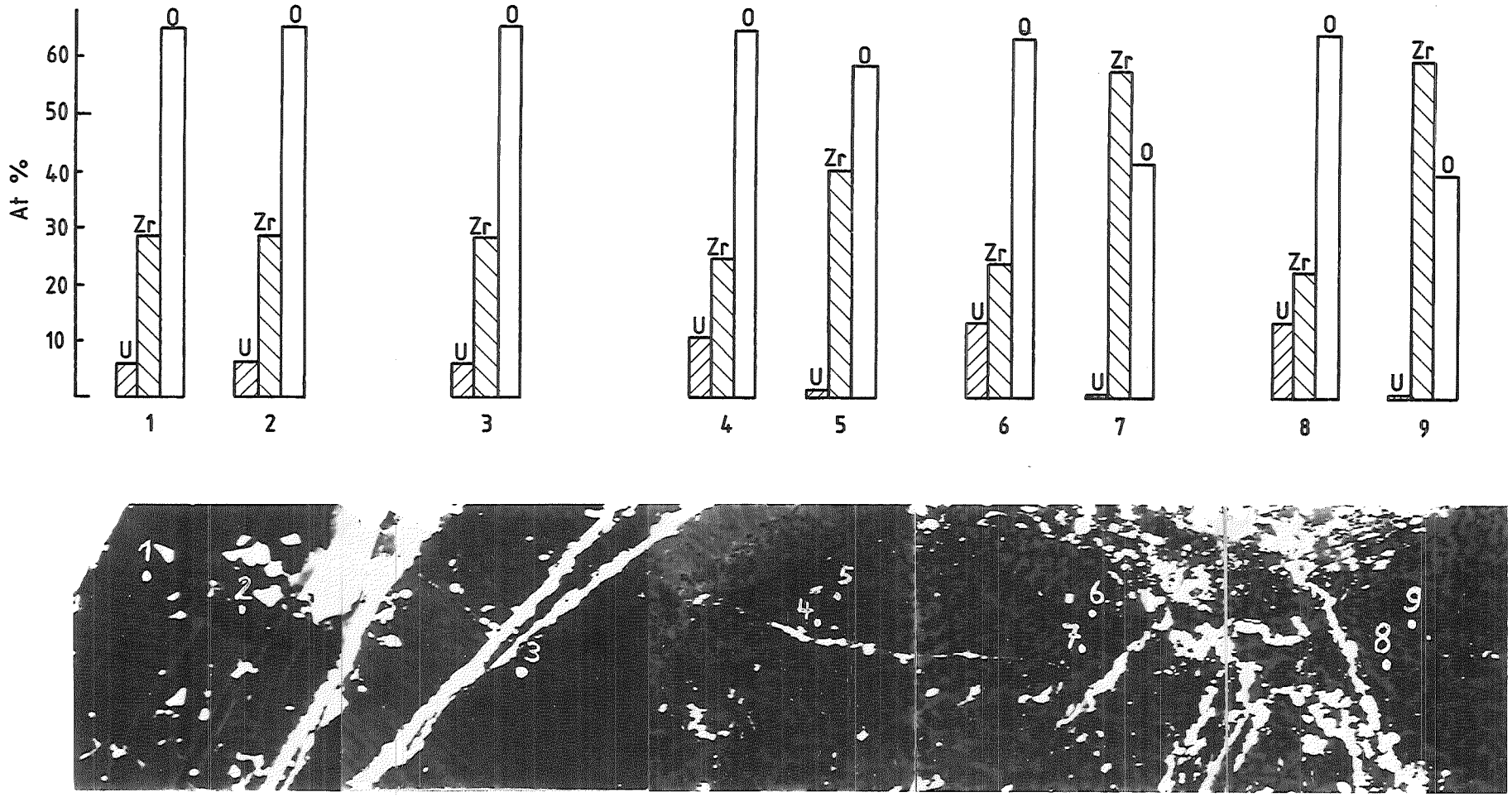

FIG.1-11: SCANNING ELECTRON MICROSCOPE PICTURE FROM THE OUTER REGION OF THE REFROZEN MELT AND THE MICROPROBE RESULTS AT THE MARKED POSITIONS (CROSS SECTION AT 50 MM FOR ESSI-1)

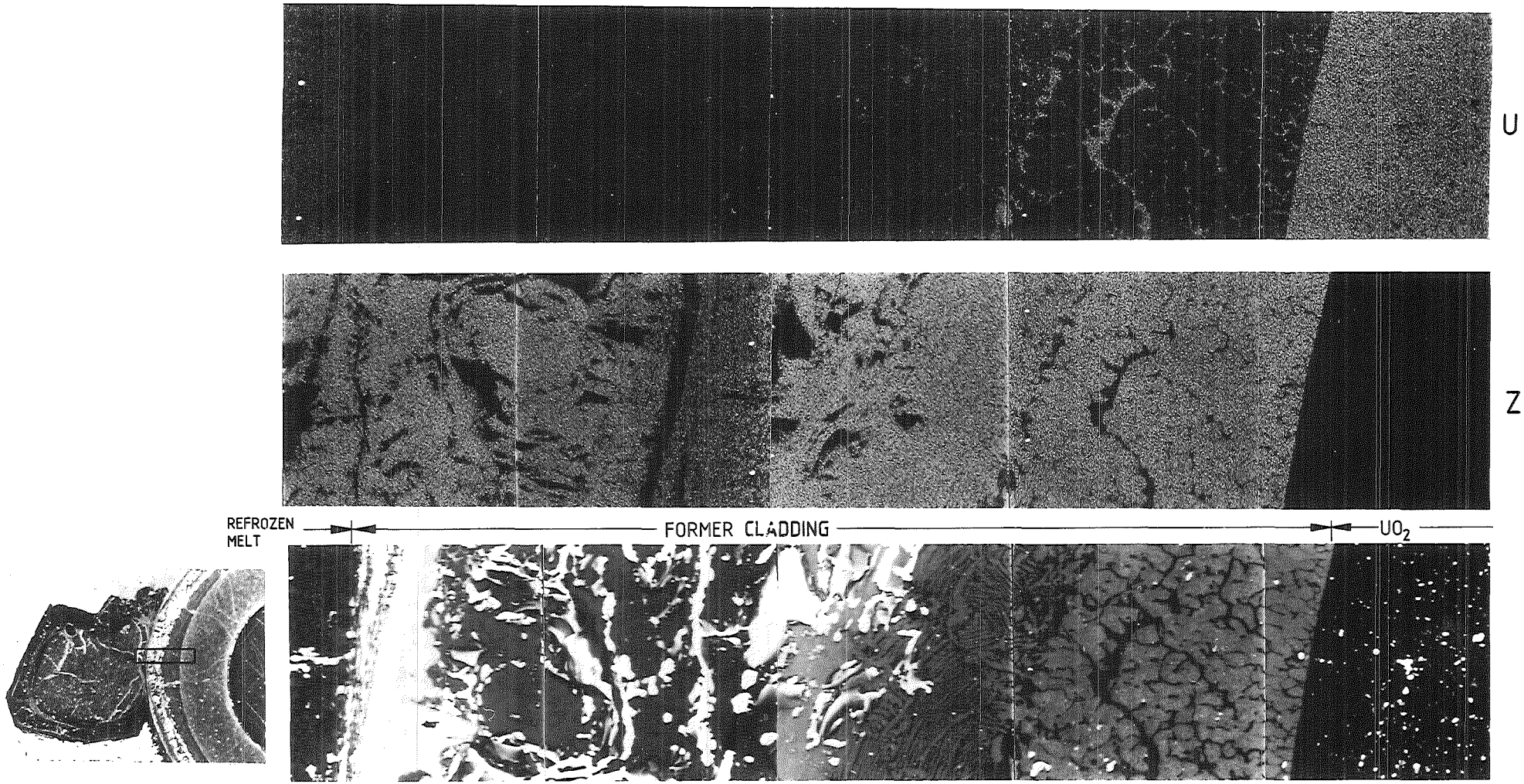

FIG.1-12: SCANNING ELECTRON MICROSCOPE PICTURE FROM THE FORMER CLADDING REGION AND ELEMENT DISTRIBUTIONS FOR ZR AND U (CROSS SECTION AT 50 MM FOR ESSI-1)

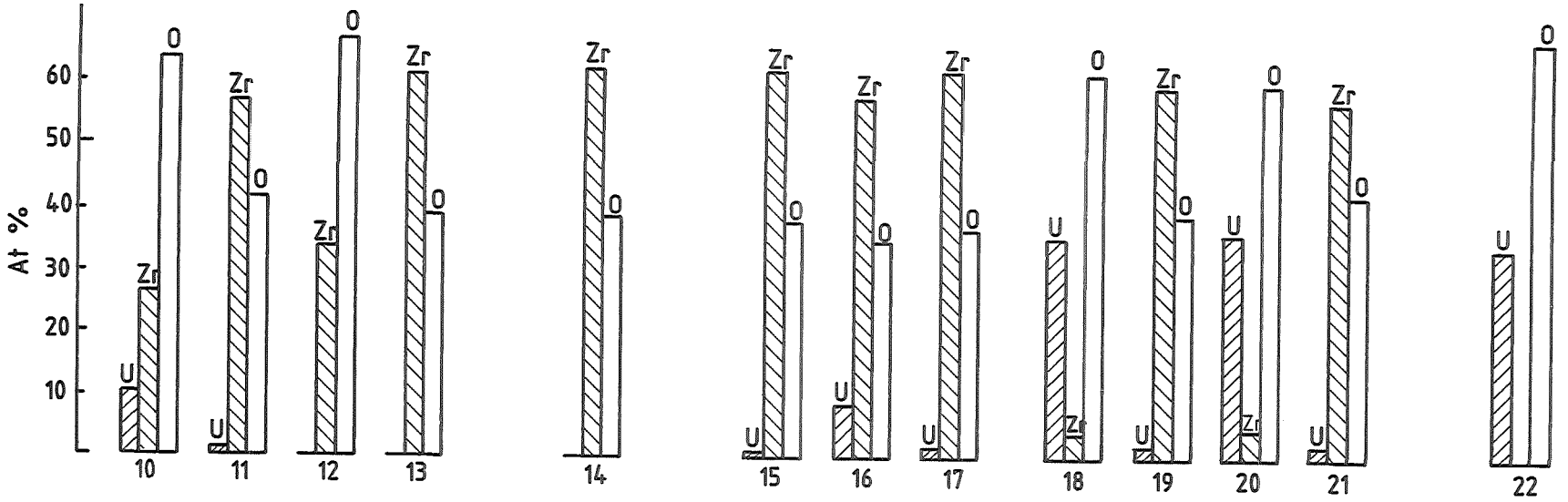

FIG.1-13: SCANNING ELECTRON MICROSCOPE PICTURE FROM THE FORMER CLADDING REGION AND THE MICROPROBE RESULTS AT THE MARKED POSITIONS (CROSS SECTION AT 50 MM FOR ESSI-1)

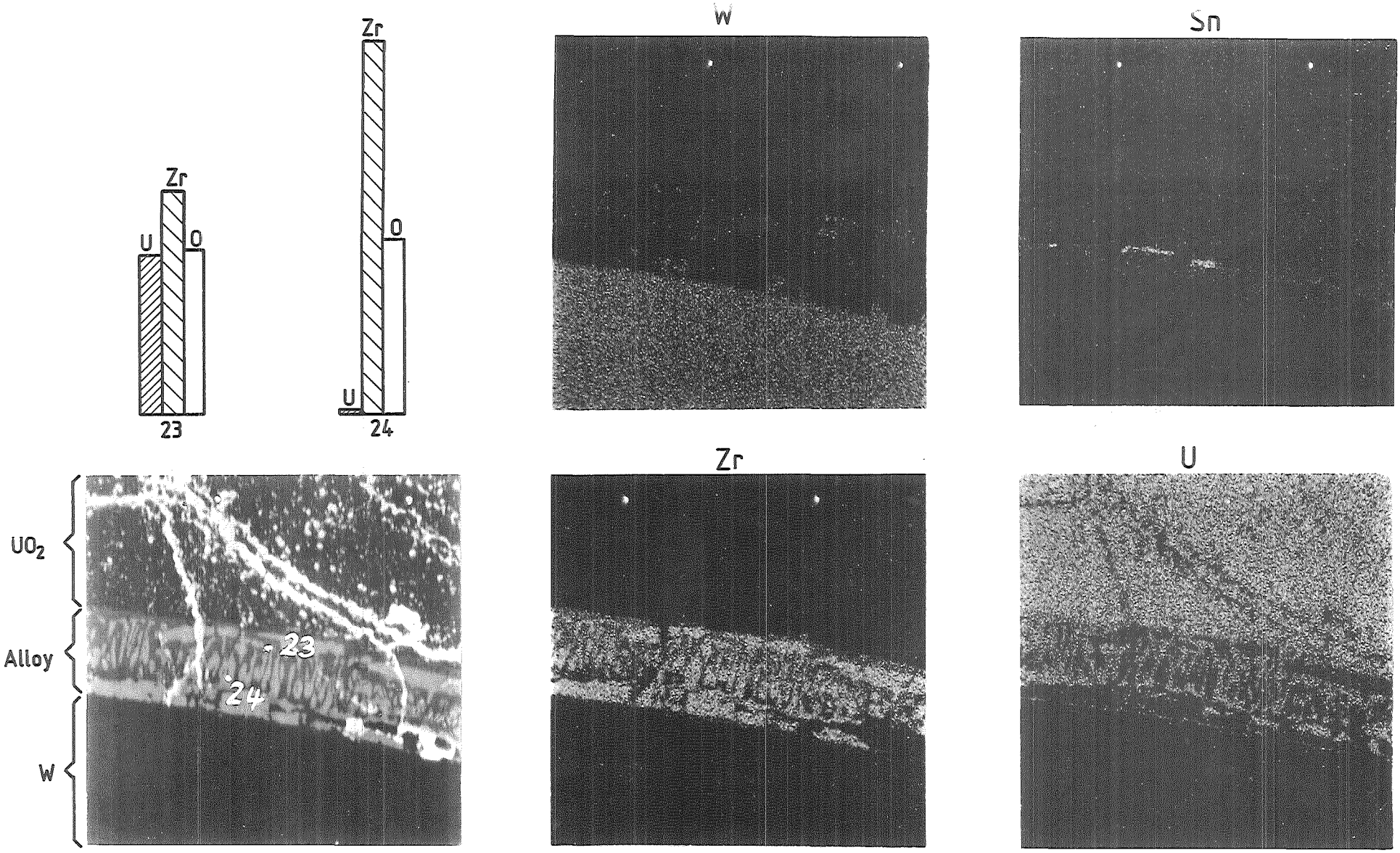

FIG.1-14: MICROPROBE INVESTIGATION OF THE FORMER GAP BETWEEN TUNGSTEN HEATER AND UO2-PELLET IN THE CROSS SECTION AT 50 MM FOR ESSI-1

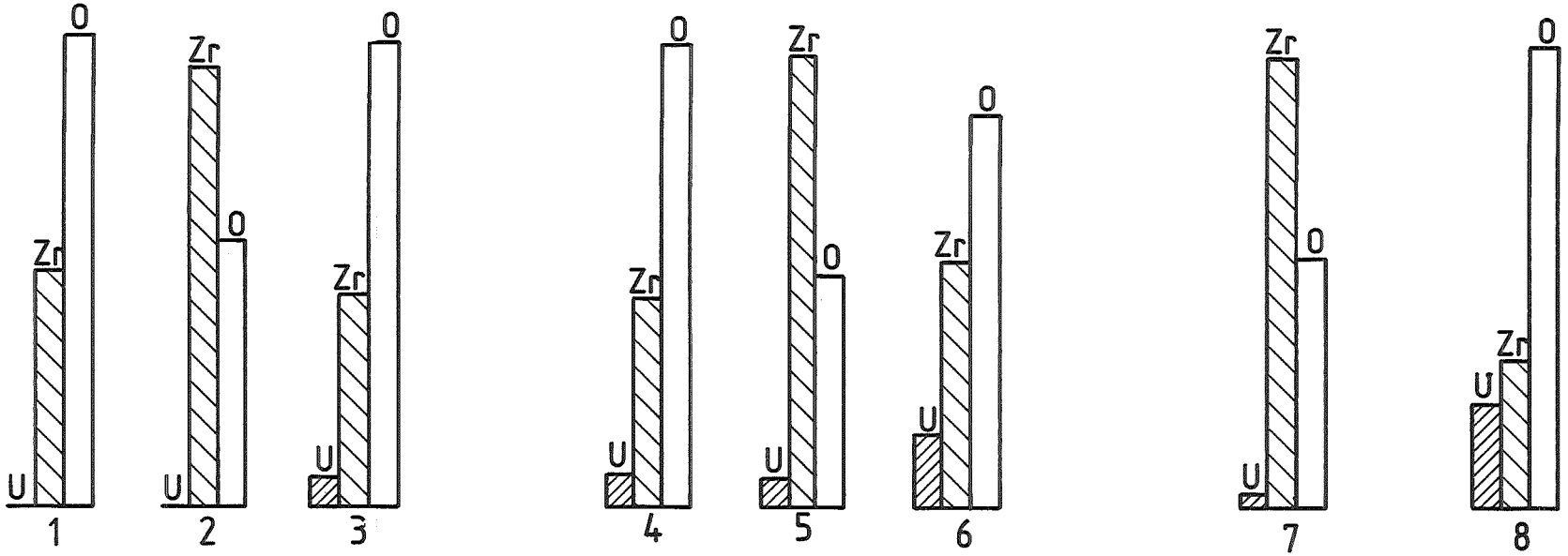

HAGEN ET AL. KFK-REPORT 3768

PNS KfK IT

FIG.1-15: MICROPROBE INVESTIGATION AT DIFFERENT LOCATIONS (SEE FIG.1-16) OF THE CROSS SECTION AT 188 MM FOR ESSI-1

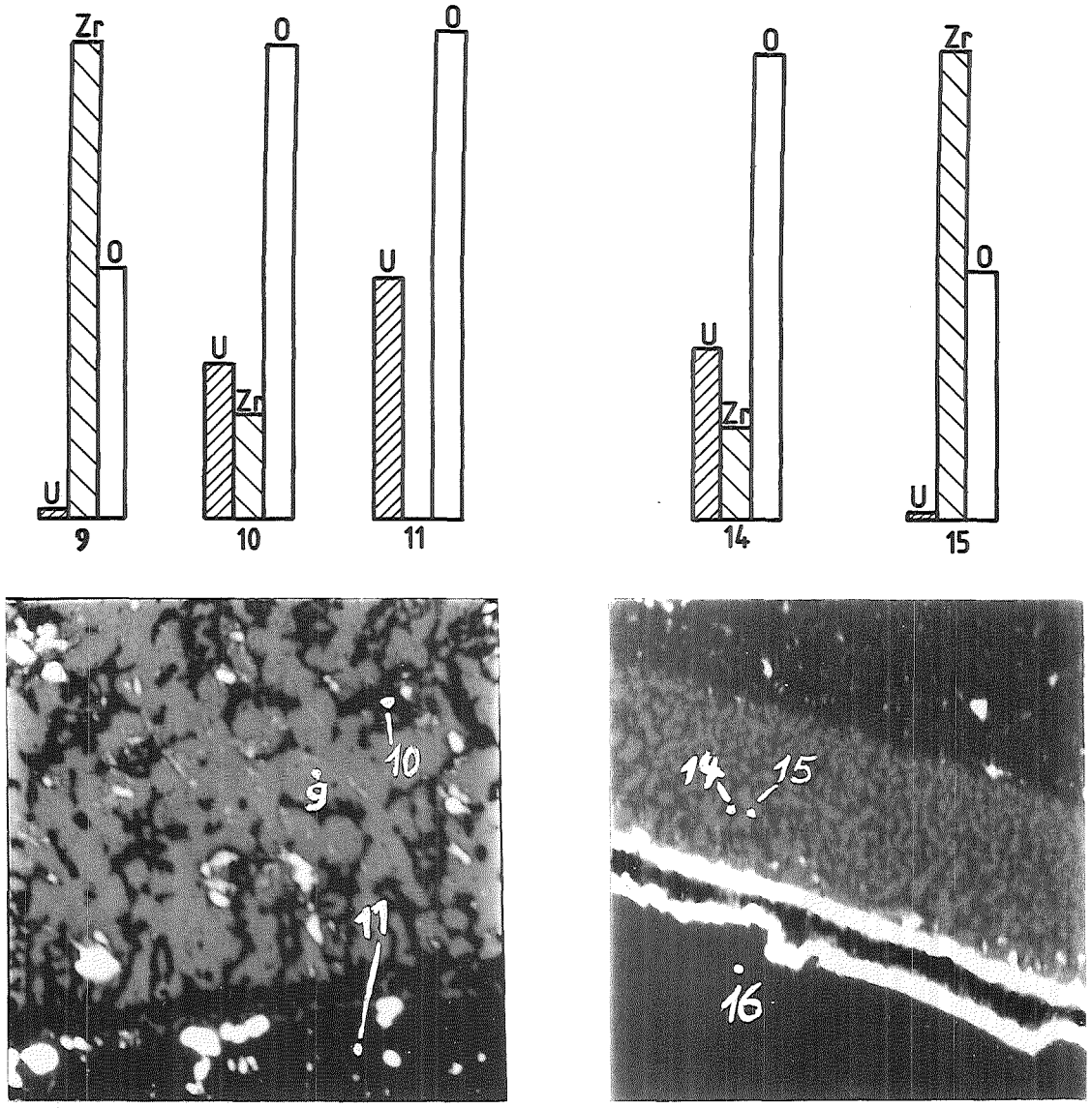

FIG.1-16: MICROPROBE INVESTIGATION AT DIFFERENT LOCATIONS OF THE CROSS SECTION AT 188 MM FOR ESSI-1

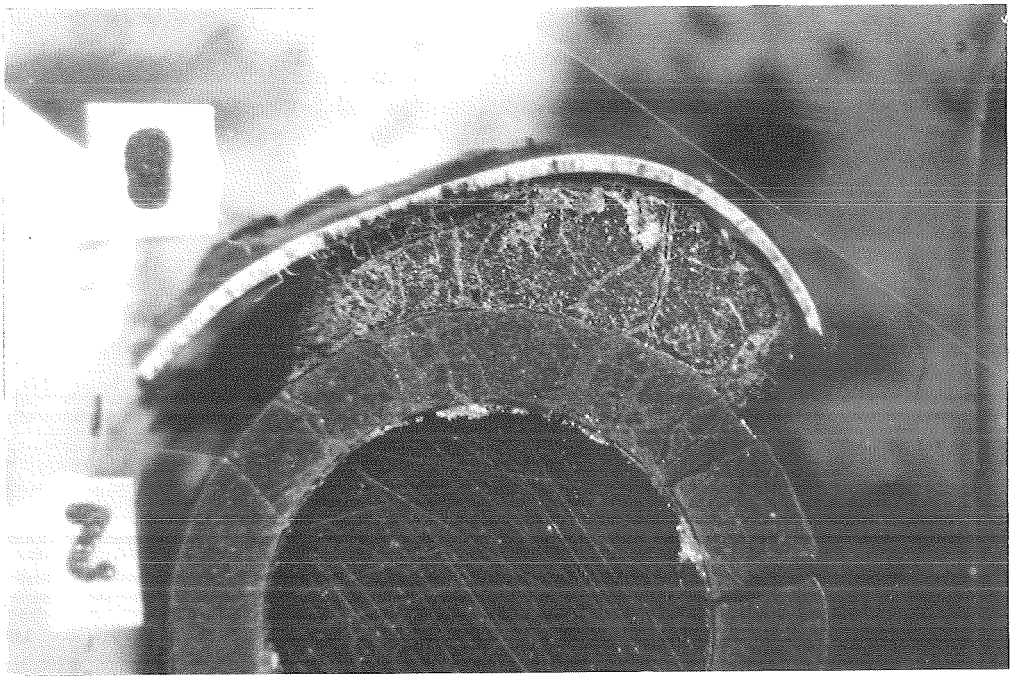

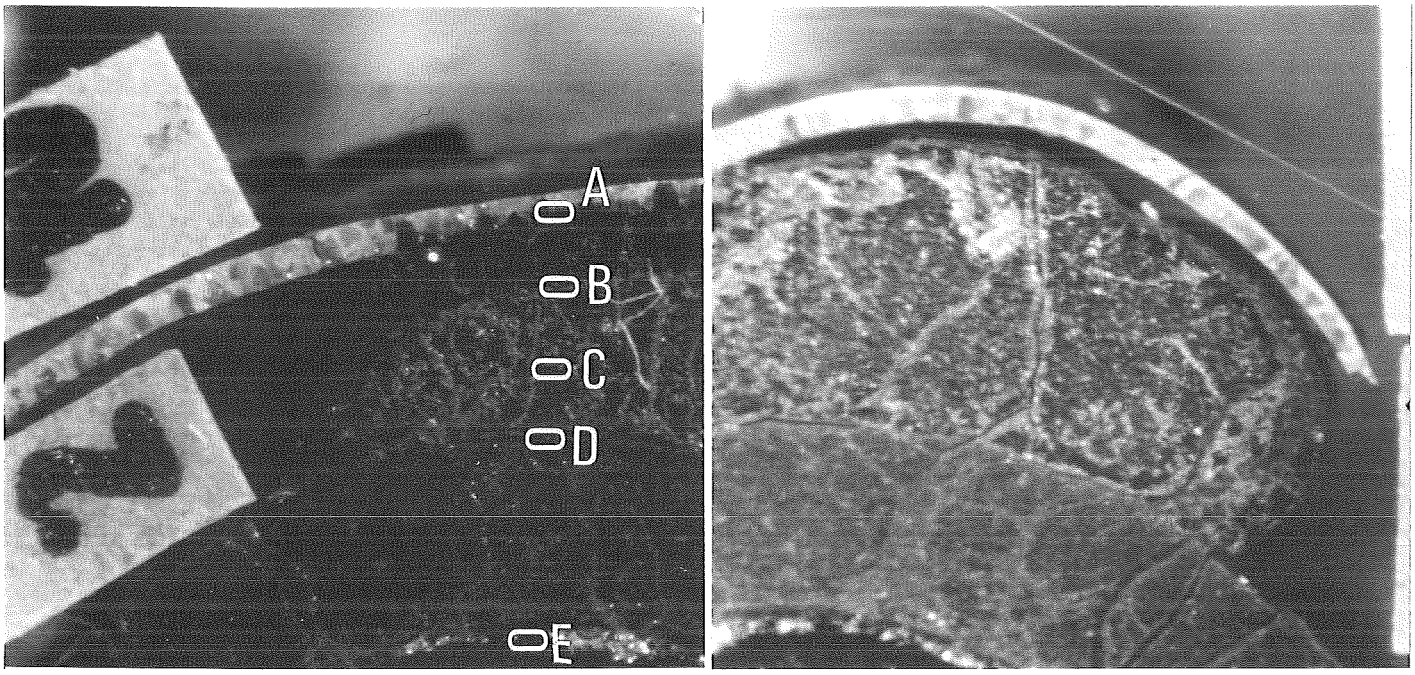

Fig. 1-16a: Locations of microprobe measurements of the cross section at 188mm elevation from test ESSI-1.

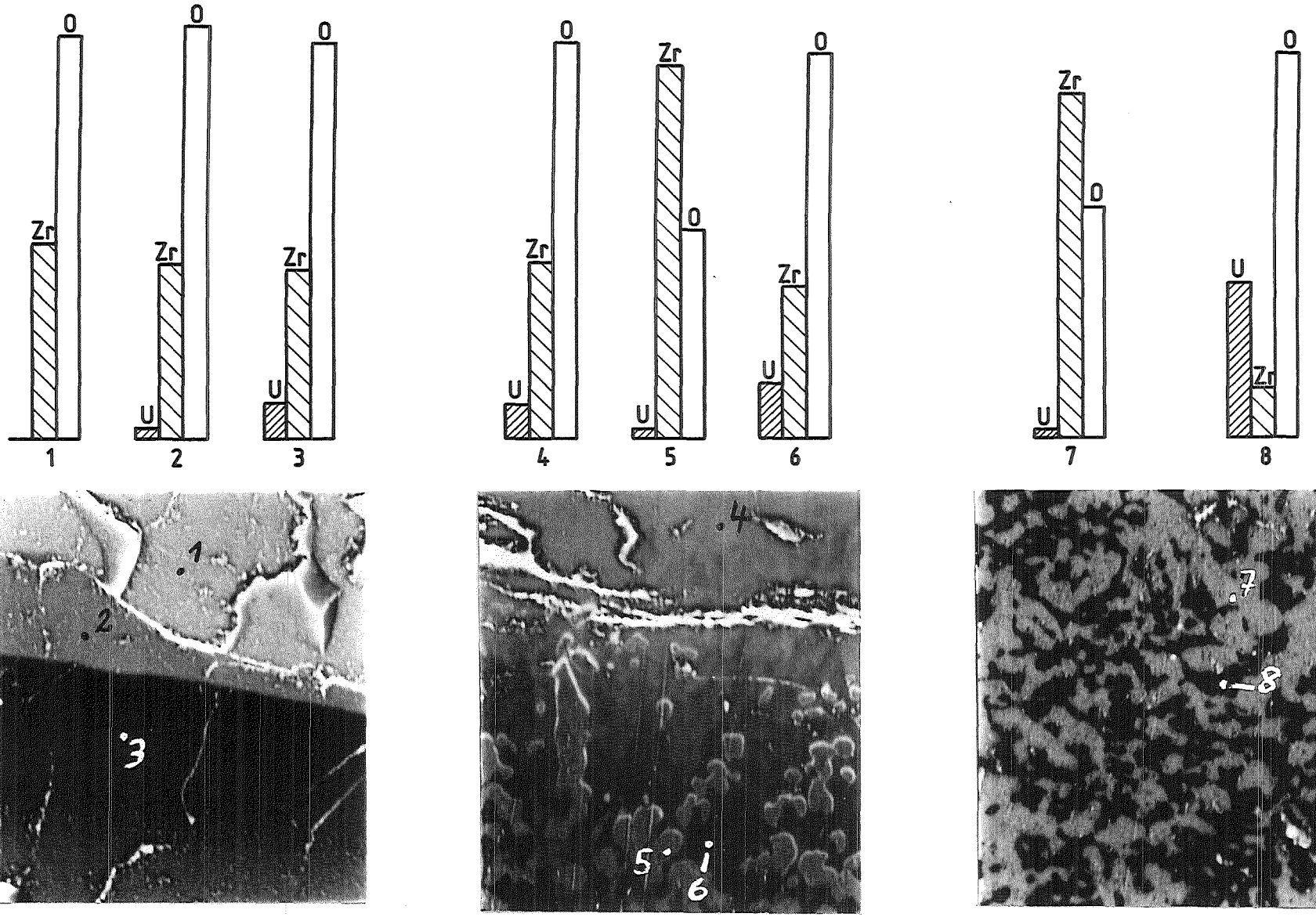

FIG.1-17: MICROPROBE INVESTIGATION AT DIFFERENT LOCATIONS (SEE FIG.1-18a) OF THE CROSS SECTION AT 105 MM FOR ESSI-1

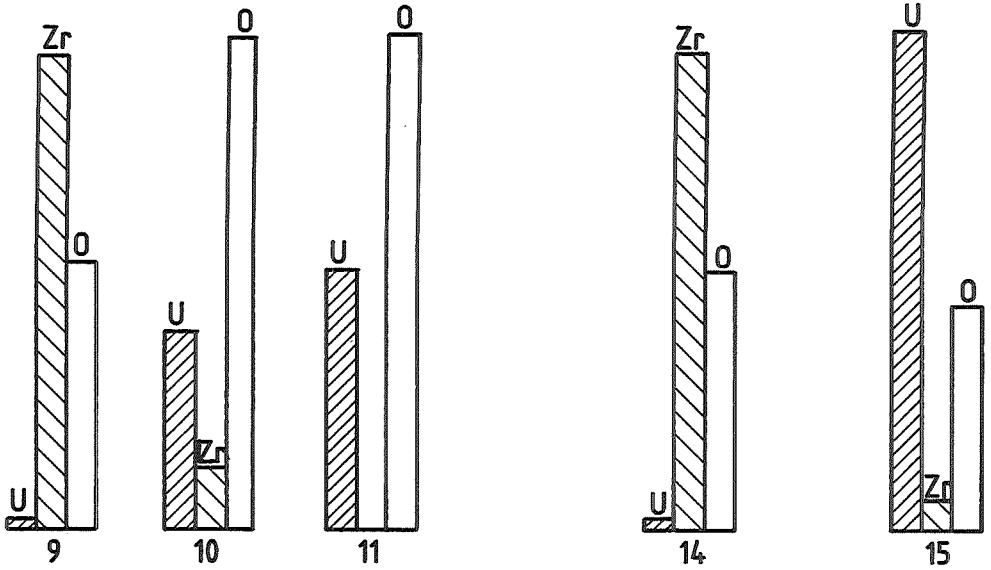

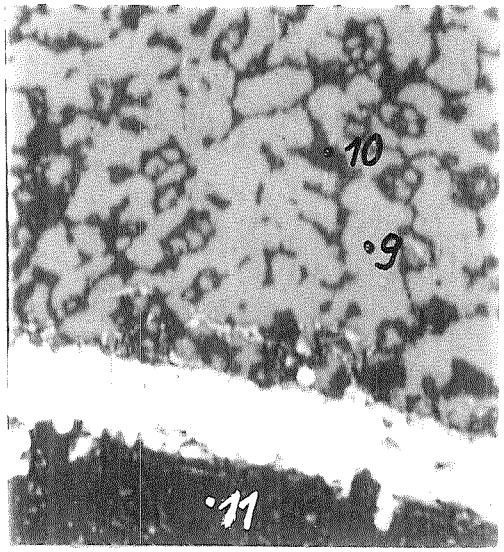

D

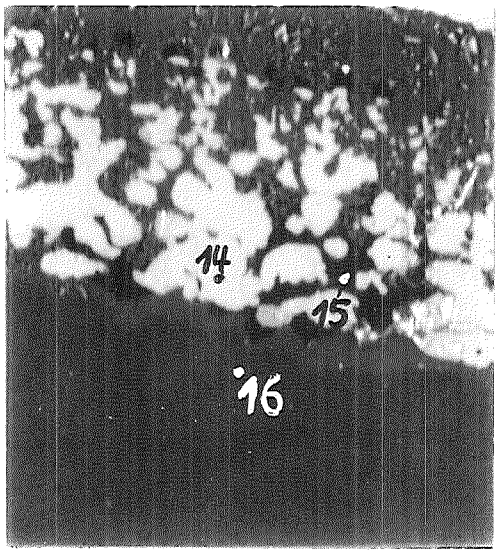

E

FIG.1-18: MICROPROBE INVESTIGATION AT DIFFERENT LOCATIONS OF THE CROSS SECTION AT 105 MM FOR ESSI-1

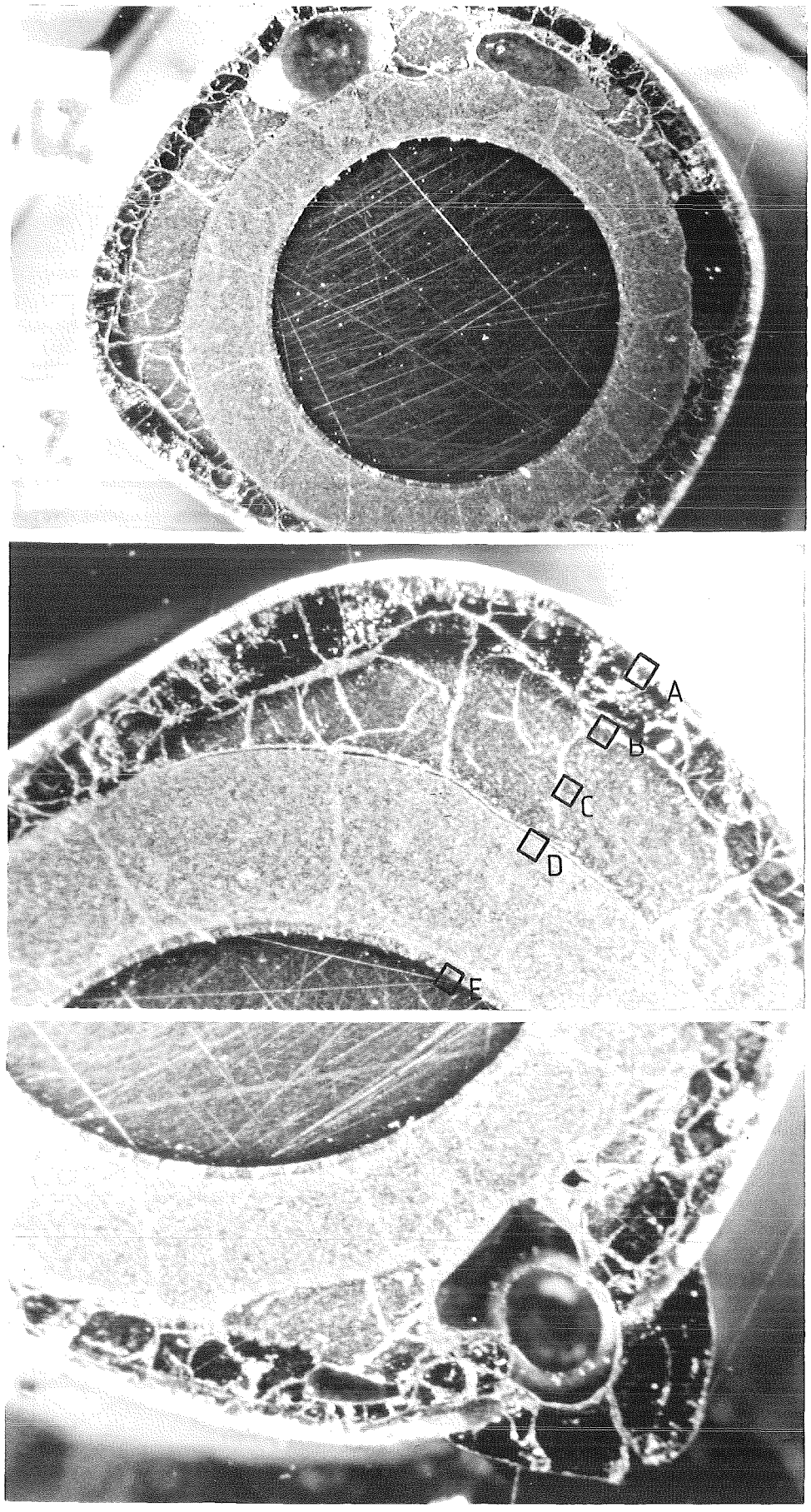

Fig.1-18a: Locations of microprobe measurements of the cross section at 105mm elavation from test ESSI-1

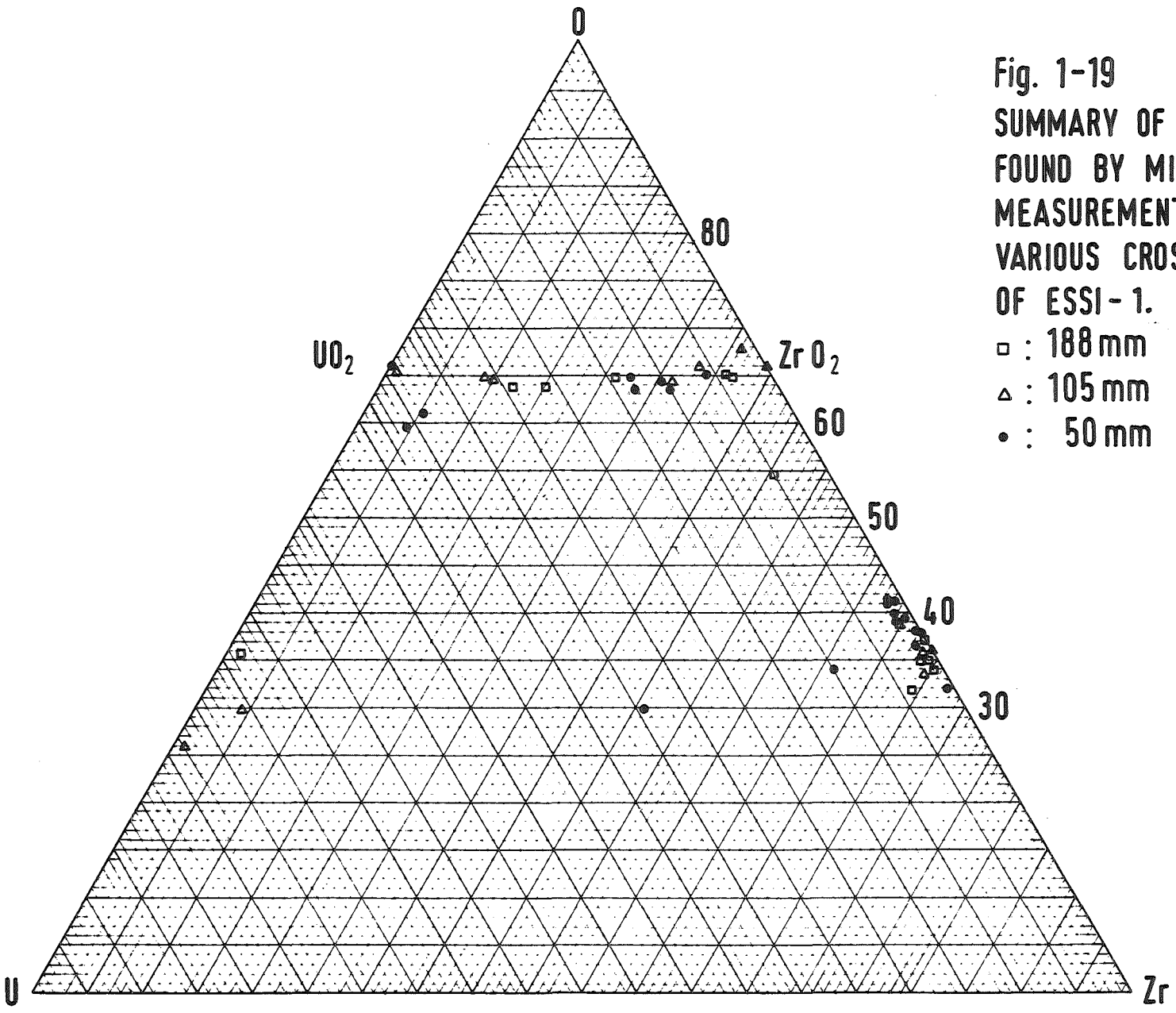

Fig. 1-19
SUMMARY OF COMPOSITIONS FOUND BY MICROPROBE MEASUREMENTS FROM VARIOUS CROSS SECTIONS OF ESSI-1.
□ : 188 mm
△ : 105 mm
• : 50 mm

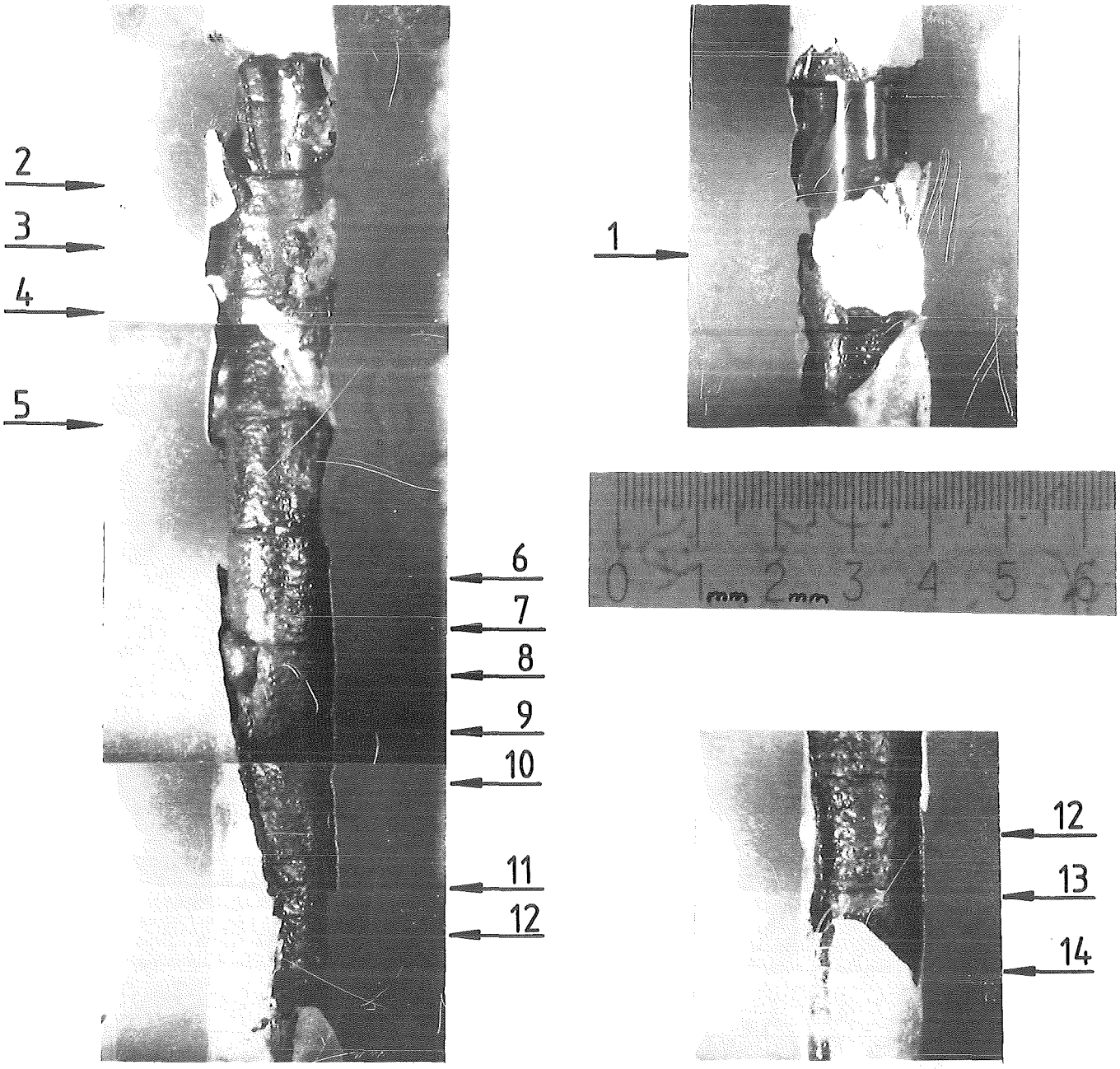

FIG.1-20: LOCATIONS OF ENLARGED VIEWS FROM THE UPPER PART OF THE FUEL ROD SIMULATOR ESSI-1 GIVEN IN THE FOLLOWING FIGURES

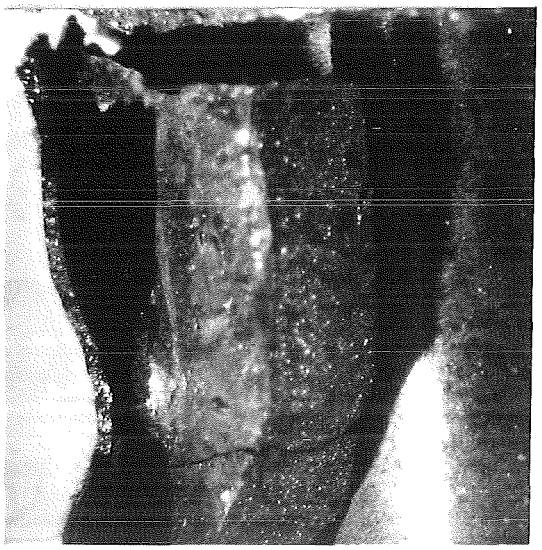

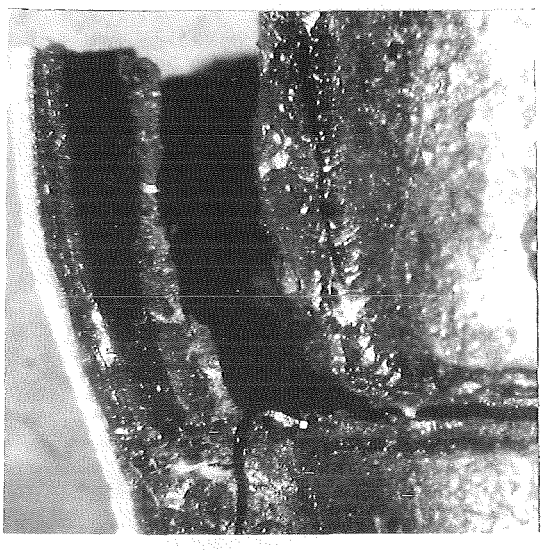

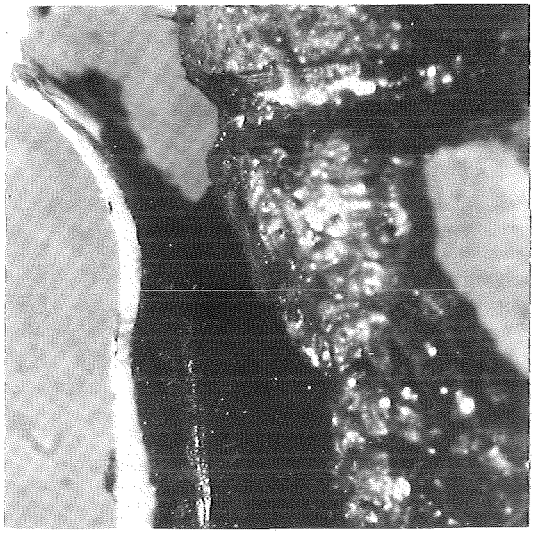

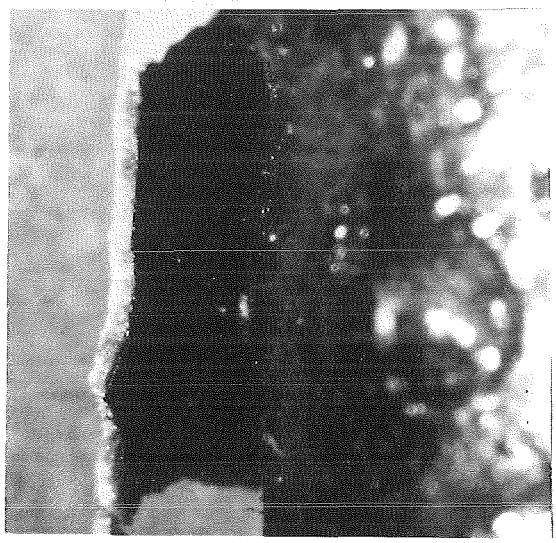

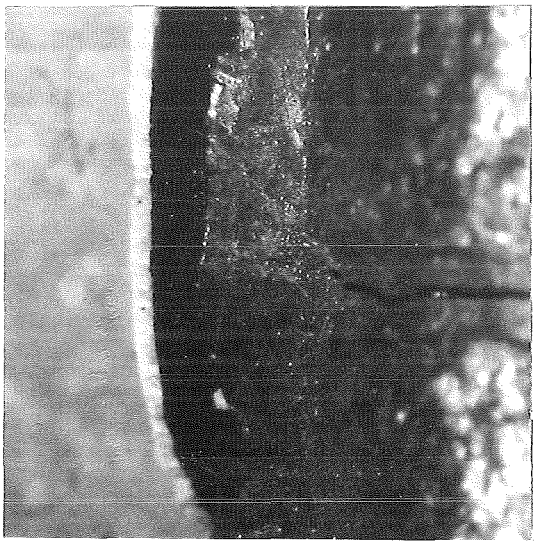

FIG.1-21: ENLARGED VIEWS FROM THE UPPER PART OF THE FUEL ROD SIMULATOR ESSI-1 (POSITIONS SEE FIG.1-20)

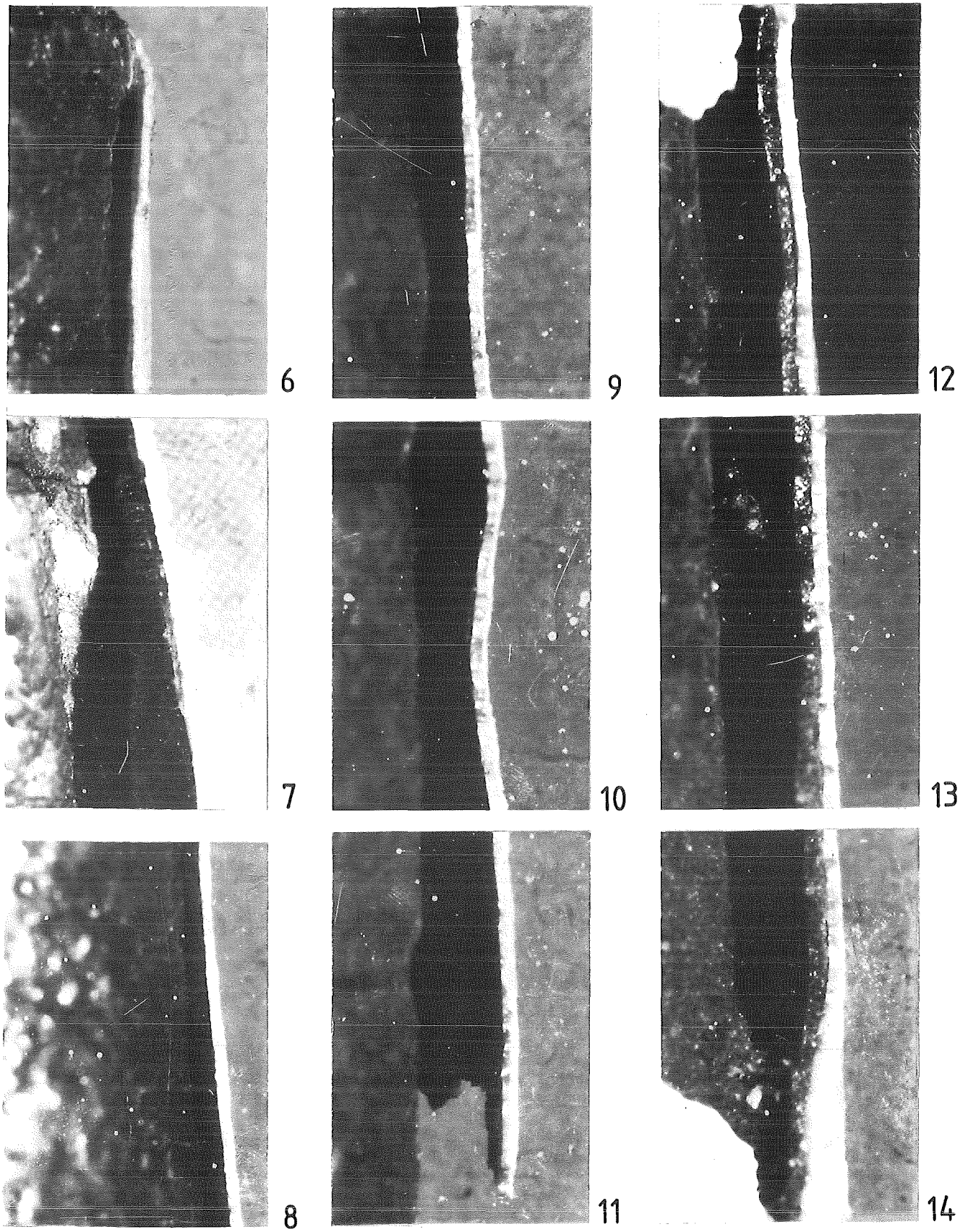

FIG.1-22: ENLARGED VIEWS FROM THE UPPER PART OF THE FUEL ROD SIMULATOR ESSI-1 (POSITIONS SEE FIG.1-20)

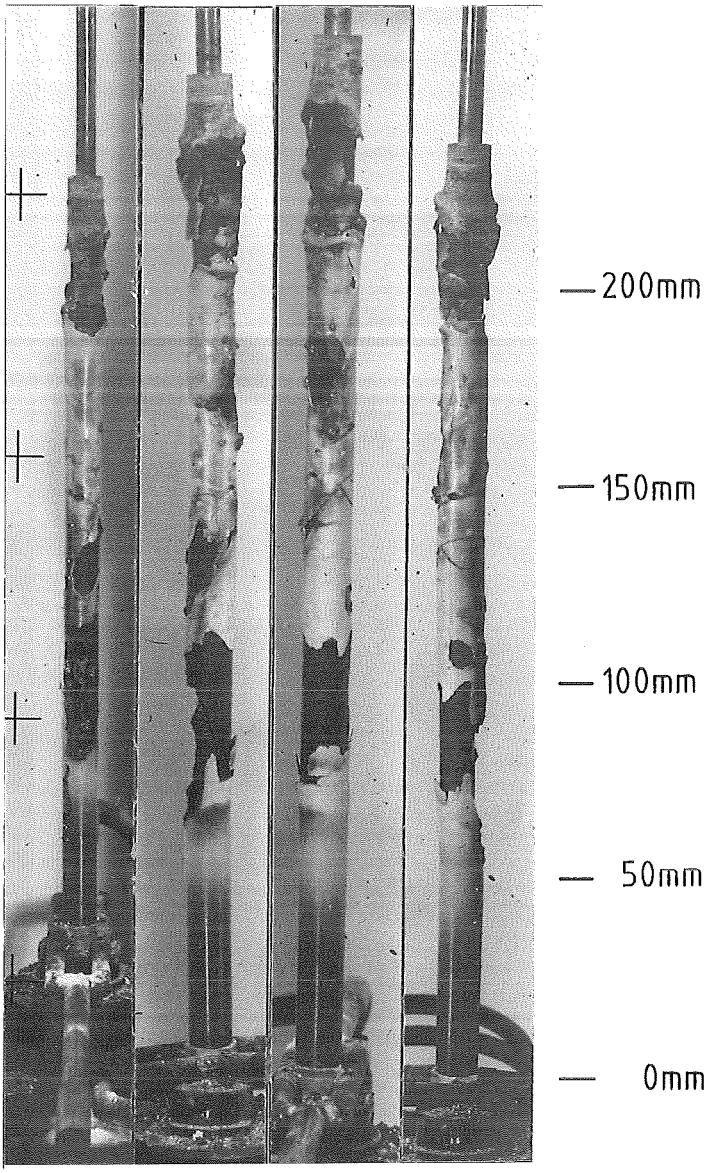

FIG. 2-1: POSTTEST APPEARANCE OF THE FUEL ROD SIMULATOR AND SCALE OF THE CROSS SECTION ELEVATIONS FOR ESSI-2

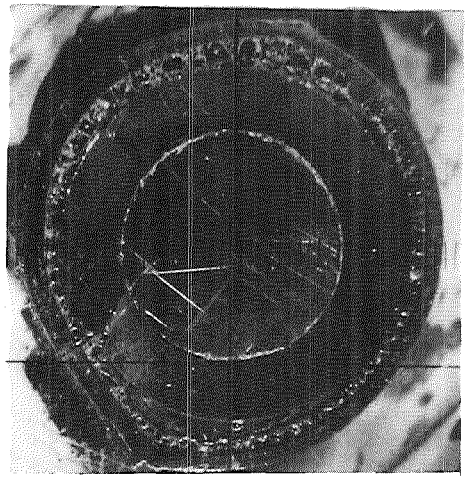

225mm

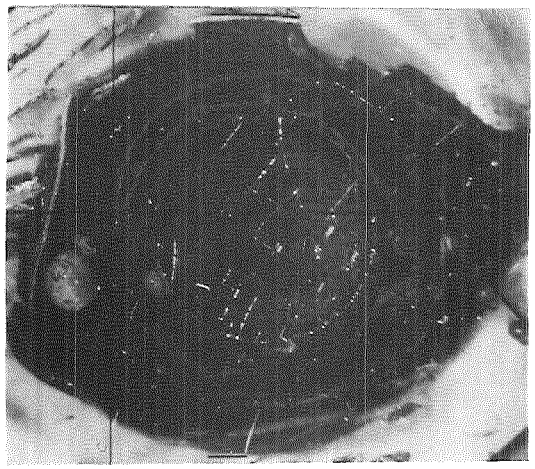

210mm

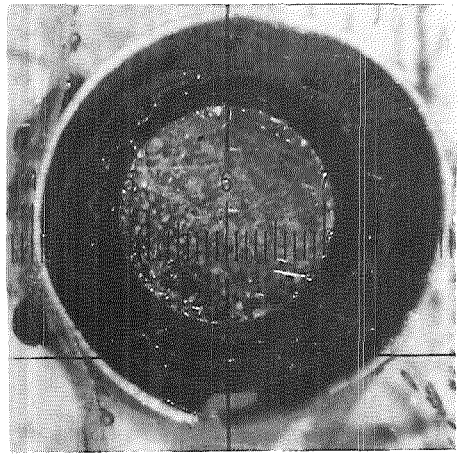

180mm

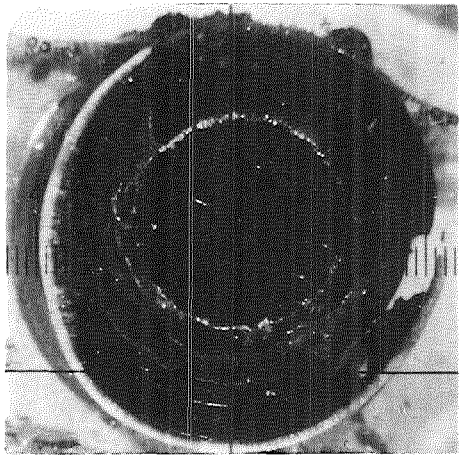

168mm

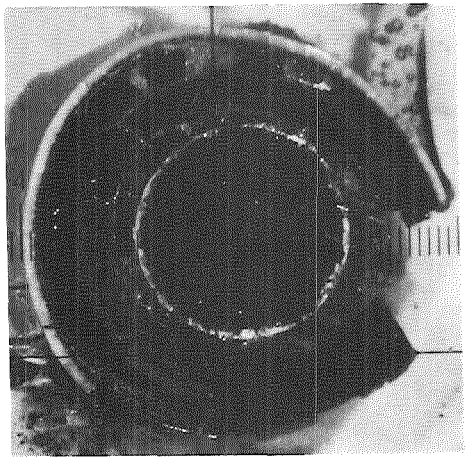

162mm

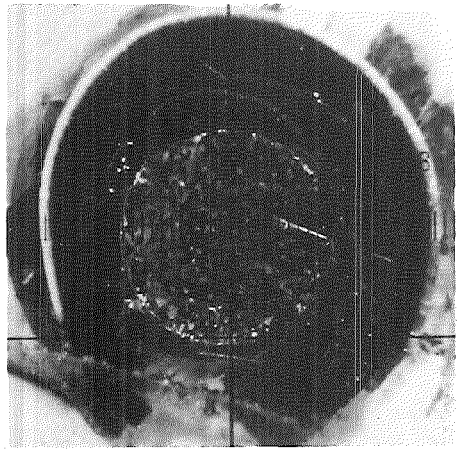

152mm

Fig.2-2: Cross Sections of Test ESSI-2

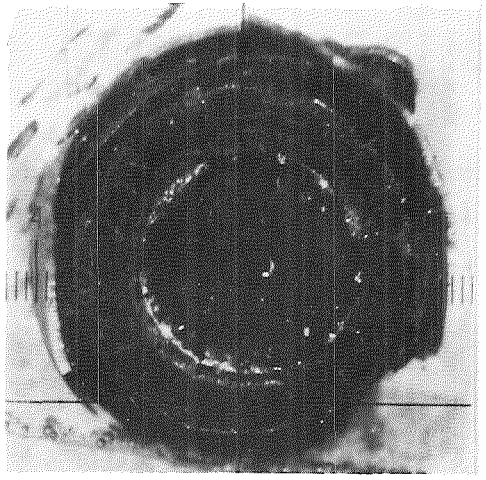

115mm

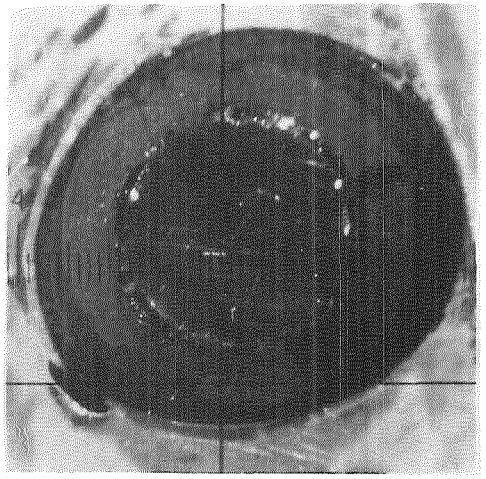

100mm

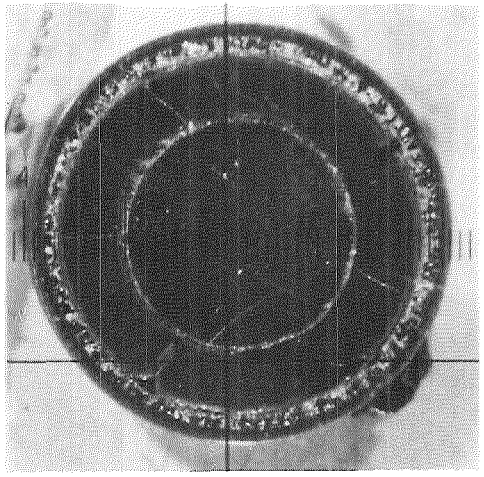

50mm

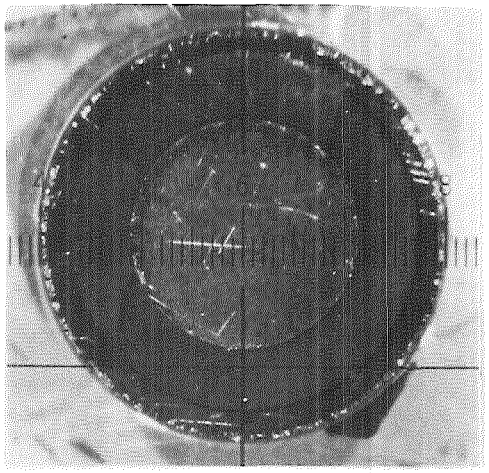

35mm

KfK

Fig.2-3: Cross Sections of Test ESSI-2

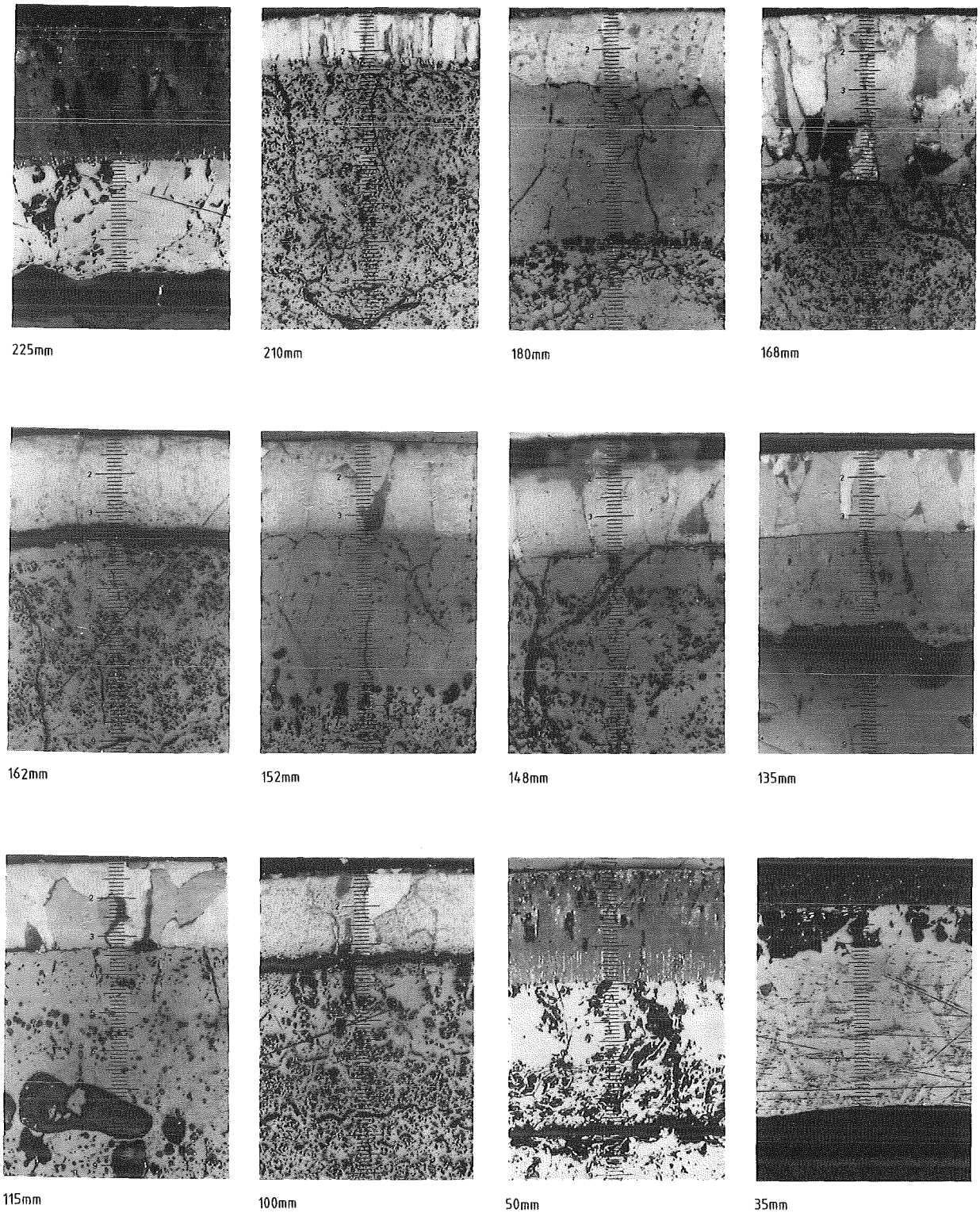

Fig. 2-4 : Enlarged View (100x) of Cross Sections From ESSI-2

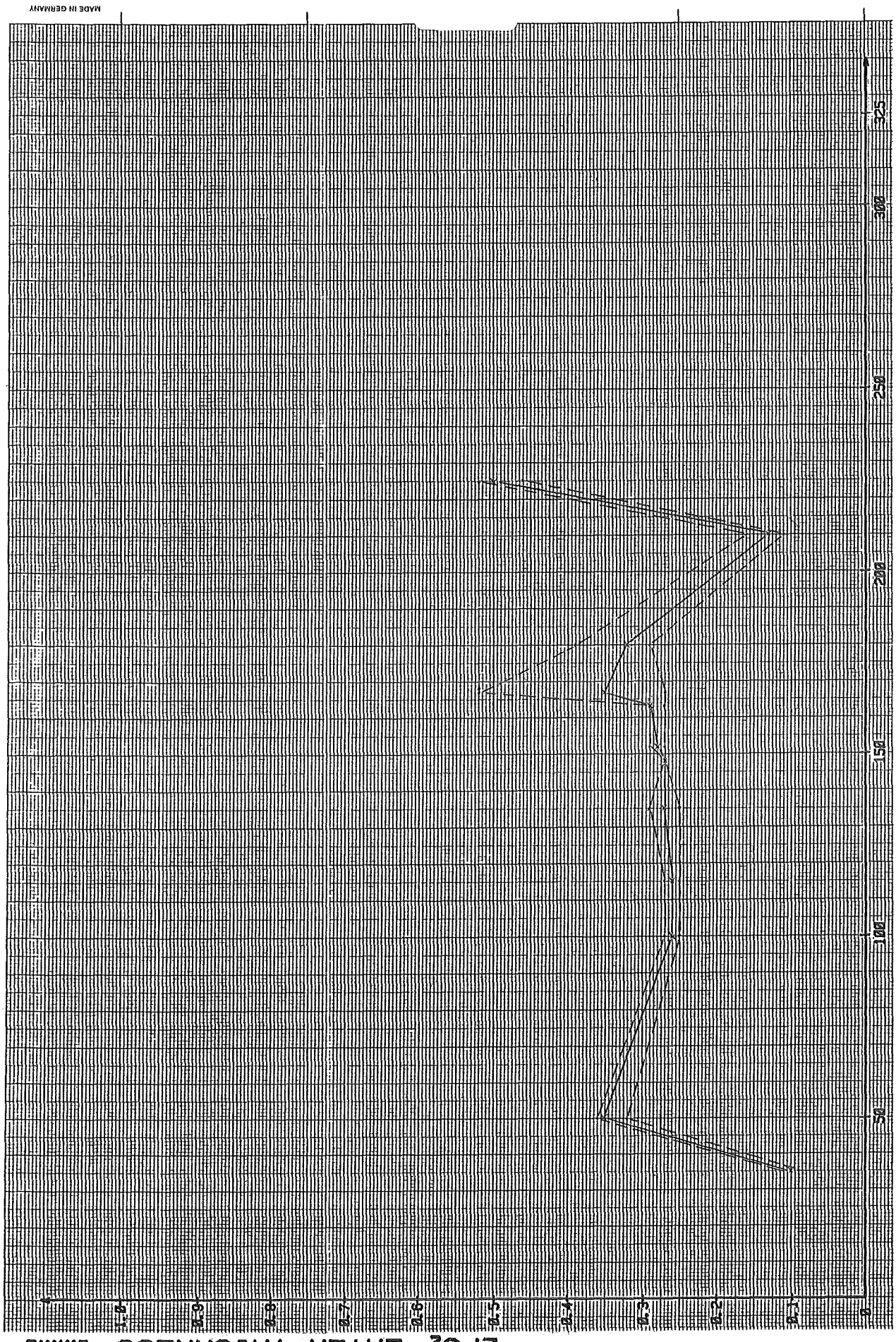

Fig.2-A: Zirconoxid layer thickness for test ESSI-2 (———maximum or minimum value; ——mean value)

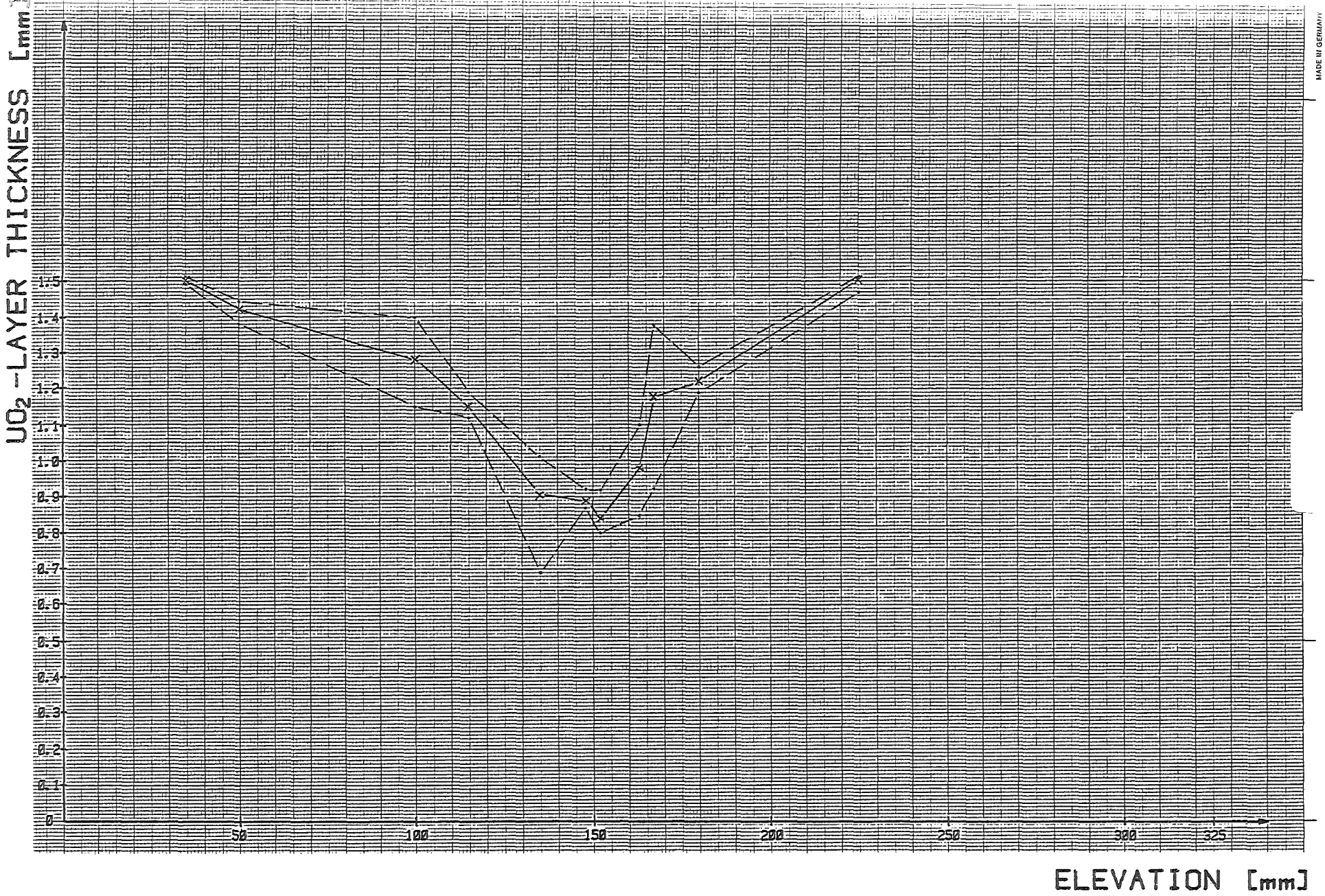

Fig. 2-B : Uranium oxide layer thickness for test ESSI-2 (---maximum or minimum value; —— mean value)

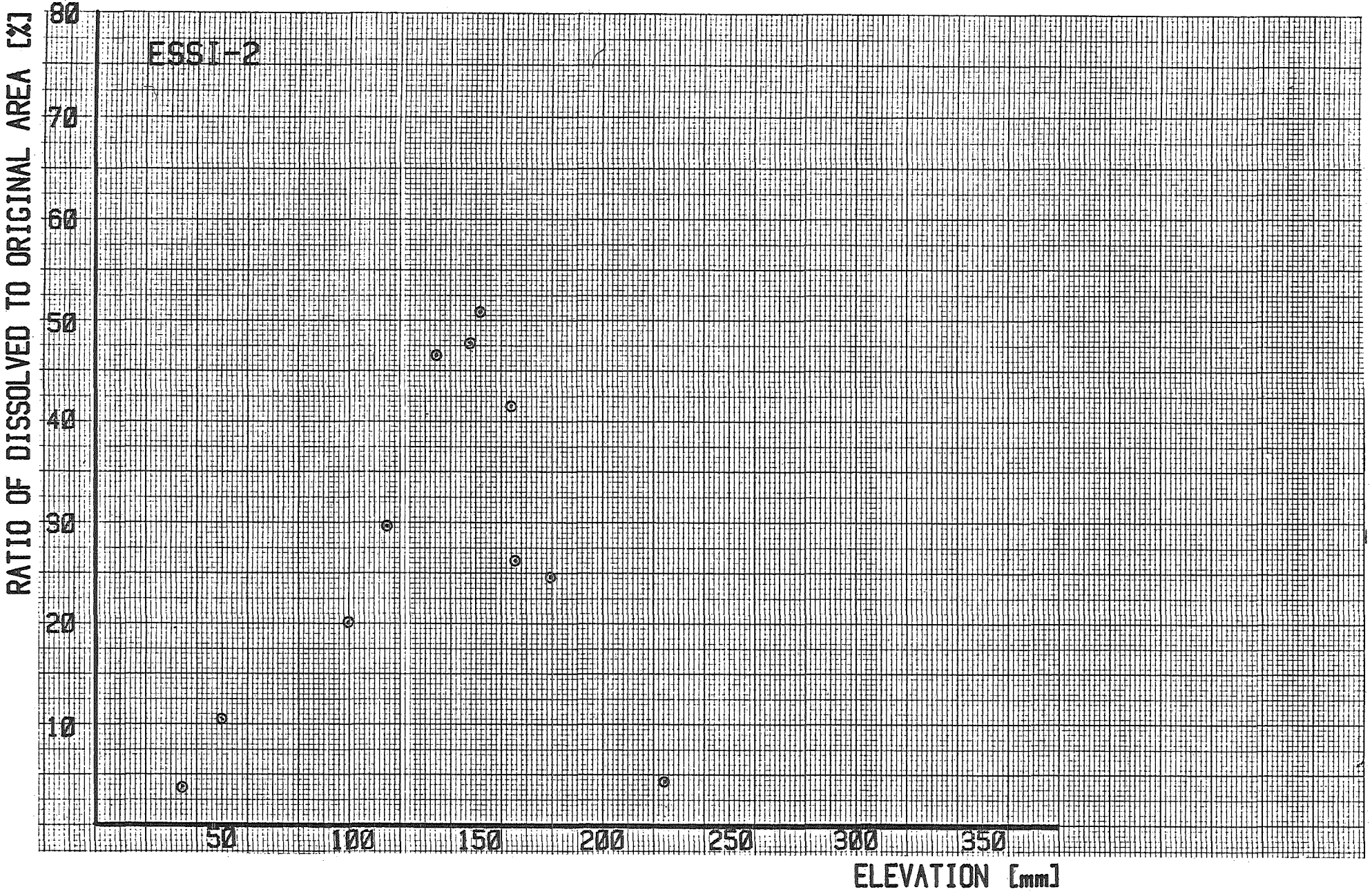

Fig.: 2-C
Dissolution of the UO_2-pellet at different elevations (ESSI-2)

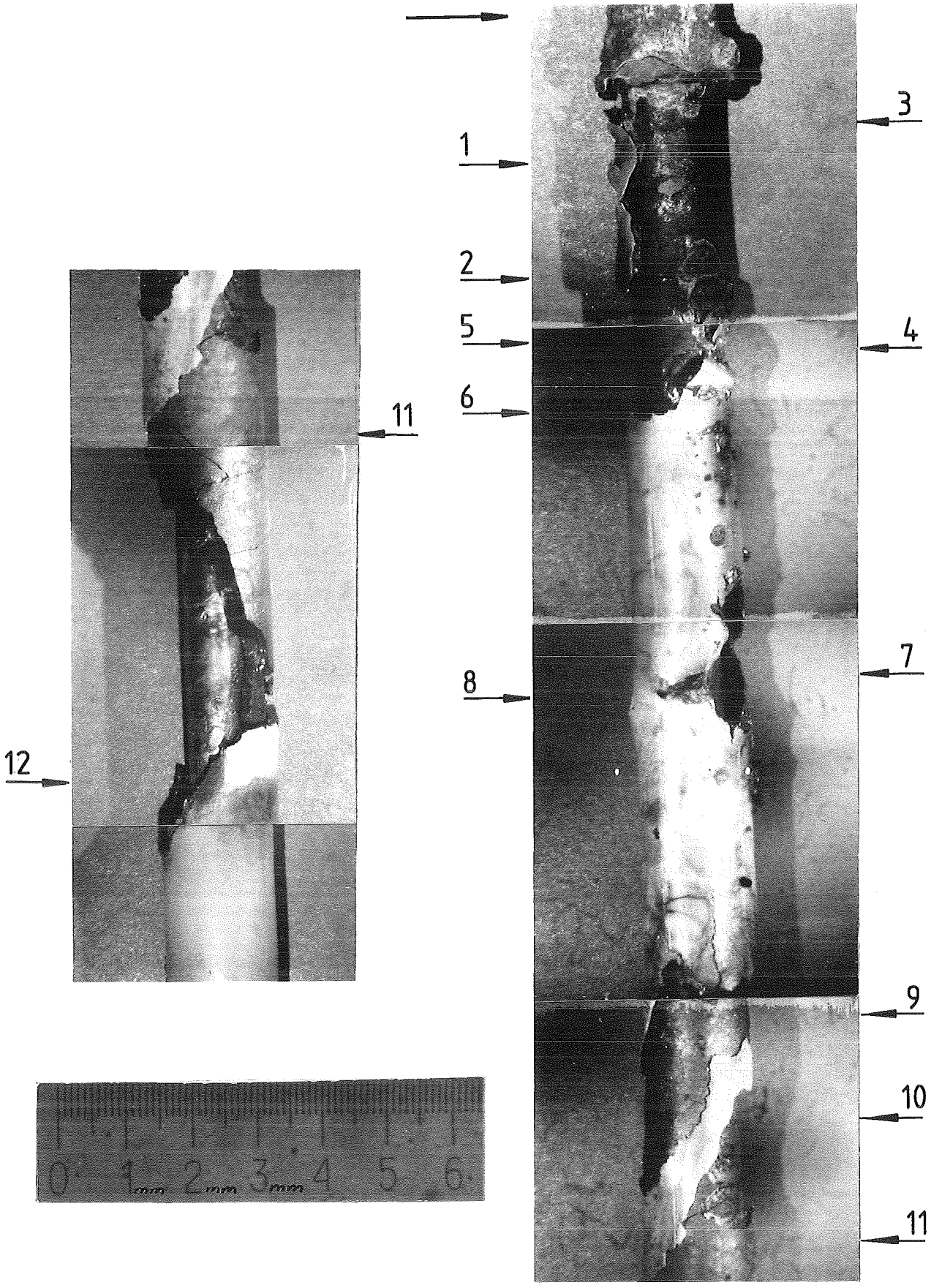

FIG.2-10: LOCATIONS OF ENLARGED VIEWS OF THE FUEL ROD SIMULATOR ESSI-2 GIVEN IN THE FOLLOWING FIGURES

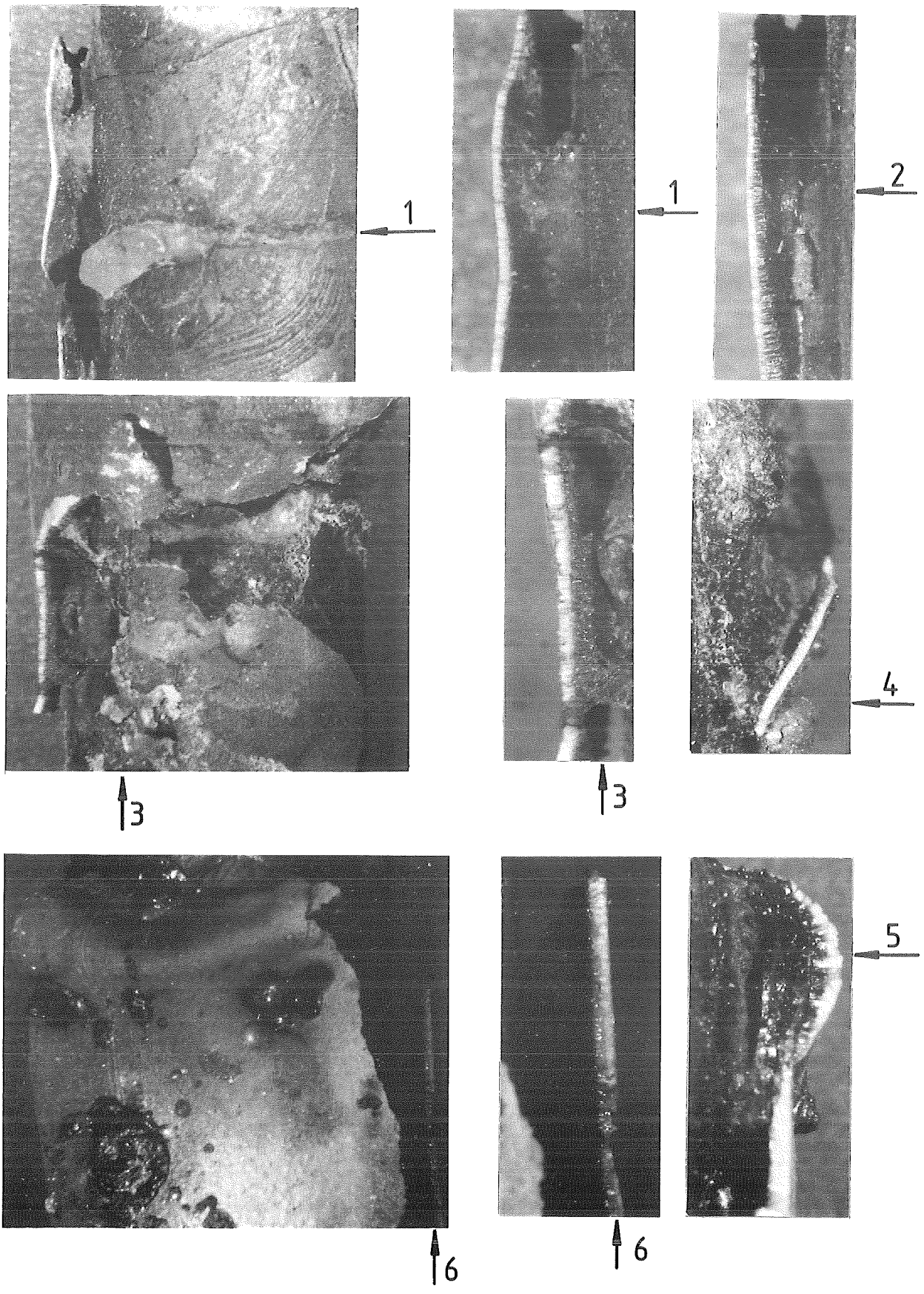

FIG.2-11: DETAILS OF THE FUEL ROD SIMULATOR ESSI-2
(POSITION SEE FIG.2-10)

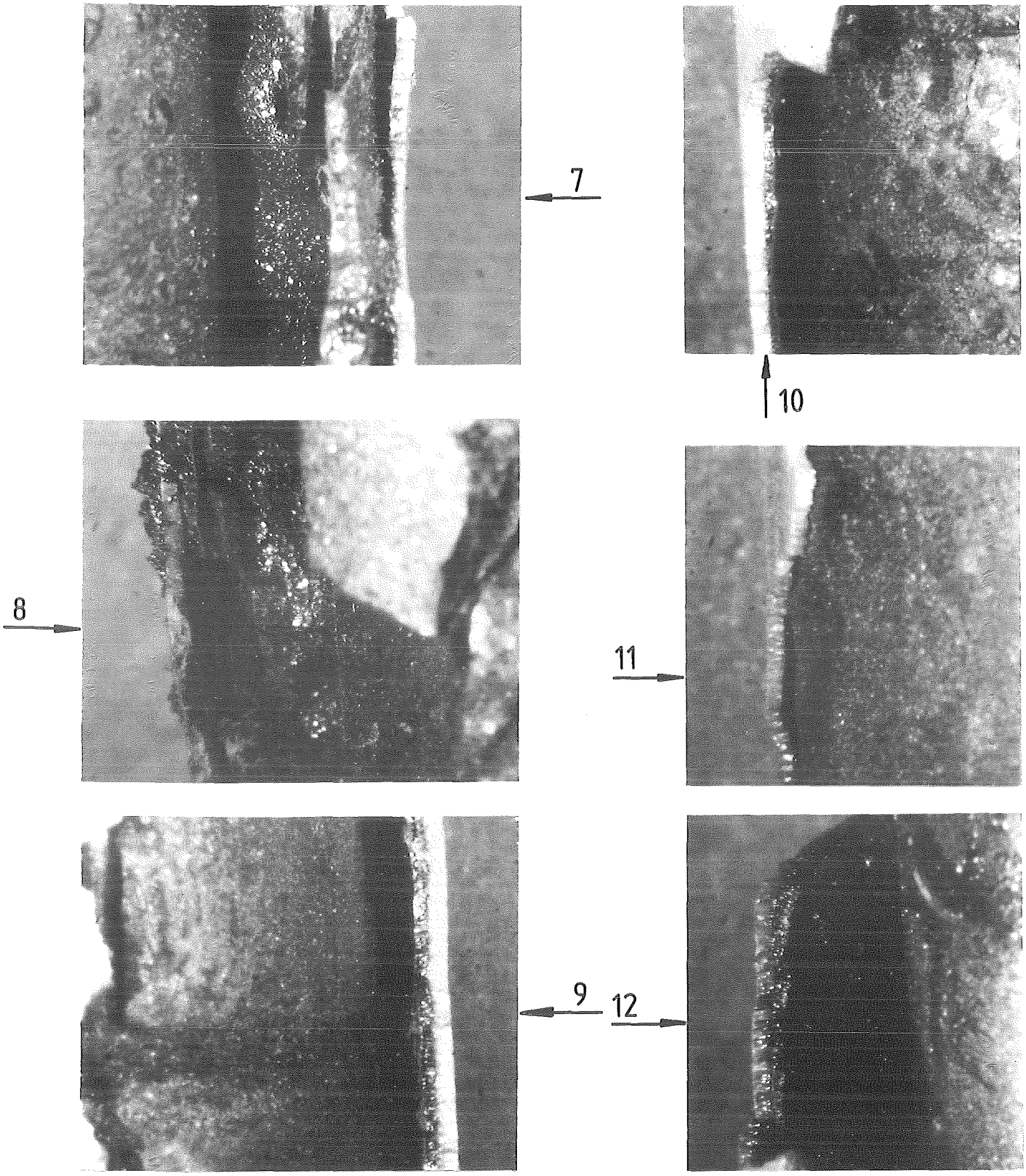

FIG.2-12: DETAILS OF THE FUEL ROD SIMULATOR ESSI-2
(POSITION SEE FIG.2-10)

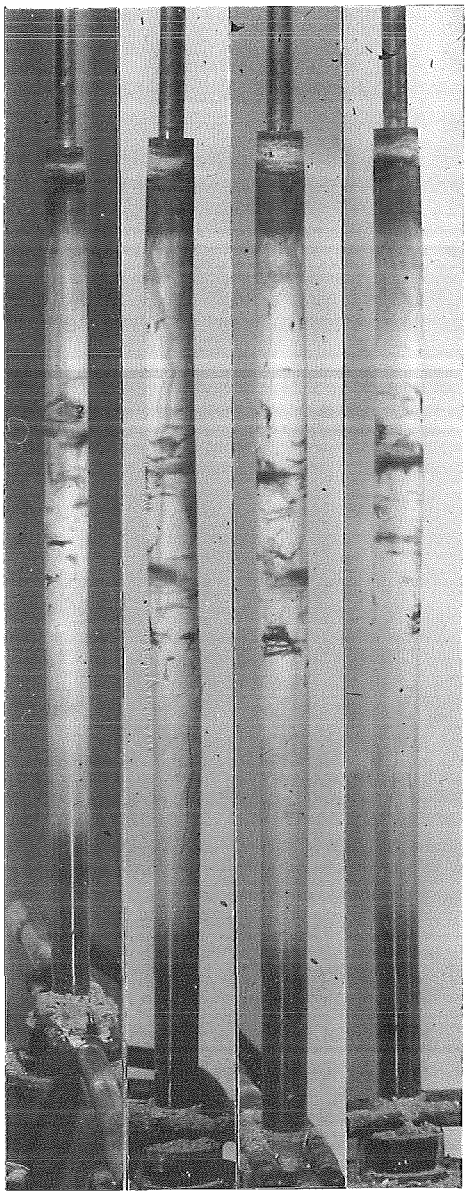

FIG. 3-1: POSTTEST APPEARANCE OF THE FUEL ROD SIMULATOR AND SCALE OF THE CROSS SECTION ELEVATIONS FOR ESSI-3

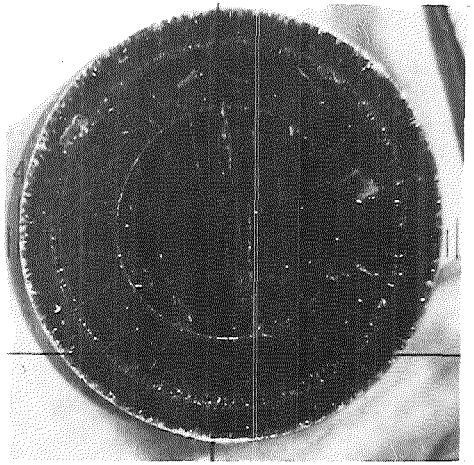

230mm

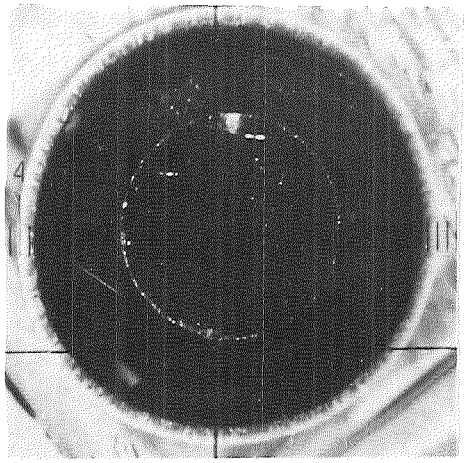

220mm

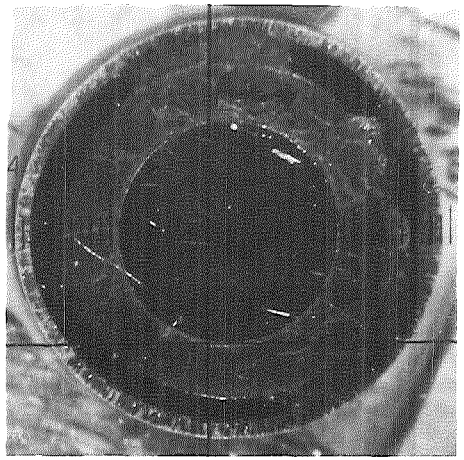

205mm

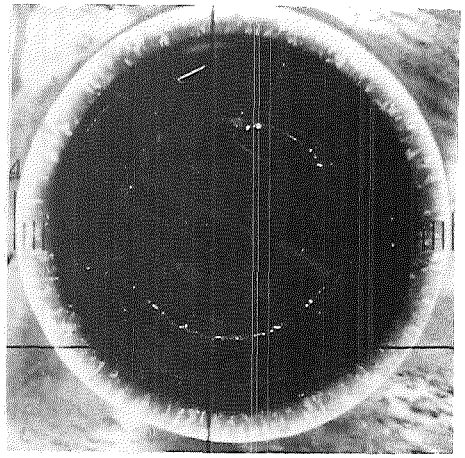

190mm

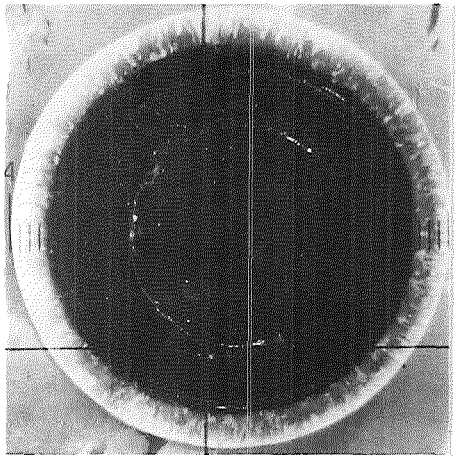

173mm

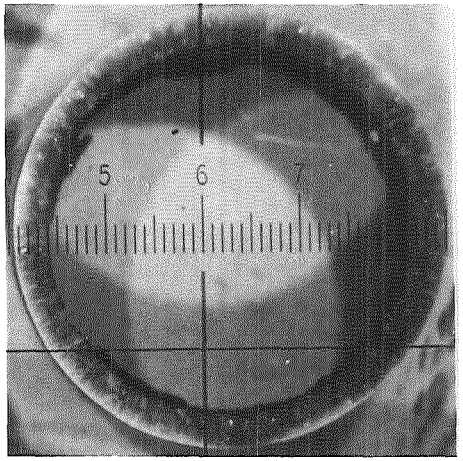

167mm

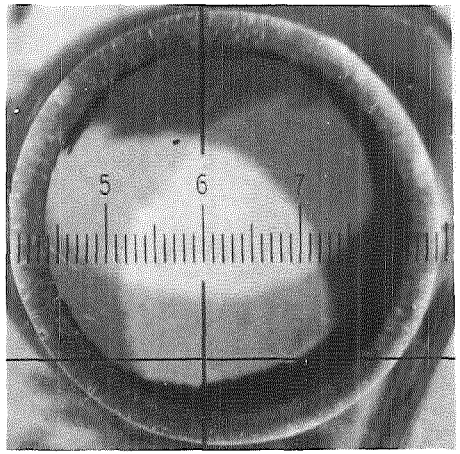

158mm

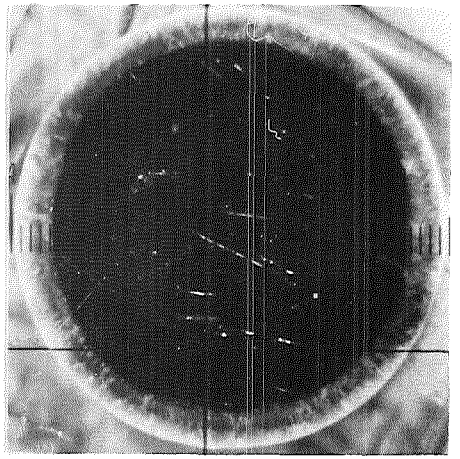

152mm

Fig.3-2: Cross Sections of Test ESSI-3

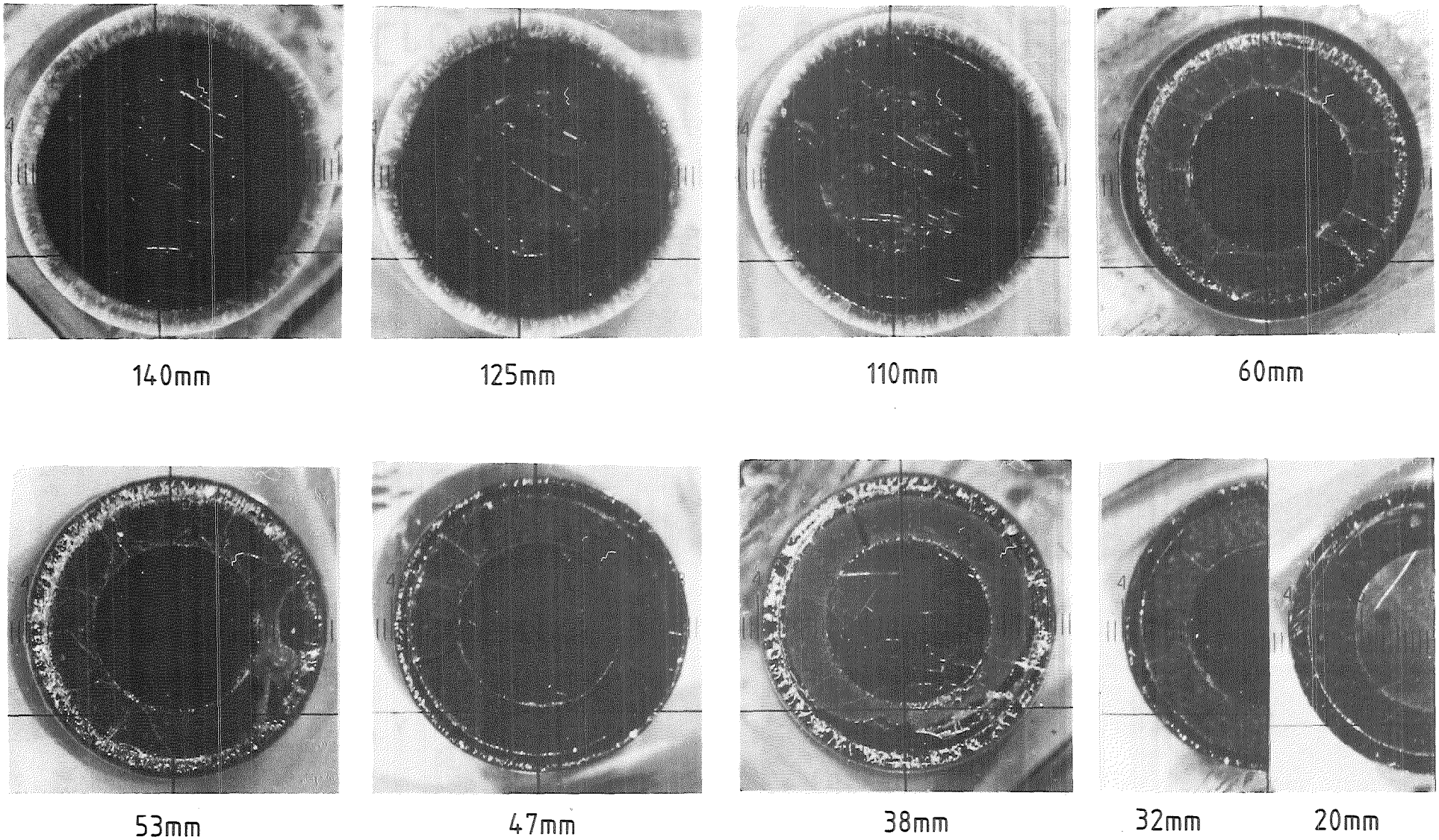

Fig.3-3: Cross Sections of Test ESSI-3

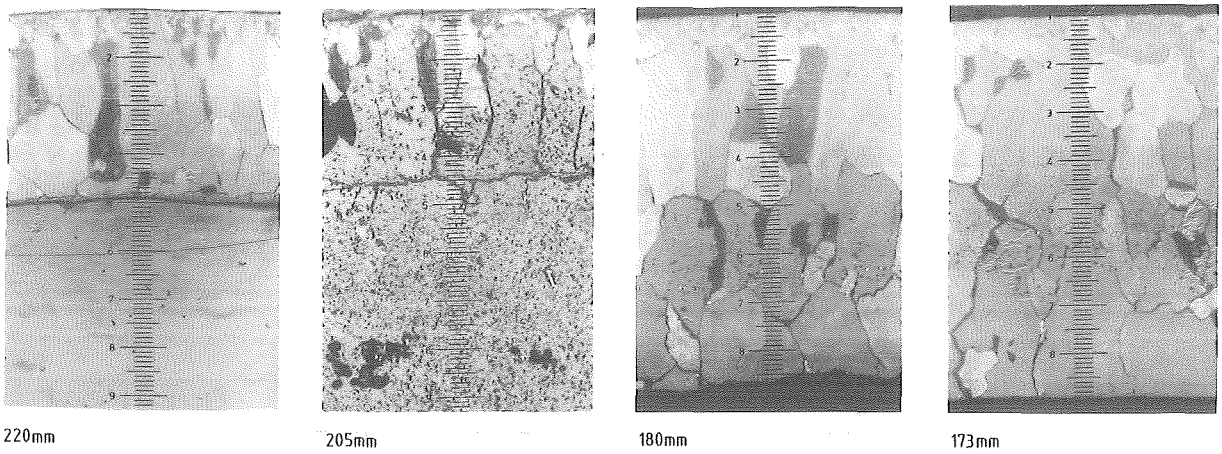

220mm 205mm 180mm 173mm

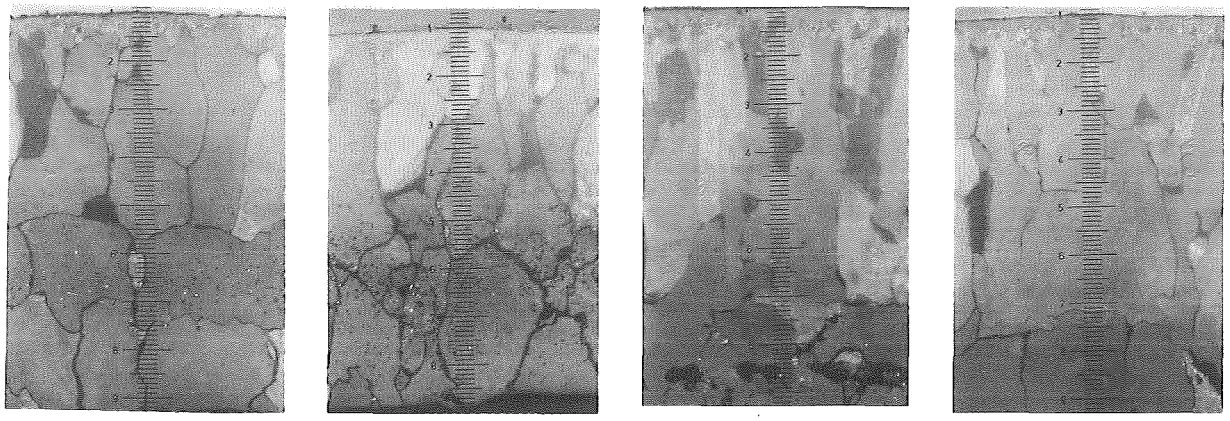

152mm 140mm 125mm 110mm

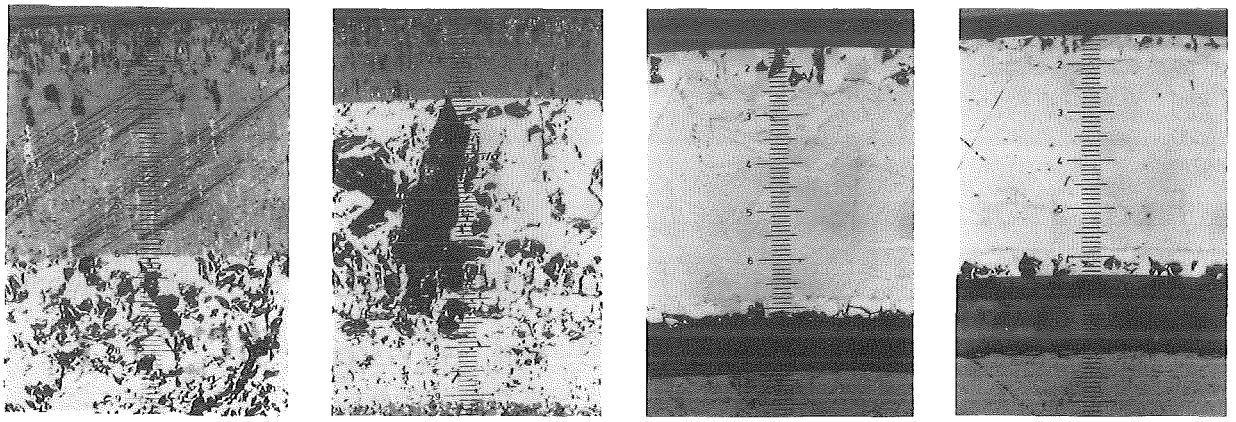

60mm 53mm 38mm 20mm

Fig.3-4 : Enlarged View (100x) of Cross Sections From ESSI-3

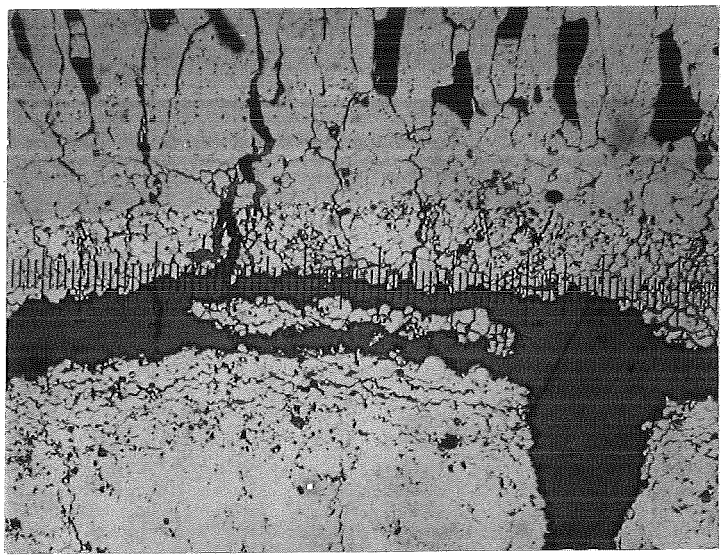

Fig. 3-5:
Transition oxidized cladding to UO_2-pellet for test ESSI-3 at 190 mm elevation

Fig.3-A: Zirconoxid layer thickness for test ESSI-3 (– – –maximum or minimum value; ——mean value)

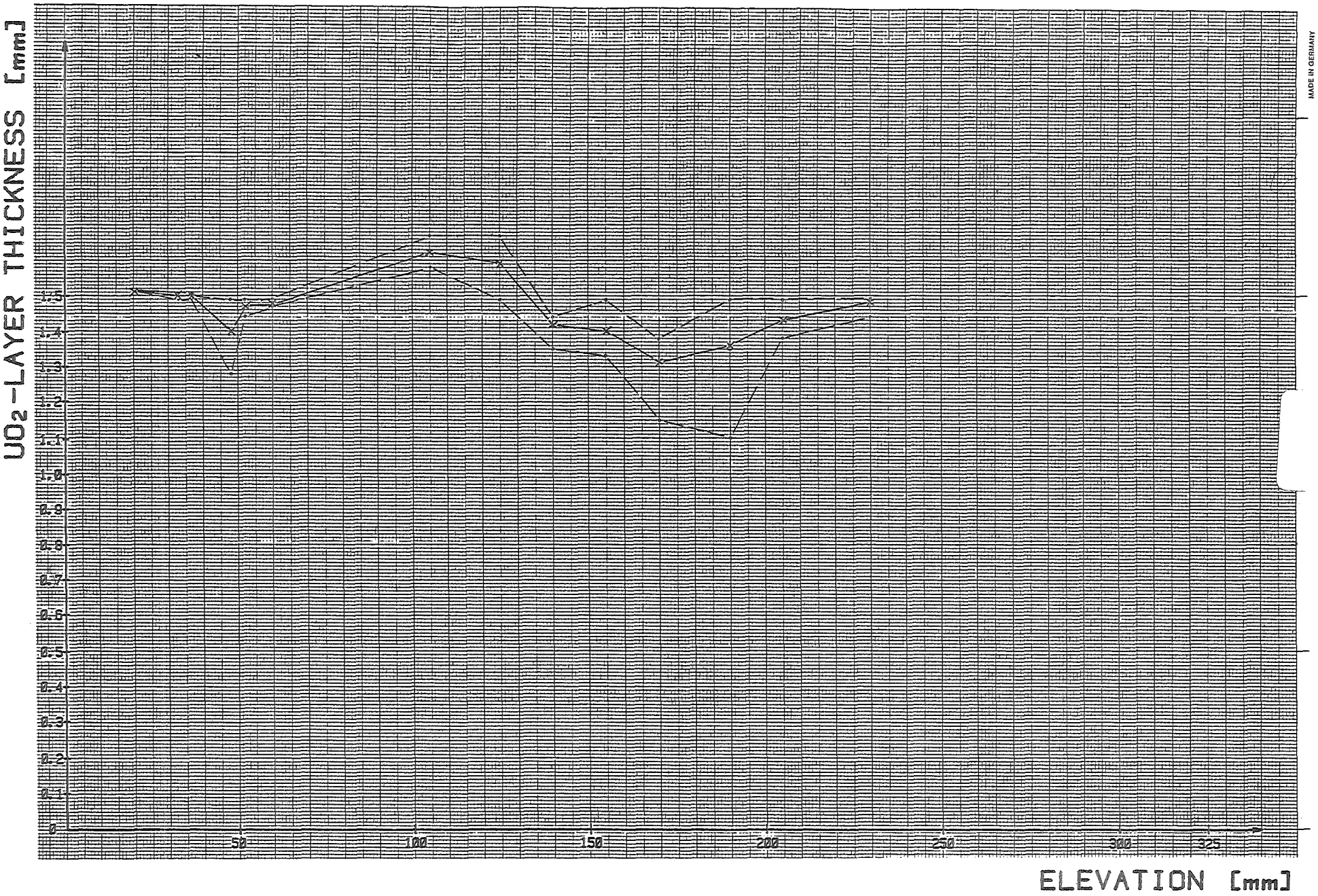

Fig.3-B : Uranium oxide layer thickness for test ESSI- 3 (---maximum or minimum value;—— mean value)

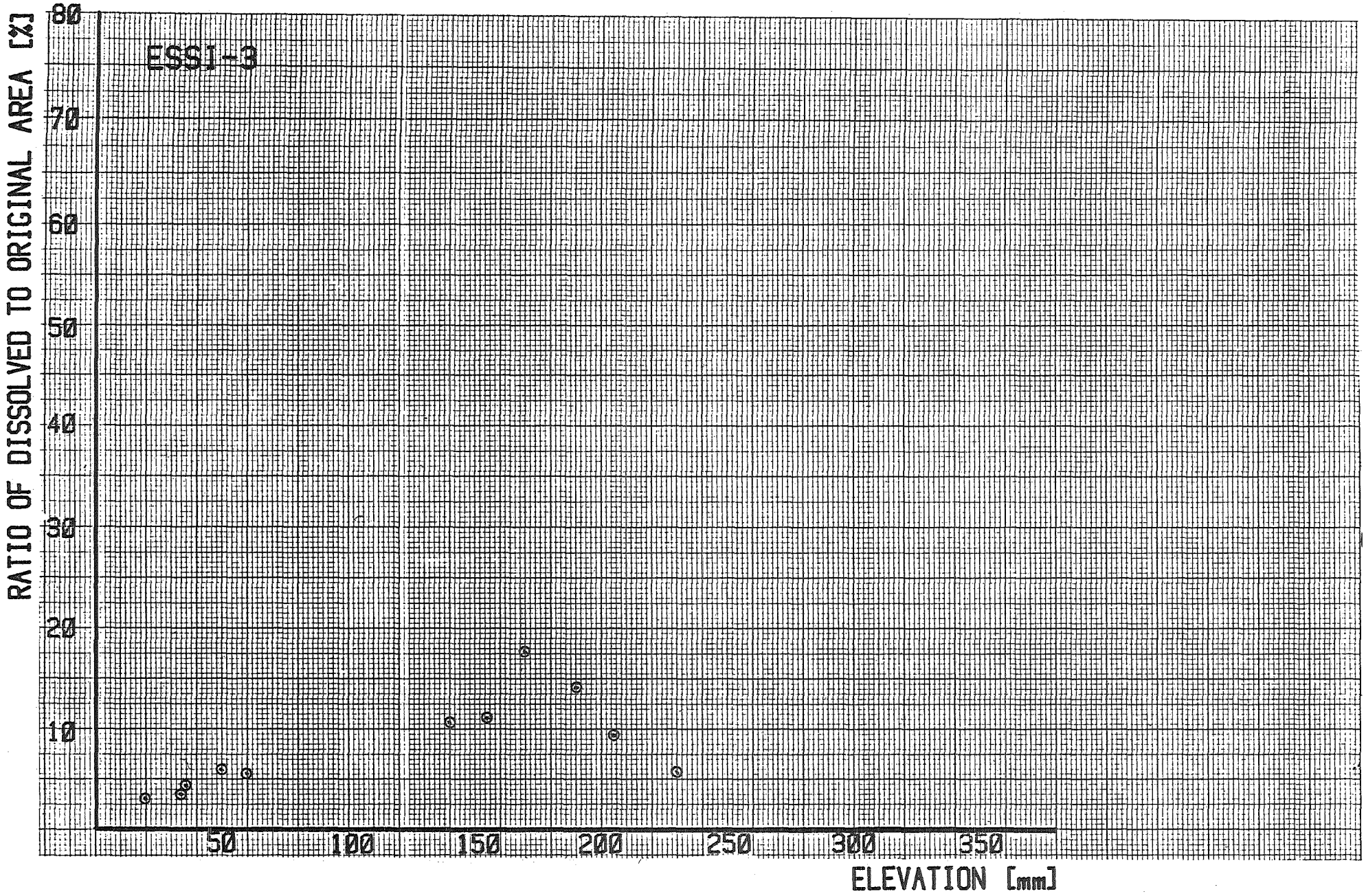

Fig.: 3-C
Dissolution of the UO_2-pellet at different elevations (ESSI-3)

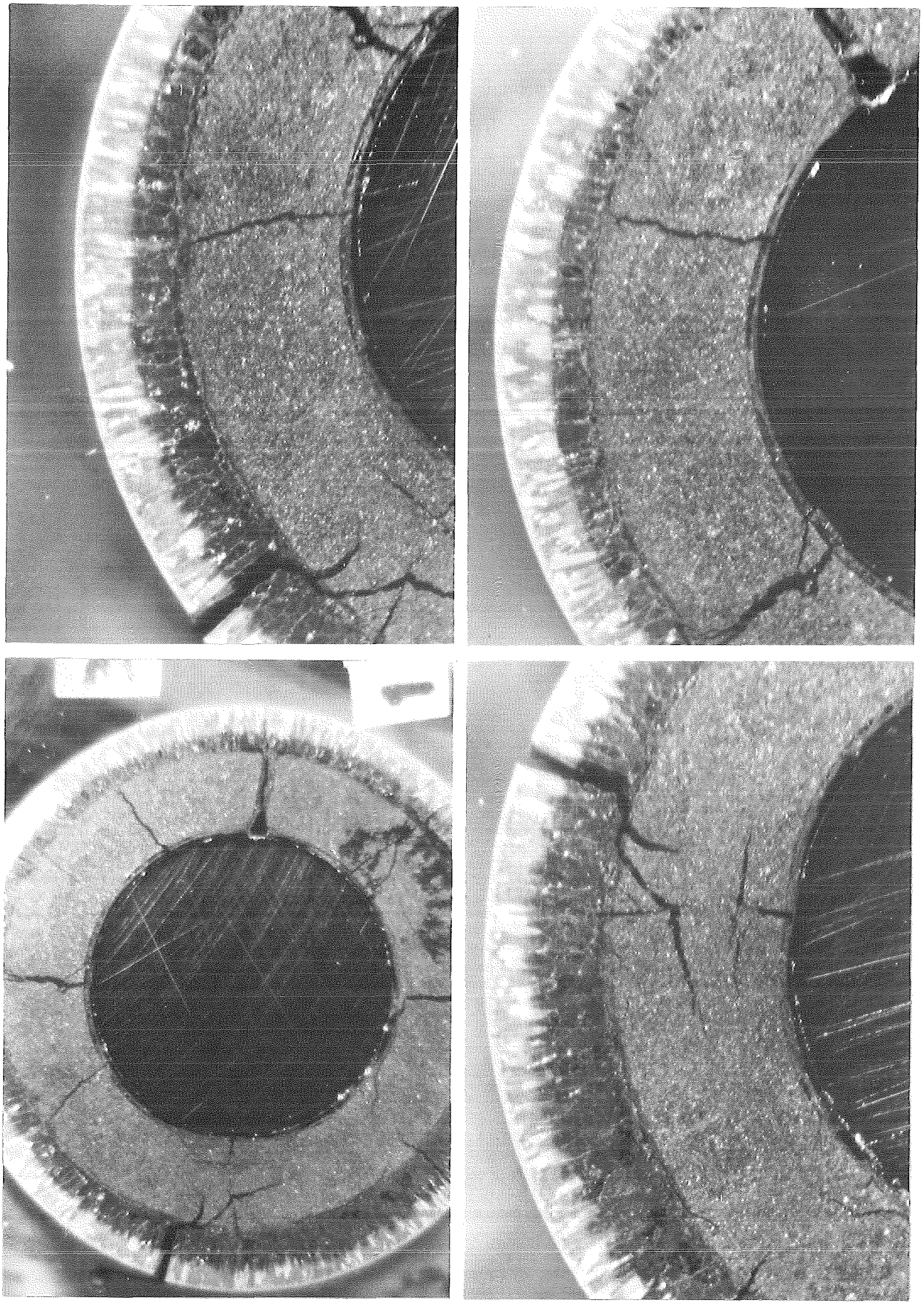

FIG.3-7: CROSS SECTION OF THE FUEL ROD SIMULATOR ESSI-3 AT 90 MM

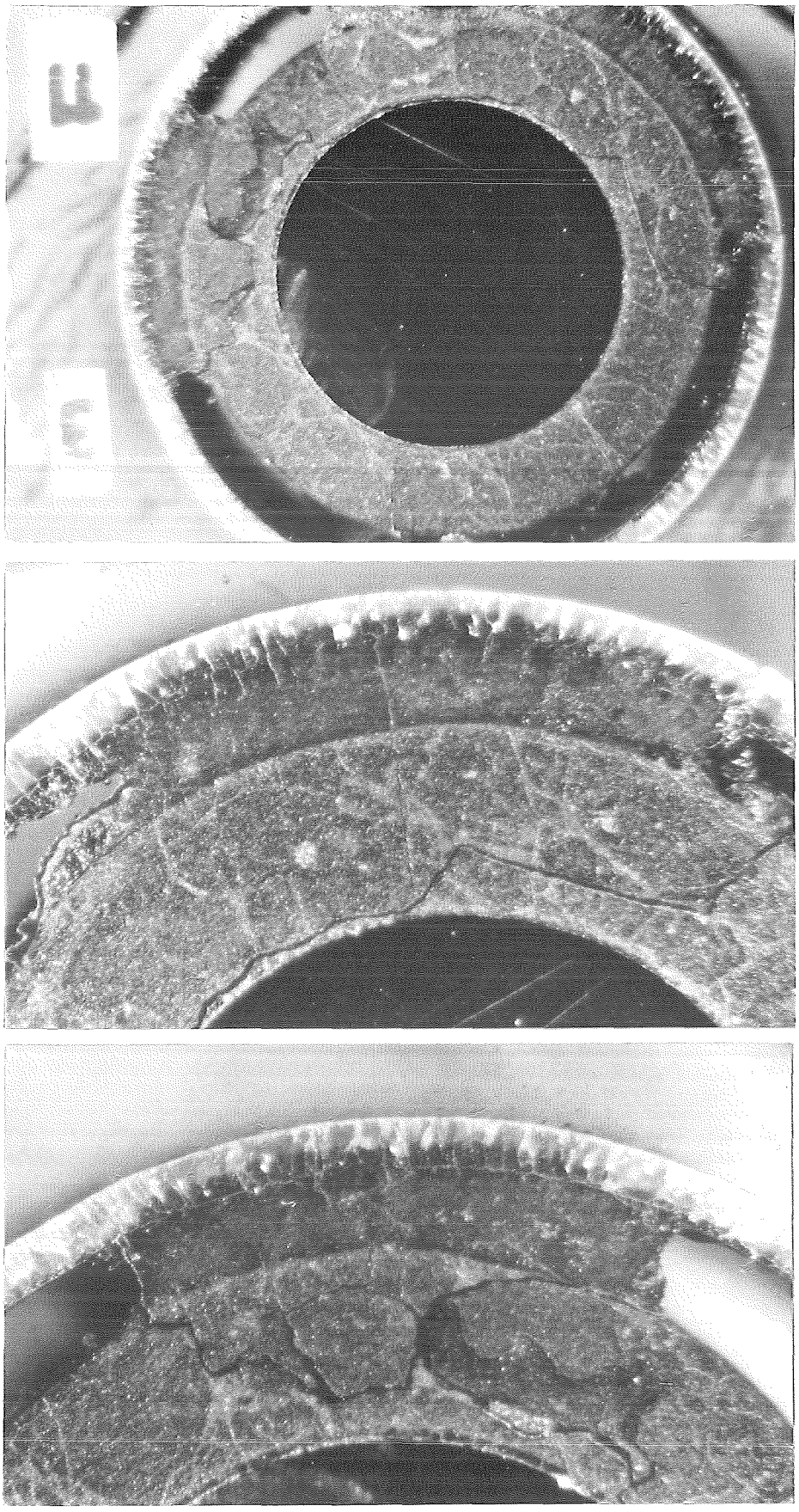

FIG.3-8: CROSS SECTION OF THE FUEL ROD SIMULATOR ESSI-3 AT 205 MM

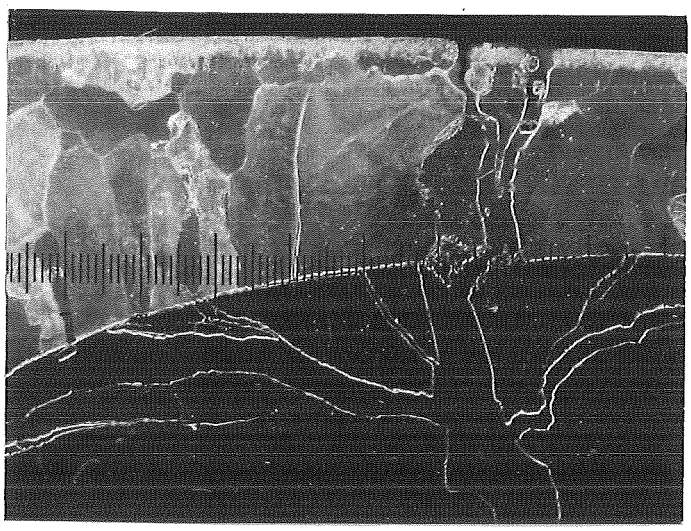

100×

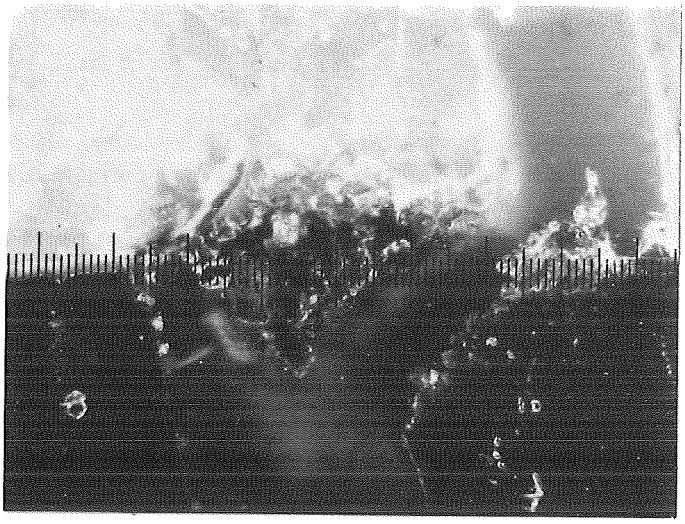

500×

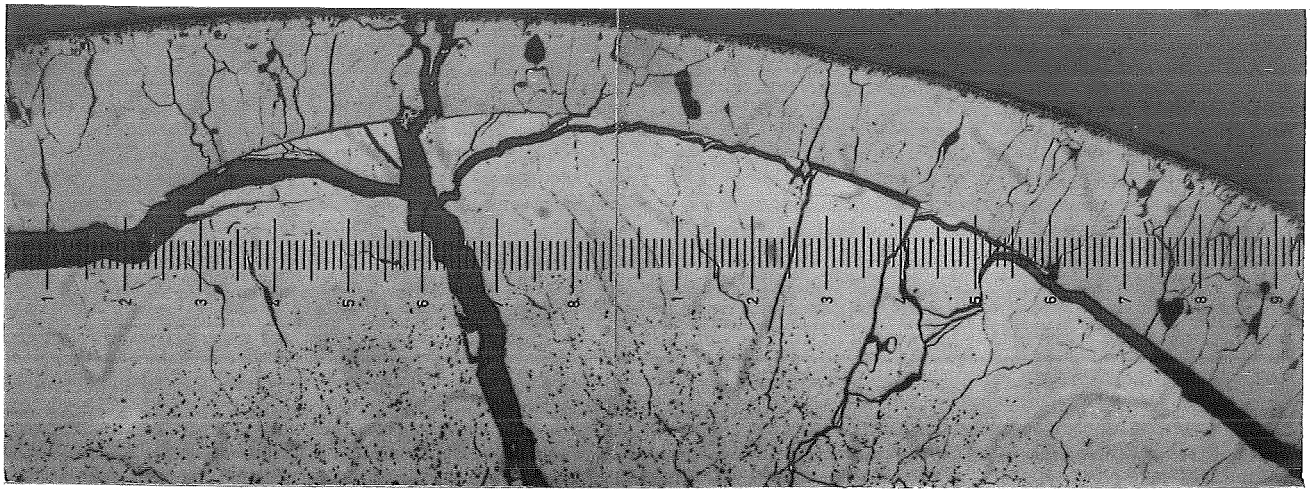

50×

50×

FIG.3-9: OXID LAYER VARIATIONS IN THE CROSS SECTION OF ESSI-3 AT THE 205 MM ELEVATION

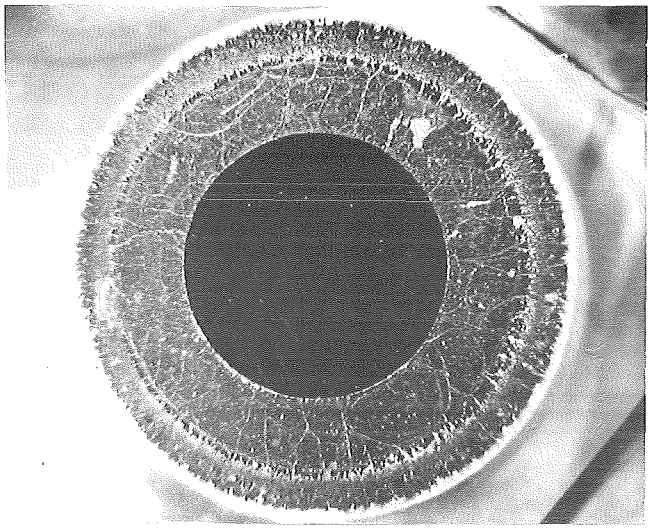

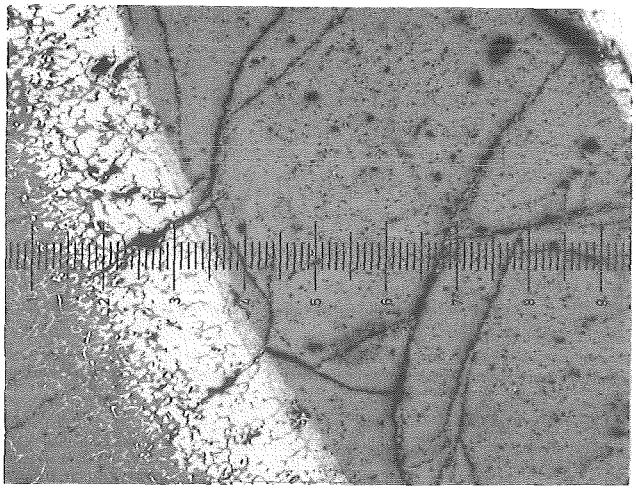

50x

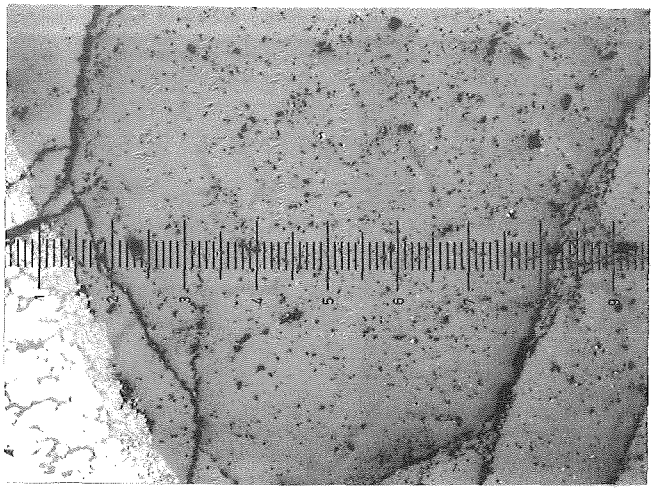

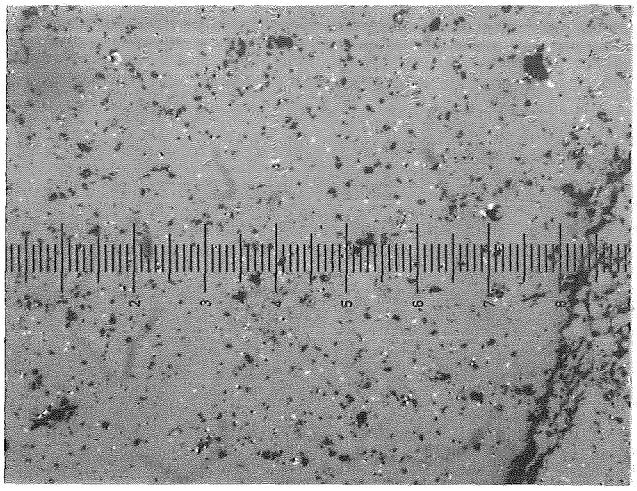

200x

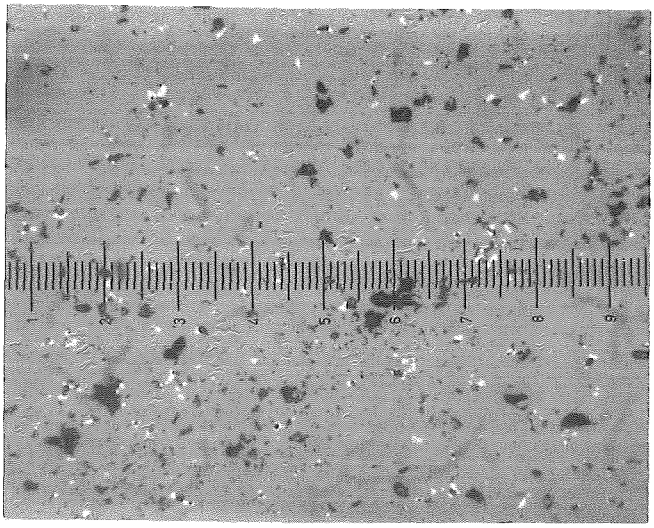

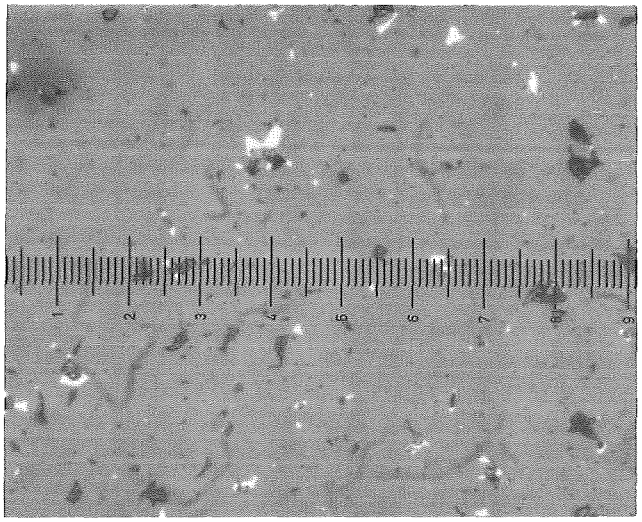

1000x

FIG.3-10: INCREASED ENLARGEMENT OF THE ESSI-3 CROSS SECTION AT THE 230 MM ELEVATION

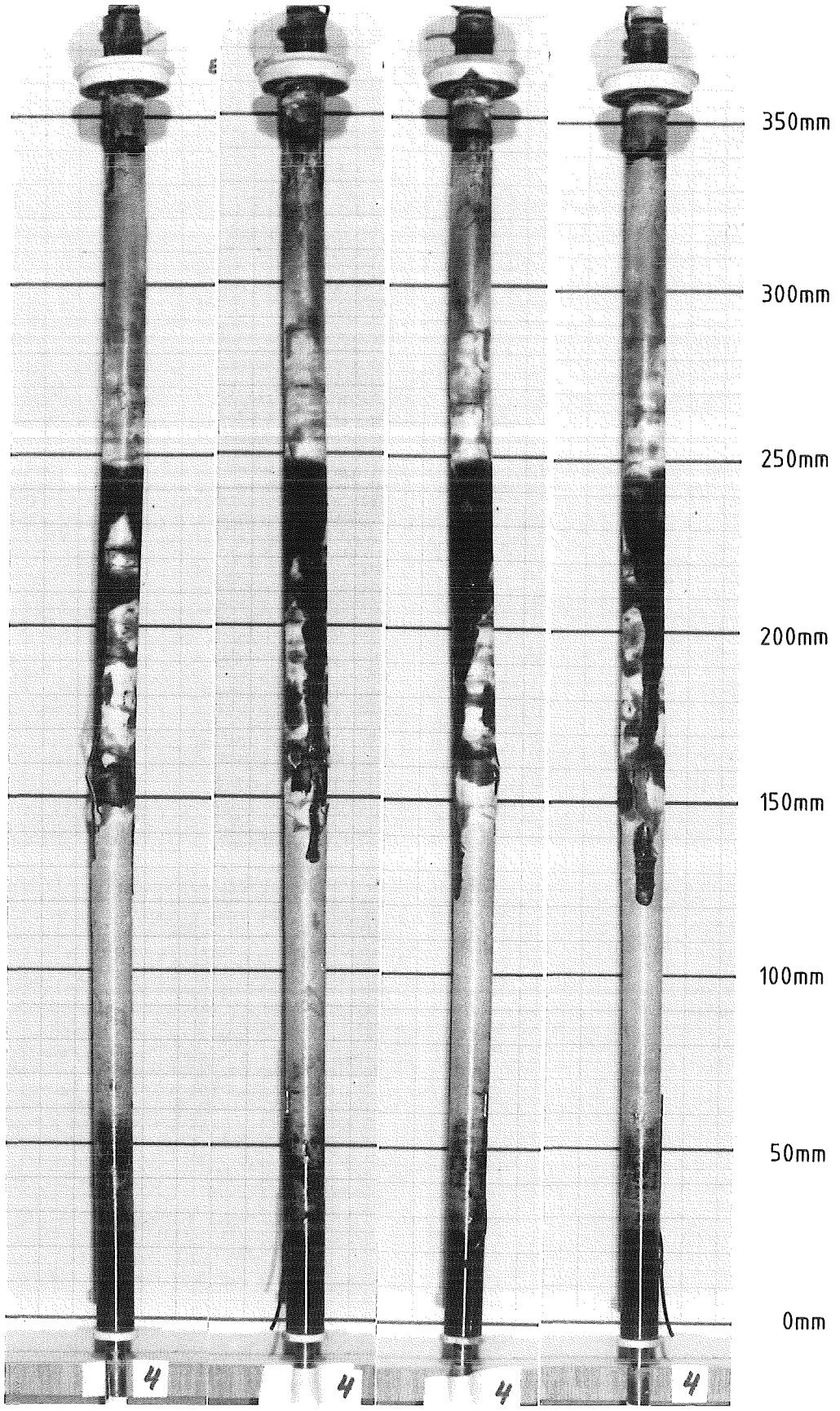

FIG. 4-1: POSTTEST APPEARANCE OF THE FUEL ROD SIMULATOR AND SCALE OF THE CROSS SECTION ELEVATIONS FOR ESSI-4

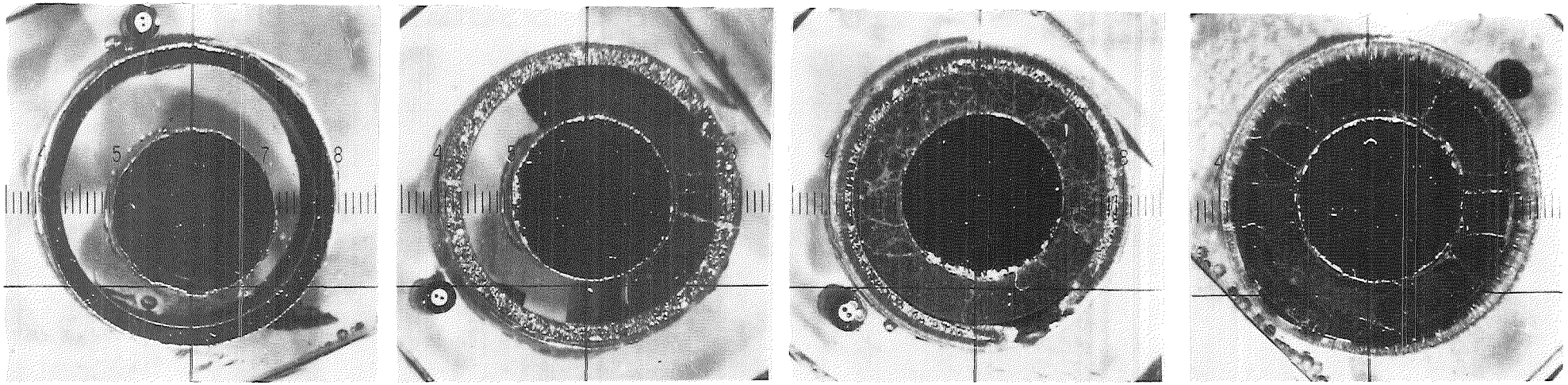

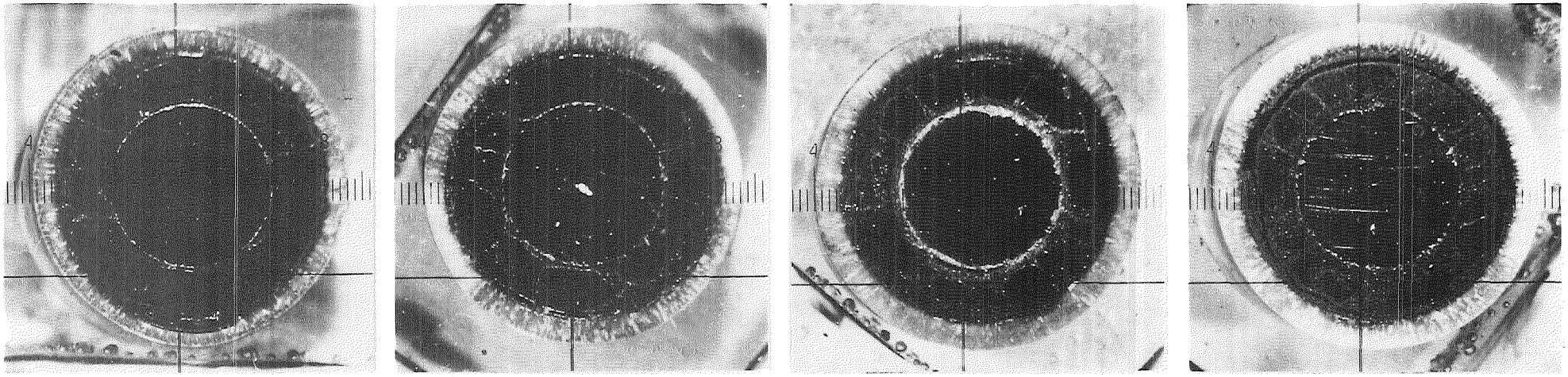

KfK

Fig.4-2: Cross Sections of Test ESSI-4

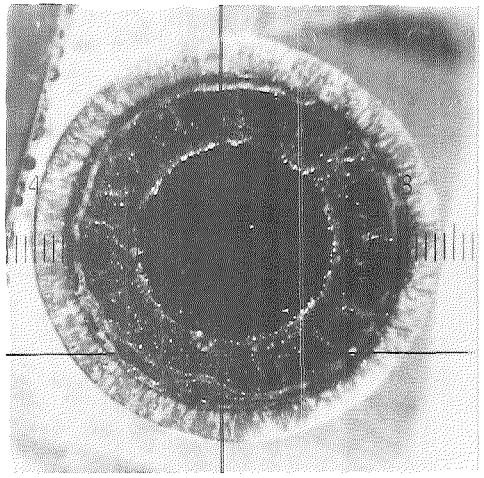

265mm

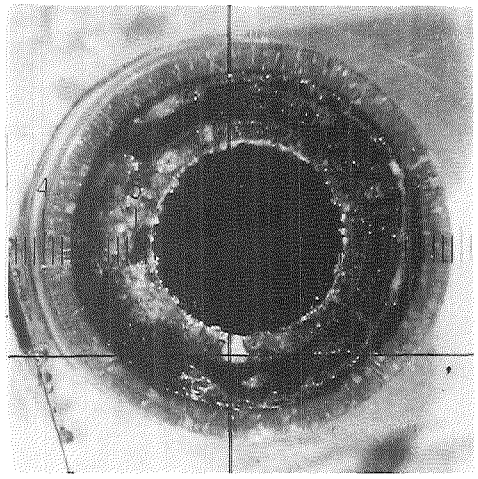

253mm

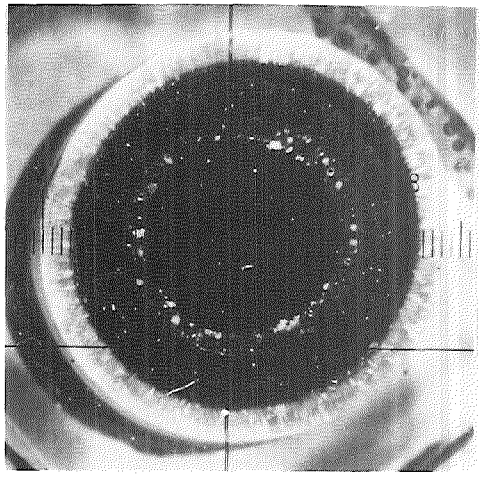

247mm

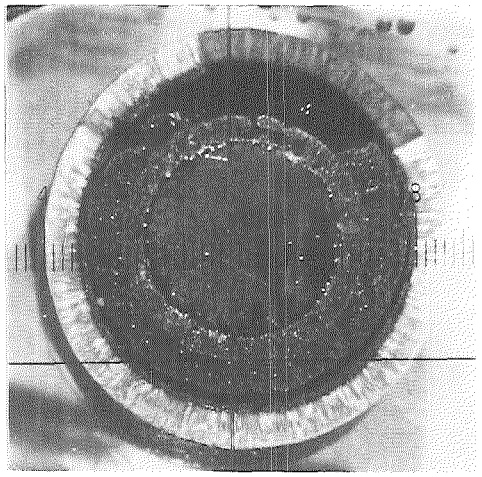

230mm

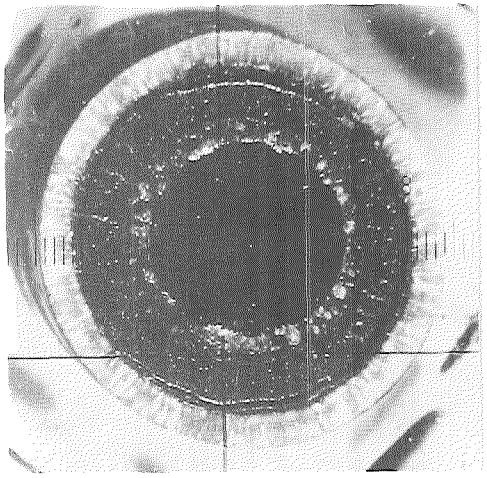

210mm

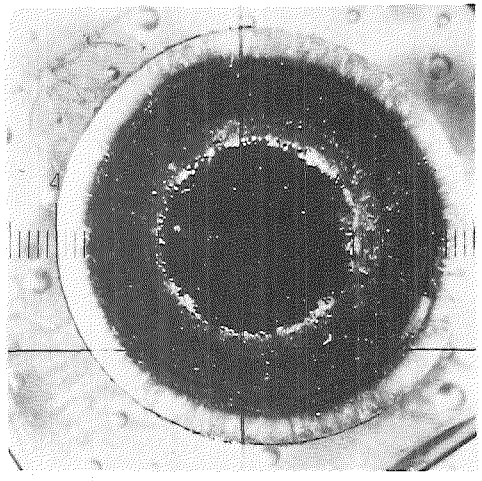

198mm

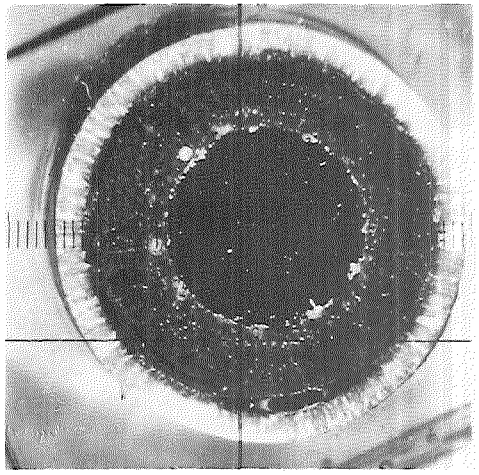

192mm

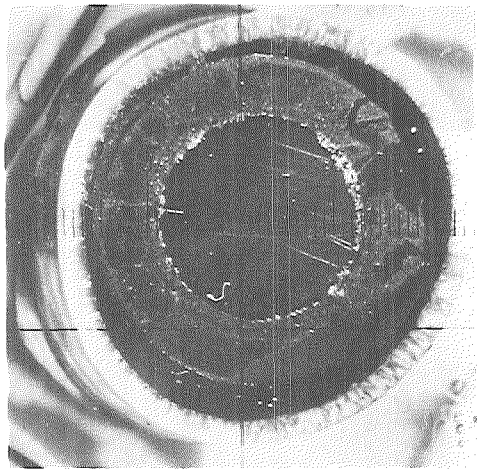

175mm

KfK

Fig.4-3: Cross Sections of Test ESSI-4

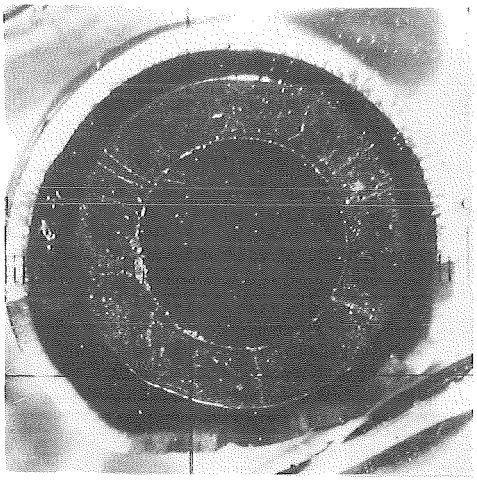

155mm

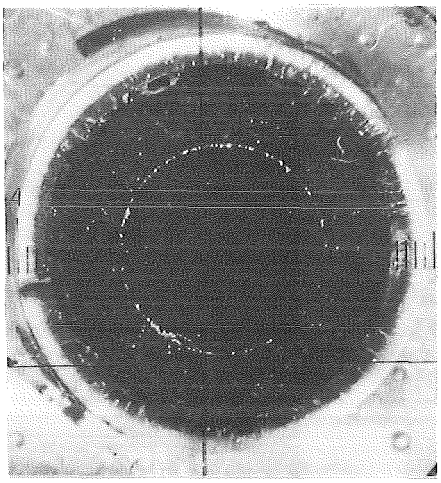

143mm

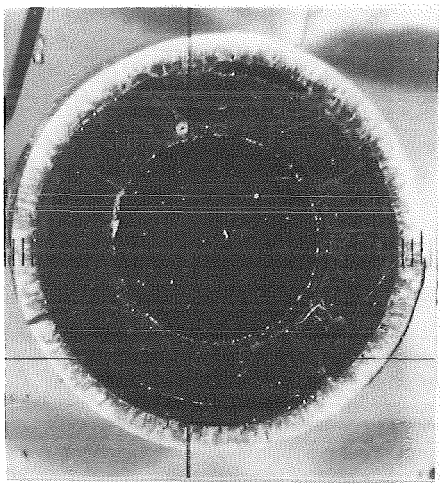

137mm

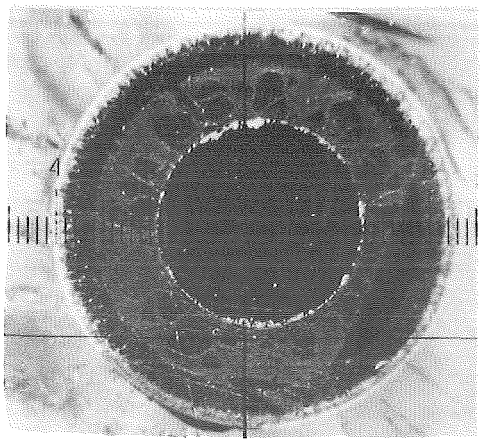

130mm

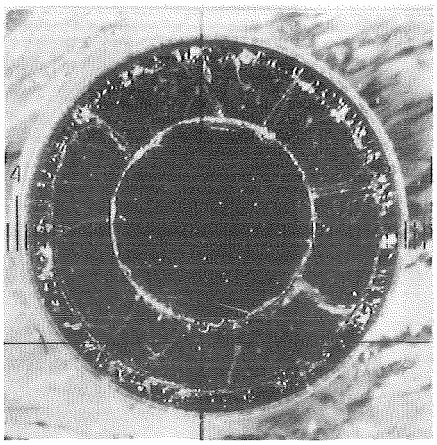

103mm

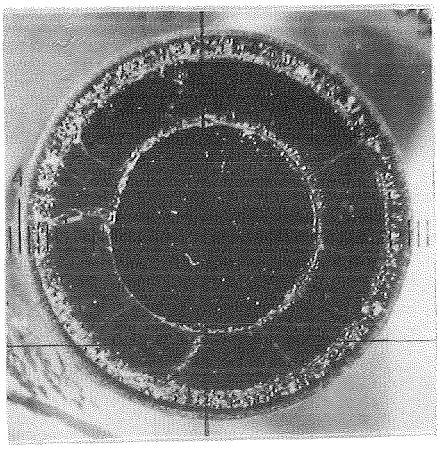

97mm

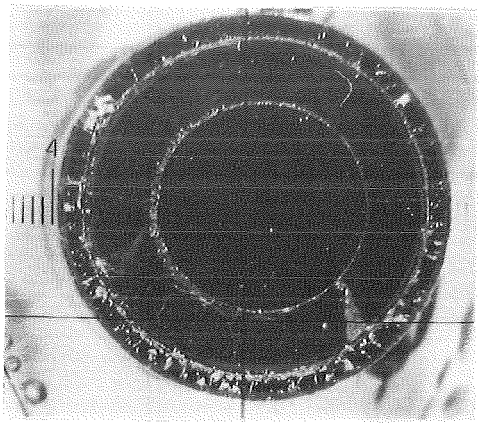

80mm

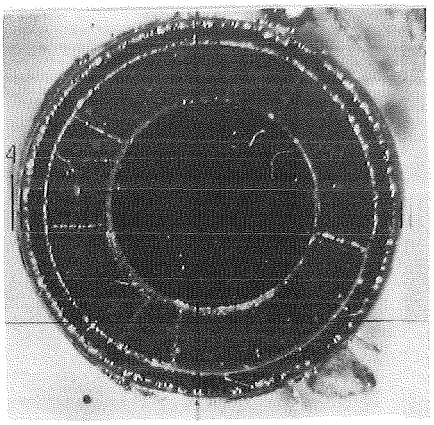

65mm

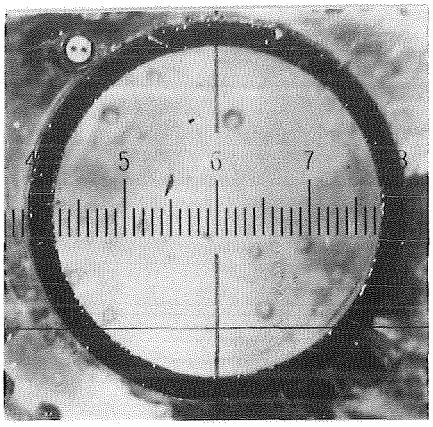

50mm

KfK

Fig.4-4: Cross Sections of Test ESSI-4

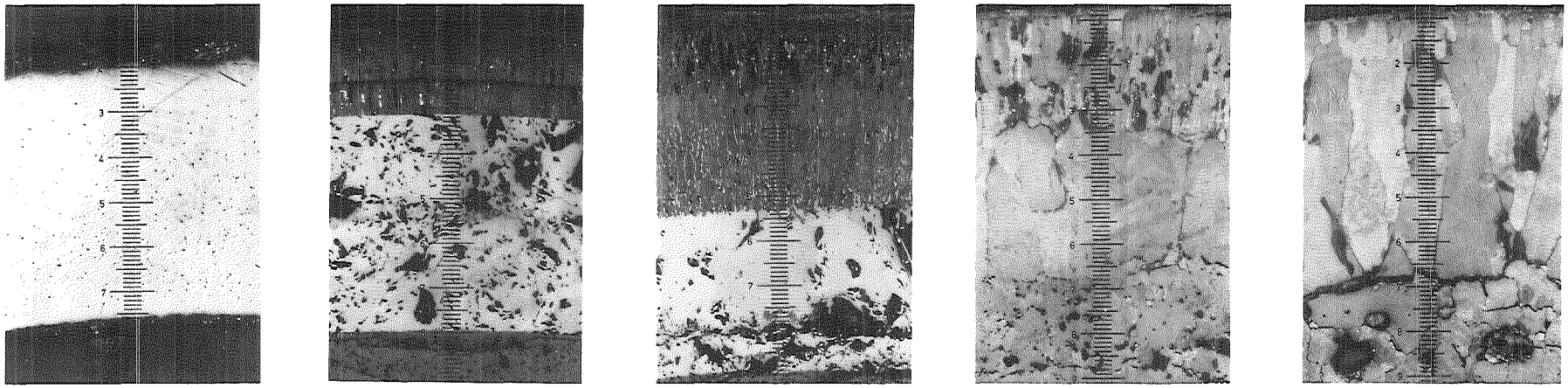

345mm 335mm 325mm 313mm 295mm

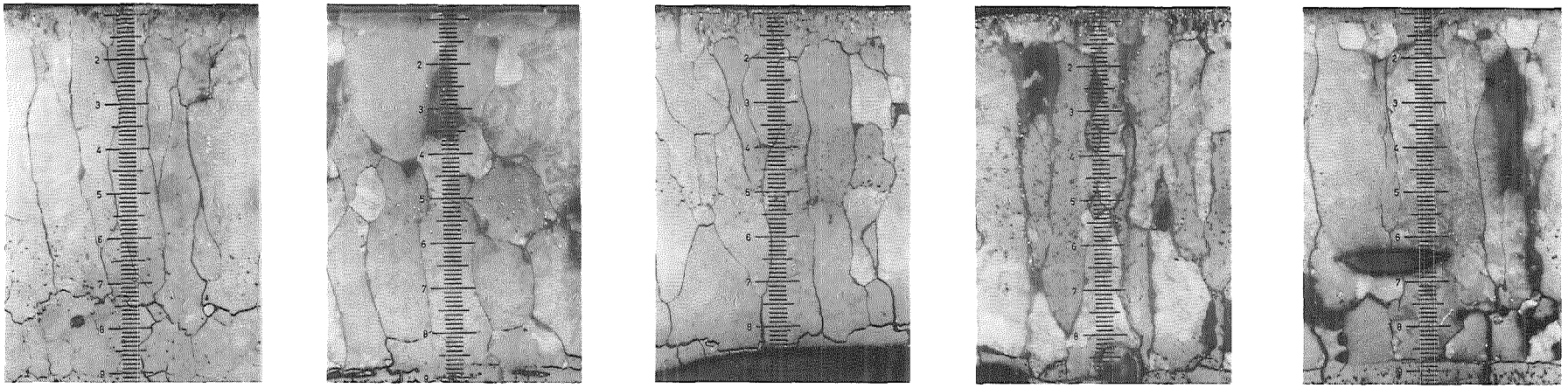

277mm 265mm 247mm 230mm 210mm

Fig. 4-5 : Enlarged View (100x) of Cross Sections From ESSI-4

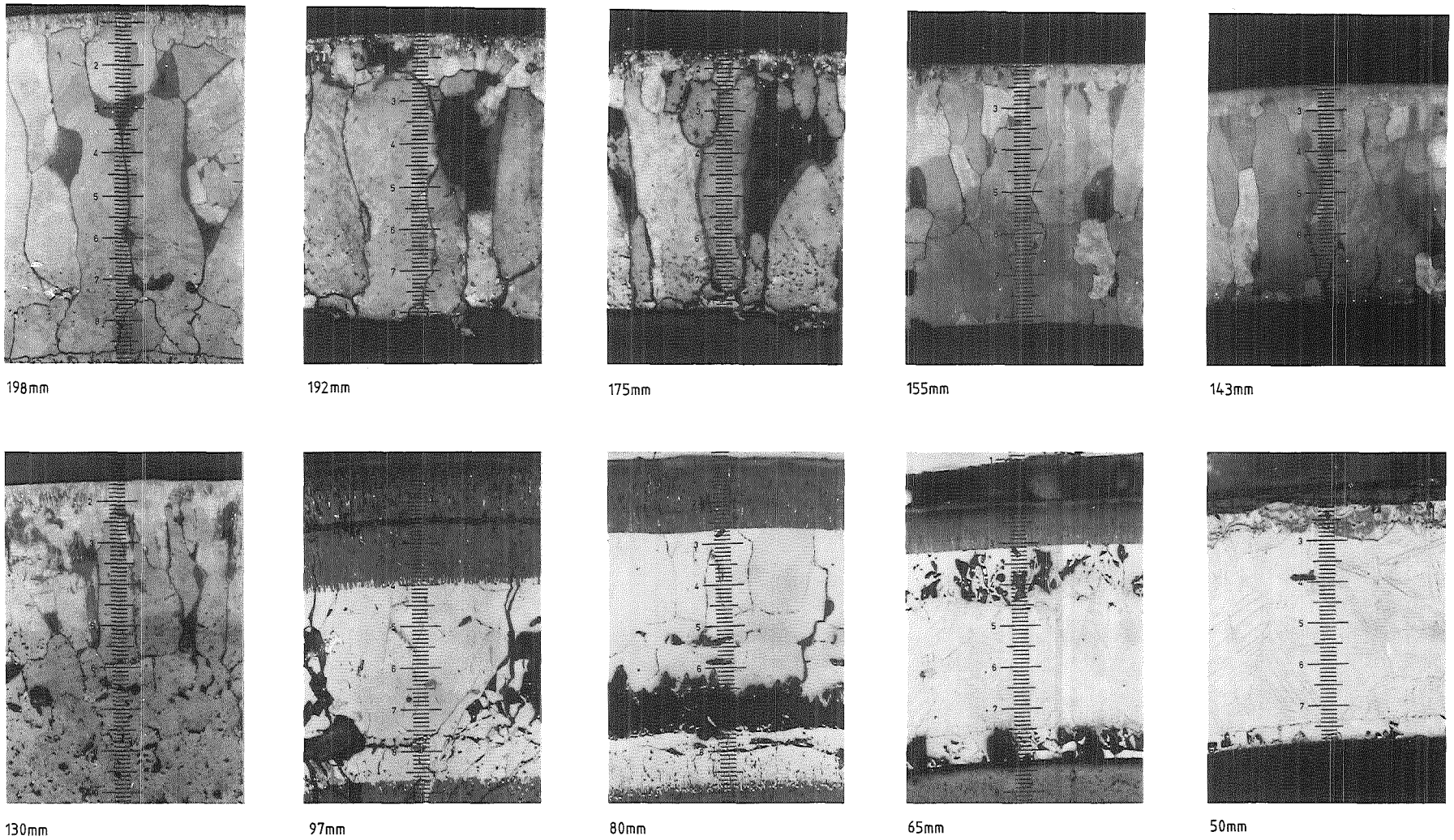

Fig. 4-6 : Enlarged View (100x) of Cross Sections From ESSI- 4

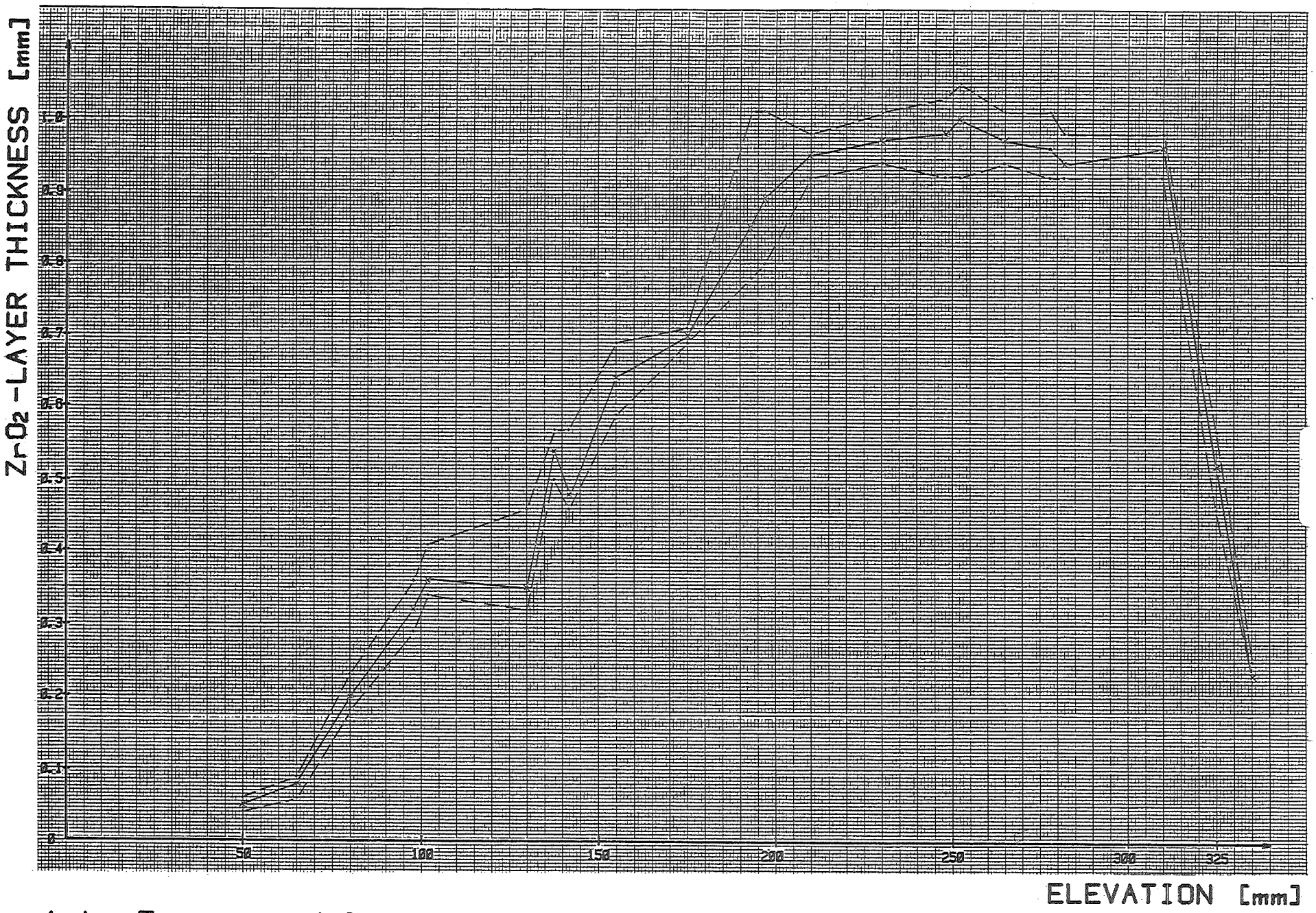

Fig.4-A: Zirconoxid layer thickness for test ESSI- 4 (– – – maximum or minimum value; —— mean value)

Fig. 4-B : Uranium oxide layer thickness for test ESSI- 4 (---maximum or minimum value; —— mean value)

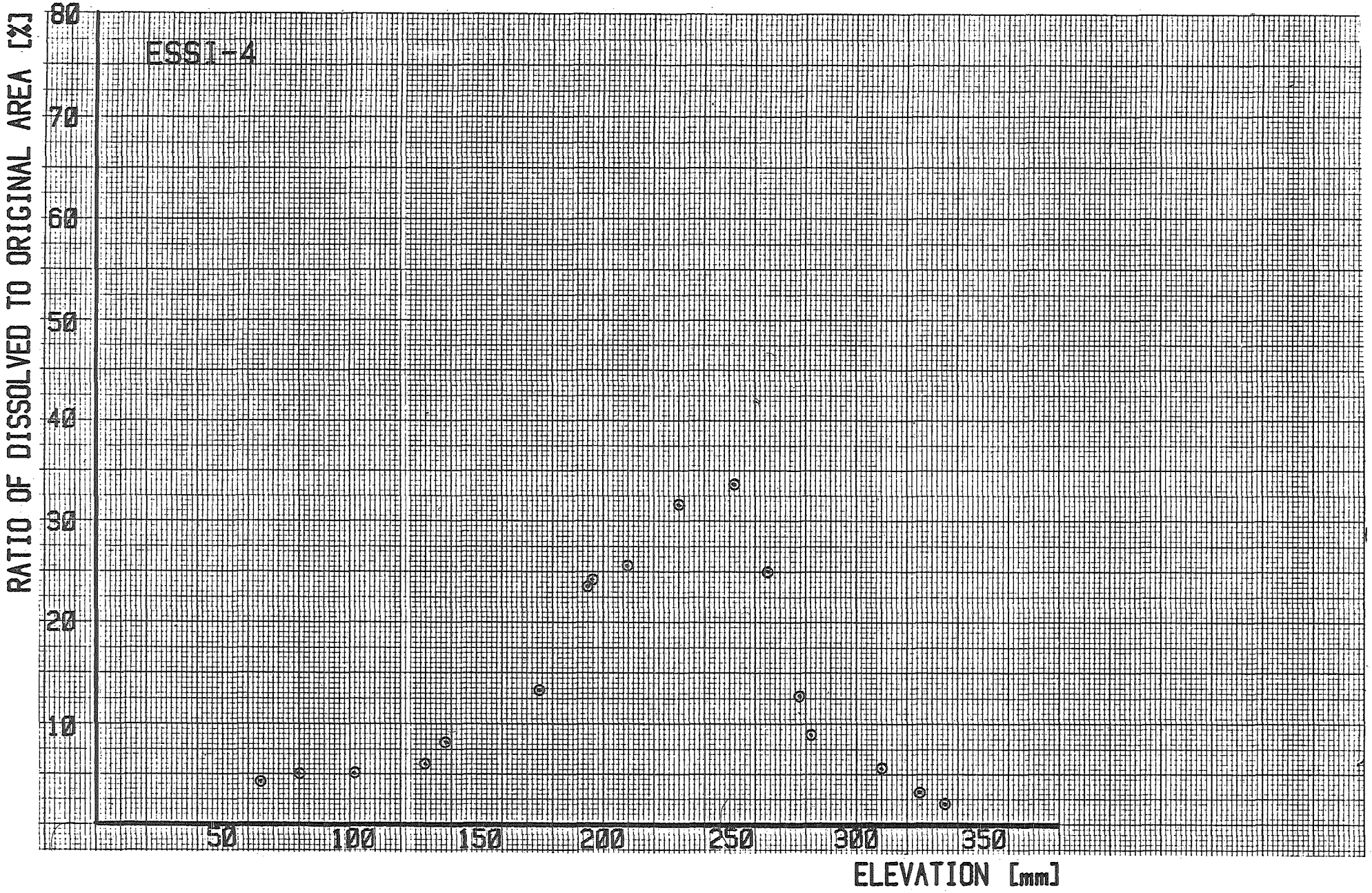

Fig.: 4-C
Dissolution of the UO_2-pellet at different elevations (ESSI-4)

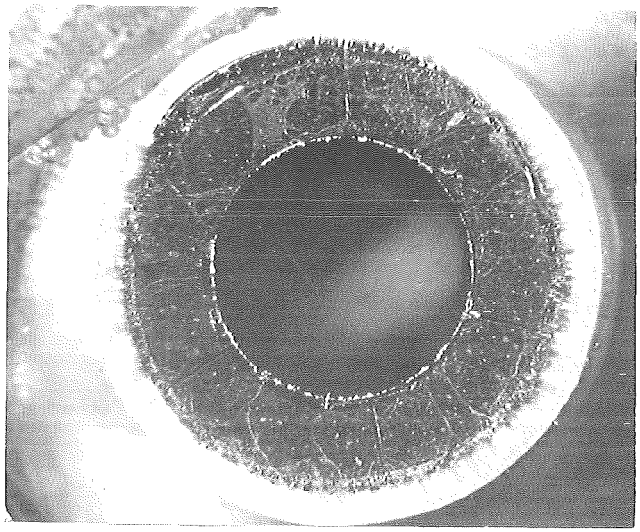

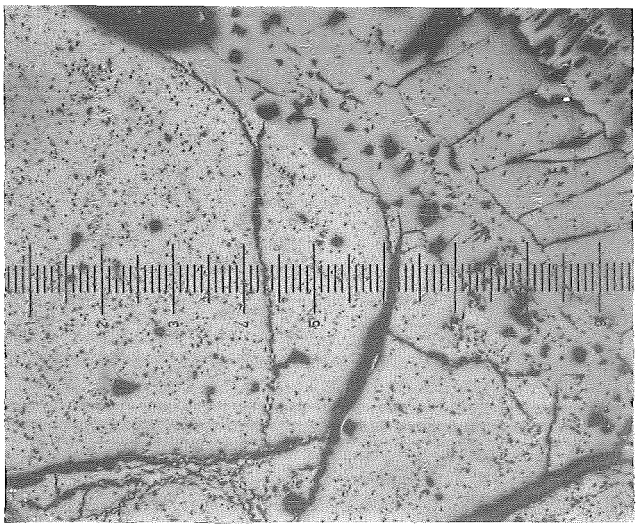

50×

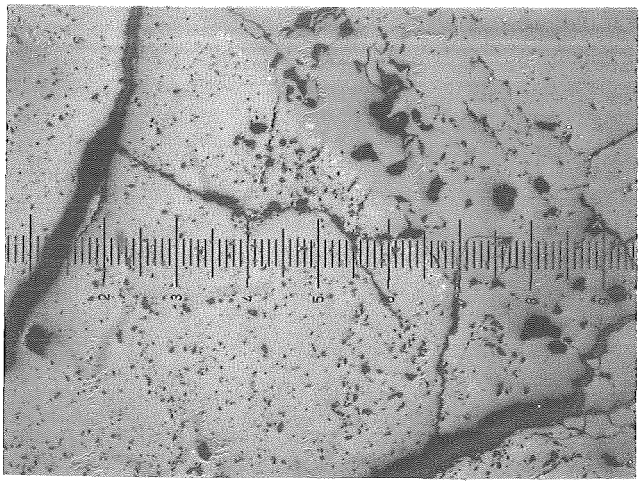

100×

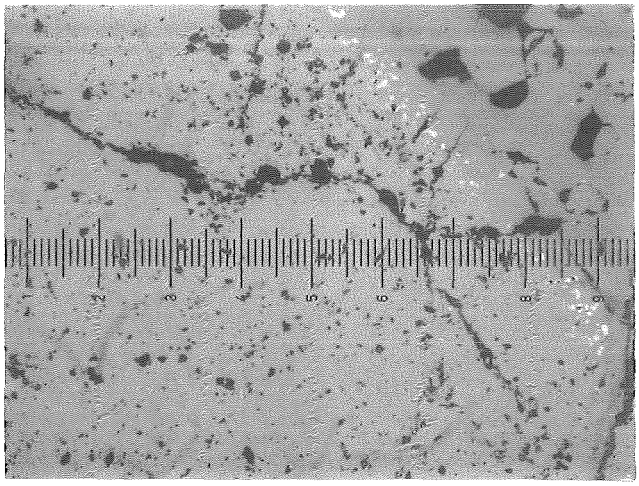

200×

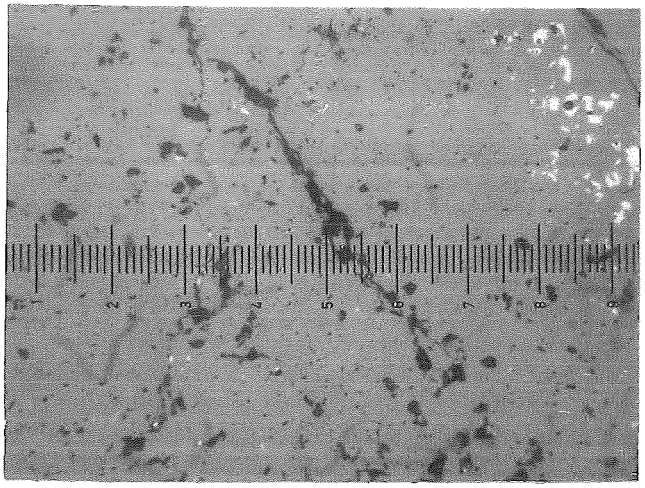

500×

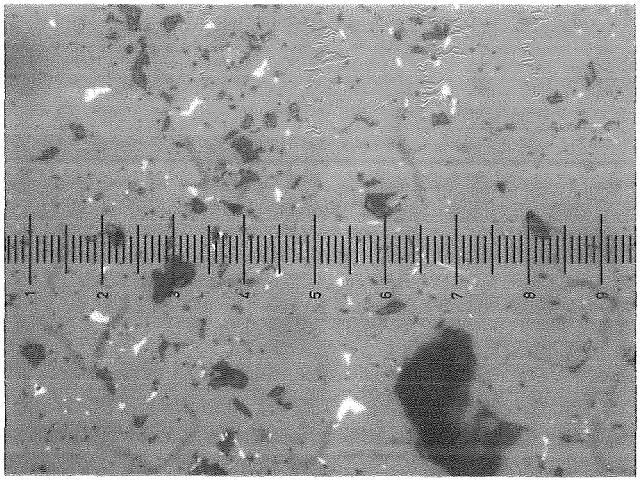

1000×

FIG.4-7: CONTACT BETWEEN UO2 AND OXIDIZED CLADDING IN THE ESSI-4 CROSS SECTION AT 310 MM SHOWN IN DIFFERENT ENLARGEMENTS

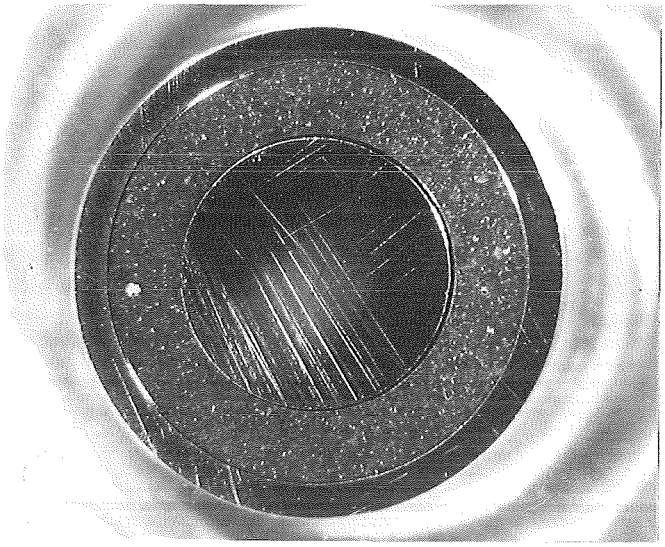

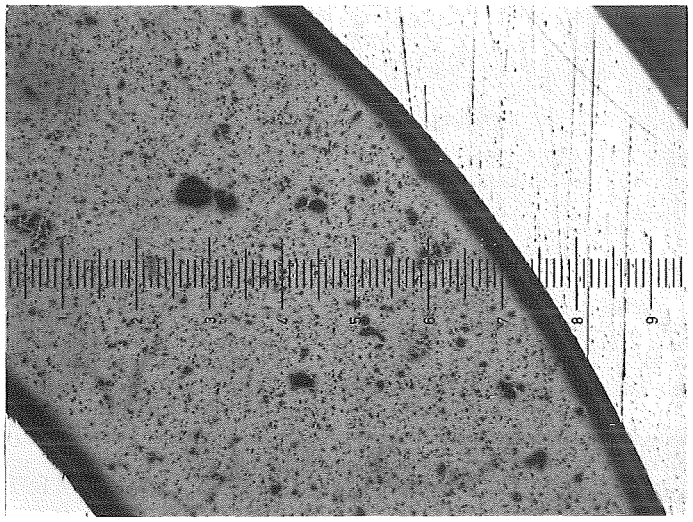

50×

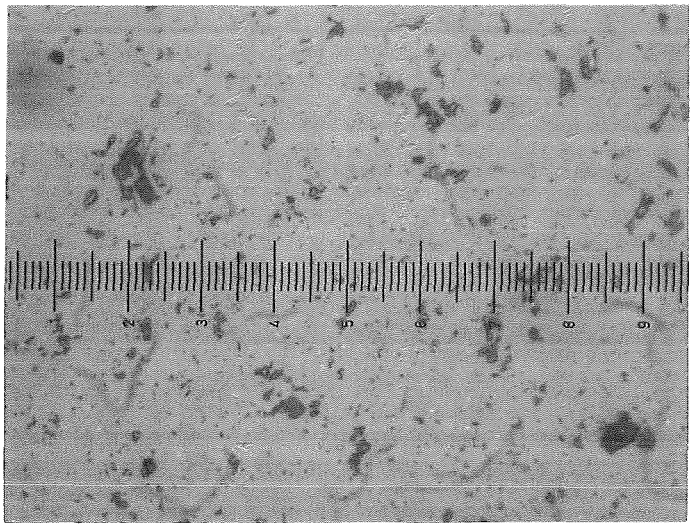

1000×

FIG.4-8: CROSS SECTION OF THE UNHEATED FUEL ROD SIMULATOR SHOWN IN DIFFERENT ENLARGEMENTS

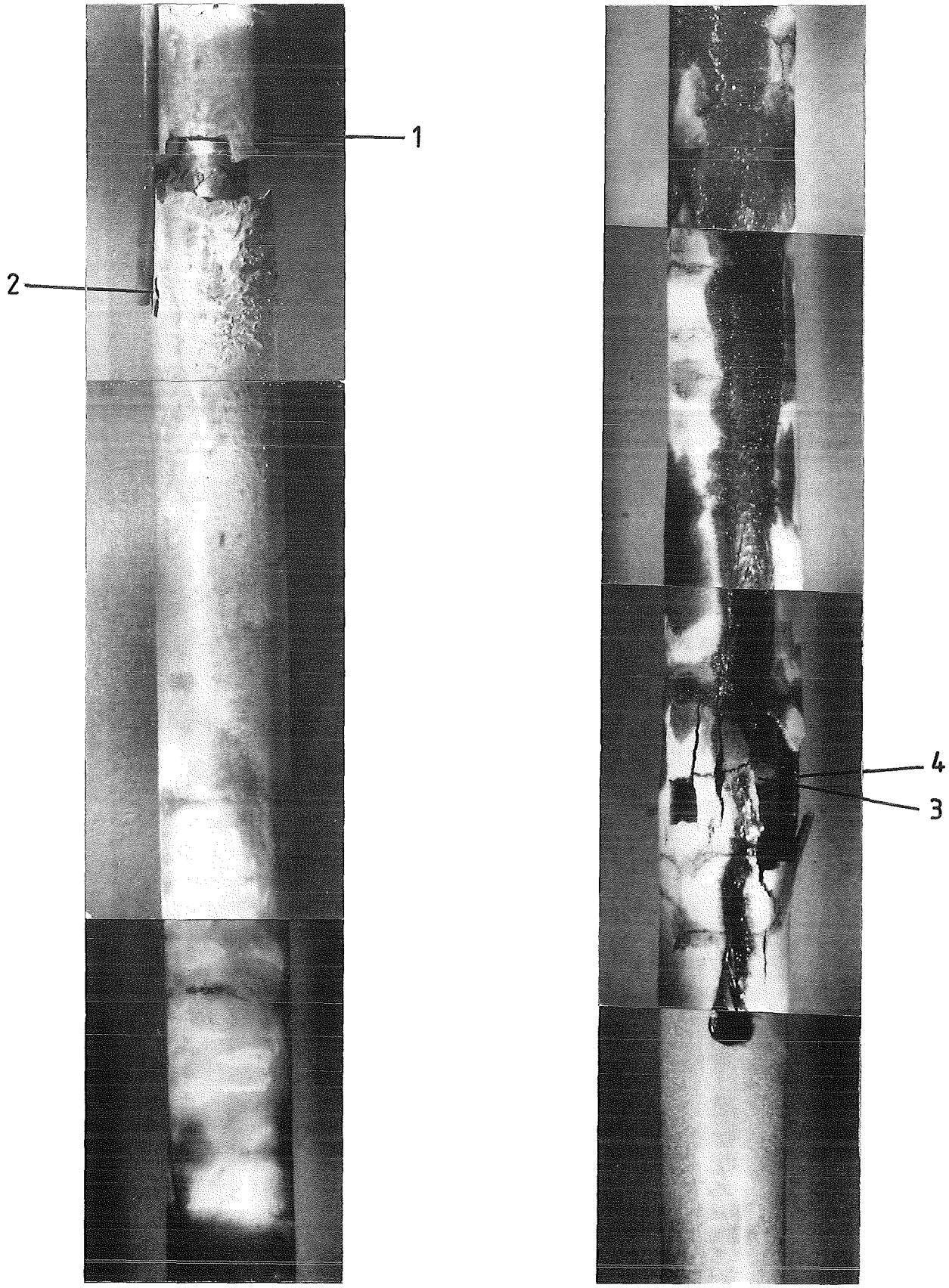

FIG.4-9: LOCATIONS OF ENLARGED VIEWS OF THE FUEL ROD SIMULATOR ESSI-4

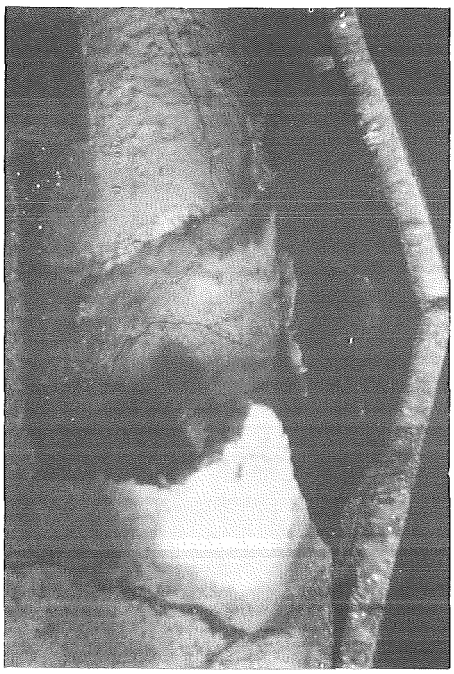

3 6x

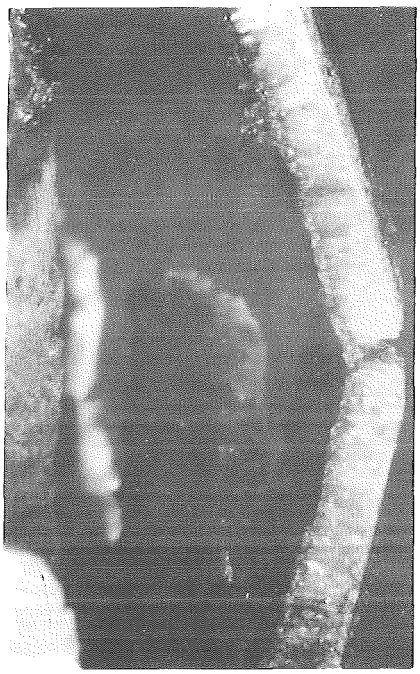

3 12x

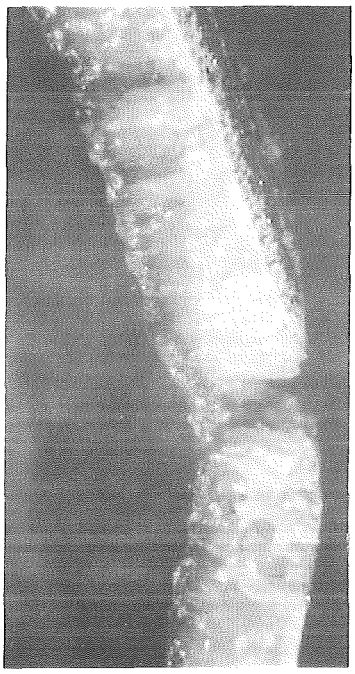

3 25x

4 6x

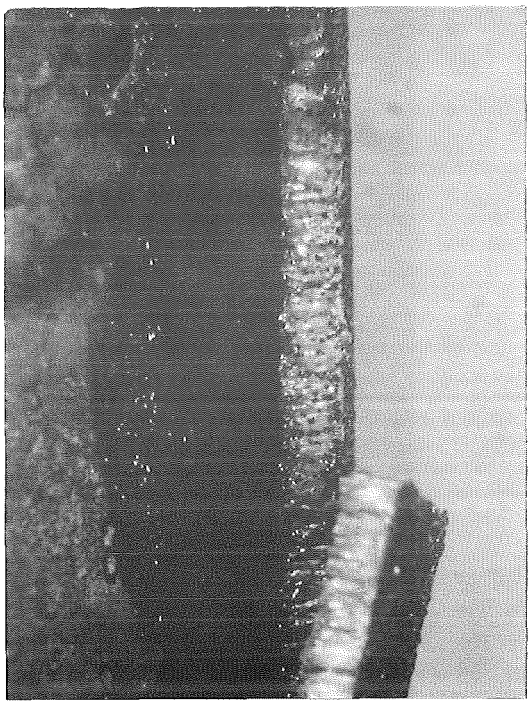

4 12x

FIG.4-10: ENLARGED VIEWS OF THE FUEL ROD SIMULATOR ESSI-4 (POSITION SEE FIG.4-9)

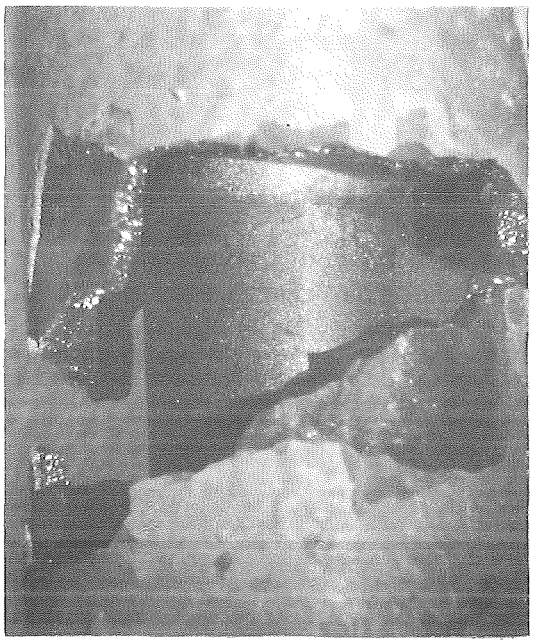

1 6x

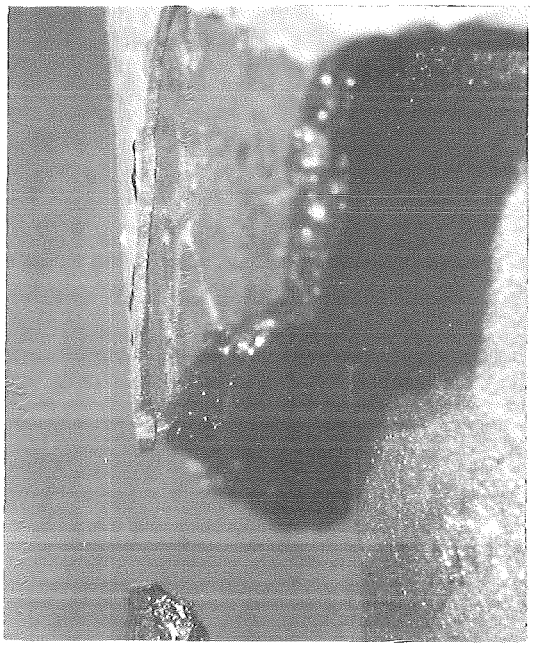

1 12x

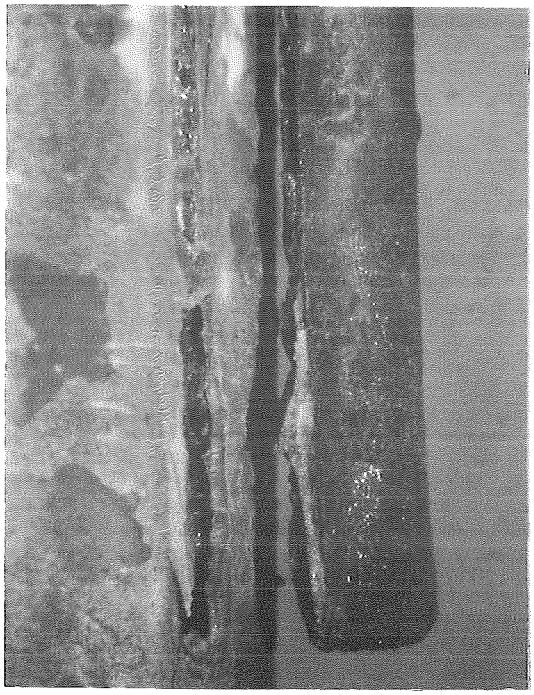

2 12x

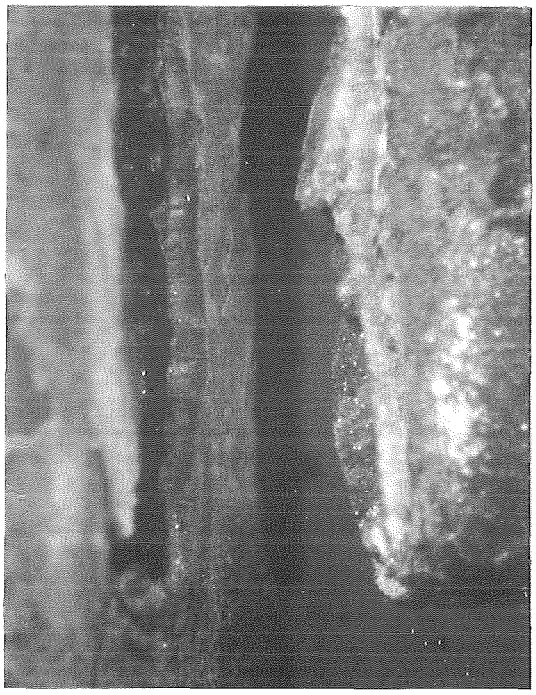

2 25x

FIG.4-11: ENLARGED VIEWS OF THE FUEL ROD SIMULATOR ESSI-4
(POSITION SEE FIG.4-9)

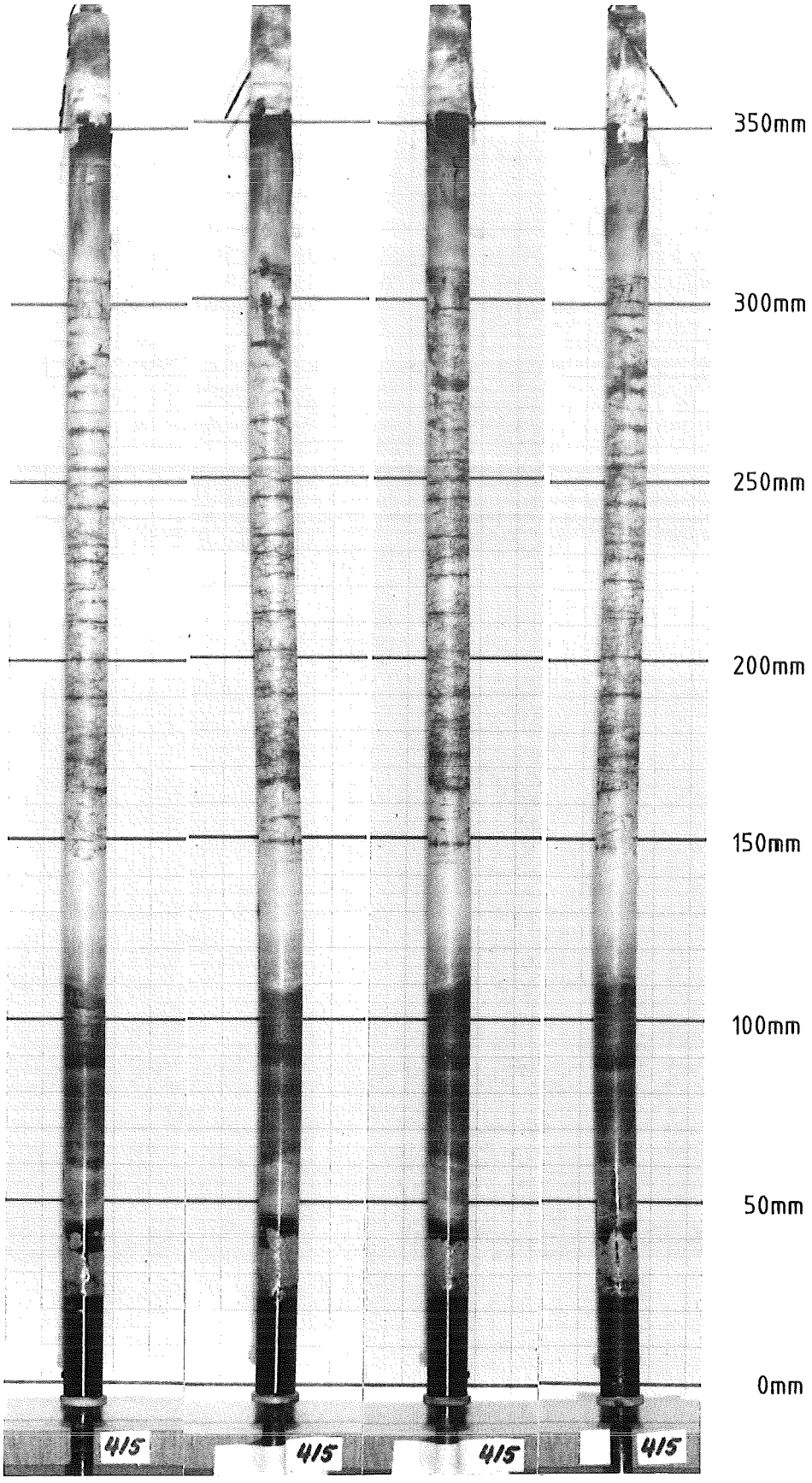

FIG.4/5-1: POSTTEST APPEARANCE OF THE FUEL ROD SIMULATOR AND SCALE OF THE CROSS SECTION ELEVATIONS FOR ESSI-4/5

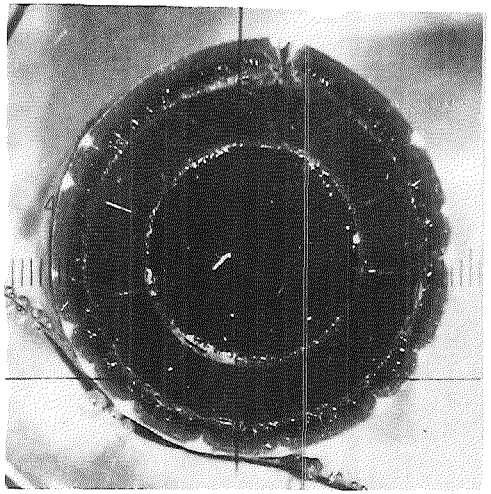

325mm

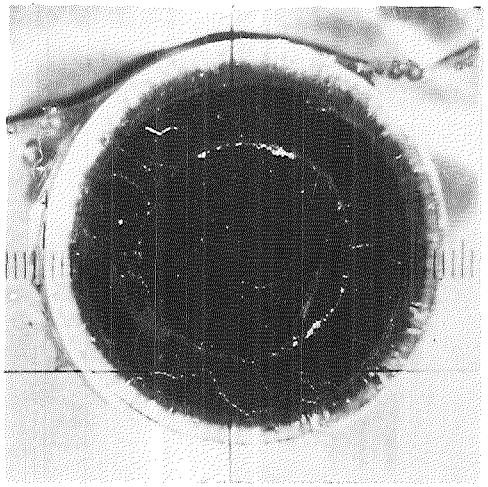

310mm

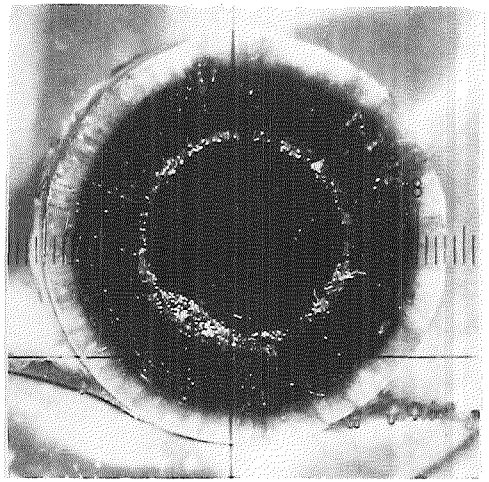

280mm

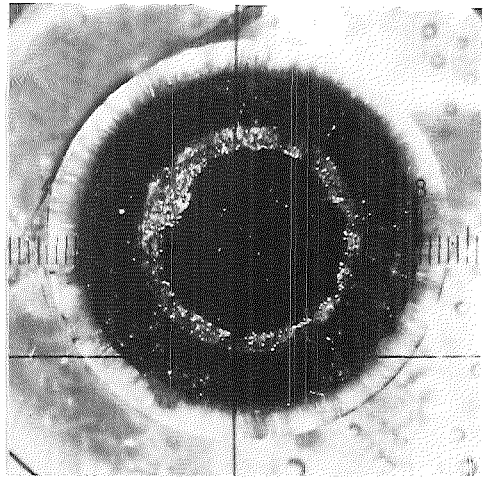

265mm

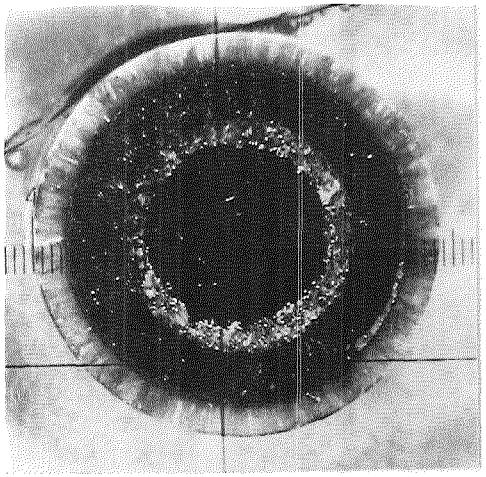

250mm

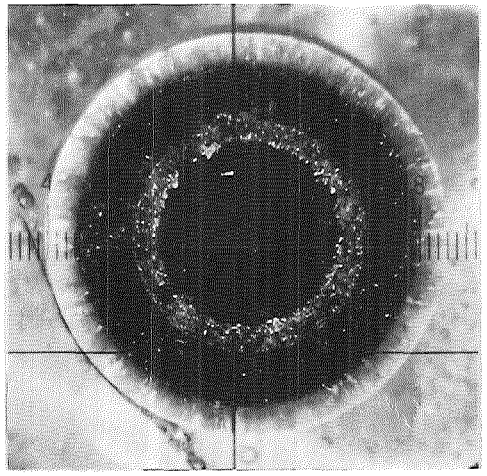

240mm

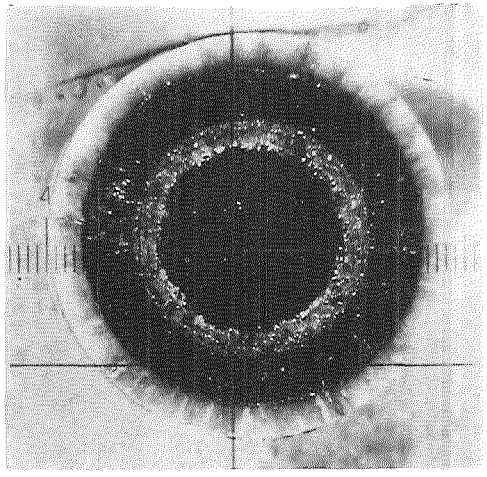

225mm

KfK

Fig. 4/5-2 : Cross Sections of Test ESSI-4/5

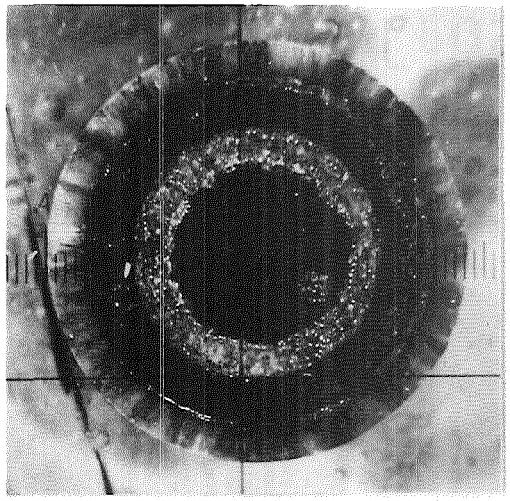

210mm

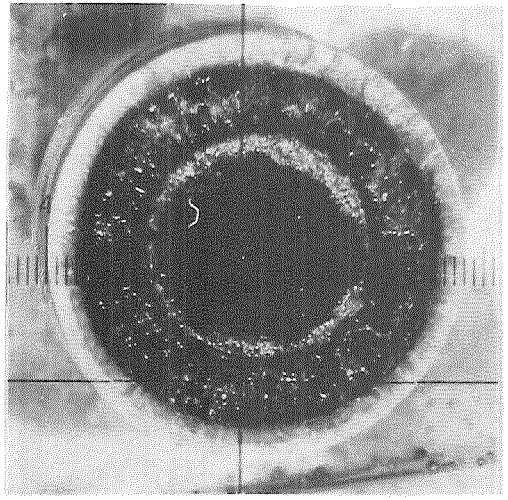

155mm

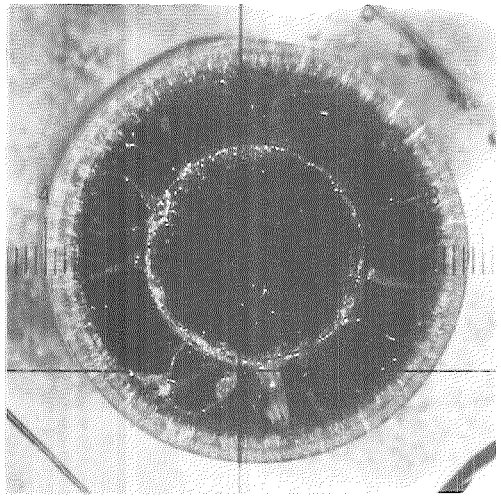

115mm

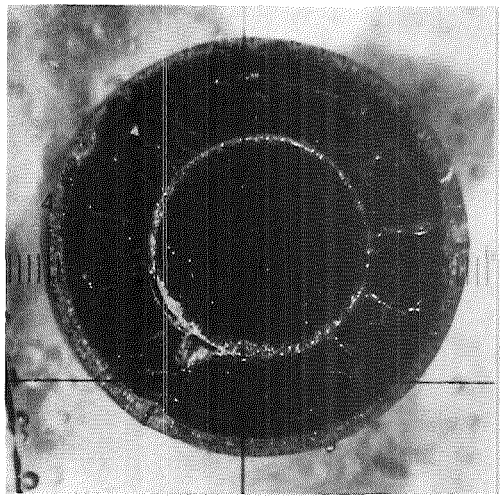

100mm

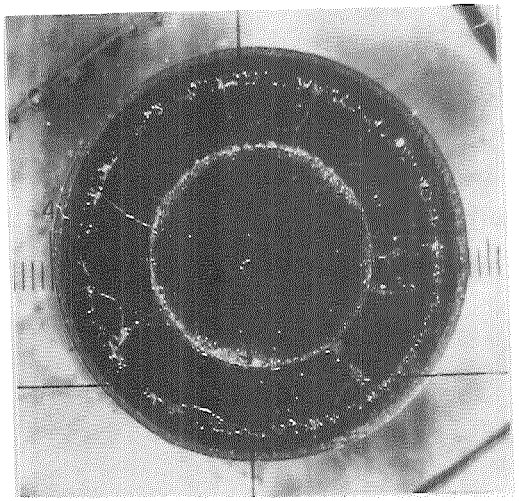

85mm

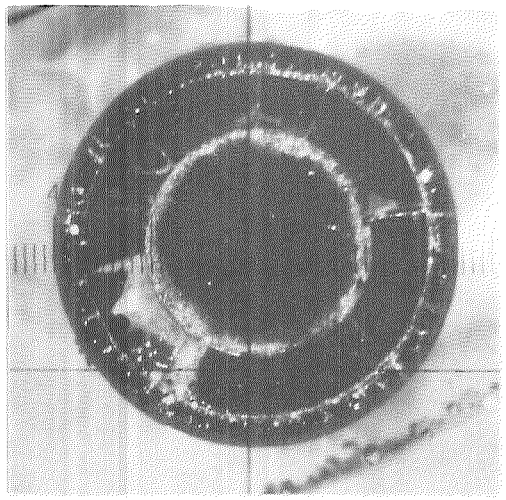

65mm

KfK

Fig. 4/5-3 : Cross Sections of Test ESSI-4/5

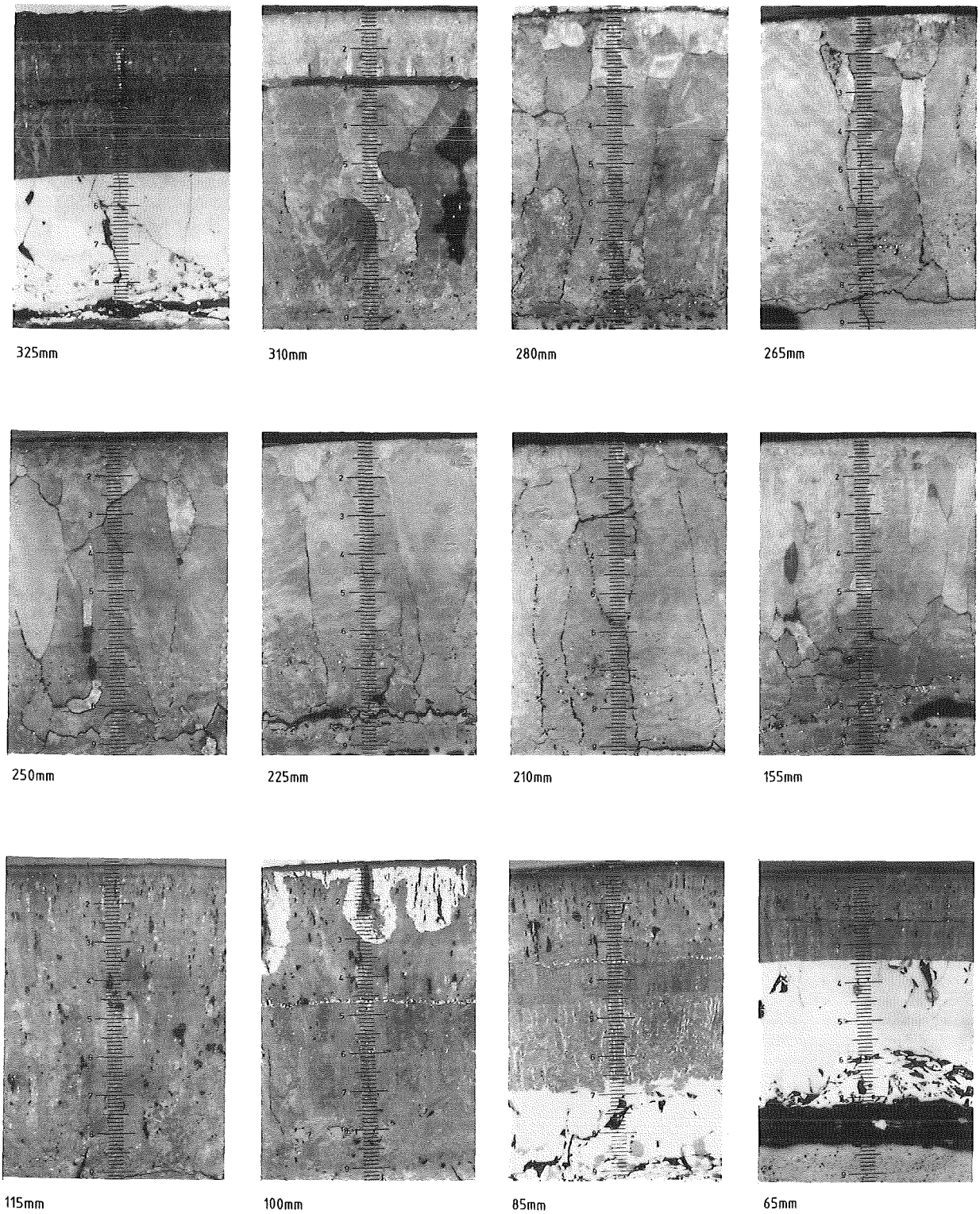

Fig. 4/5-4 : Enlarged View (100x) of Cross Sections From ESSI-4/5

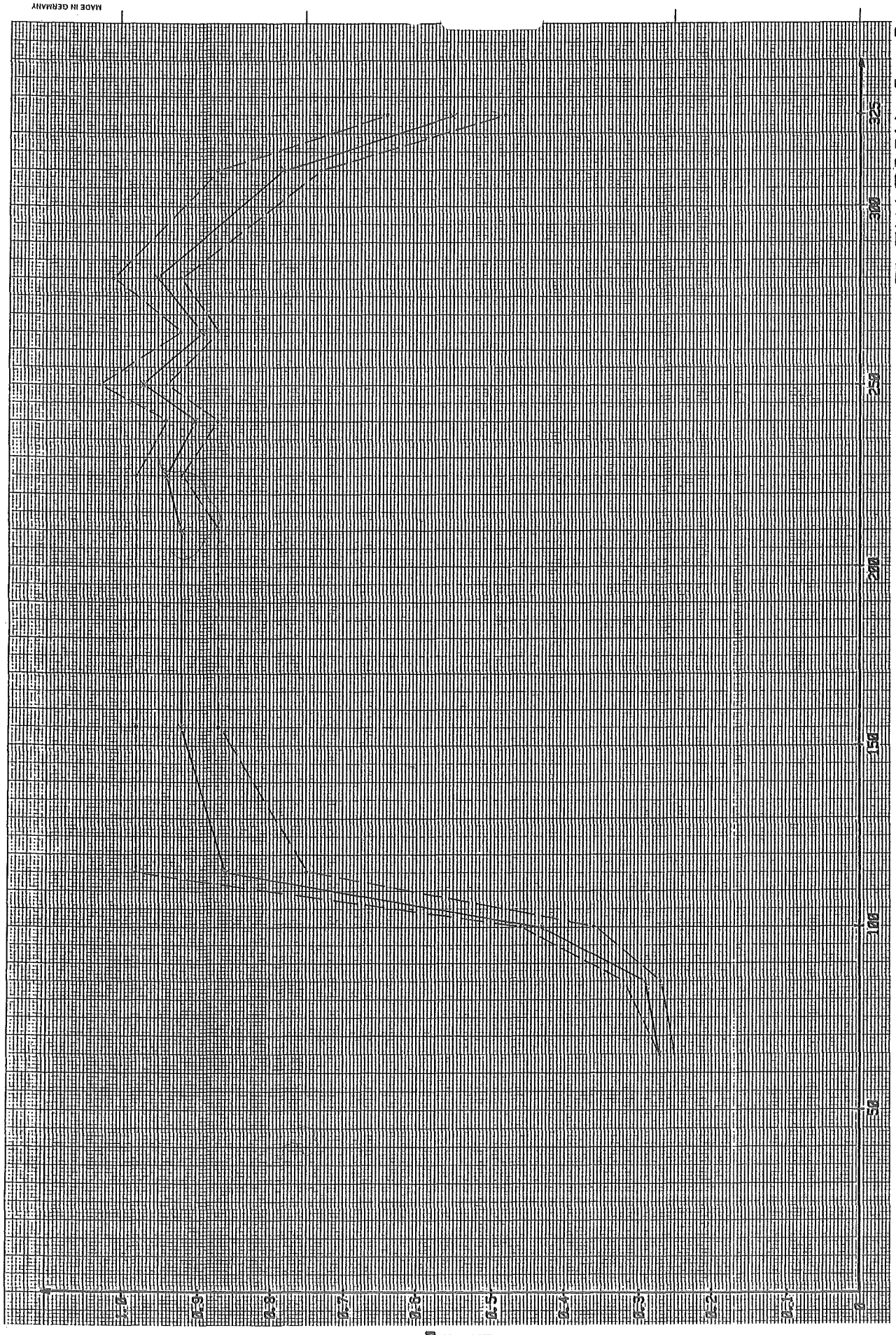

Fig.4/5-A:Zirconoxid layer thickness for test ESSI-4/5(- - -maximum or minimum value; ——mean value)

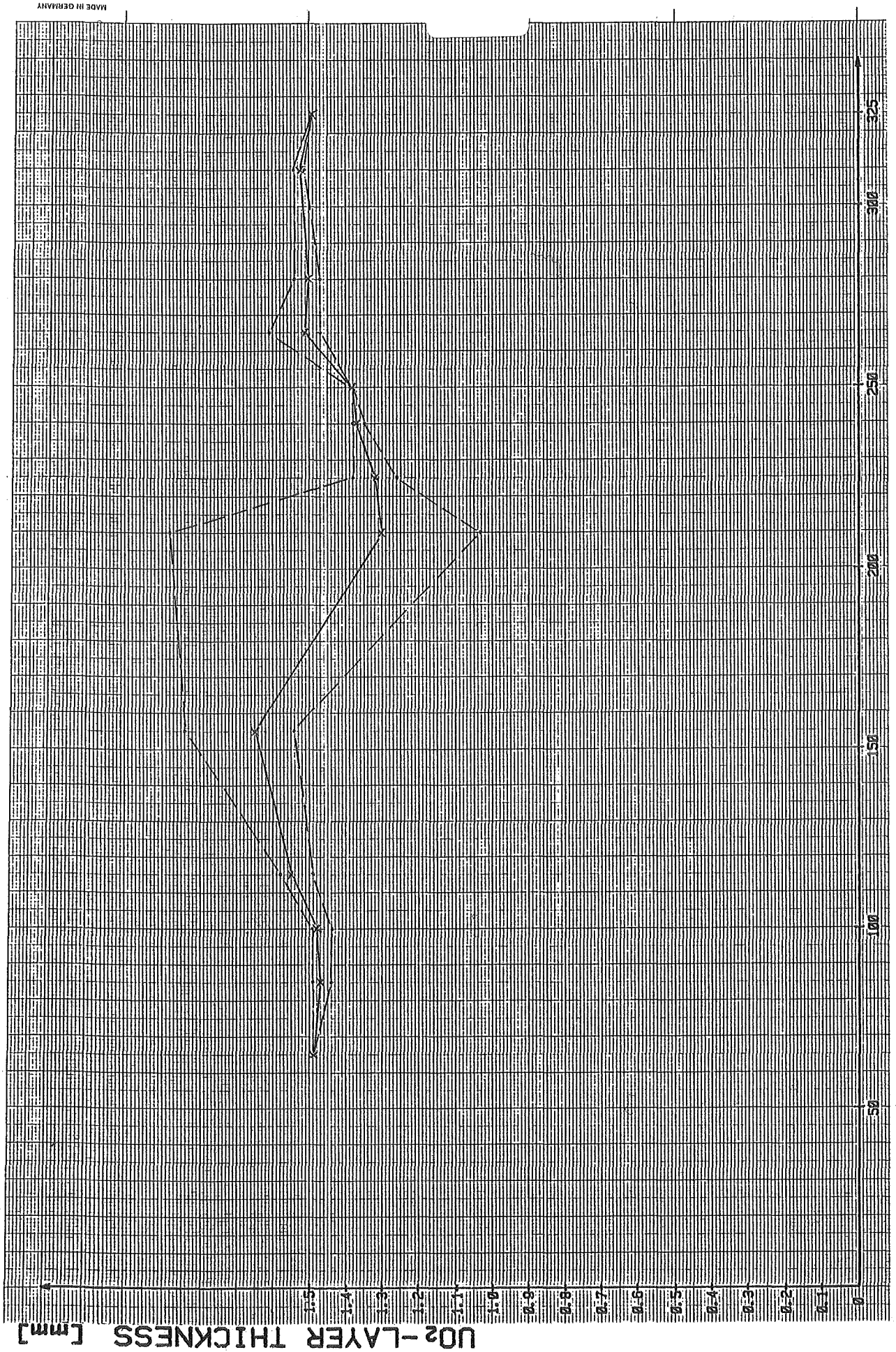

Fig.4/5-B: Uranium oxide layer thickness for test ESSI-4/5 (---maximum or minimum value; —— mean value)

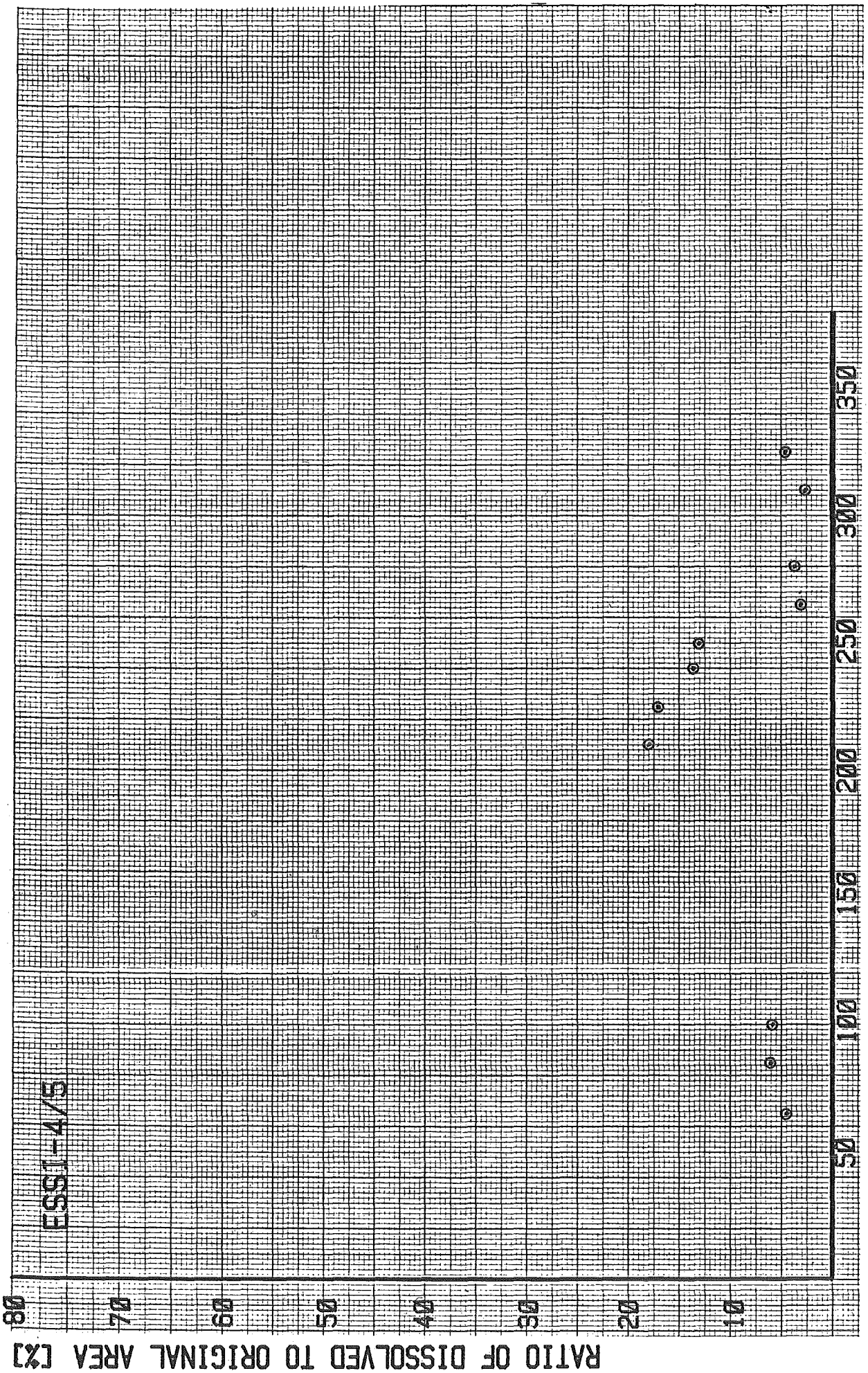

Fig.: 4/5-C
Dissolution of the UO_2-pellet at different elevations (ESSI-4/5)

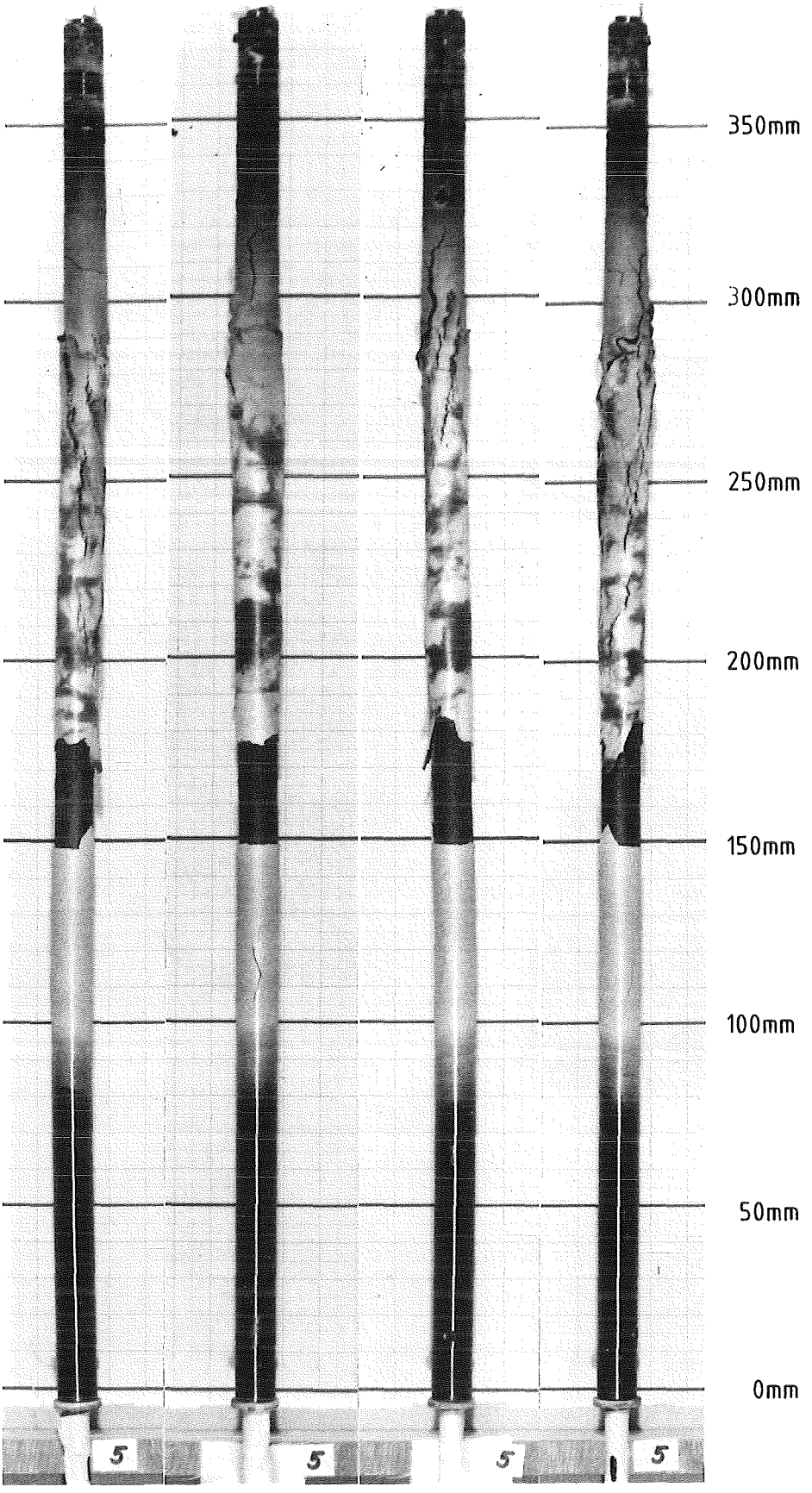

FIG. 5-1: POSTTEST APPEARANCE OF THE FUEL ROD SIMULATOR AND SCALE OF THE CROSS SECTION ELEVATIONS FOR ESSI-5

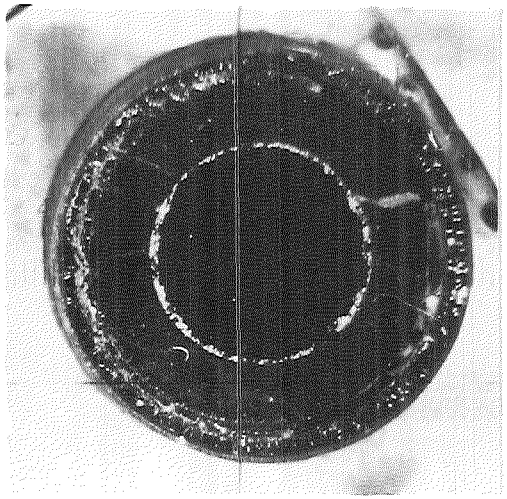

325mm

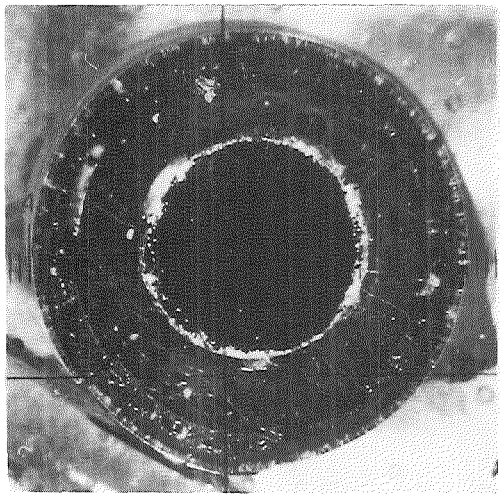

310mm

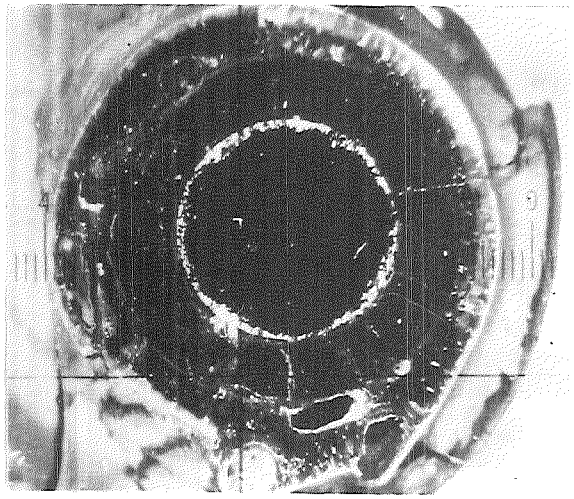

295mm

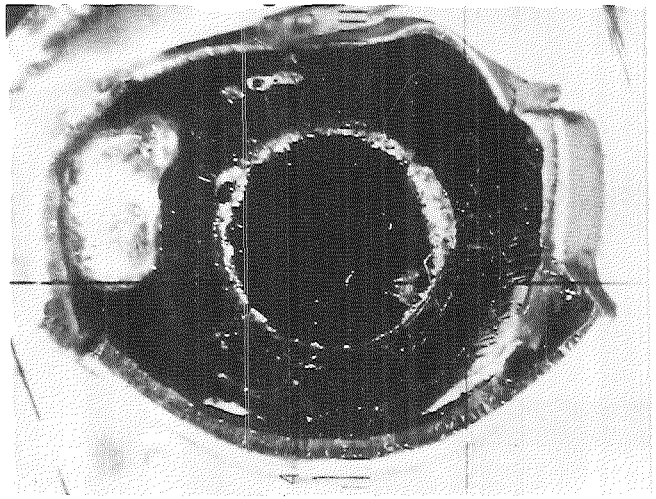

280mm

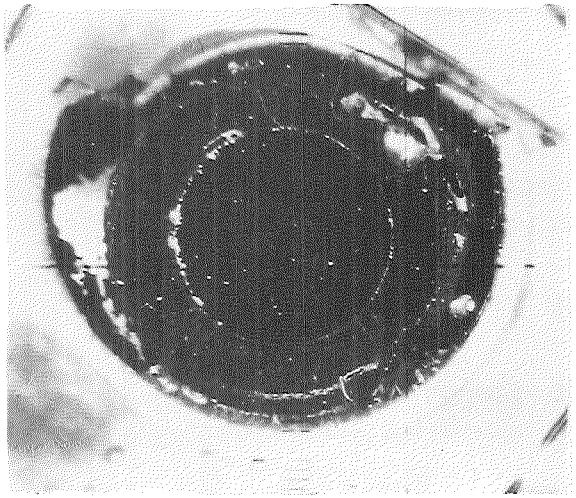

265mm

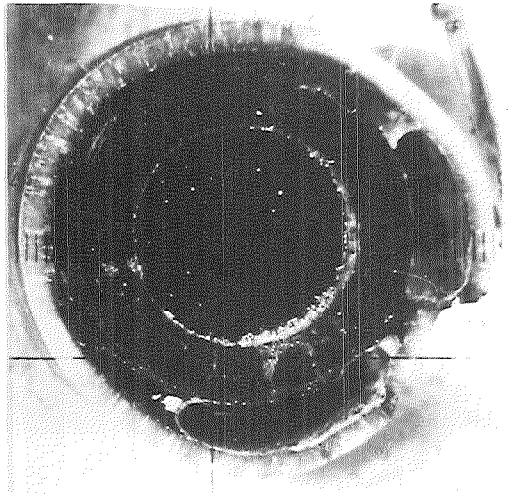

210mm

KfK

Fig. 5-2 : Cross Sections of Test ESSI-5

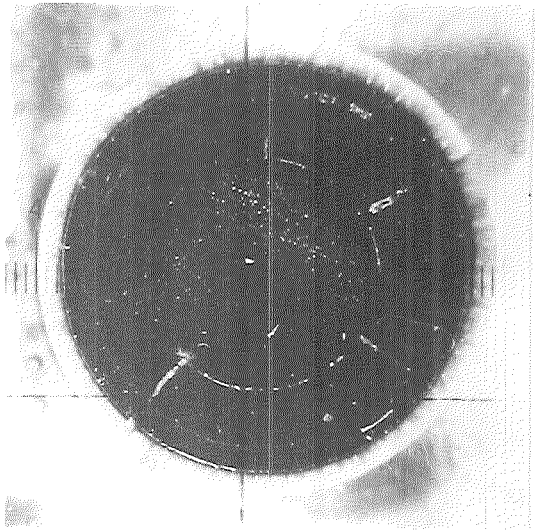

155mm

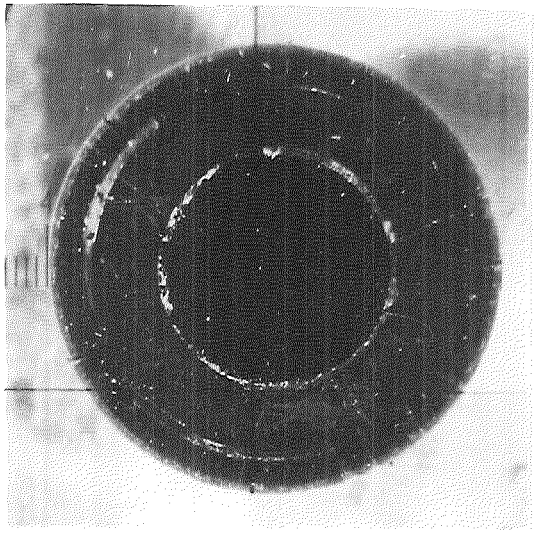

115mm

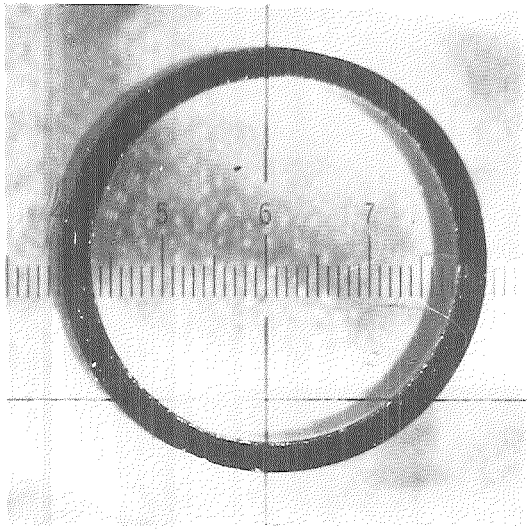

65mm

Fig. 5-3 : Cross Sections of Test ESSI-5

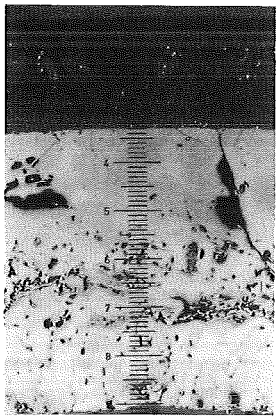

325mm

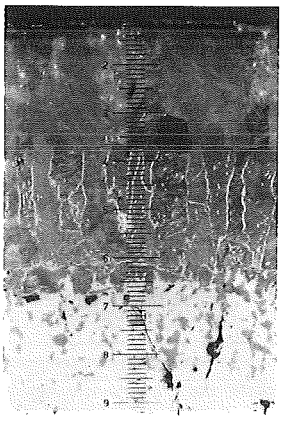

310mm

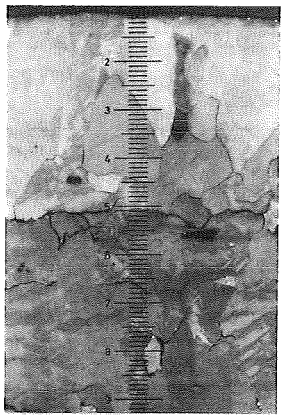

295mm

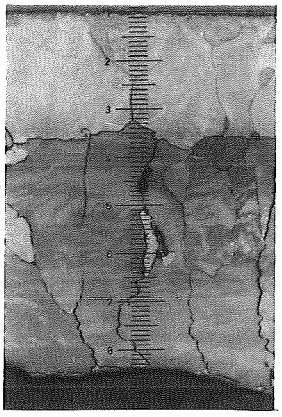

280mm

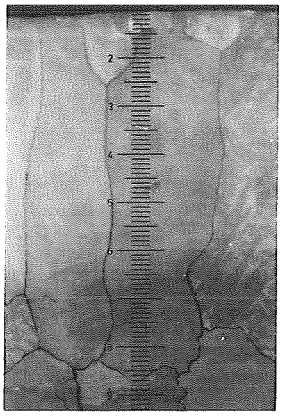

250mm

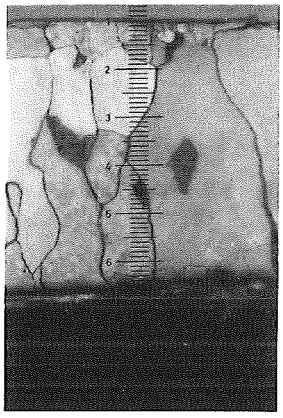

210mm

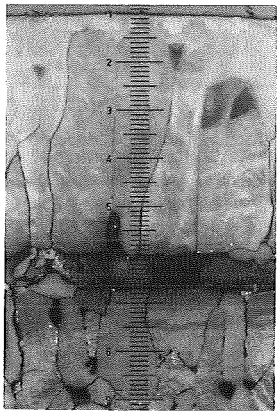

155mm

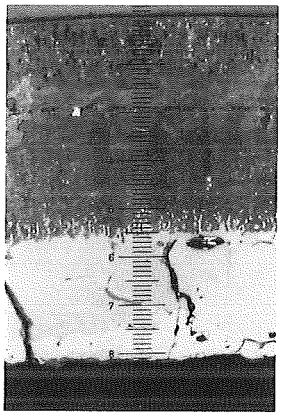

115mm

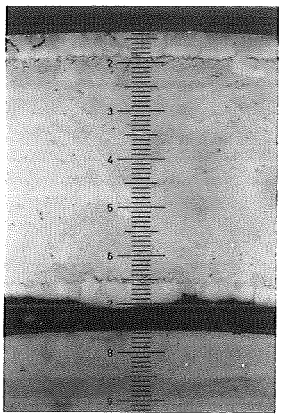

65mm

Fig. 5-4 : Enlarged View (100x) of Cross Sections From ESSI-5

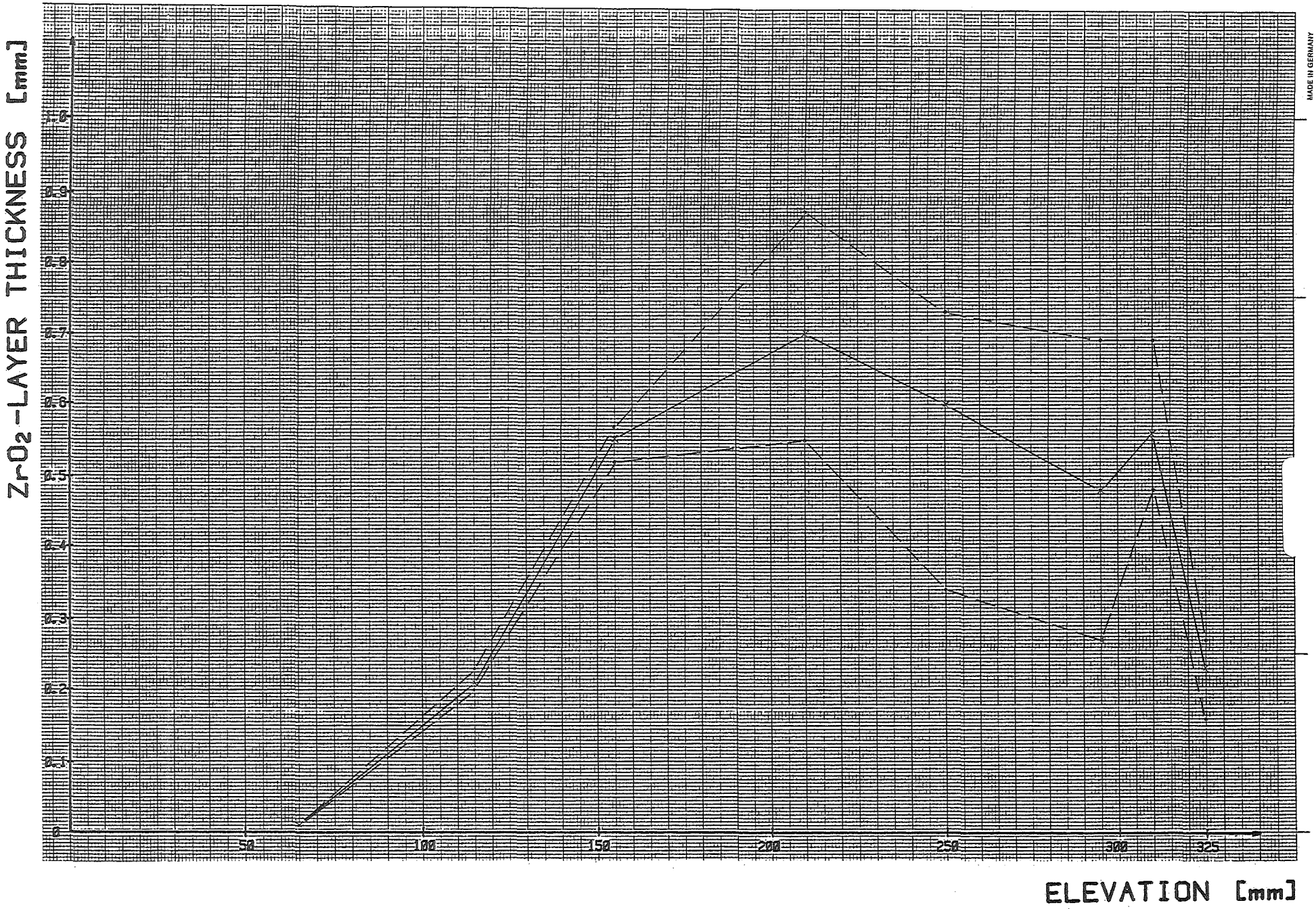

Fig.5-A: Zirconoxid layer thickness for test ESSI-5 (— — -maximum or minimum value: ——mean value)

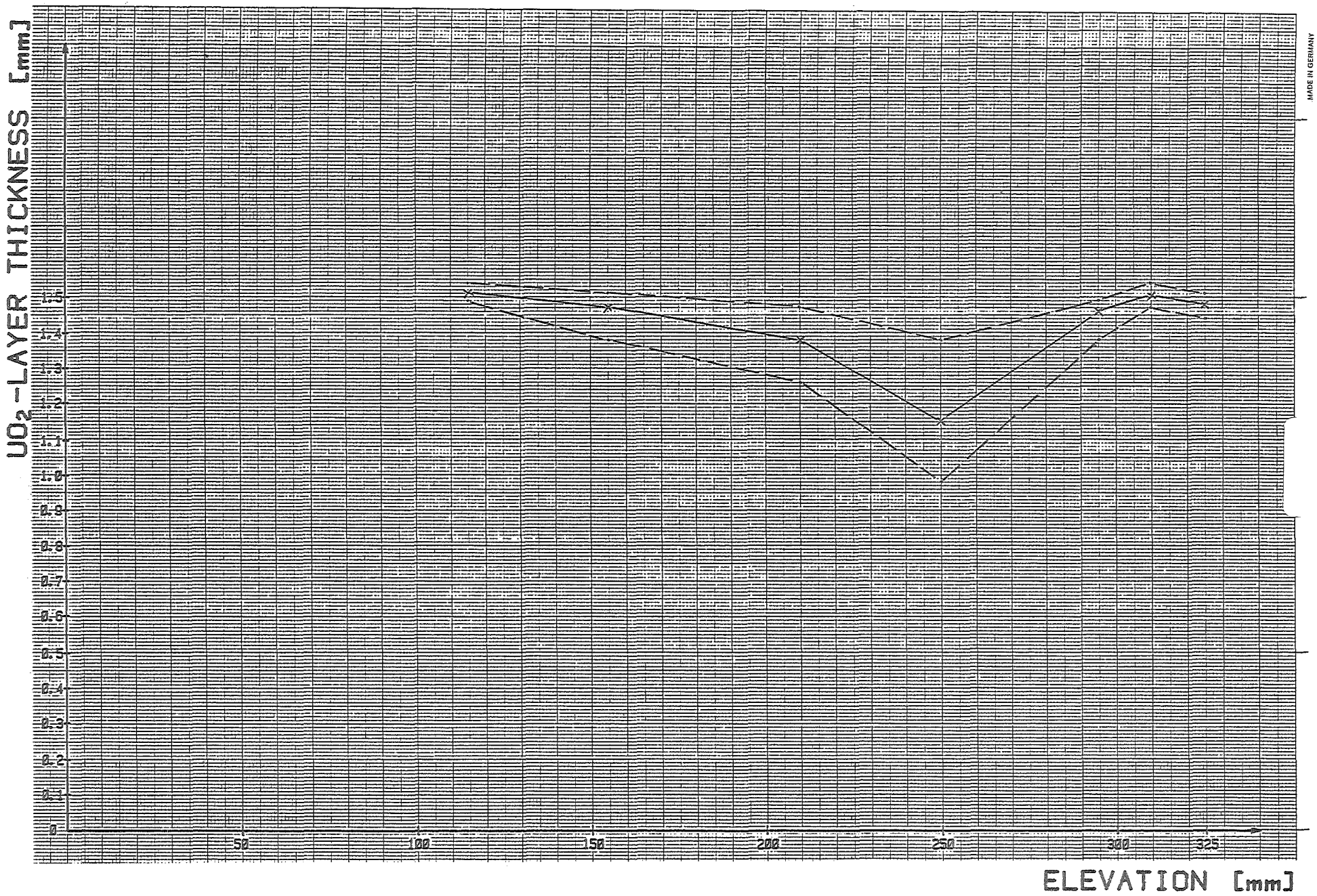

Fig.5-B : Uranium oxide layer thickness for test ESSI- 5 (---maximum or minimum value; —— mean value)

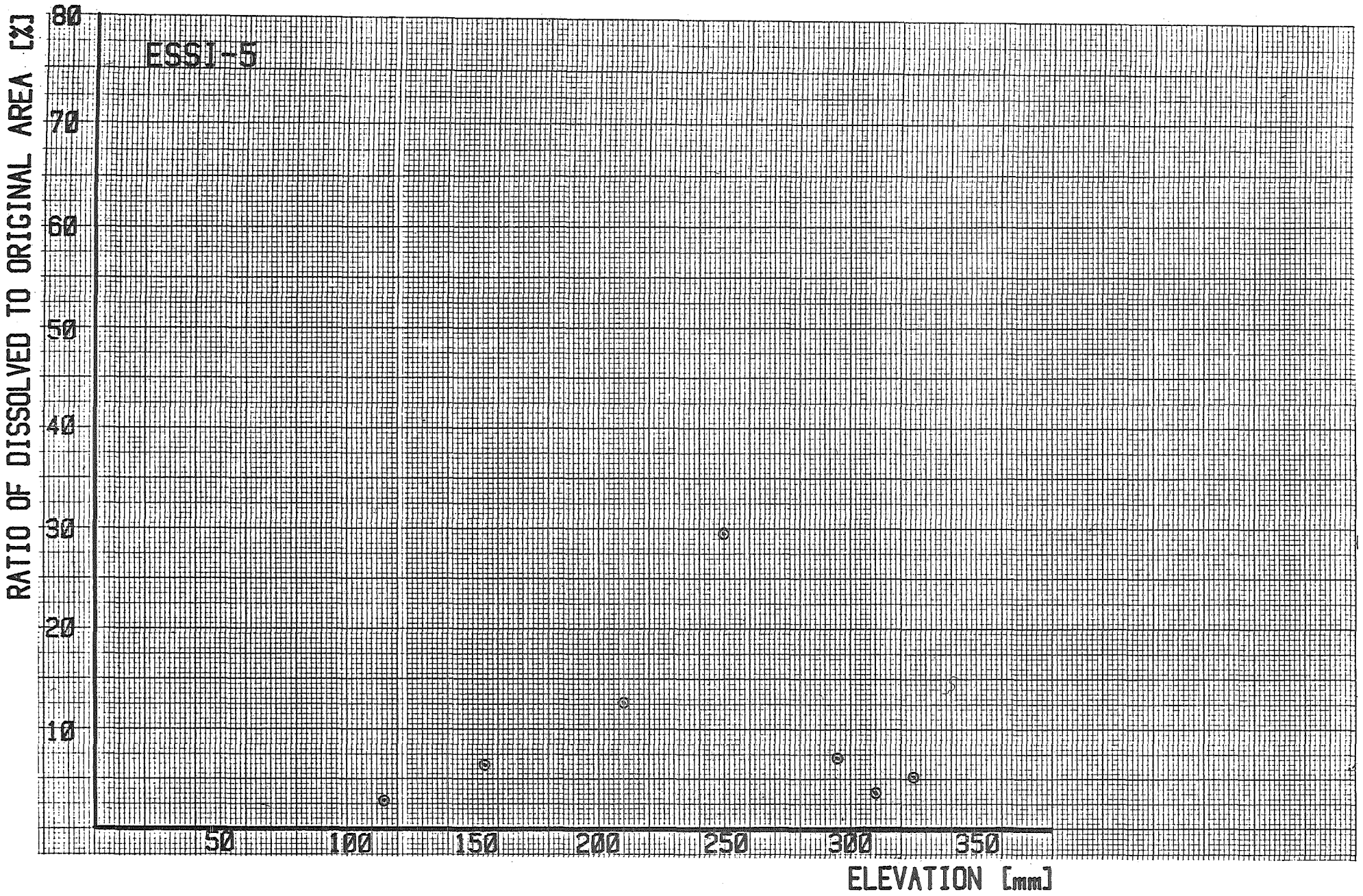

Fig.: 5-C
Dissolution of the UO_2-pellet at different elevations (ESSI-5)

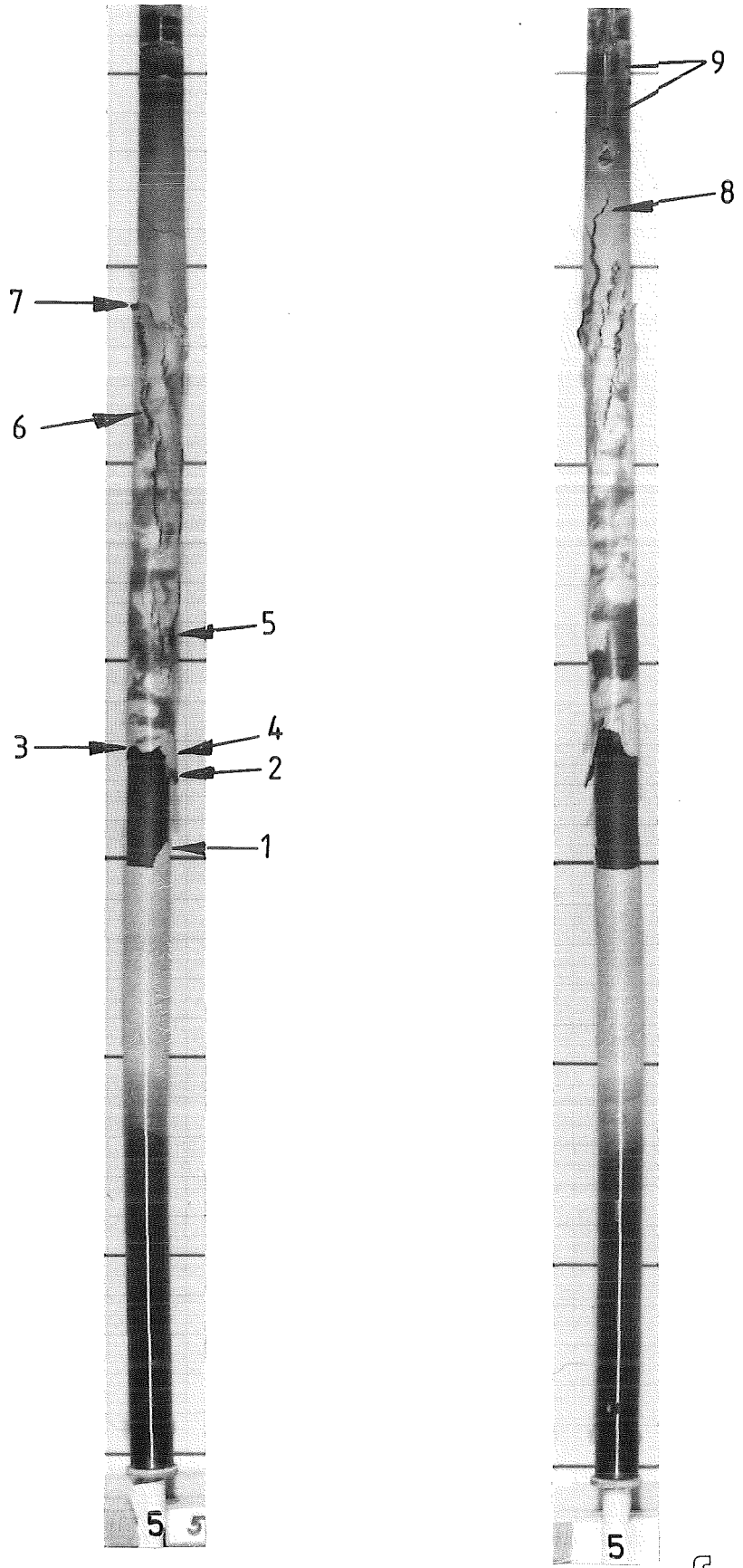

FIG.5-5: LOCATIONS OF ENLARGED VIEWS OF THE FUEL ROD SIMULATOR ESSI-5

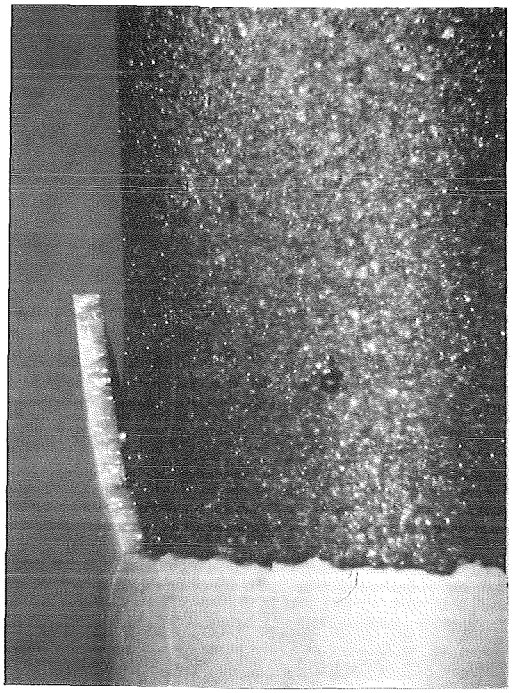

1 6×

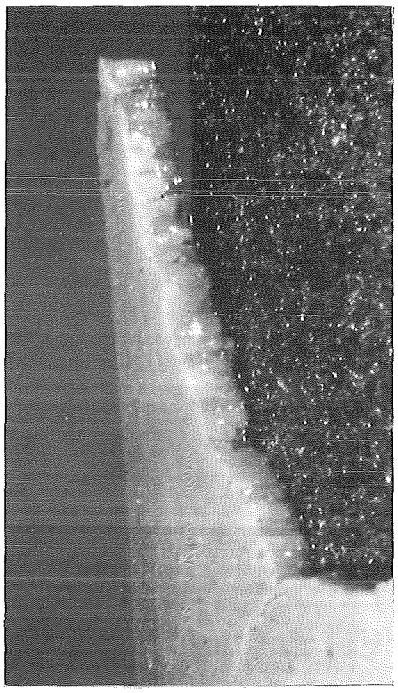

1 12×

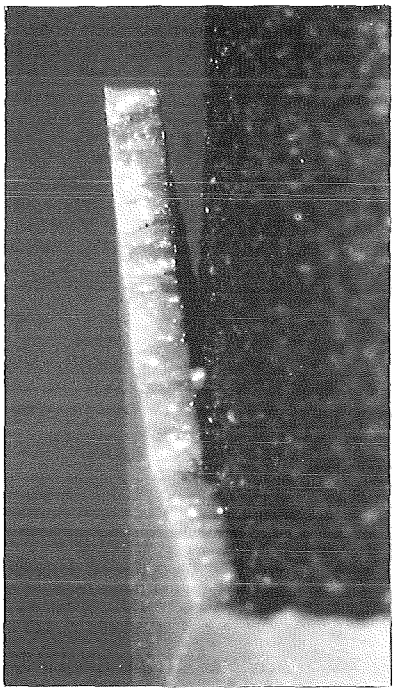

1 12× rotated

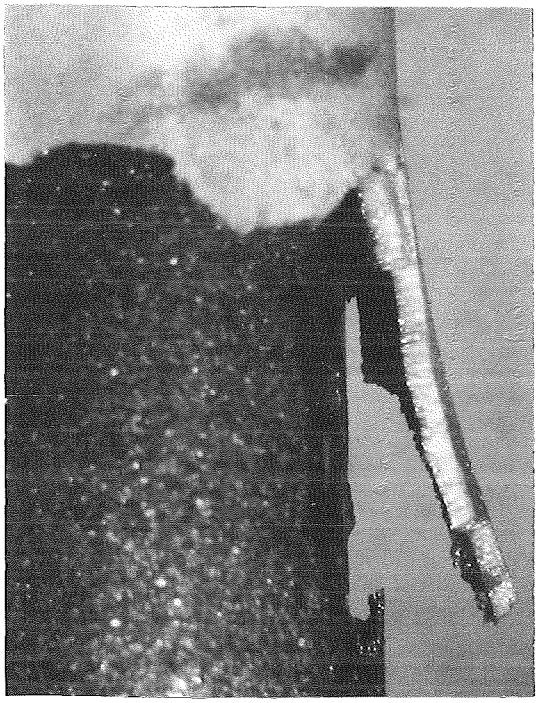

2 6×

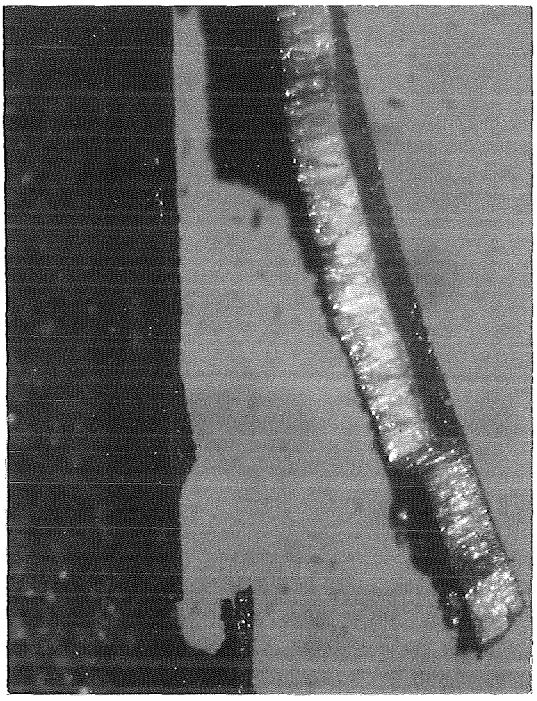

2 12×

FIG.5-6: ENLARGED VIEWS OF THE FUEL ROD SIMULATOR ESSI-5
(POSITION SEE FIG.5-5)

3 12×

4 6×

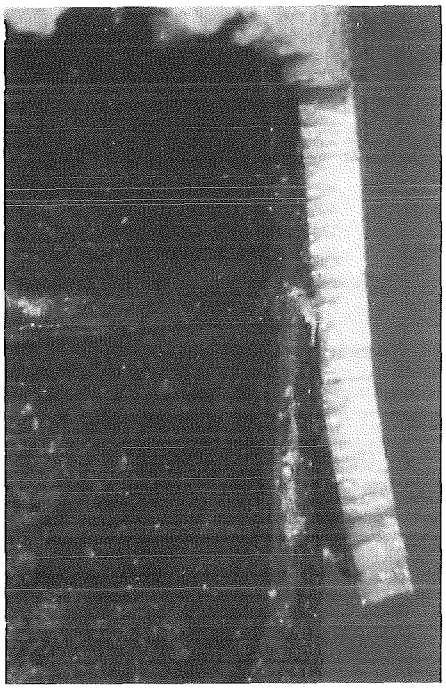

4 12×

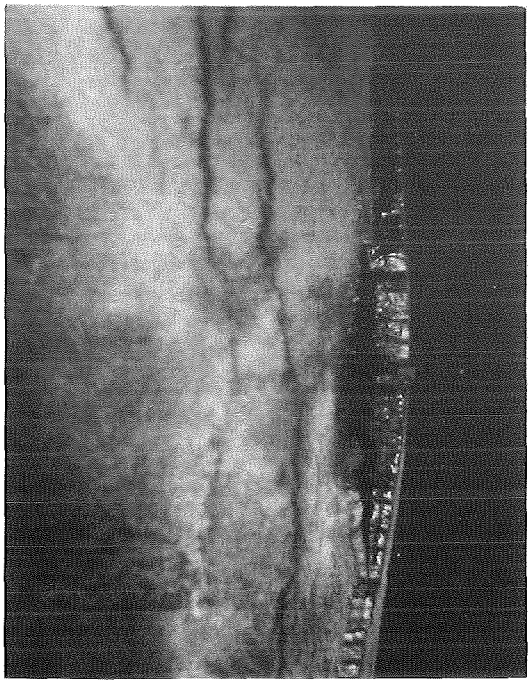

5 6×

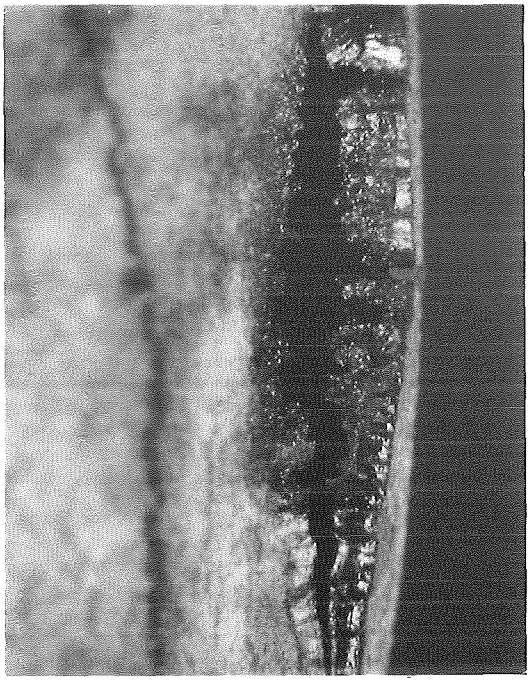

5 12×

FIG.5-7: ENLARGED VIEWS OF THE FUEL ROD SIMULATOR ESSI-5
(POSITION SEE FIG.5-5)

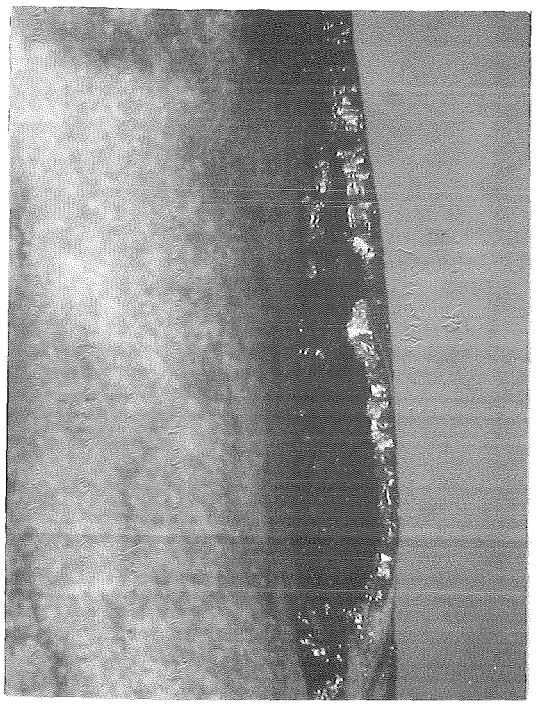

6 6x

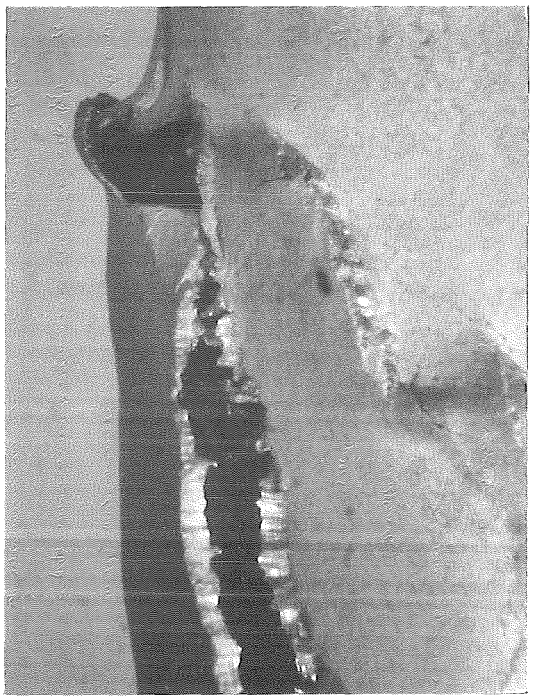

7 6x

8 6x

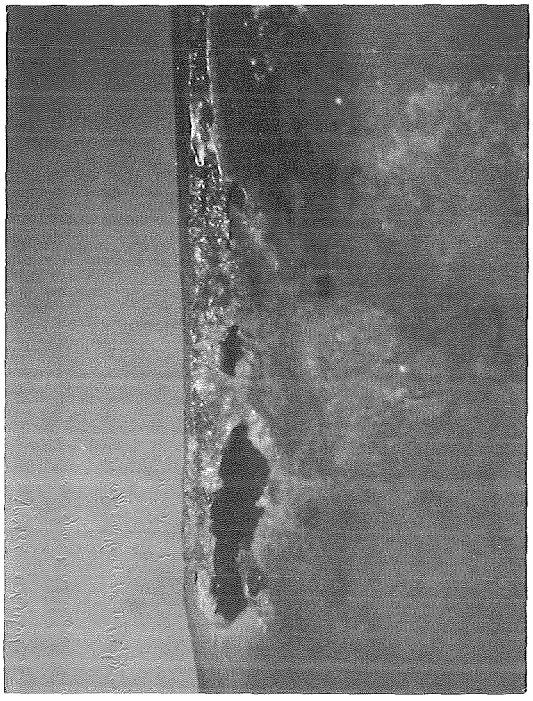

9 6x

FIG.5-8: ENLARGED VIEWS OF THE FUEL ROD SIMULATOR ESSI-5
(POSITION SEE FIG.5-5)

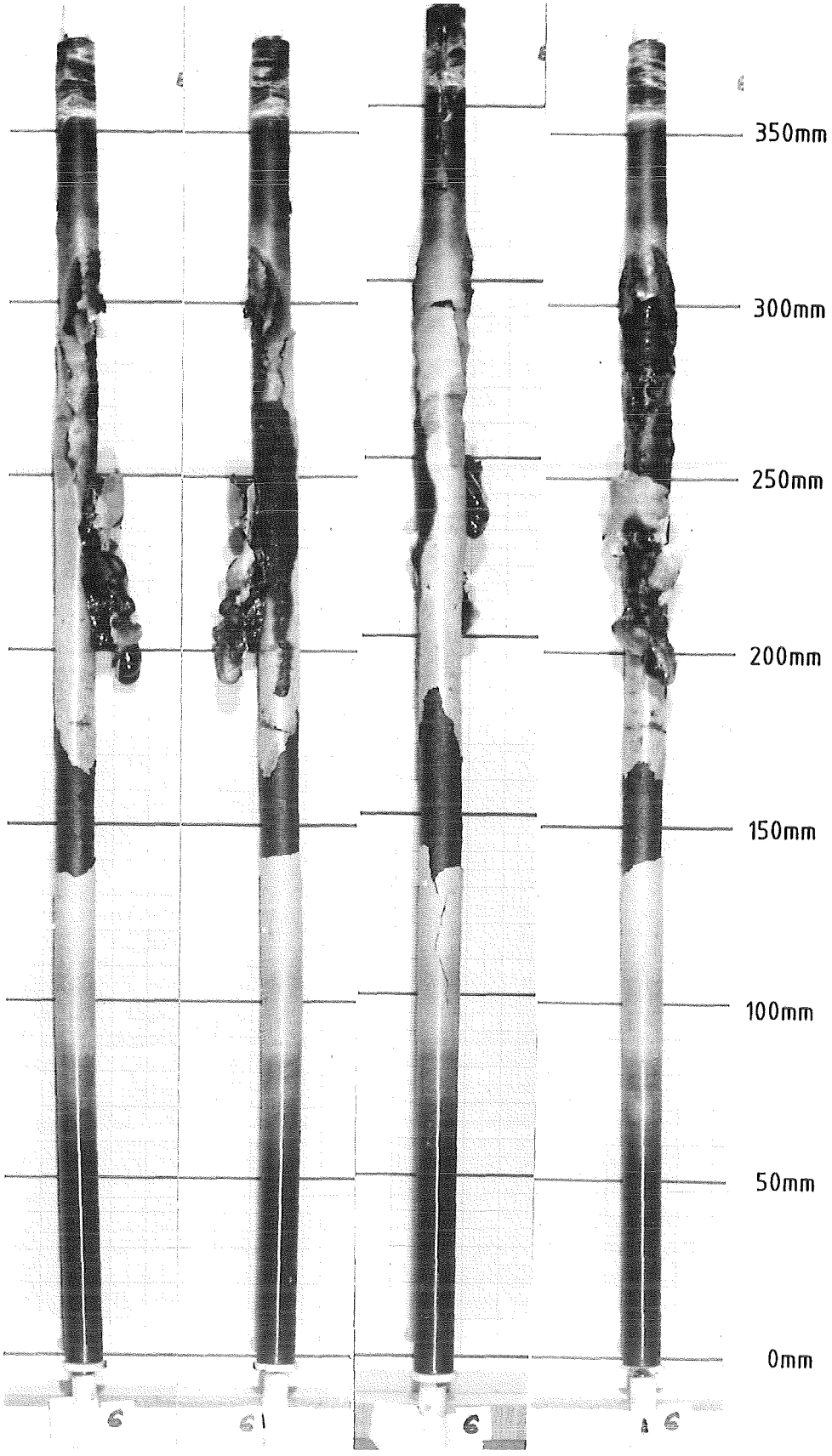

FIG. 6-1: POSTTEST APPEARANCE OF THE FUEL ROD SIMULATOR AND SCALE OF THE CROSS SECTION ELEVATIONS FOR ESSI-6

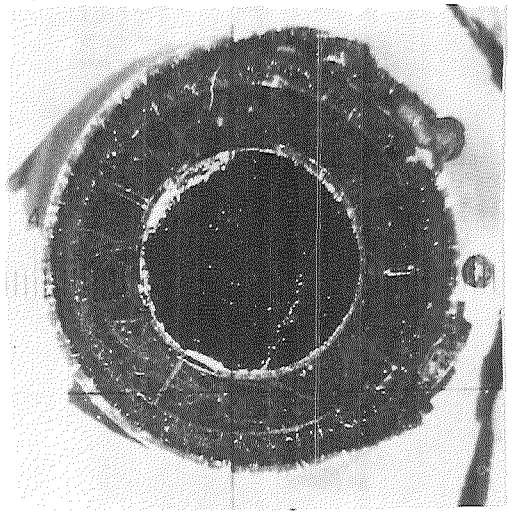

313mm

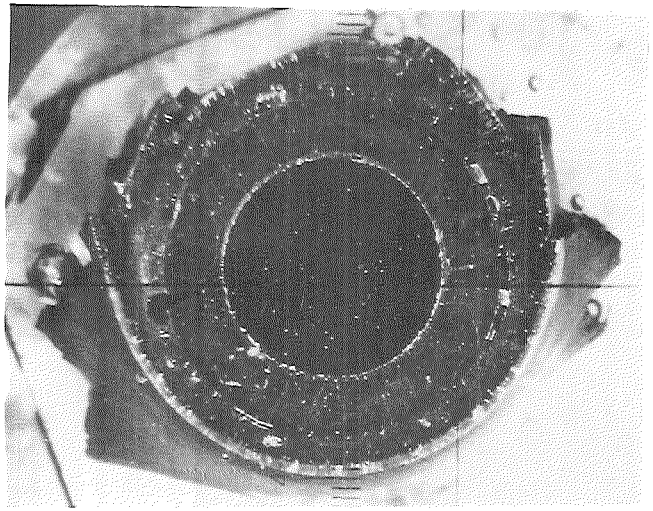

307mm

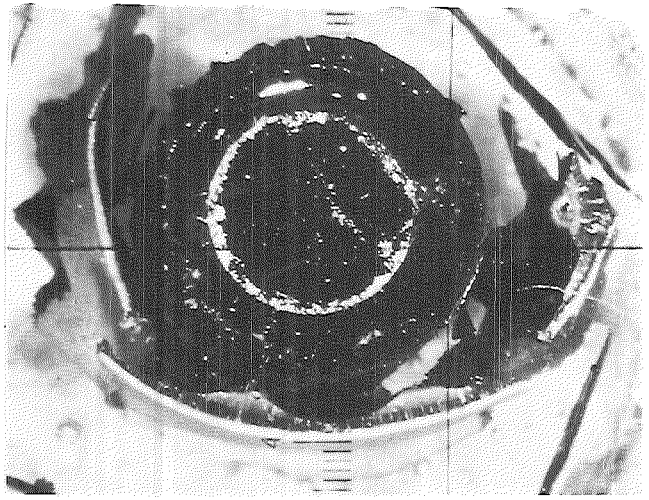

280mm

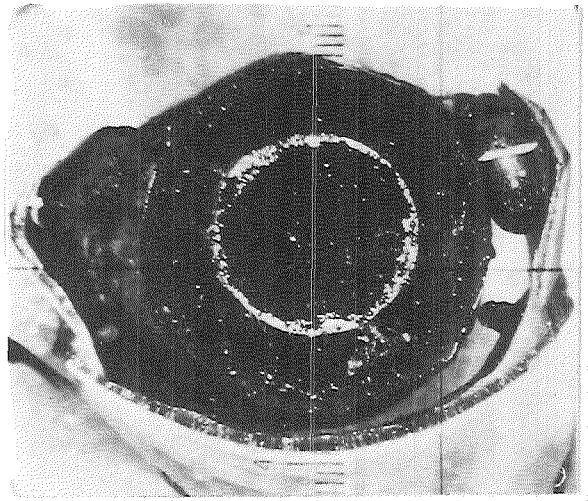

265mm

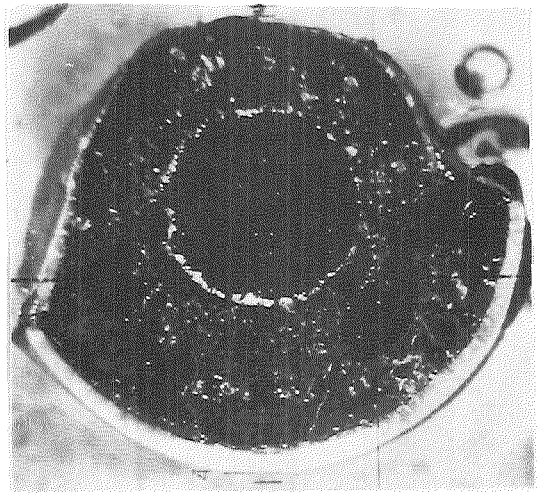

250mm

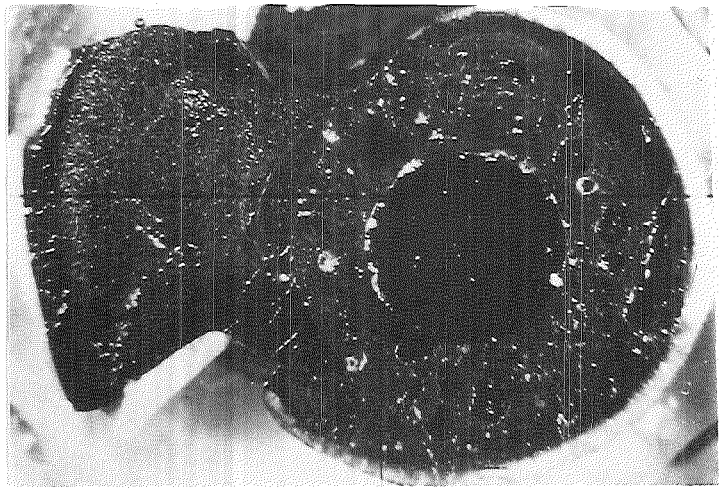

240mm

Fig. 6-2 : Cross Sections of Test ESSI-6

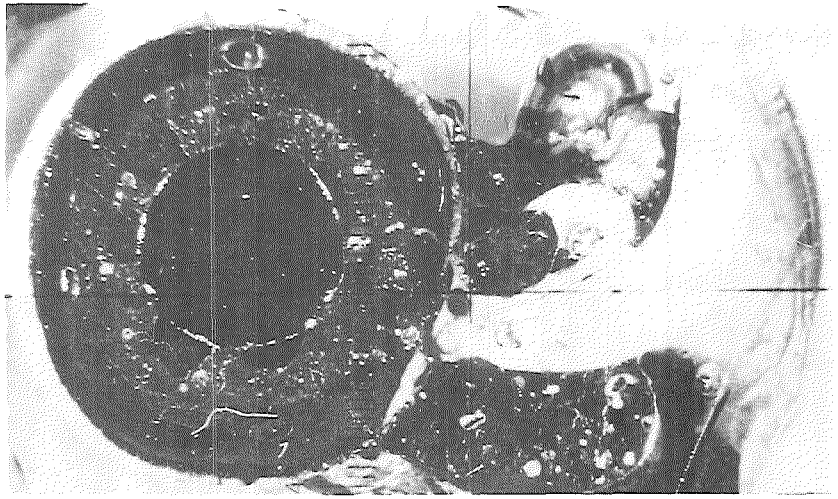

225mm

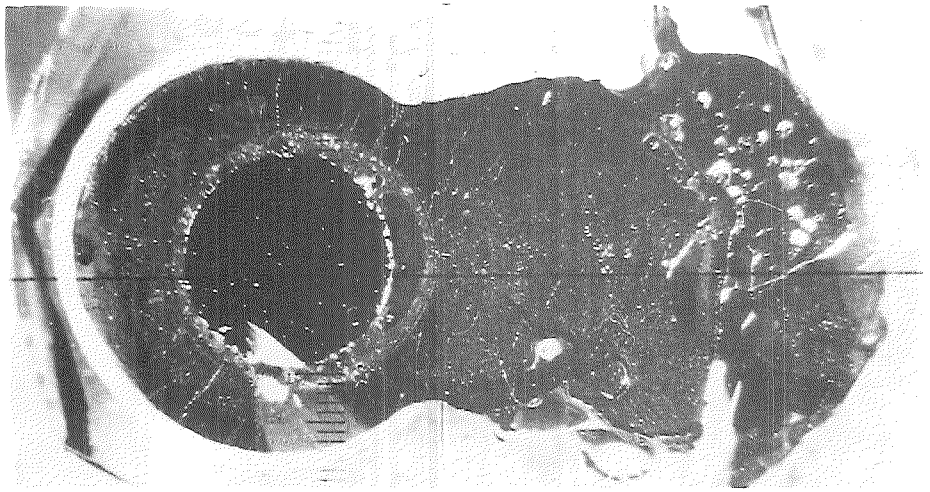

210mm

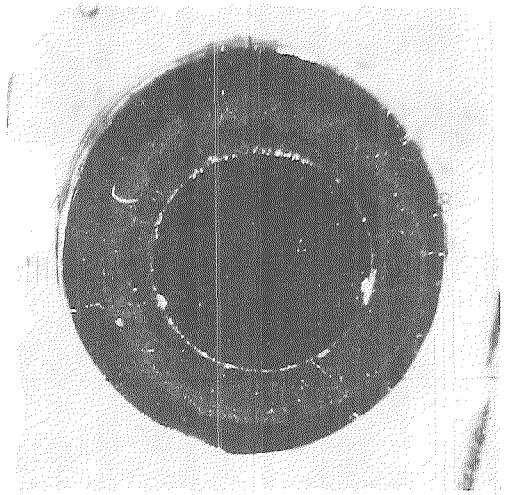

155mm

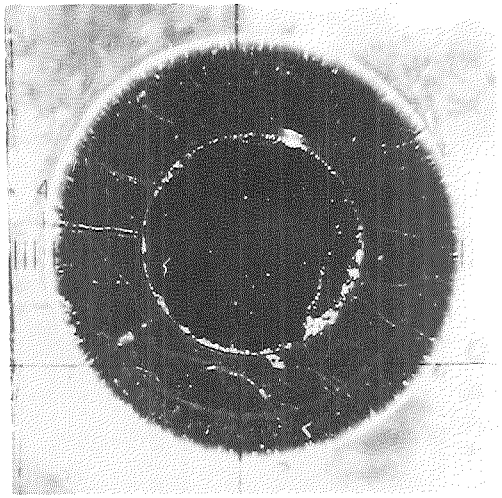

115mm

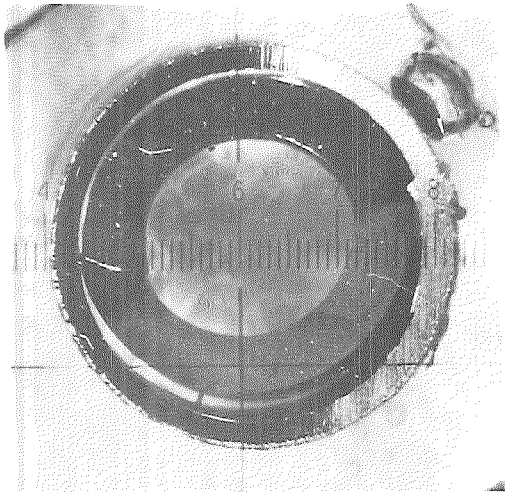

65mm

KfK

Fig. 6-3 : Cross Sections of Test ESSI-6

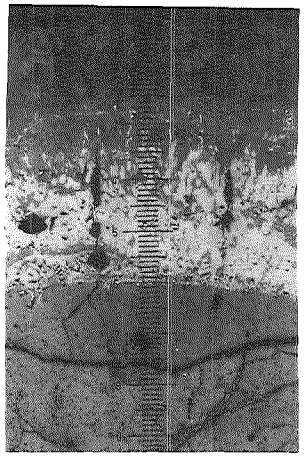

313mm

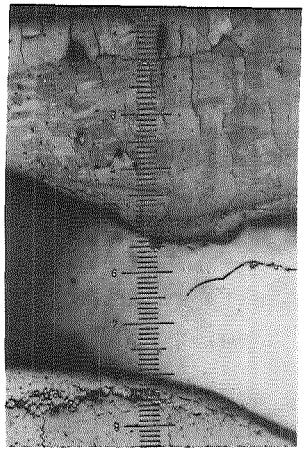

280mm

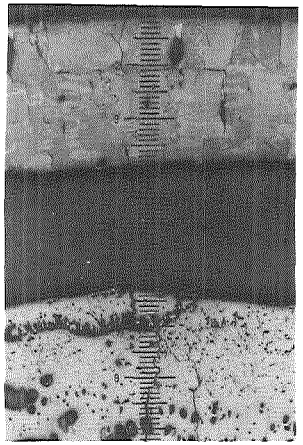

265mm

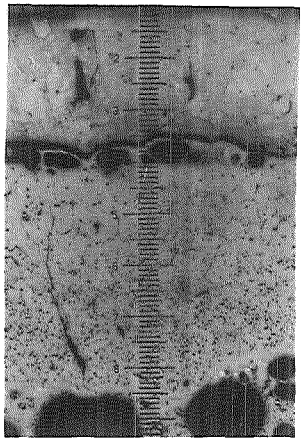

250mm

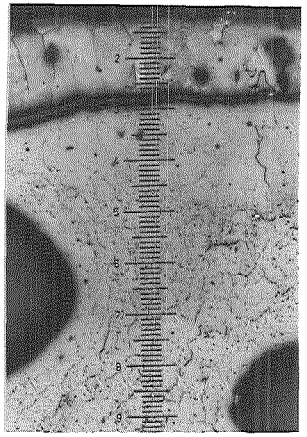

240mm

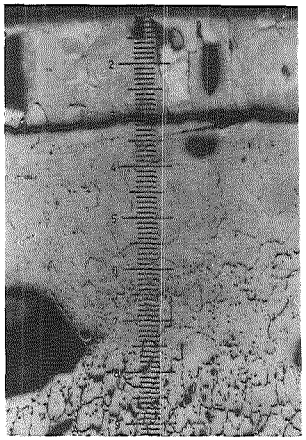

225mm

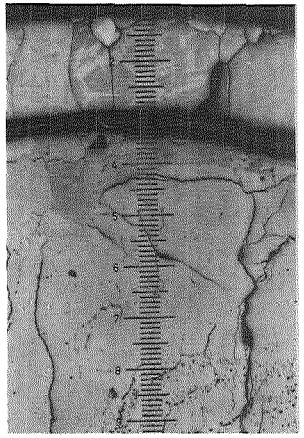

210mm

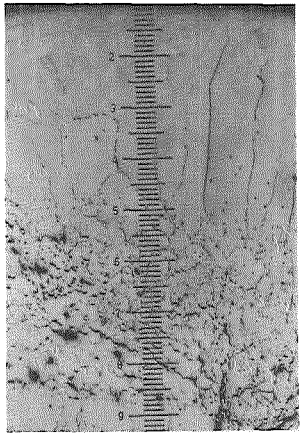

155mm

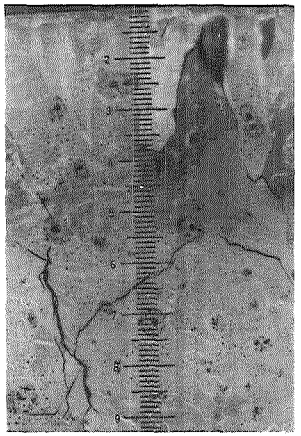

115mm

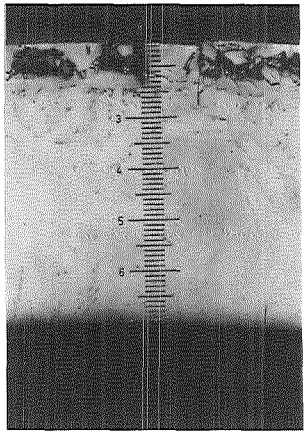

65mm

Fig. 6-4 : Enlarged View (100x) of Cross Sections From ESSI-6

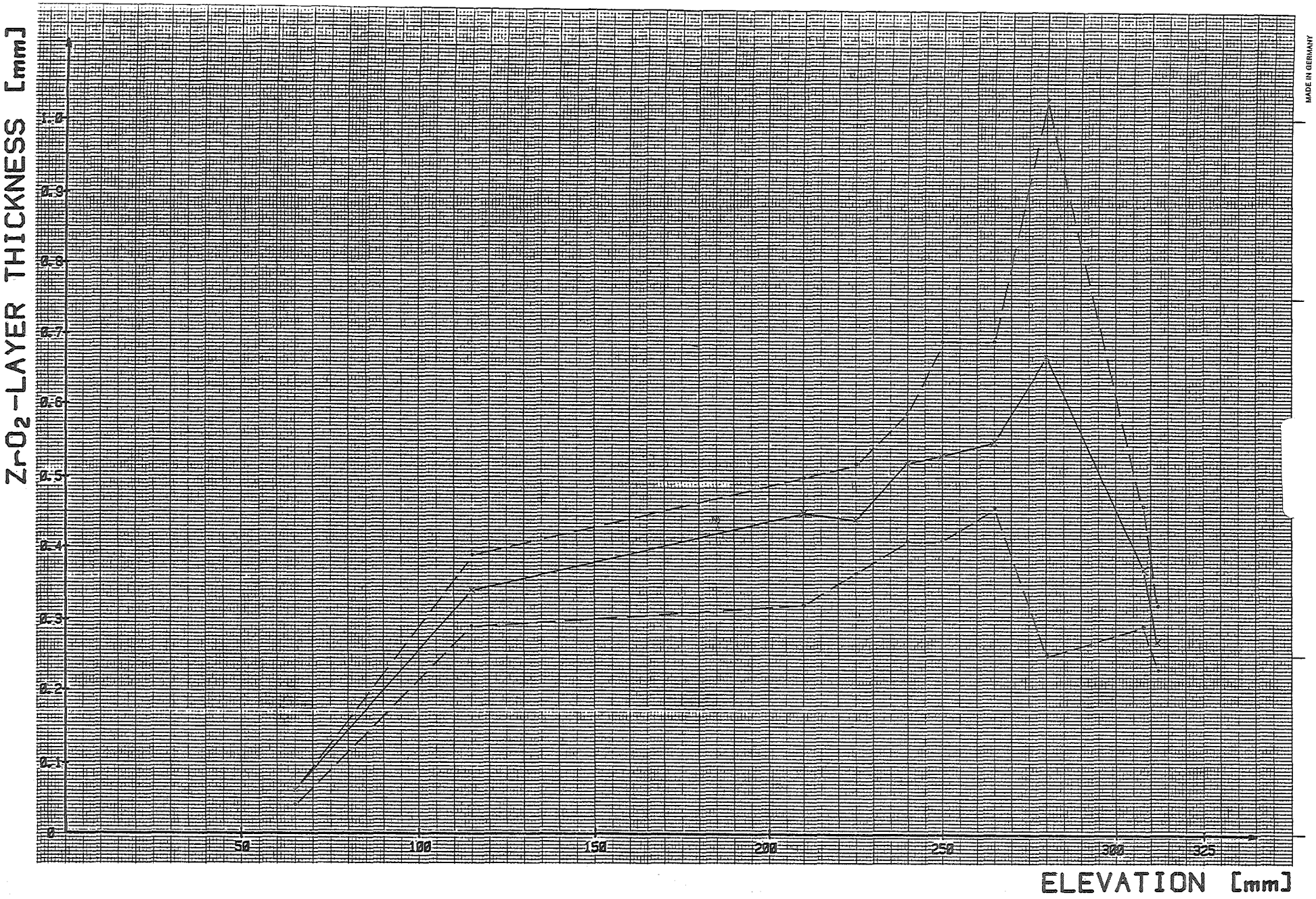

Fig.6-A: Zirconoxid layer thickness for test ESSI-6 (– – –maximum or minimum value; ——mean value)

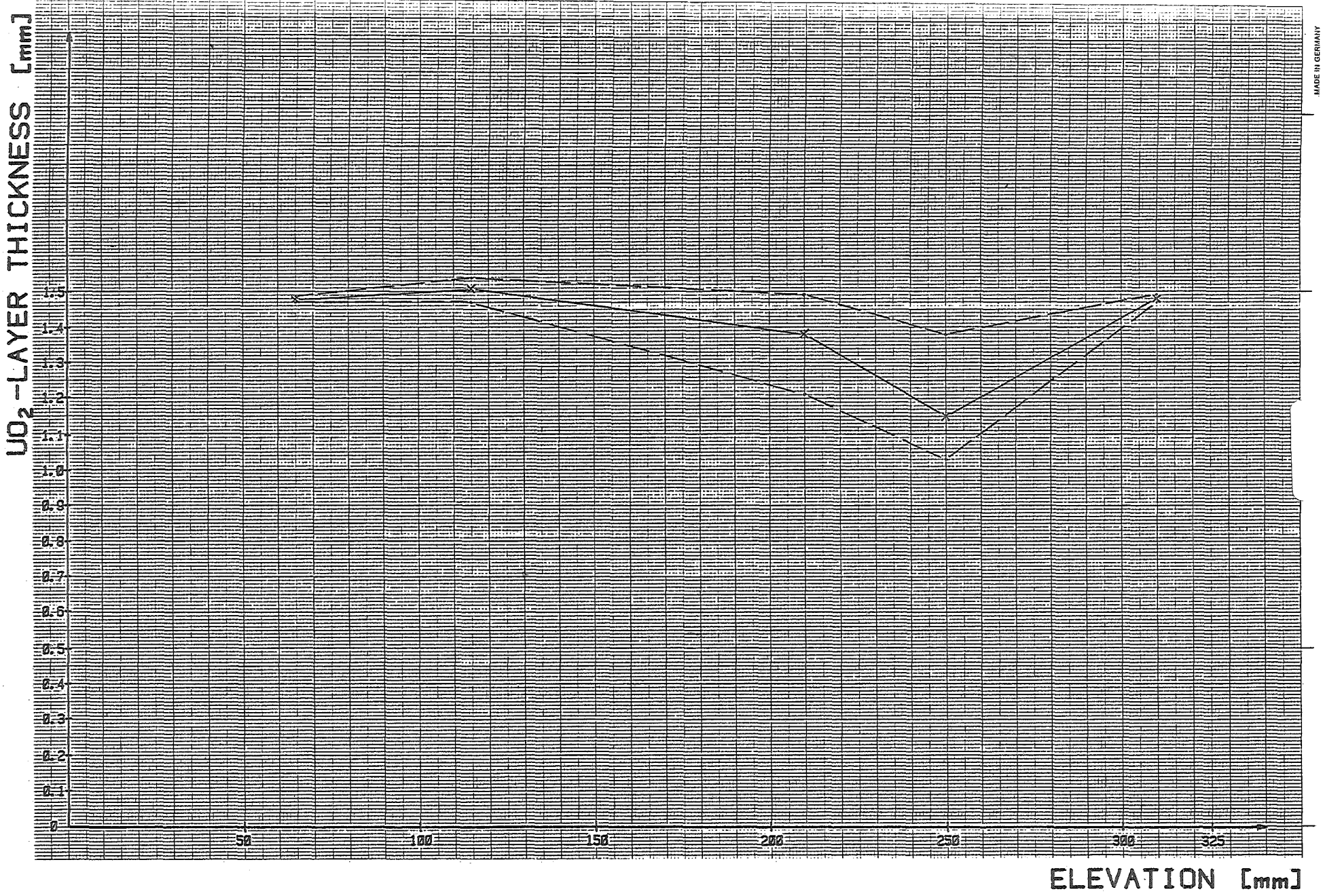

Fig. 6-B : Uranium oxide layer thickness for test ESSI- 6 (---maximum or minimum value;——mean value)

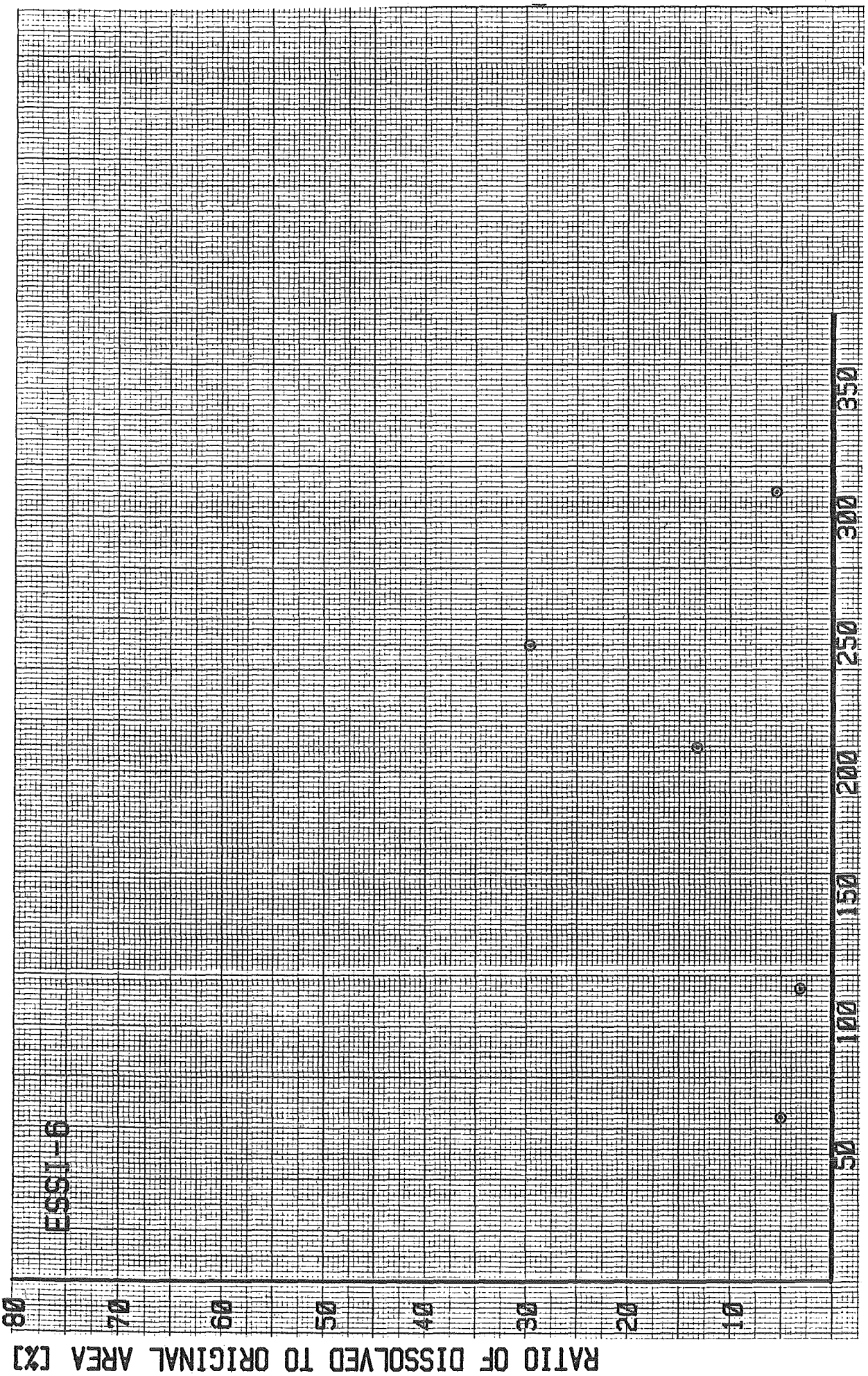

Fig.: 6-C
Dissolution of the UO_2-pellet at different elevations (ESSI-6)

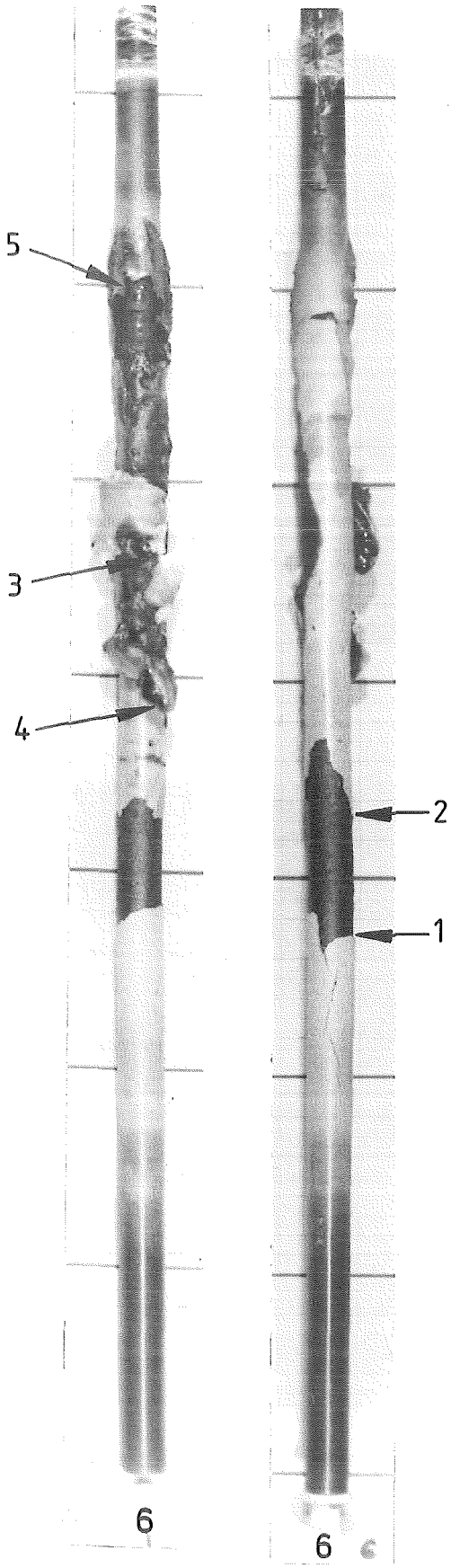

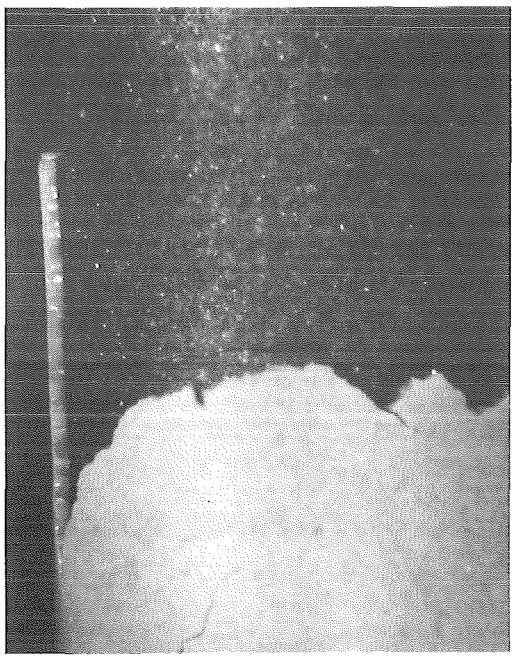

1 6×

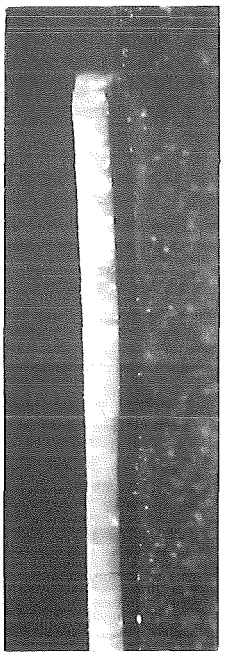

1 12×

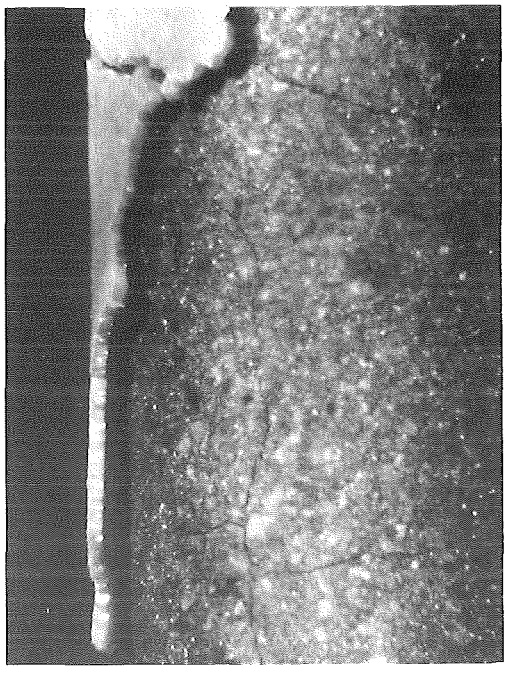

2 6×

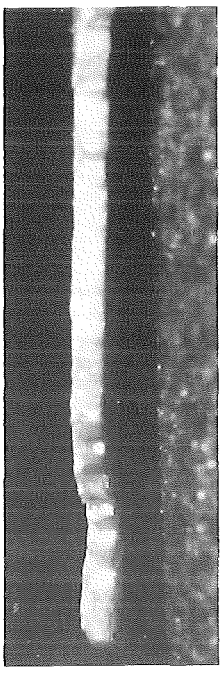

2 12×

FIG.6-5: LOCATIONS OF ENLARGED VIEWS OF THE FUEL ROD SIMULATOR ESSI-6

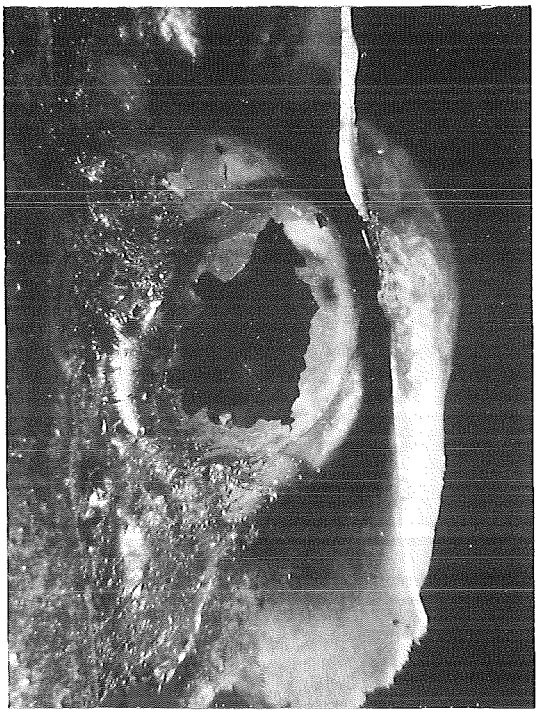

3 6×

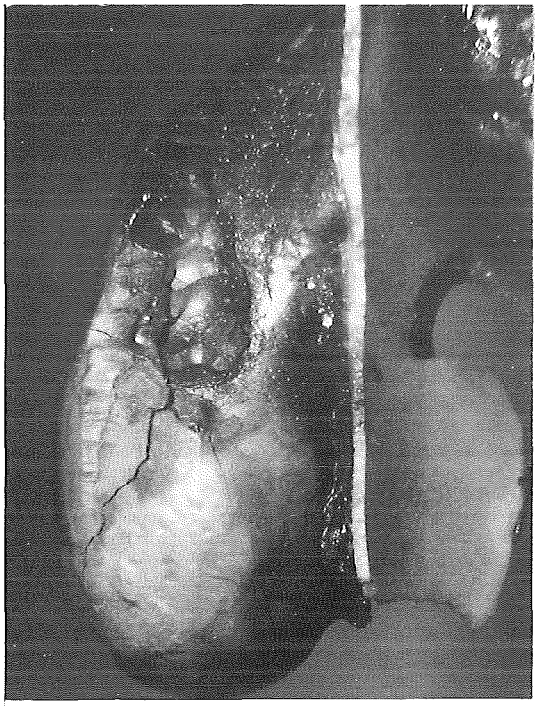

4 6×

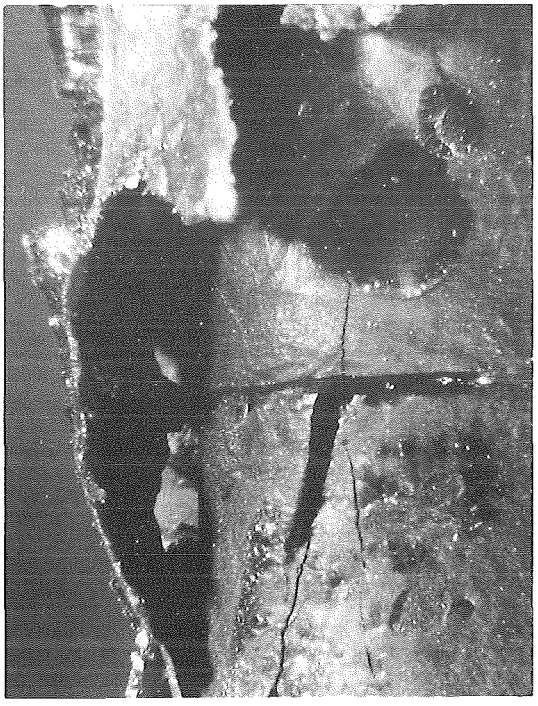

5 6×

FIG.6-6: ENLARGED VIEWS OF THE FUEL ROD SIMULATOR ESSI-6
(POSITION SEE FIG.6-5)

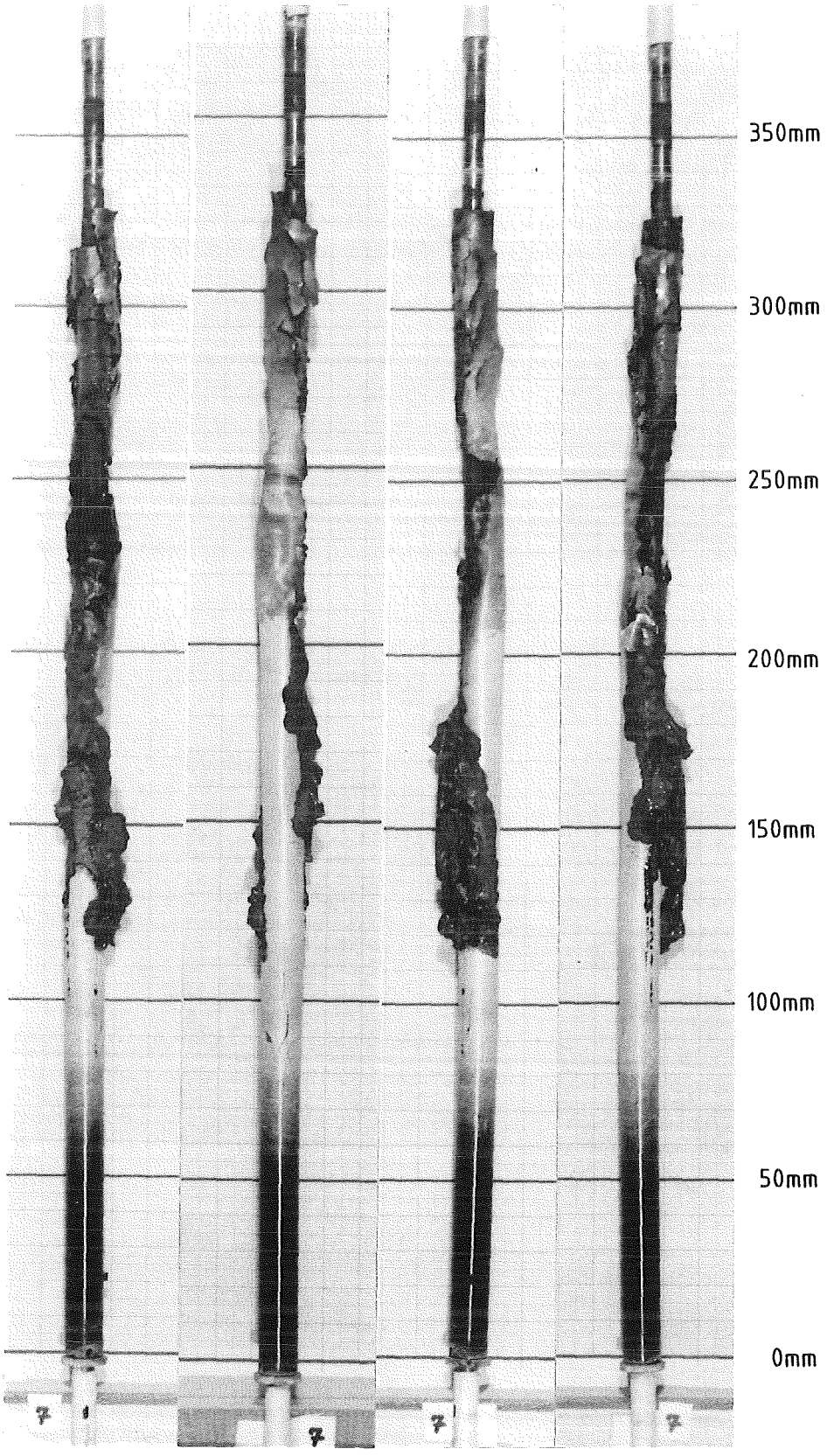

FIG. 7-1: POSTTEST APPEARANCE OF THE FUEL ROD SIMULATOR AND SCALE OF THE CROSS SECTION ELEVATIONS FOR ESSI-7

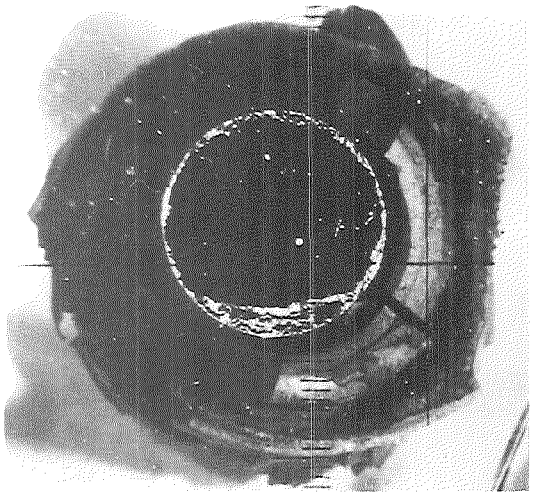

325mm

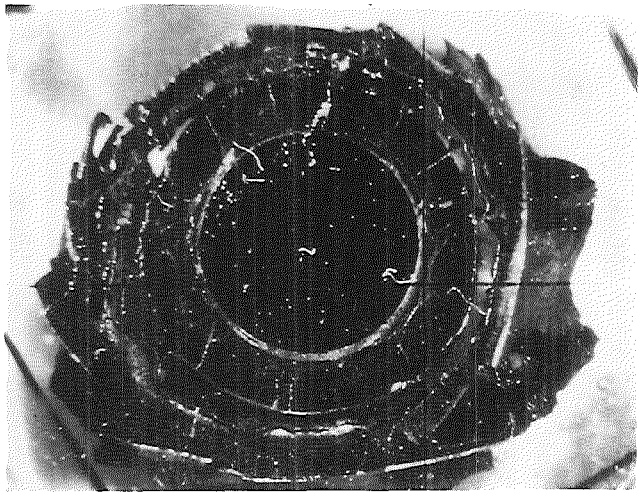

310mm

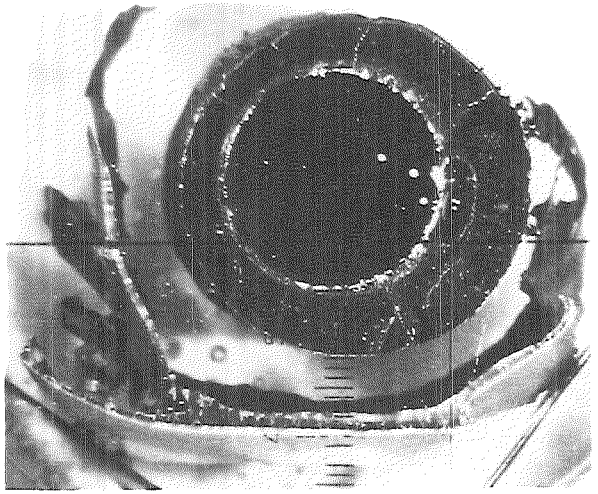

280mm

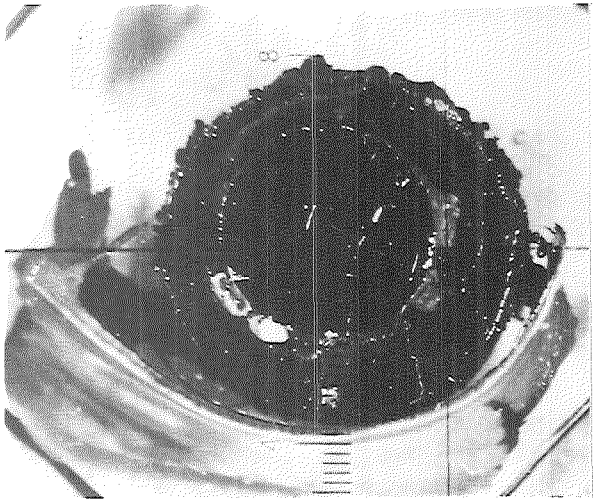

265mm

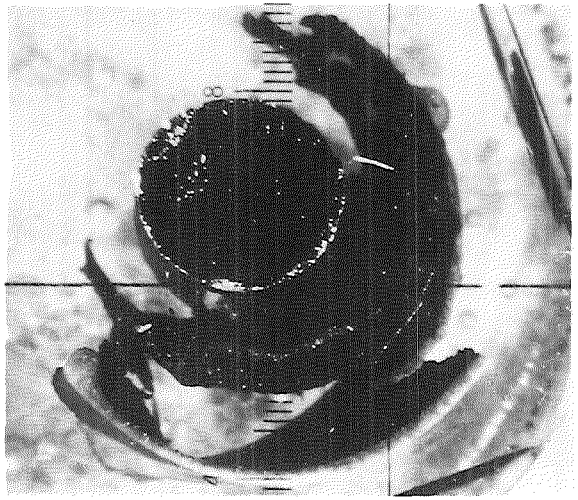

250mm

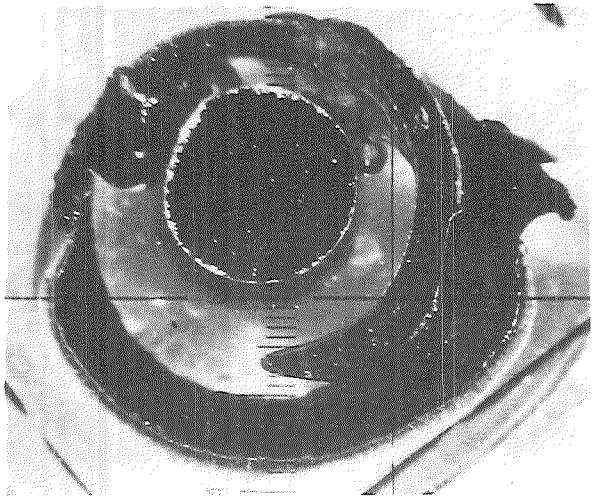

210mm

KfK

Fig. 7-2 : Cross Sections of Test ESSI-7

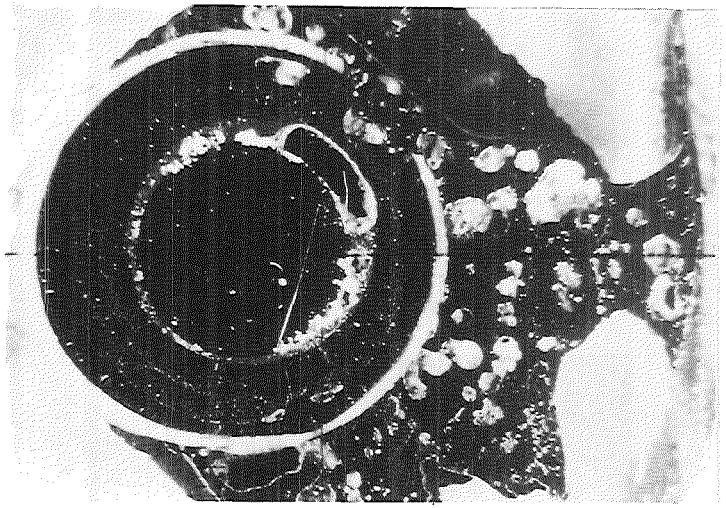

155mm

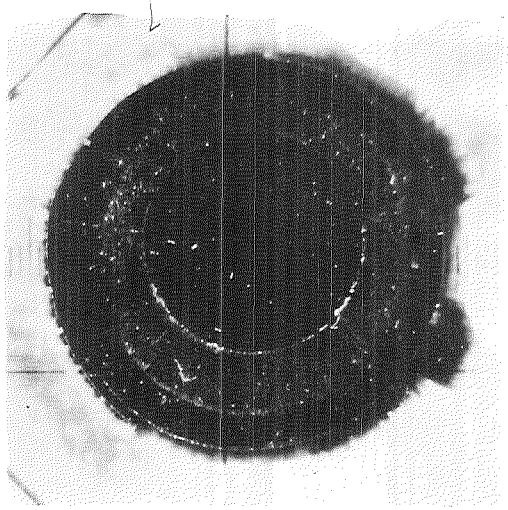

115mm

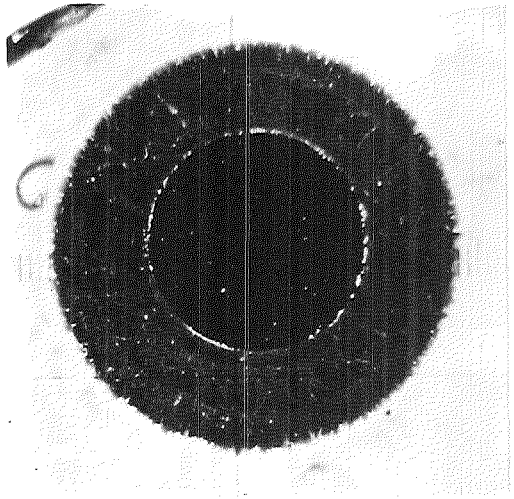

100mm

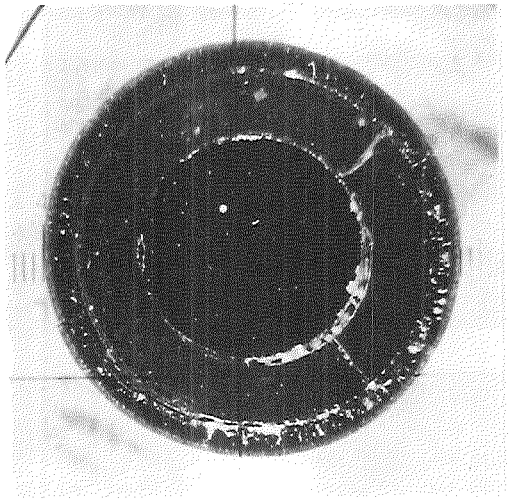

85mm

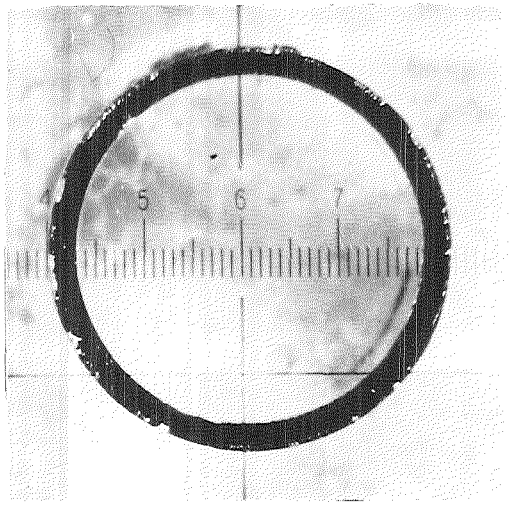

65mm

Fig. 7-3 : Cross Sections of Test ESSI-7

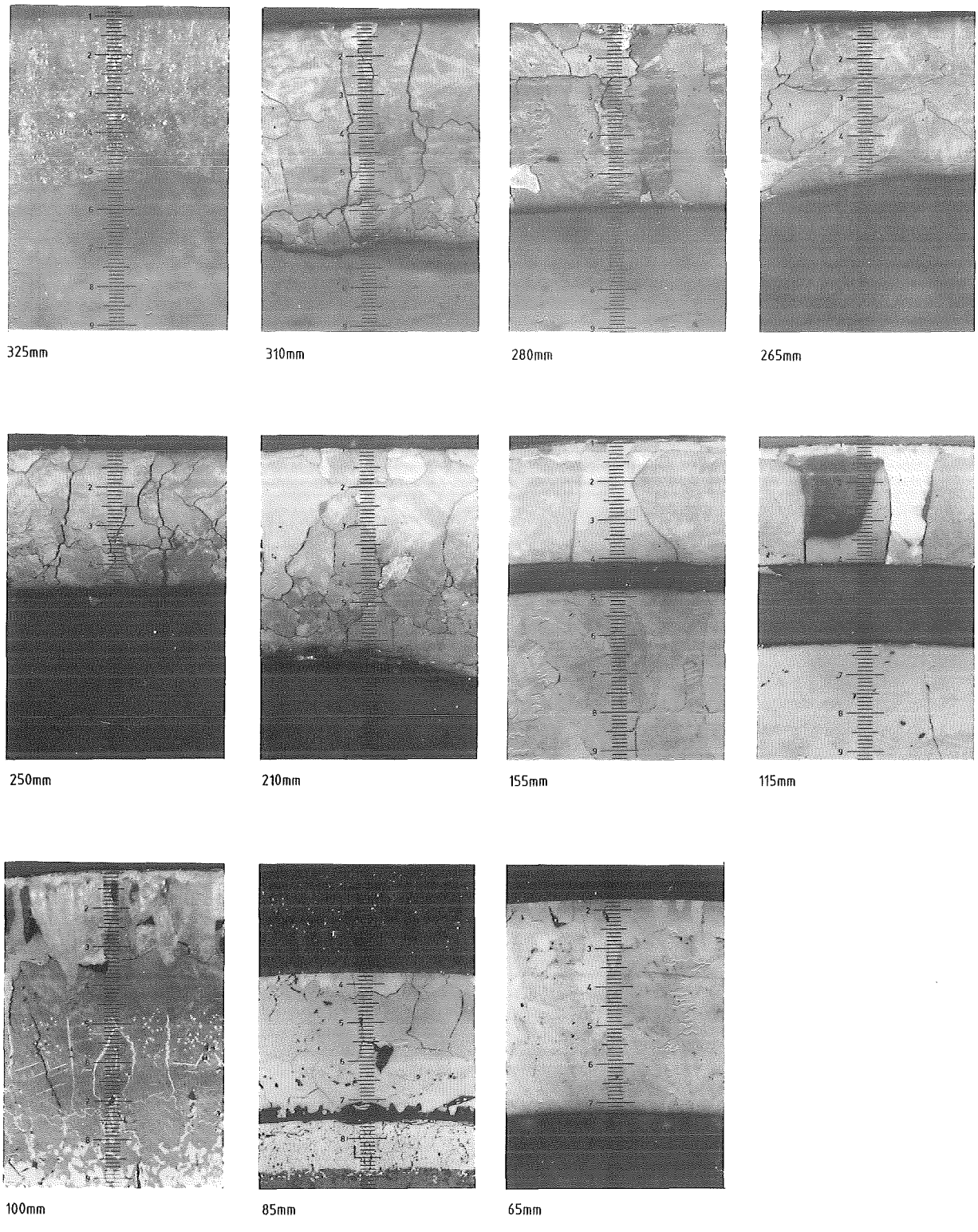

Fig.7-4: Enlarged View (100x) of Cross Sections From ESSI-7

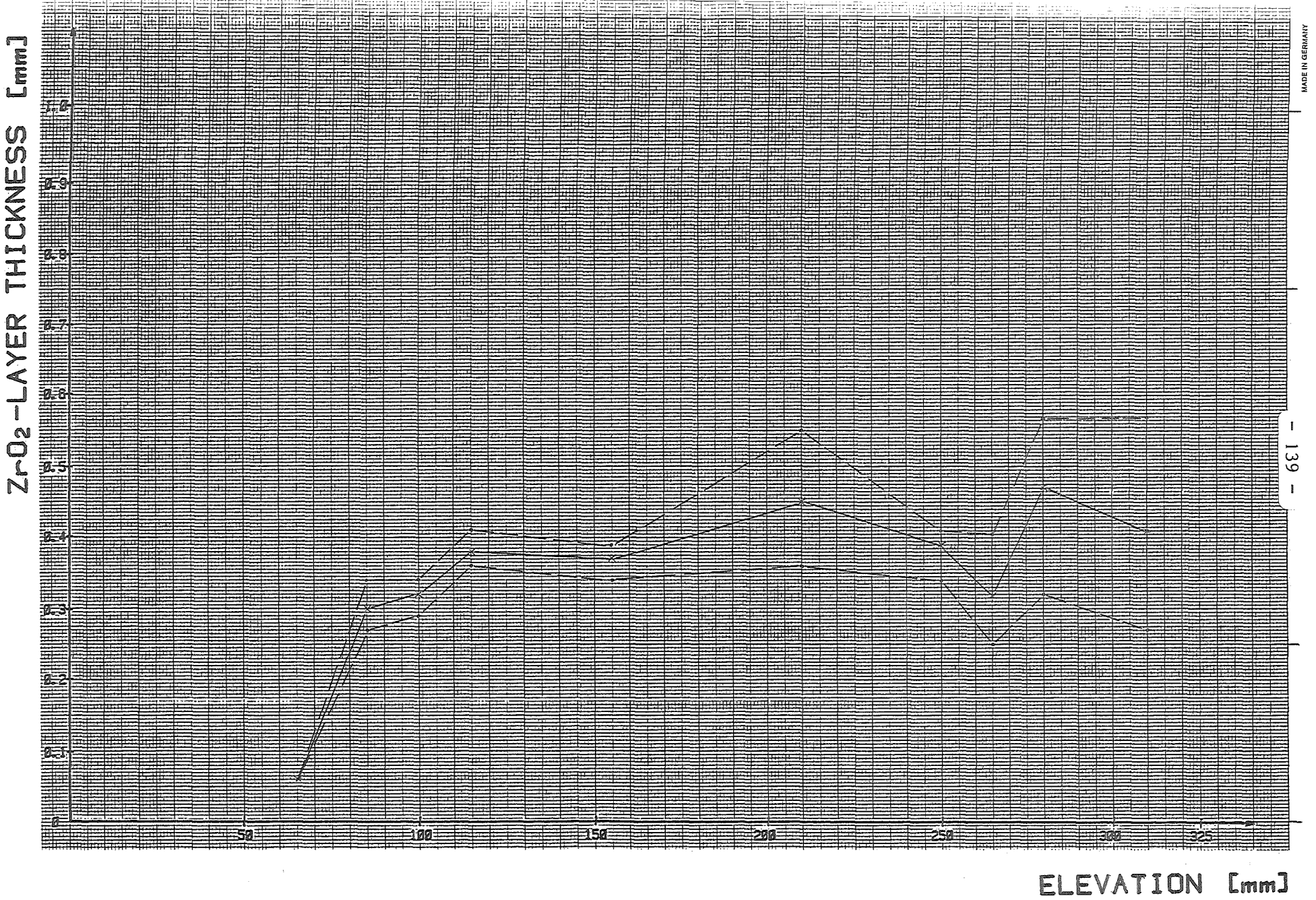

Fig.7-A: Zirconoxid layer thickness for test ESSI-7 (– – –maximum or minimum value; ——mean value)

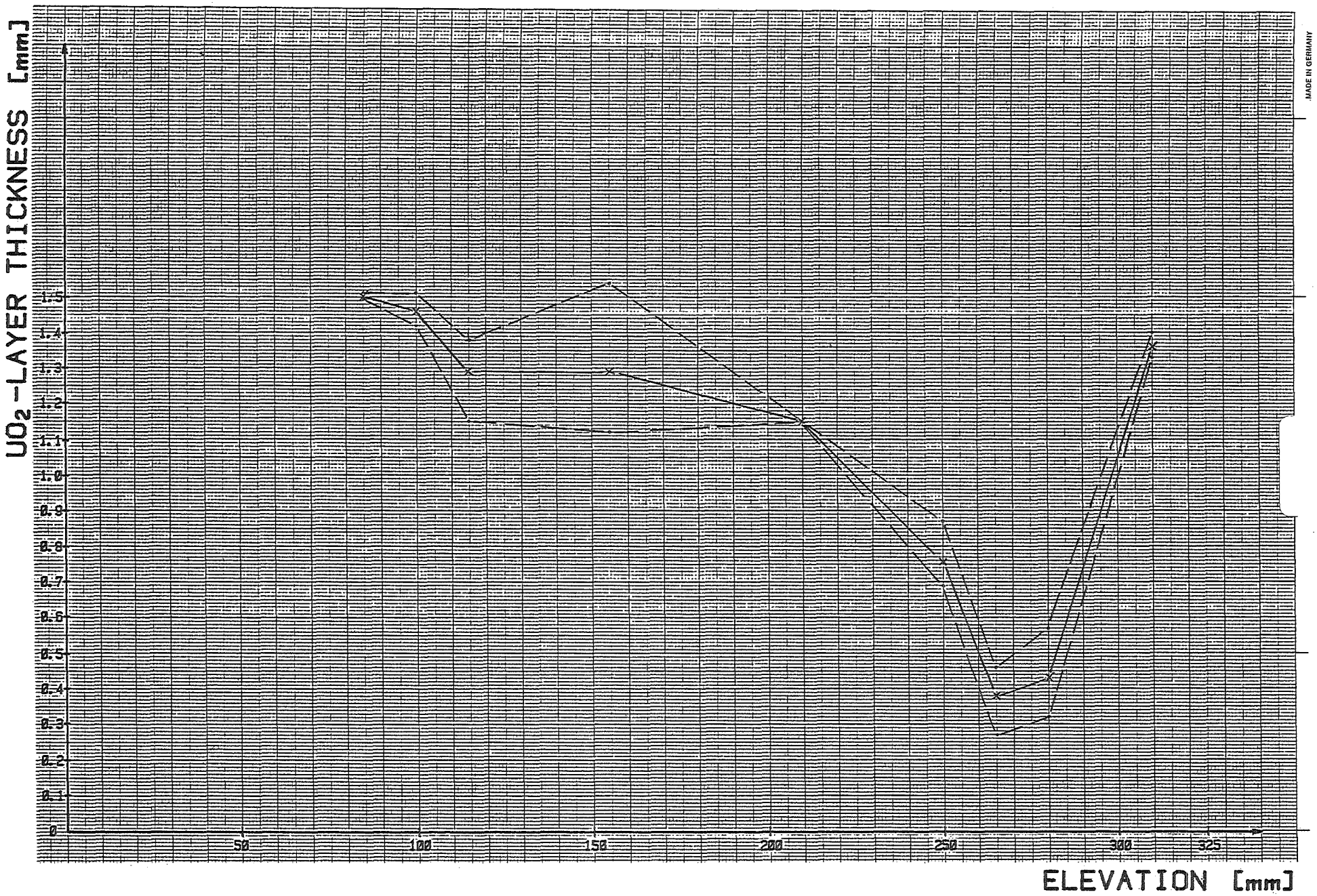

Fig. 7-B : Uranium oxide layer thickness for test ESSI- 7 (---maximum or minimum value; —— mean value)

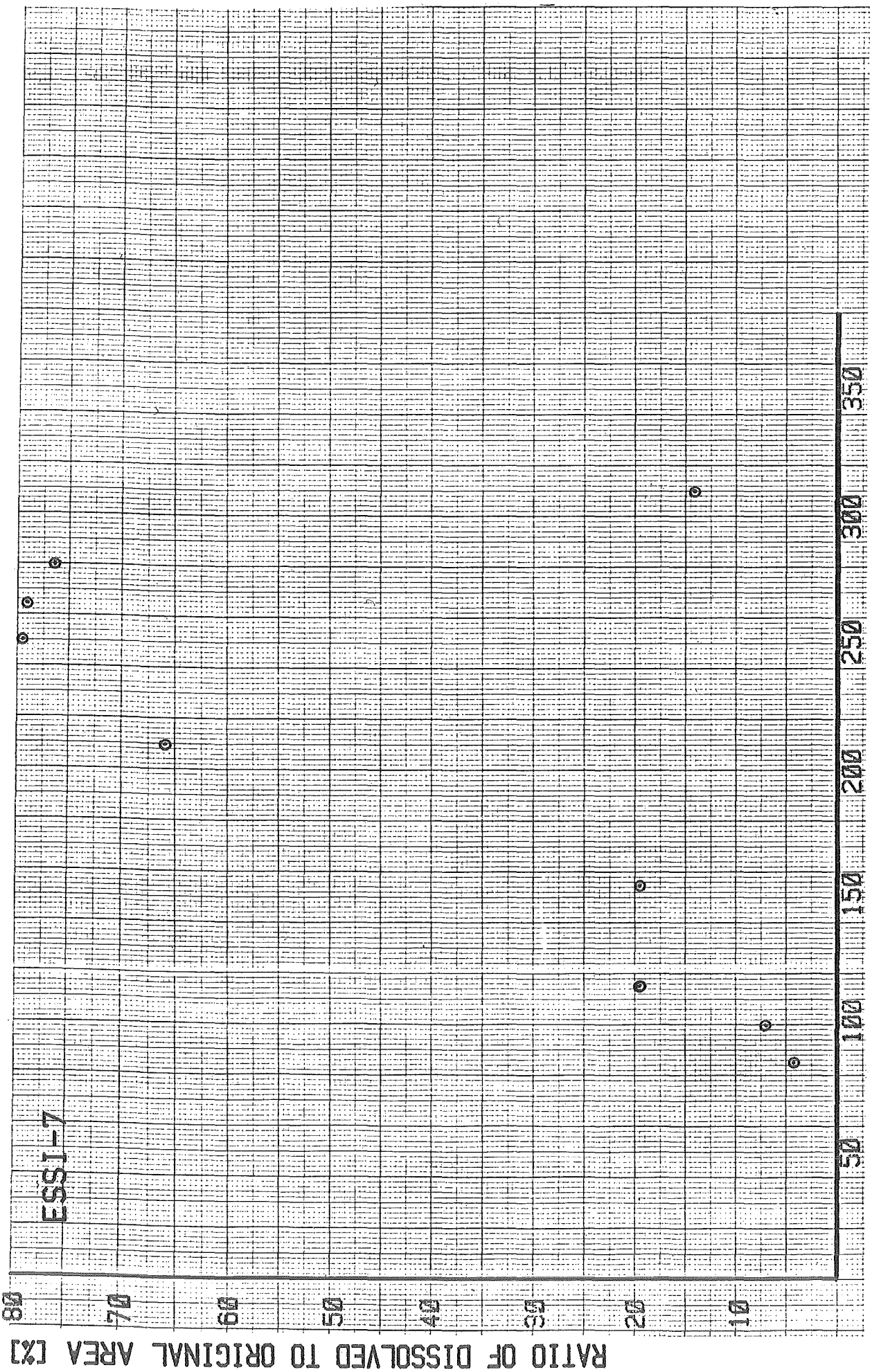

Fig.: 7-C
Dissolution of the UO_2-pellet at different elevations (ESSI-7)

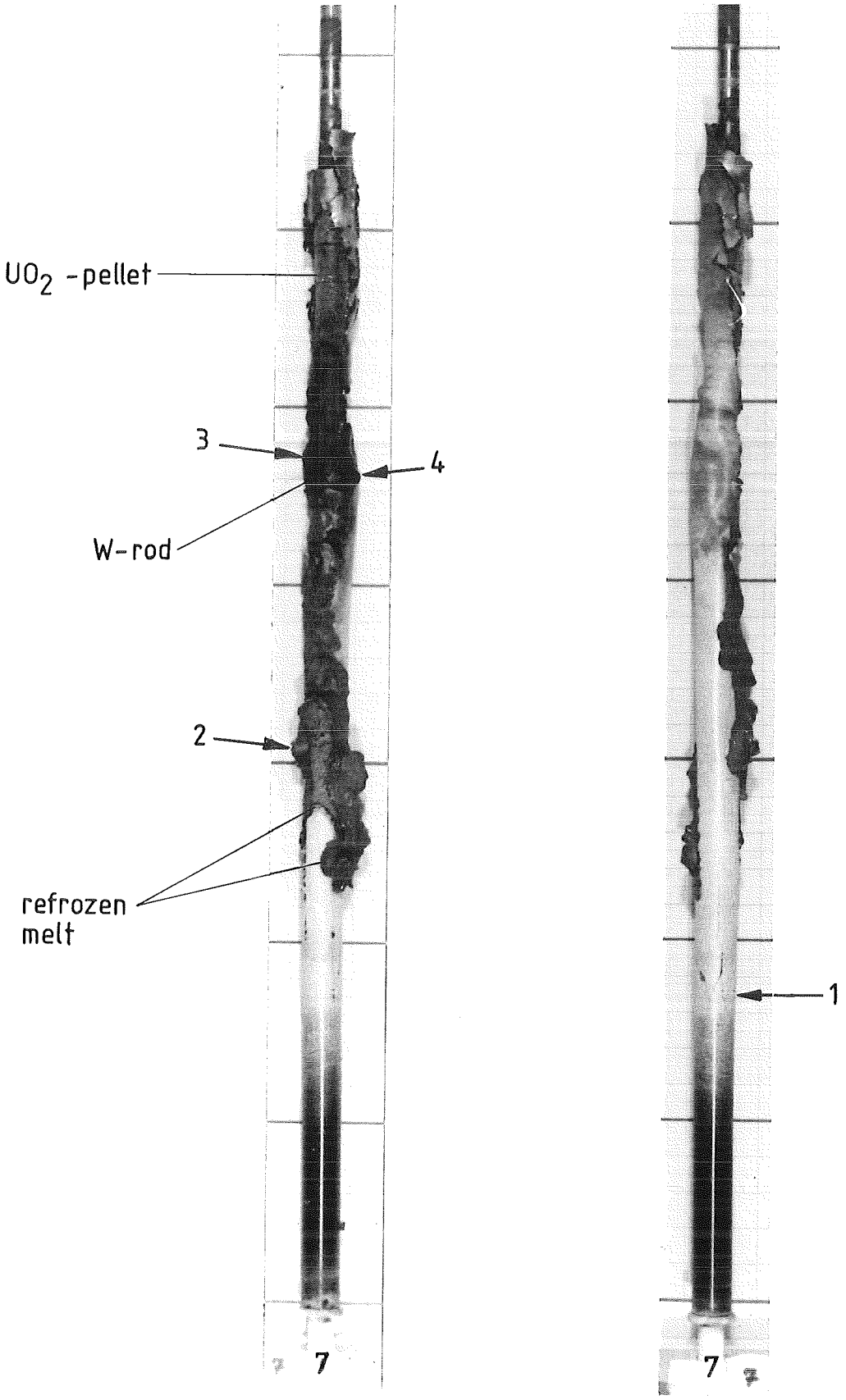

FIG.7-5: LOCATIONS OF ENLARGED VIEWS OF THE FUEL ROD SIMULATOR ESSI-7

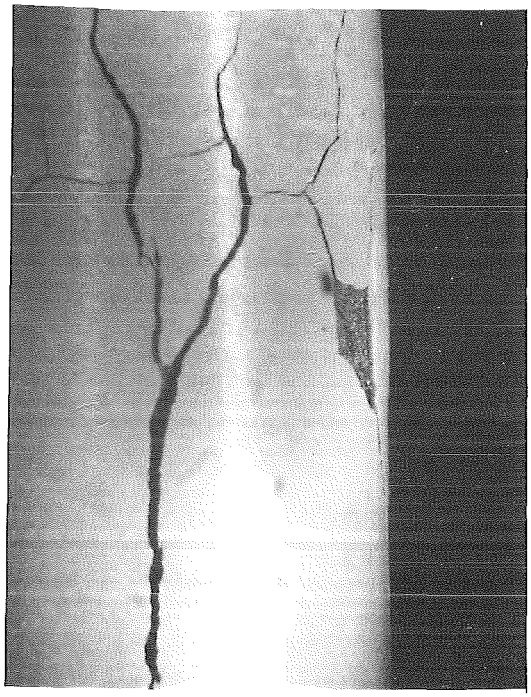

1 6×

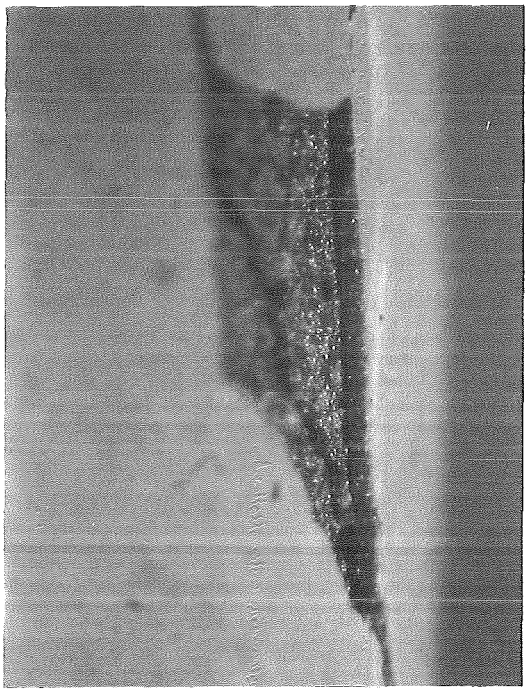

1 25×

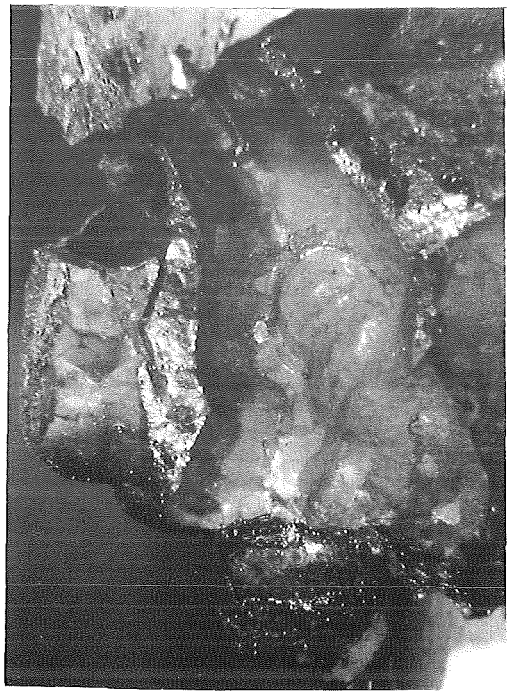

2 6×

3 6×

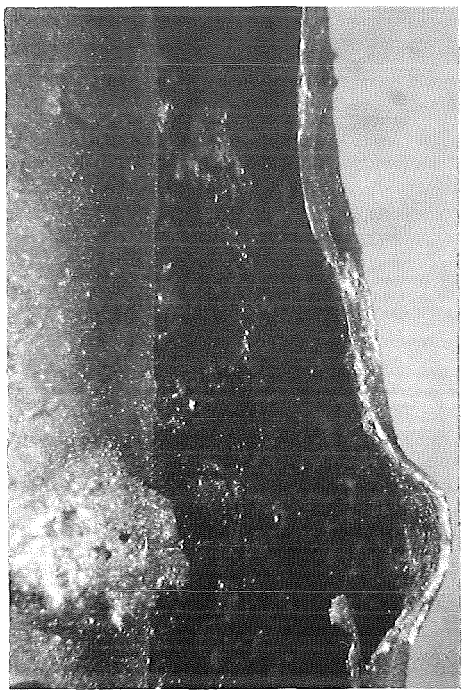

4 6×

FIG.7-6: ENLARGED VIEWS OF THE FUEL ROD SIMULATOR ESSI-7
(POSITION SEE FIG.7-5)

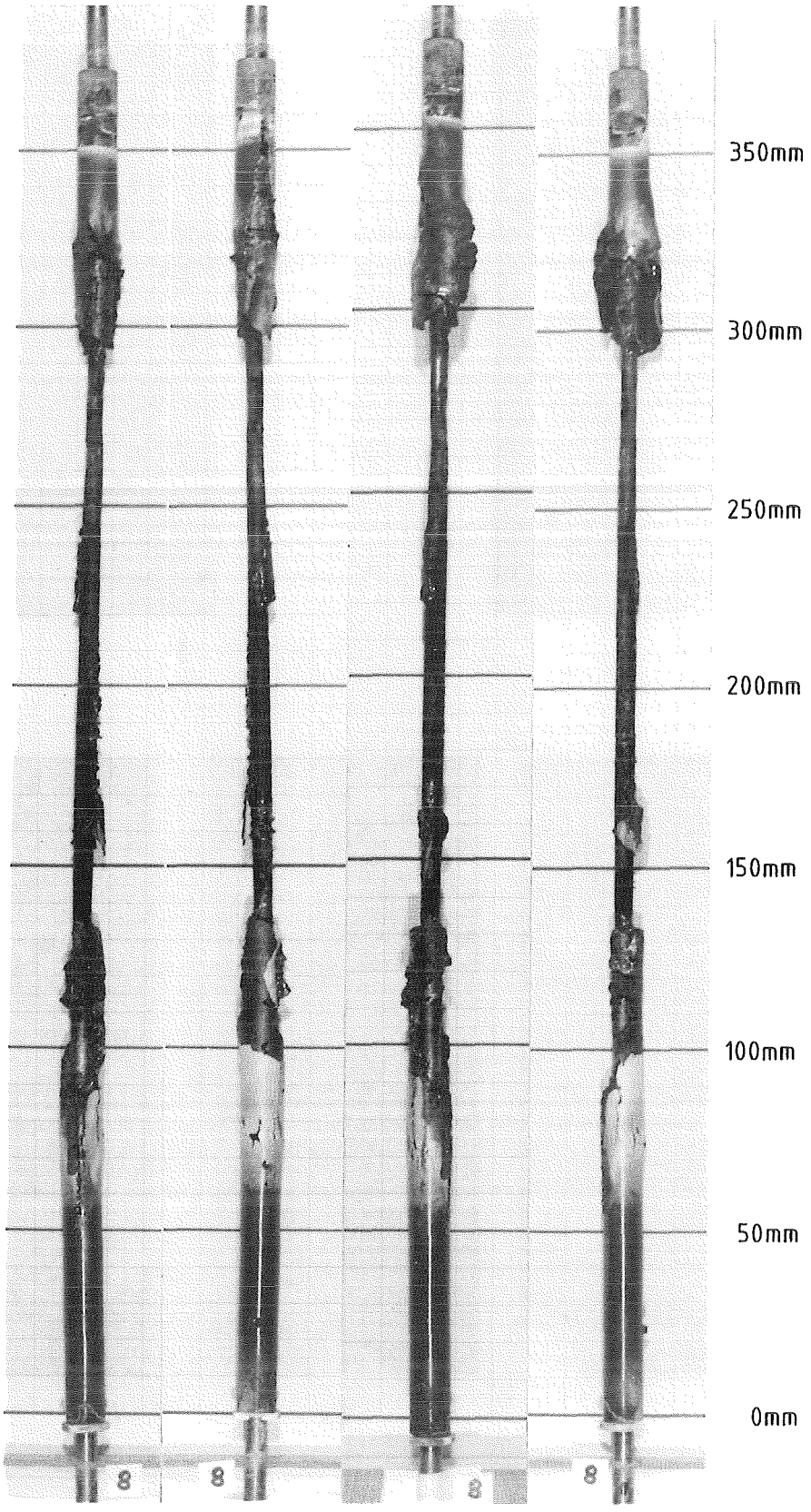

FIG. 8-1: POSTTEST APPEARANCE OF THE FUEL ROD SIMULATOR AND SCALE OF THE CROSS SECTION ELEVATIONS FOR ESSI-8

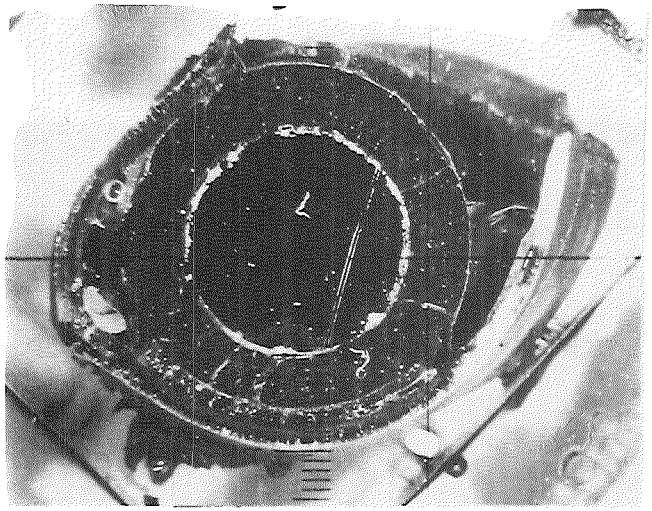

325mm

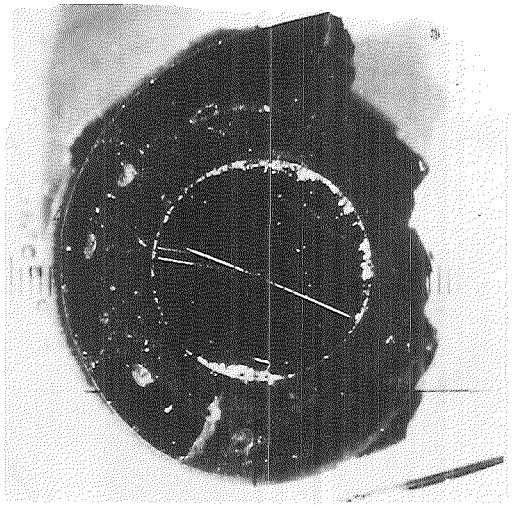

100mm

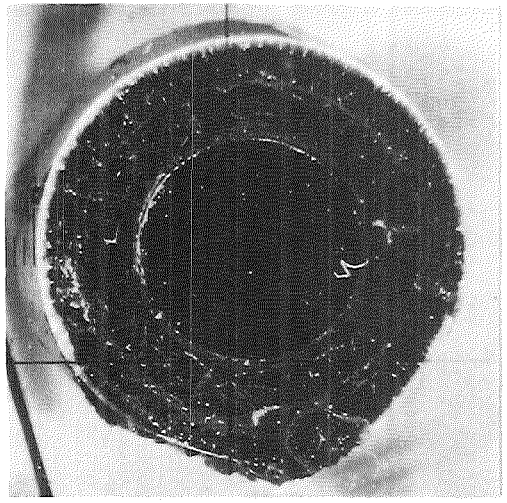

85mm

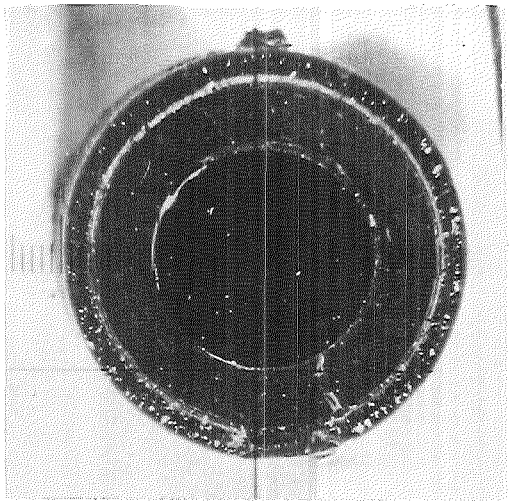

65mm

Fig. 8-2 : Cross Sections of Test ESSI-8

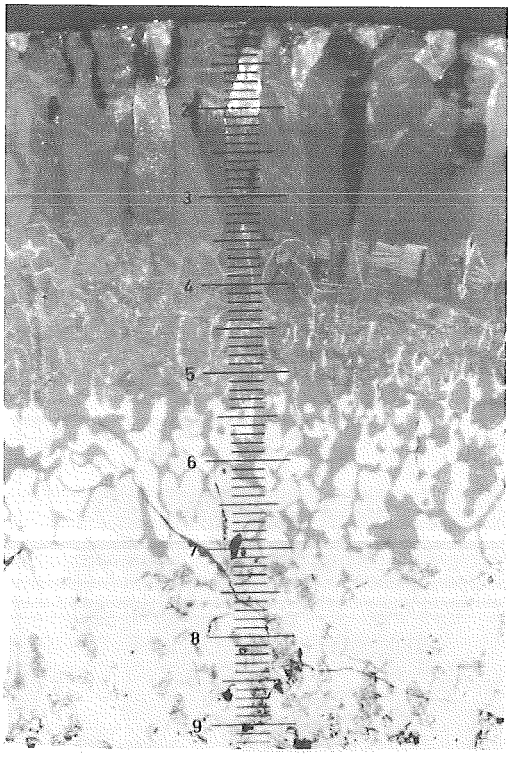

325mm

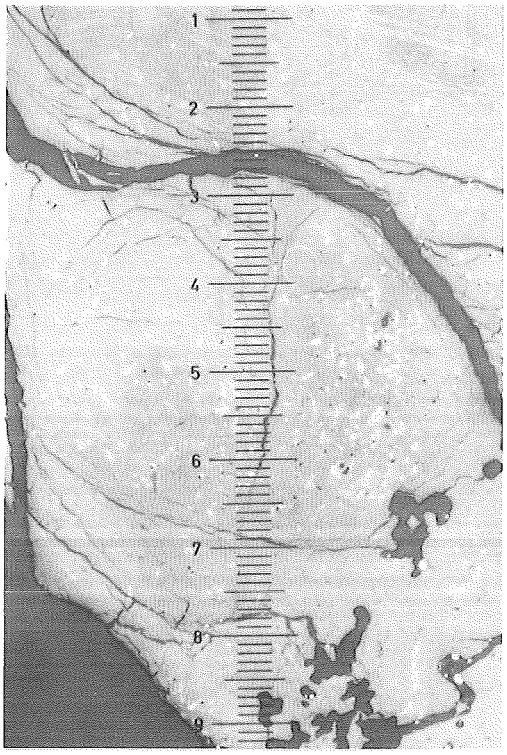

100mm

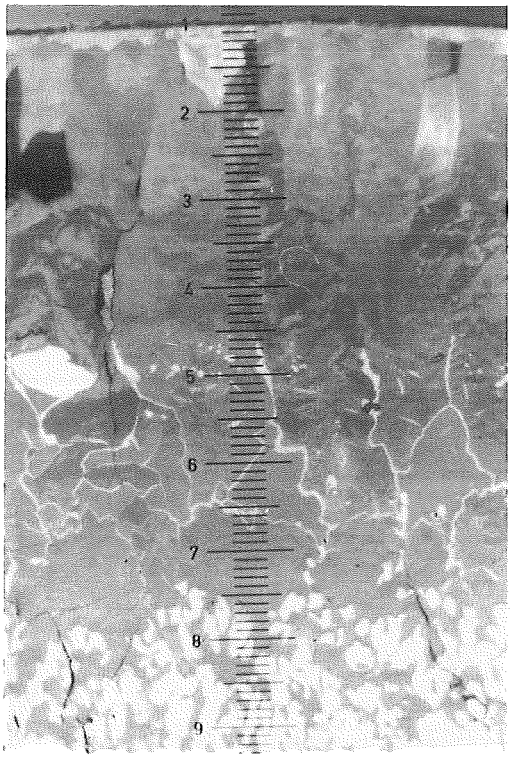

85mm

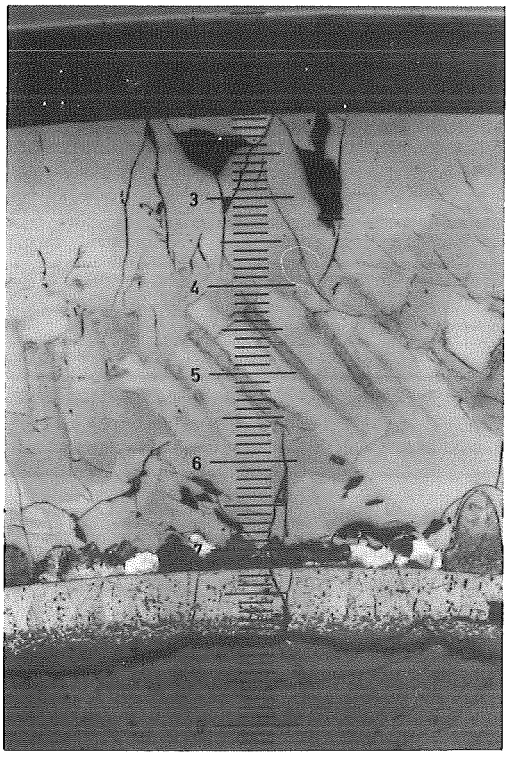

65mm

Fig. 8-3 : Enlarged View (100x) of Cross Sections From ESSI-8

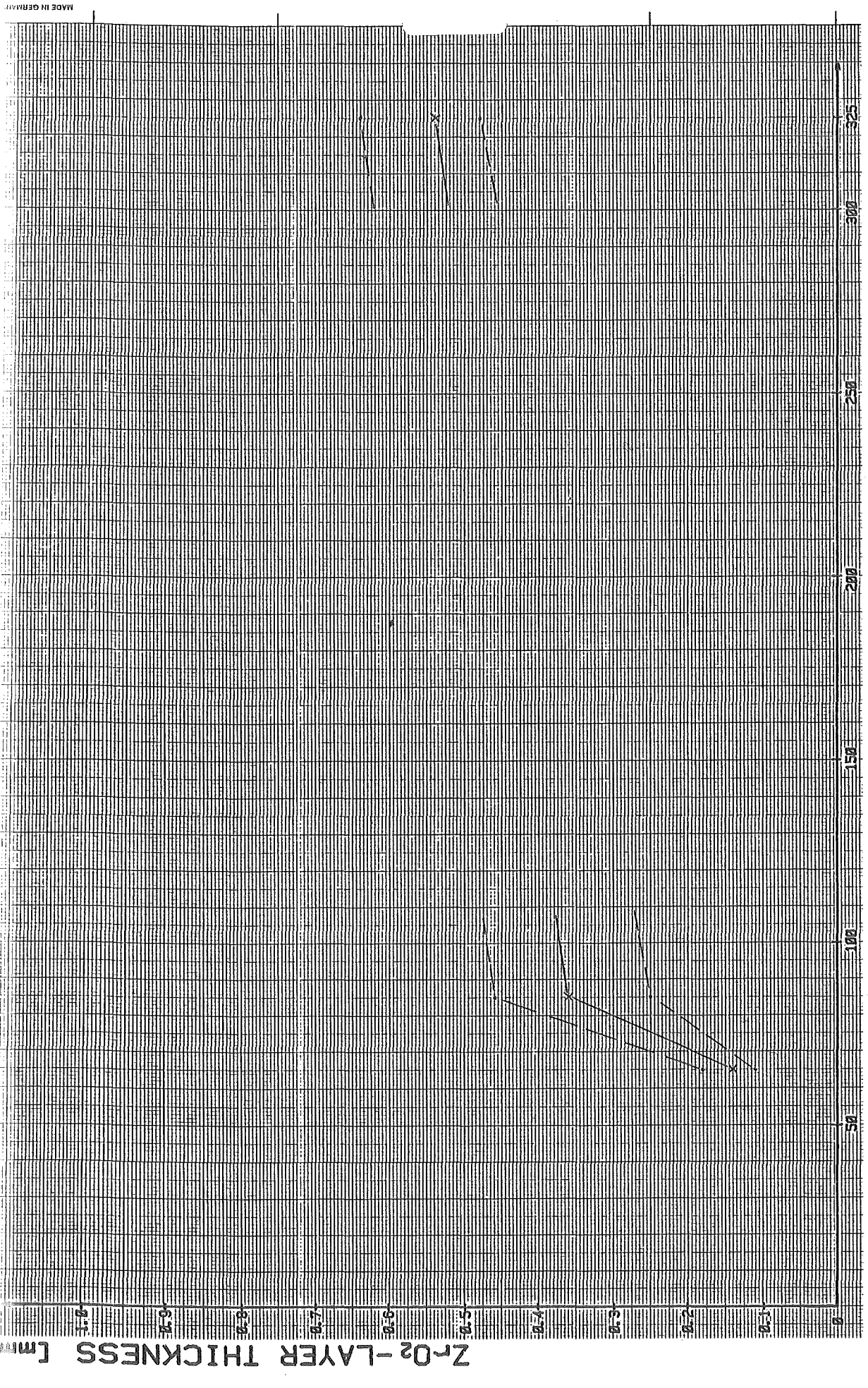

Fig.8-A: Zirconoxid layer thickness for test ESSI-8 (— — —maximum or minimum value; ——mean value)

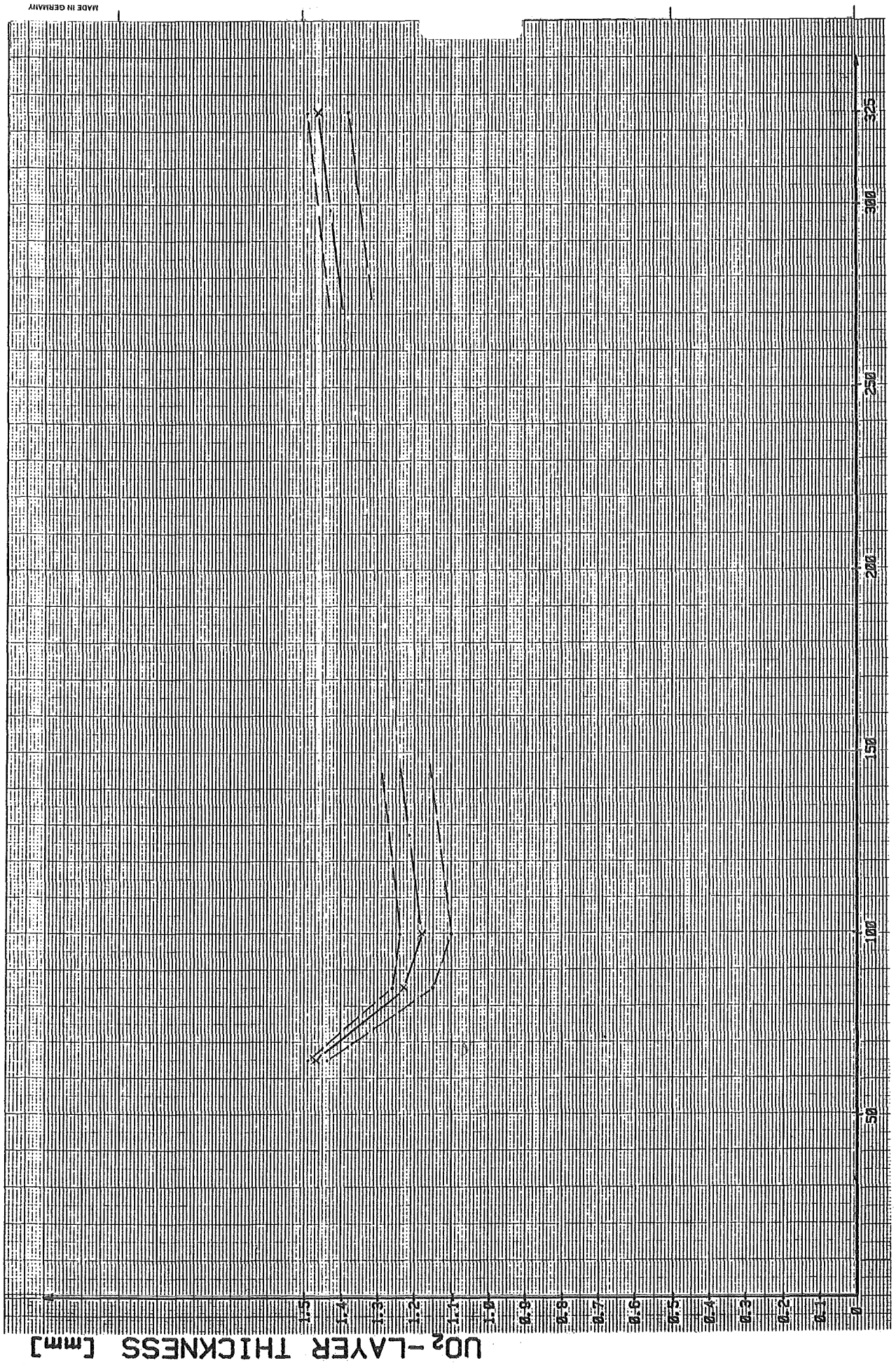

Fig.8-B : Uranium oxide layer thickness for test ESSI-8 (---maximum or minimum values ——— mean value)

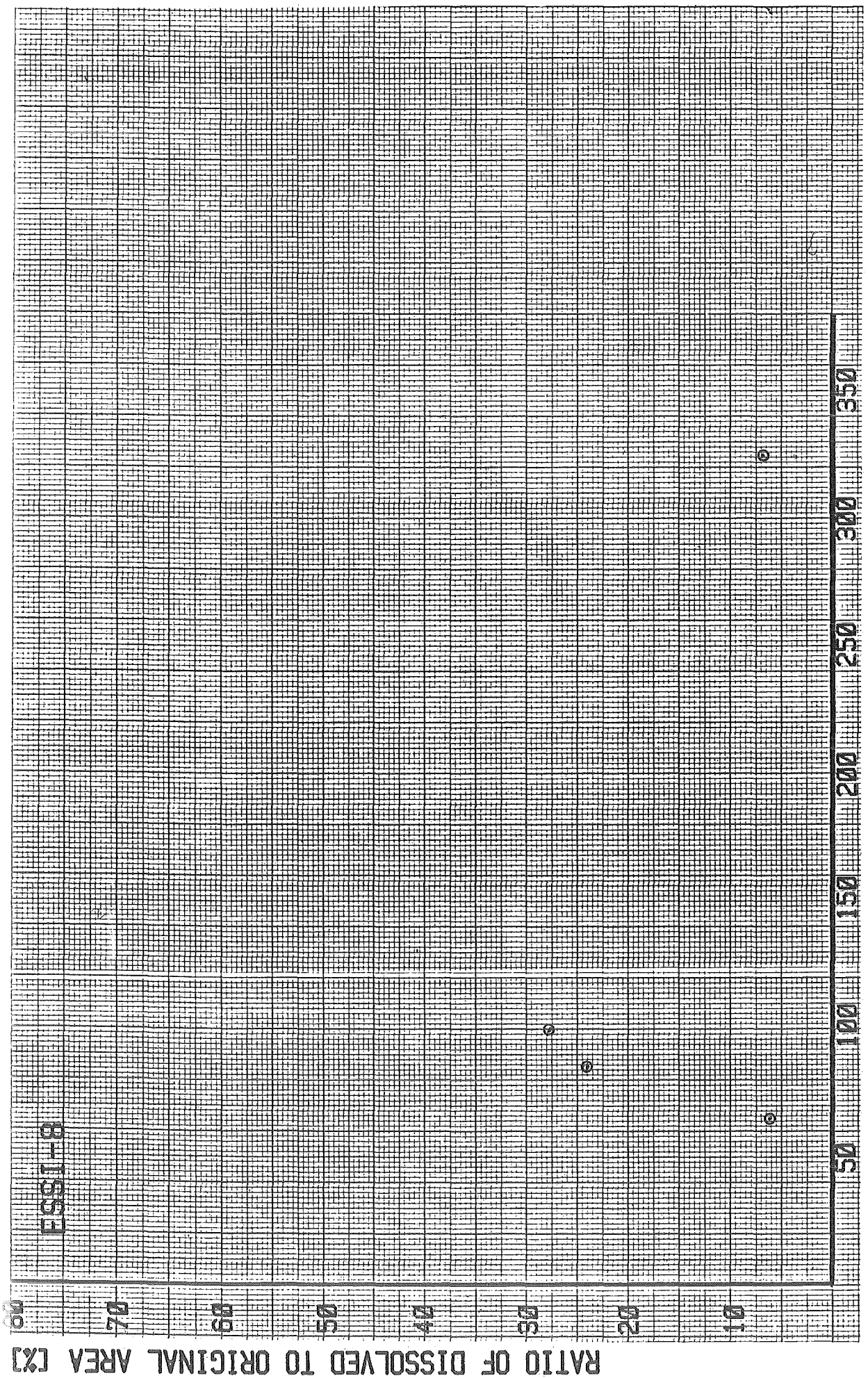

Fig.: 8-C
Dissolution of the UO_2-pellet at different elevations (ESSI-8)

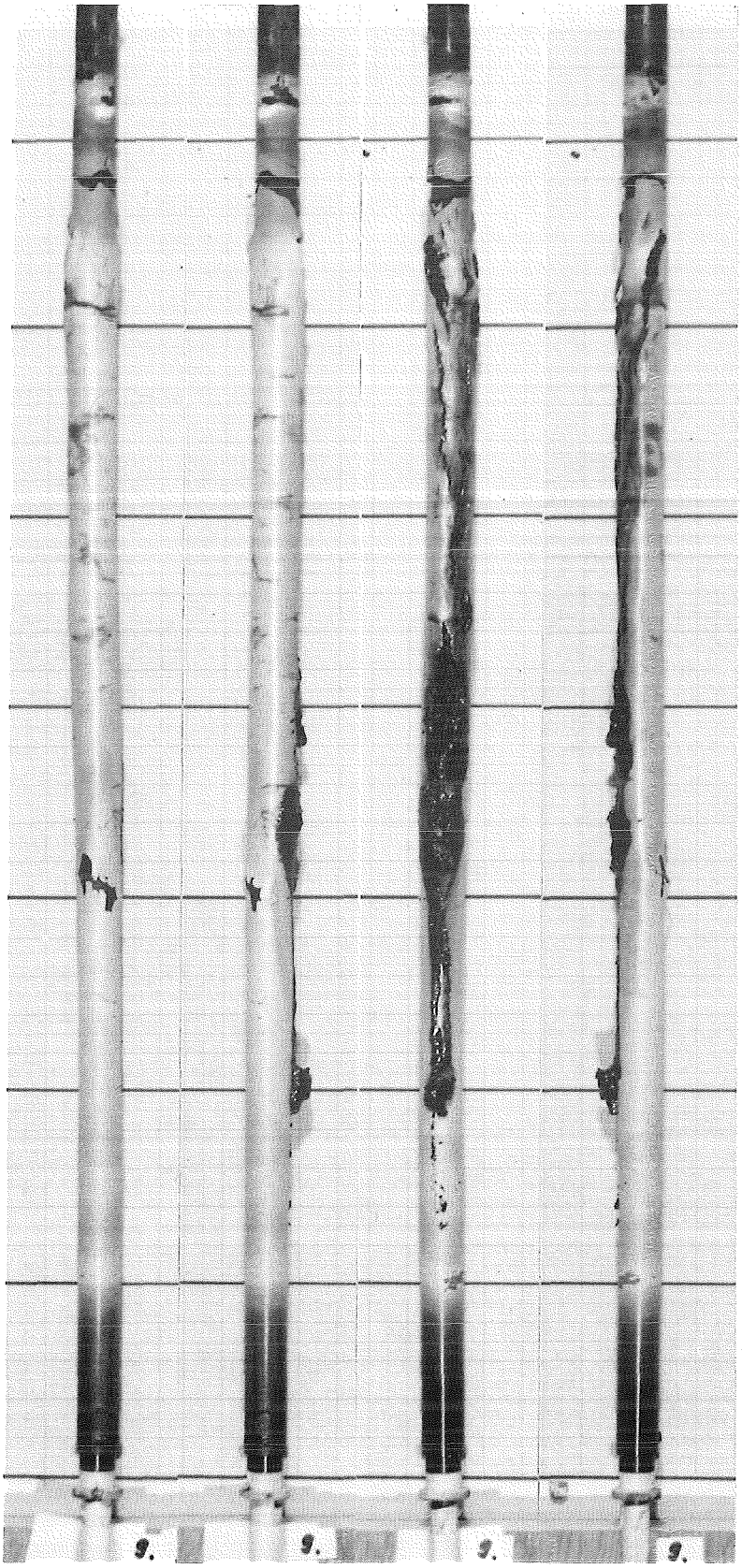

FIG. 9-1: POSTTEST APPEARANCE OF THE FUEL ROD SIMULATOR AND SCALE OF THE CROSS SECTION ELEVATIONS FOR ESSI-9

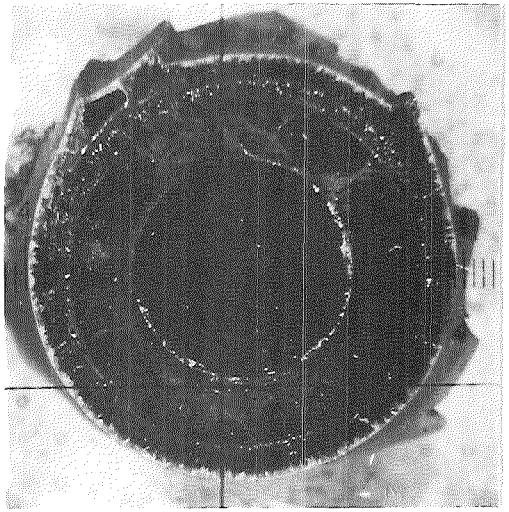

325mm

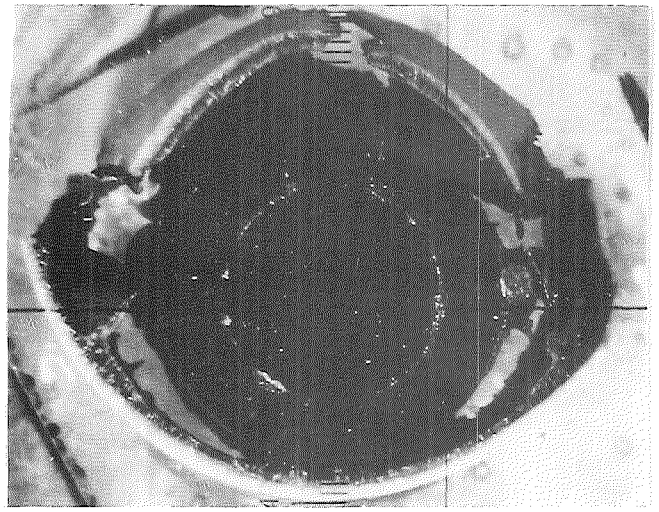

310mm

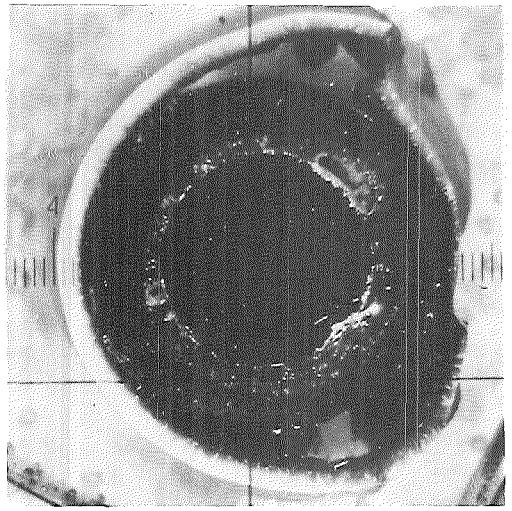

280mm

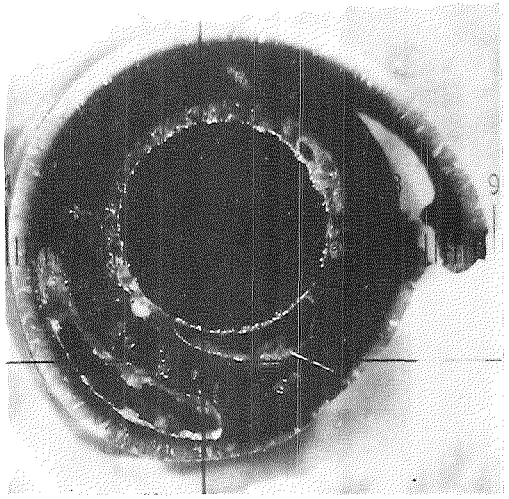

265mm

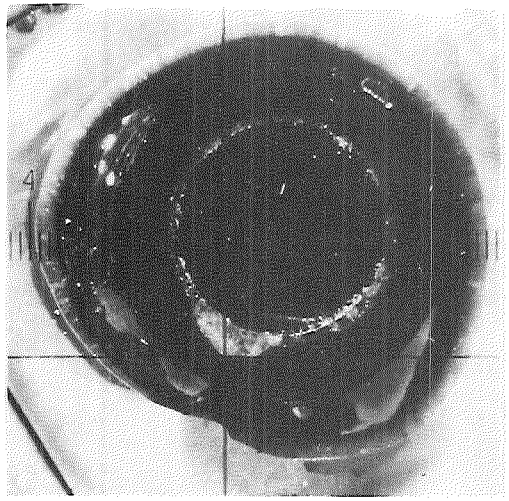

250mm

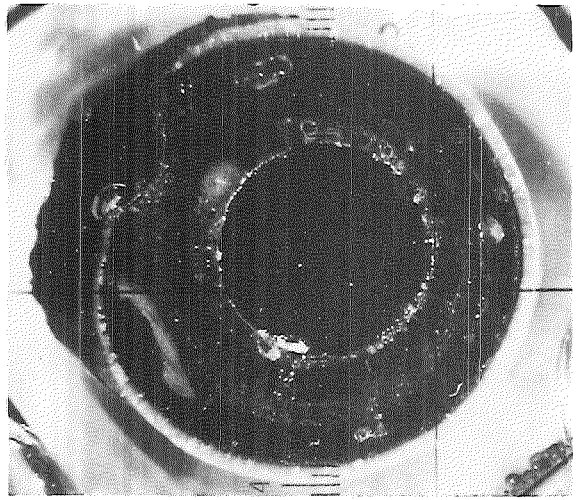

210mm

KfK

Fig. 9-2 : Cross Sections of Test ESSI-9

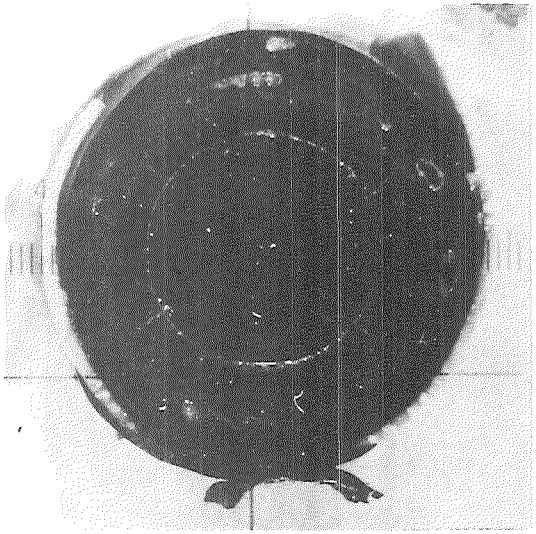

155mm

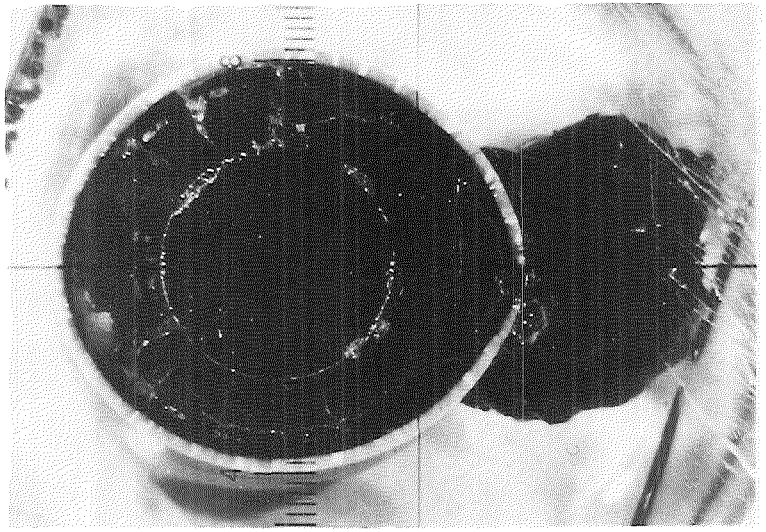

115mm

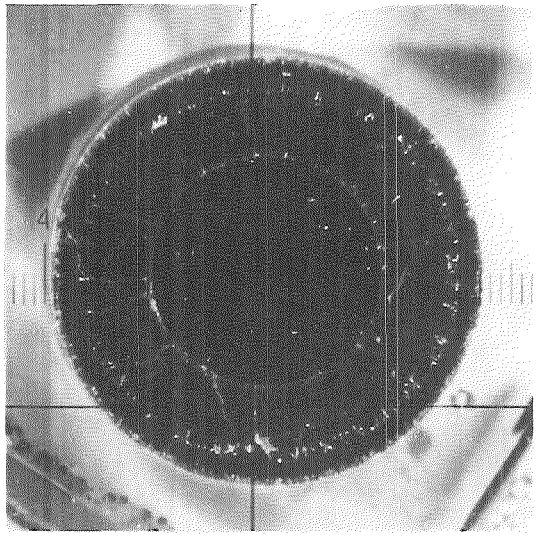

65mm

Fig. 9-3 : Cross Sections of Test ESSI-9

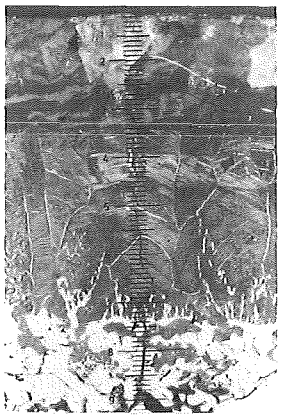

325mm

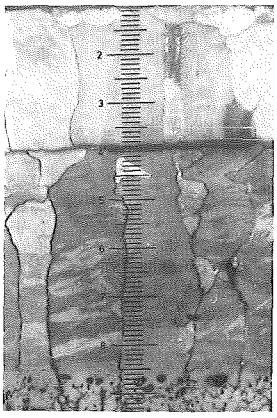

310mm

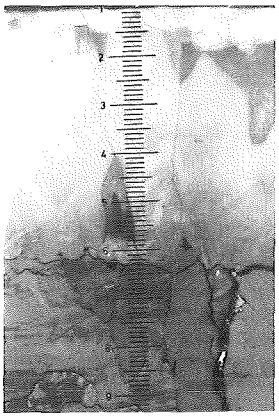

280mm

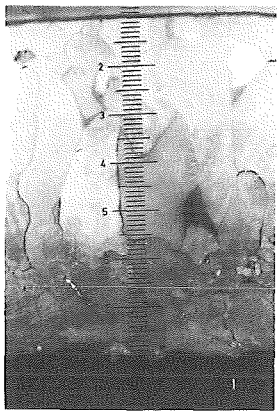

265mm

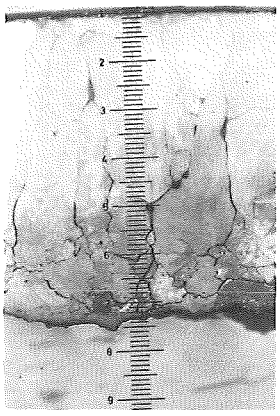

250mm

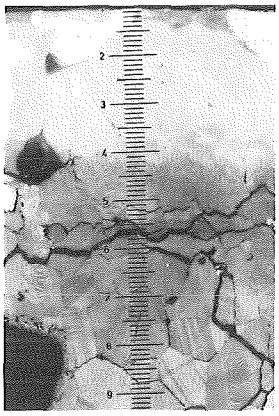

195mm

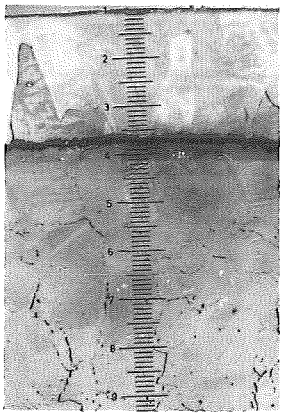

155mm

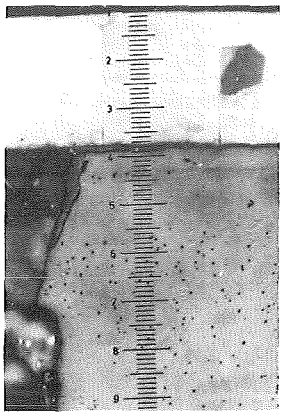

115mm

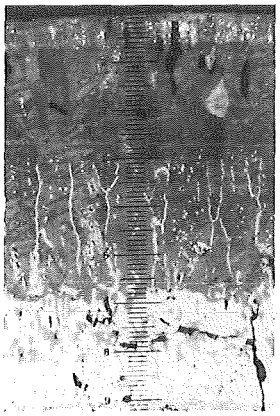

65mm

Fig. 9-4 : Enlarged View (100x) of Cross Sections From ESSI-9

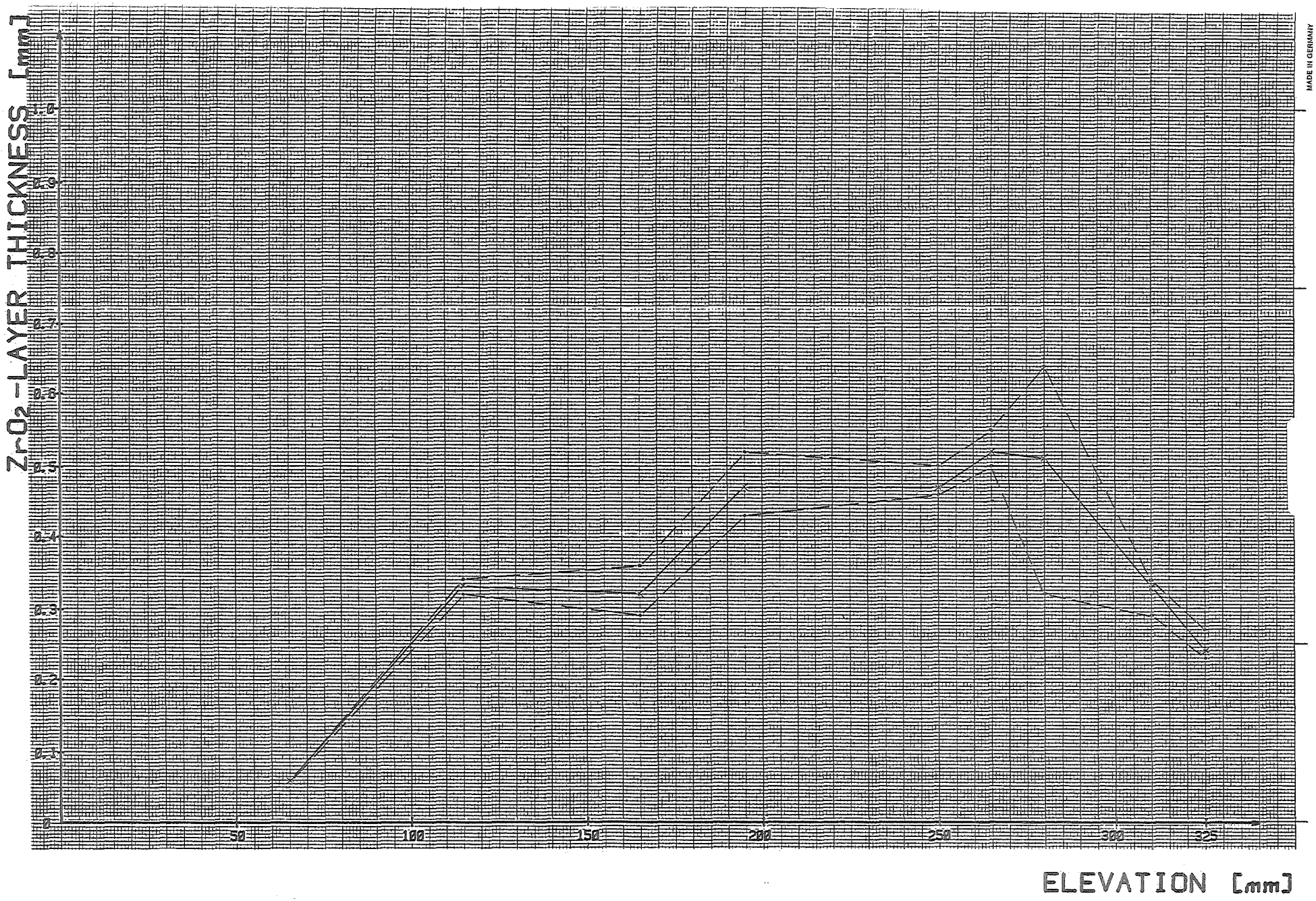

Fig.9-A: Zirconoxid layer thickness for test ESSI-9 (— — —maximum or minimum value; ——mean value)

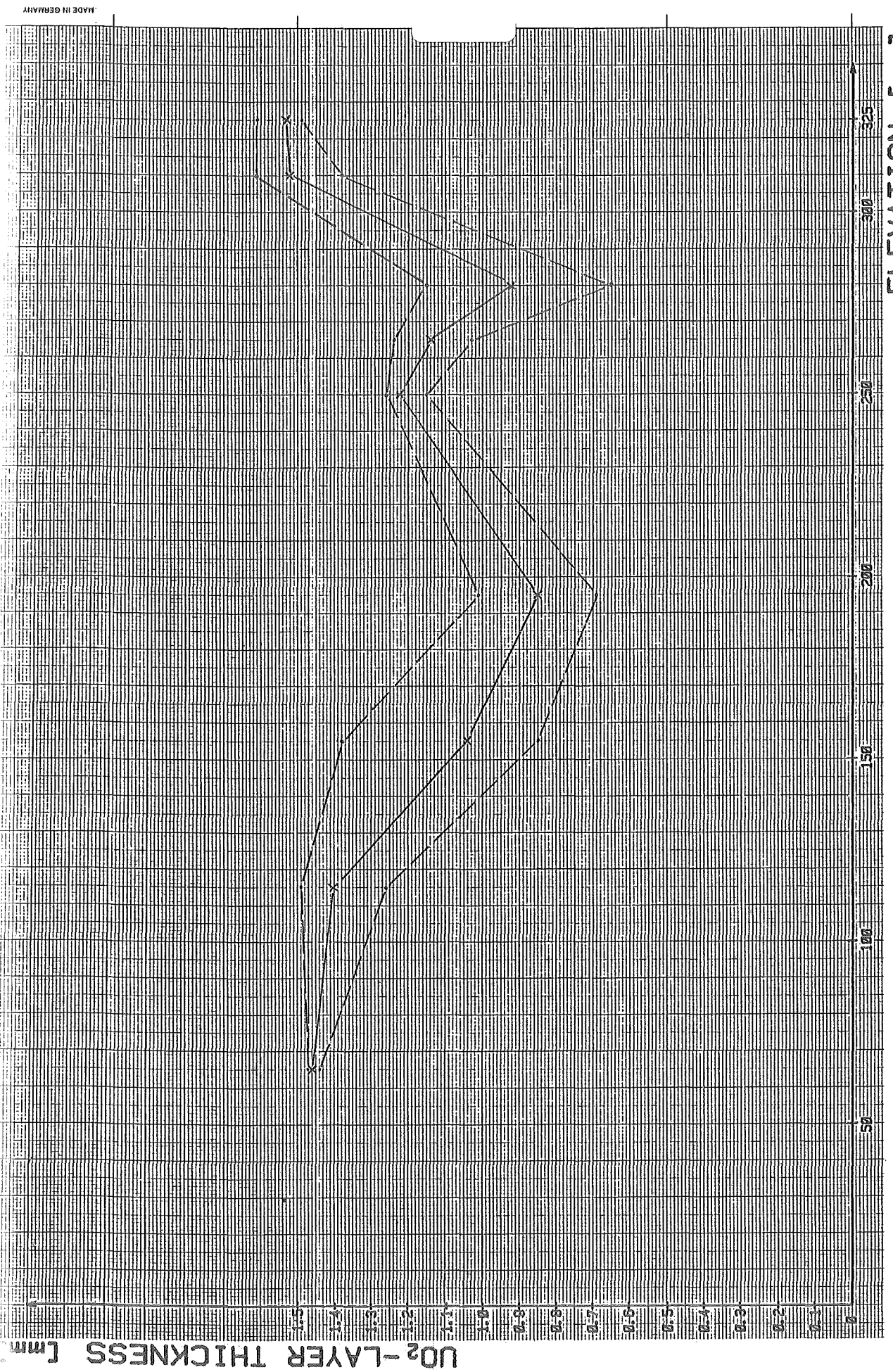

Fig.9-B : Uranium oxide layer thickness for test ESSI-9 (---maximum or minimum value; —— mean value)

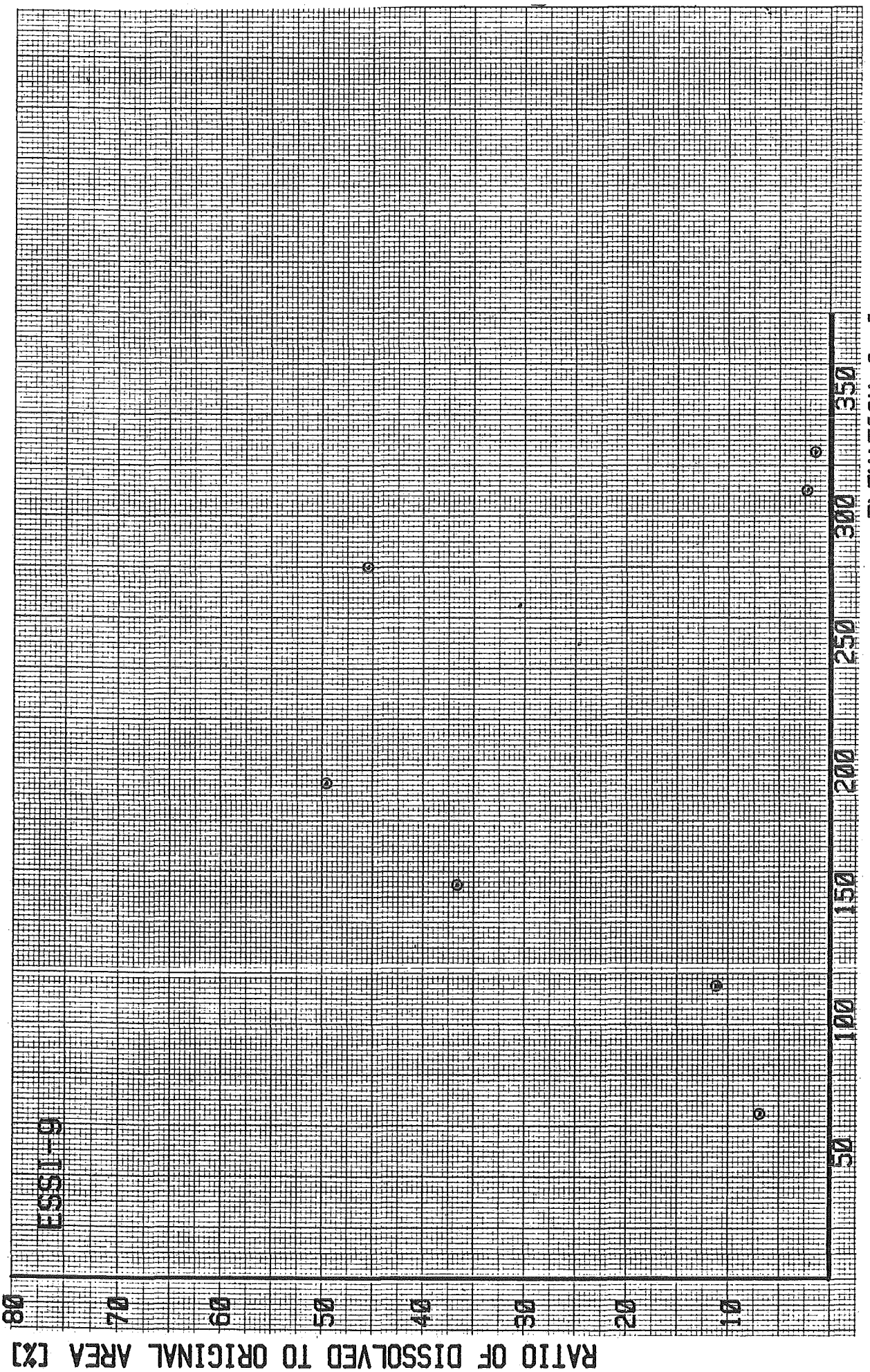

Fig.: 9-C
Dissolution of the UO_2-pellet at different elevations (ESSI-9)

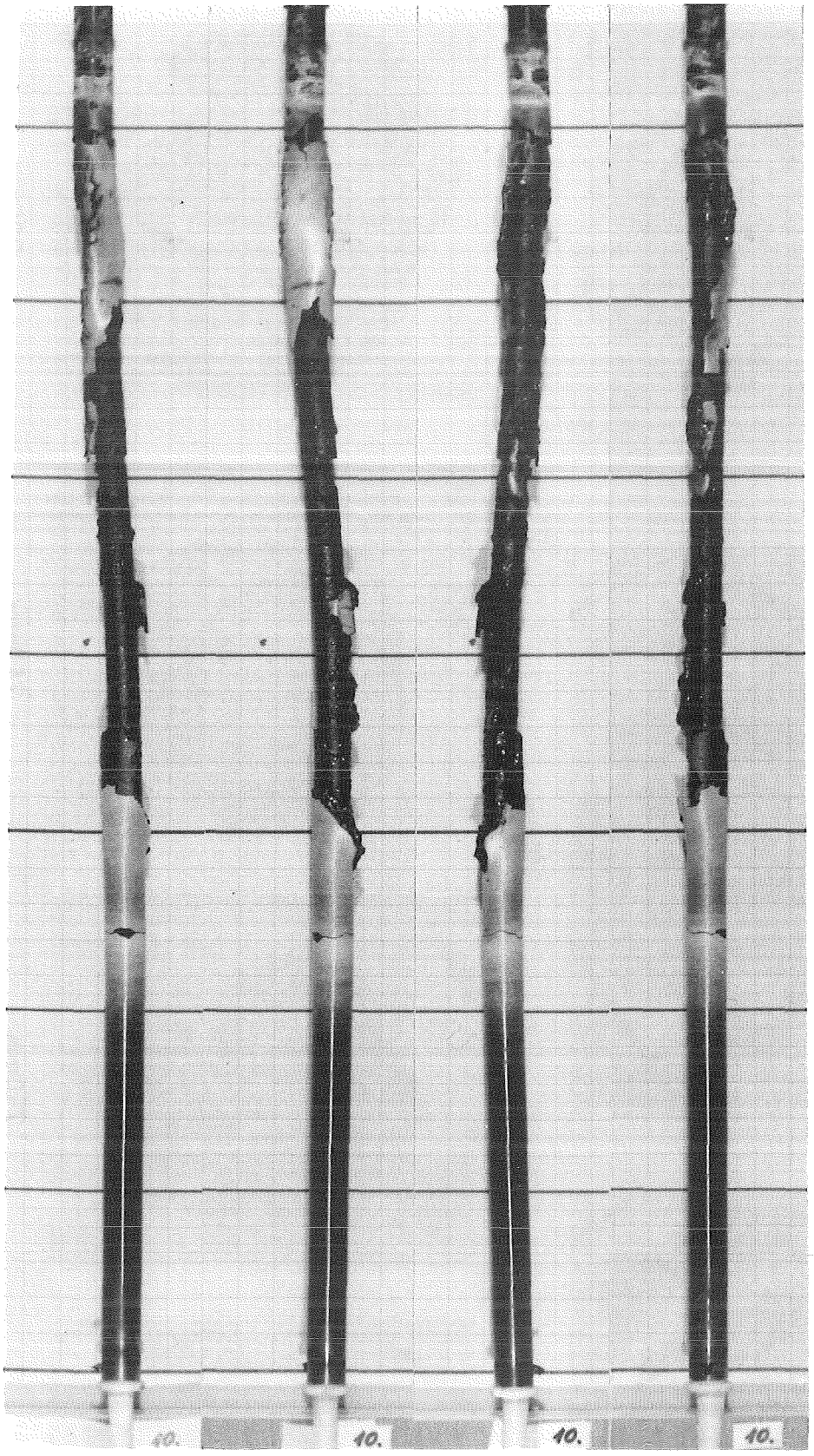

FIG. 10-1: POSTTEST APPEARANCE OF THE FUEL ROD SIMULATOR AND SCALE OF THE CROSS SECTION ELEVATIONS FOR ESSI-10

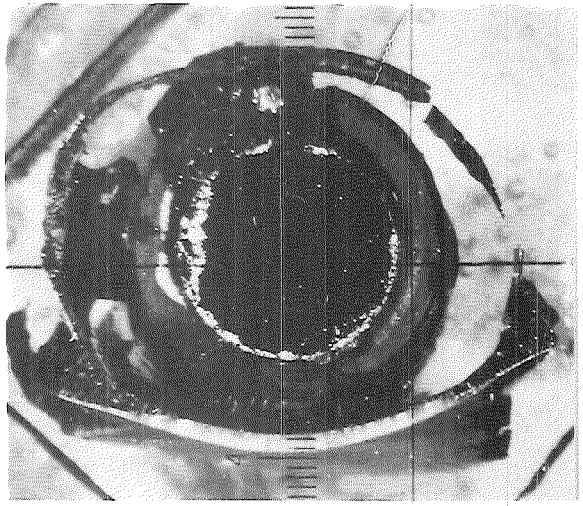

325mm

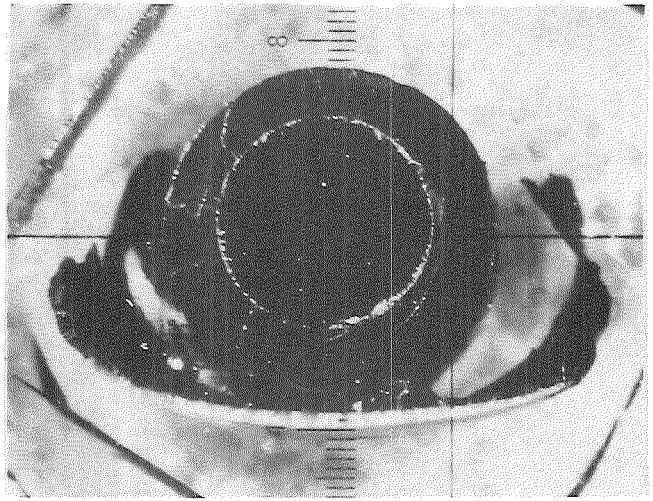

310mm

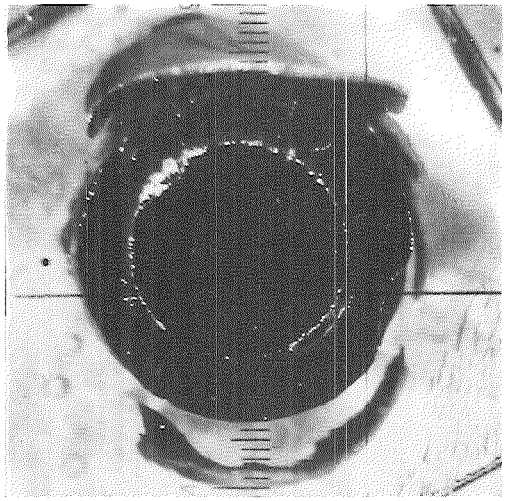

280mm

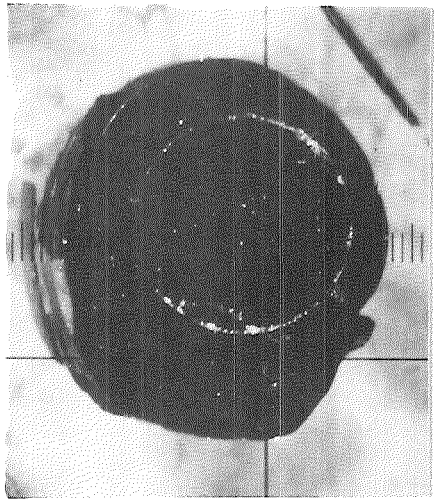

265mm

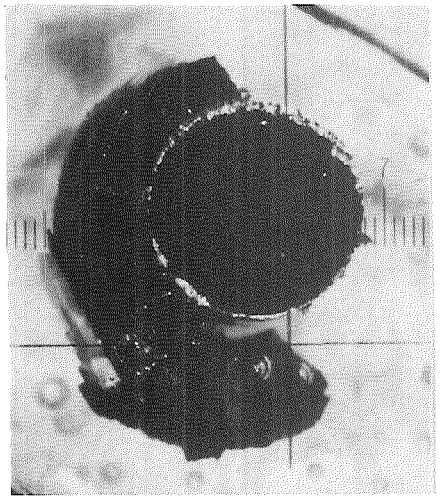

250mm

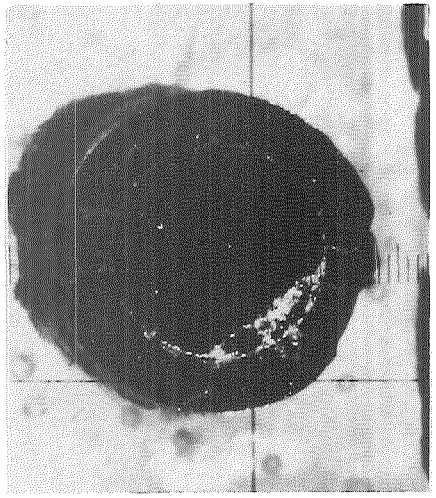

240mm

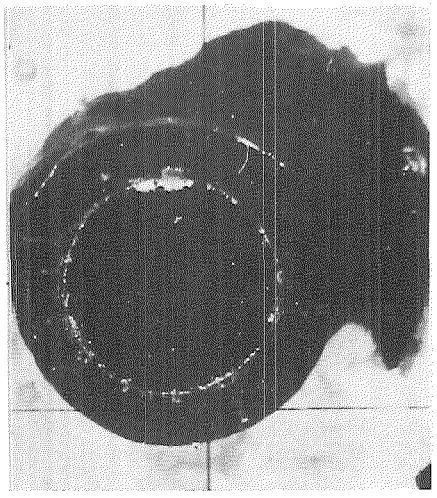

225mm

KfK

Fig. 10-2 : Cross Sections of Test ESSI-10

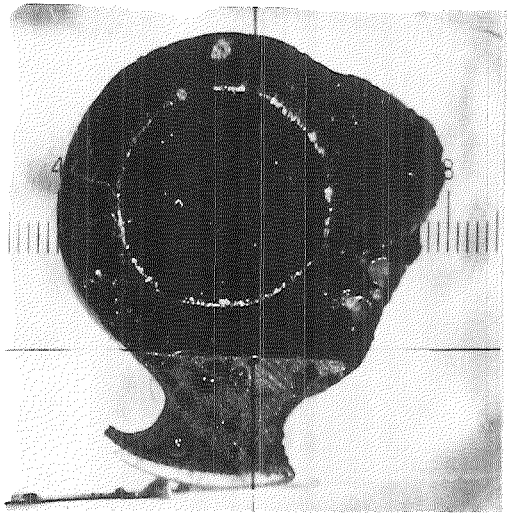

210mm

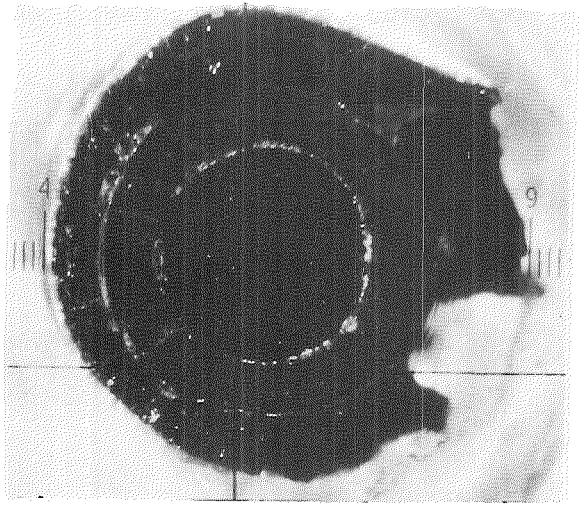

155mm

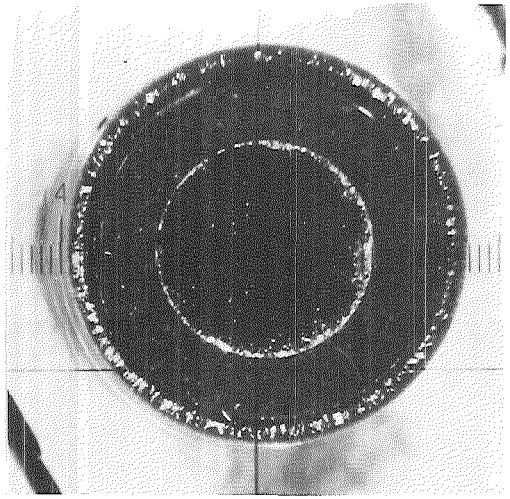

115mm

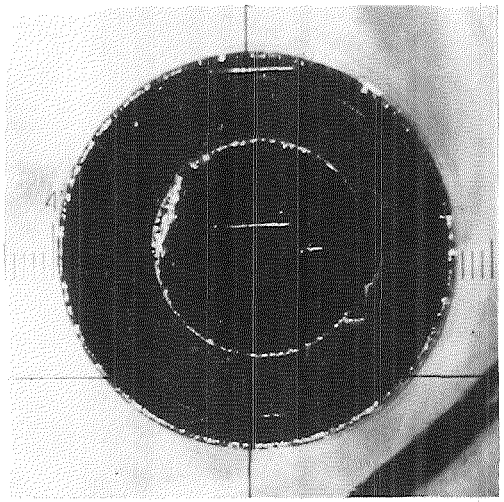

100mm

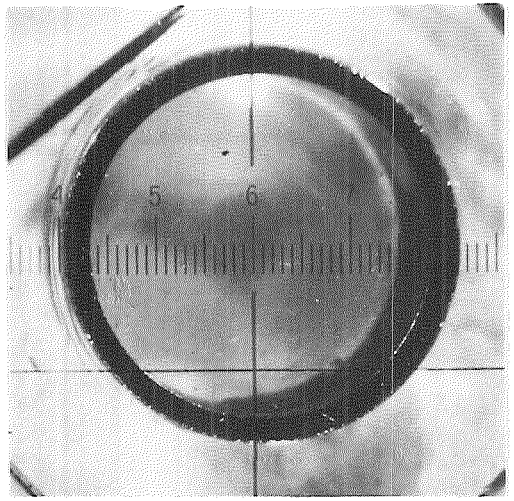

85mm

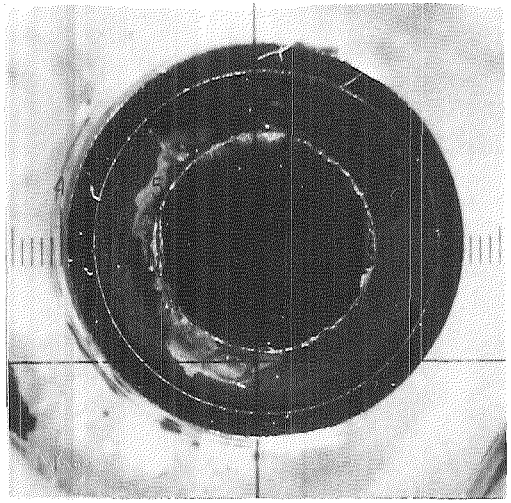

65mm

KfK

Fig. 10-3 : Cross Sections of Test ESSI-10

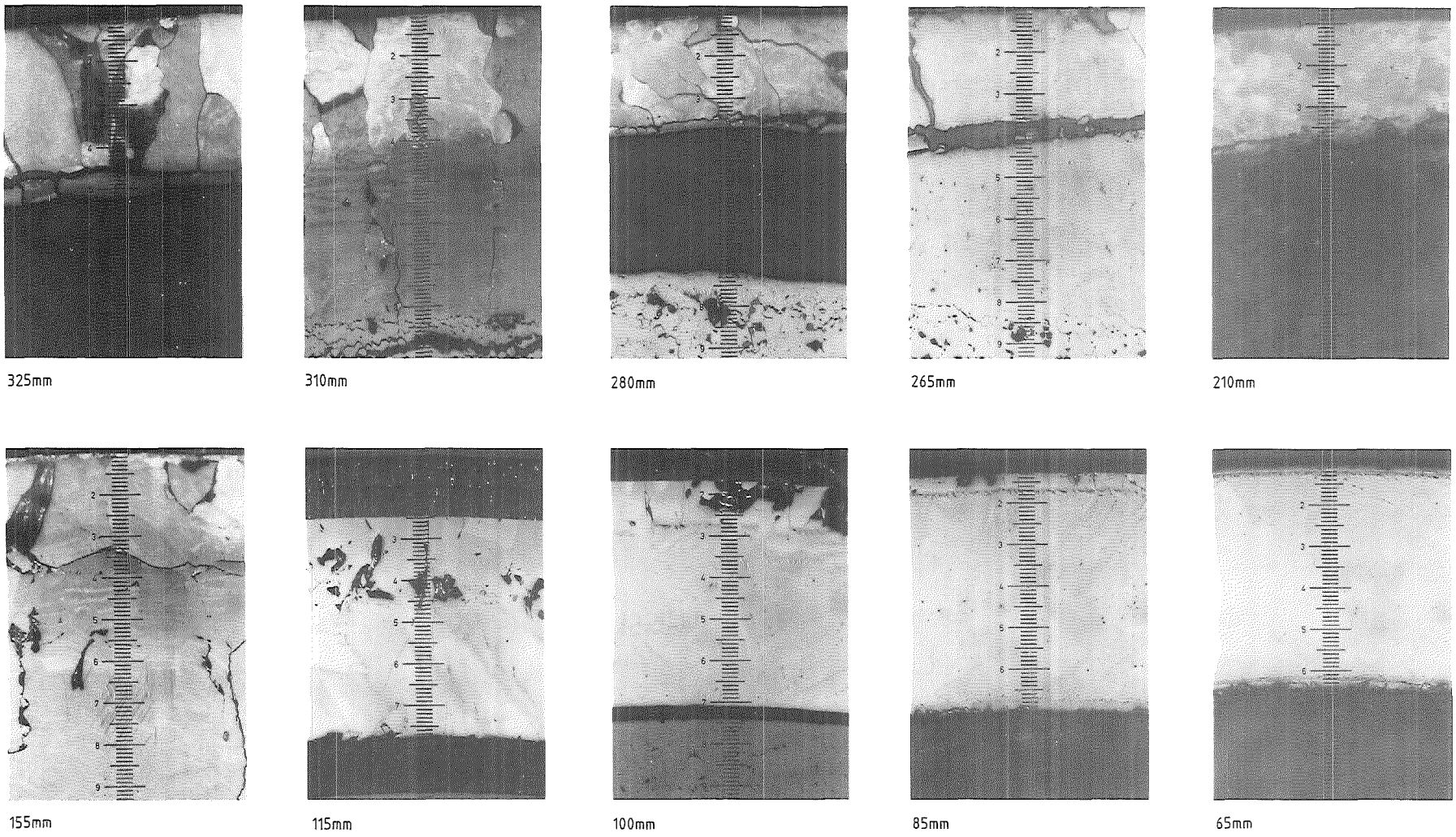

Fig. 10-4 : Enlarged View (100x) of Cross Sections From ESSI-10

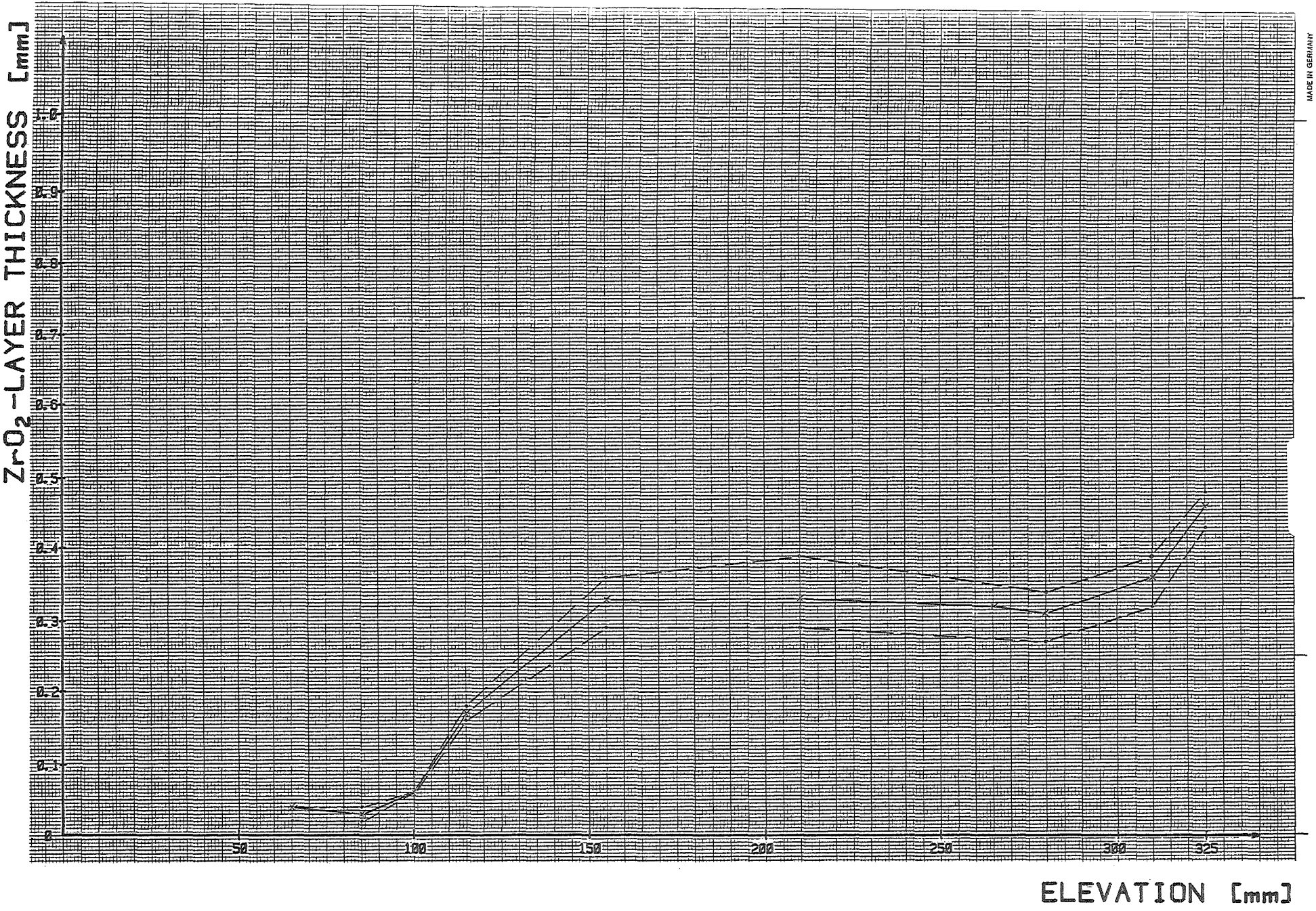

Fig.10-A: Zirconoxid layer thickness for test ESSI-10(– – –maximum or minimum value; ——mean value)

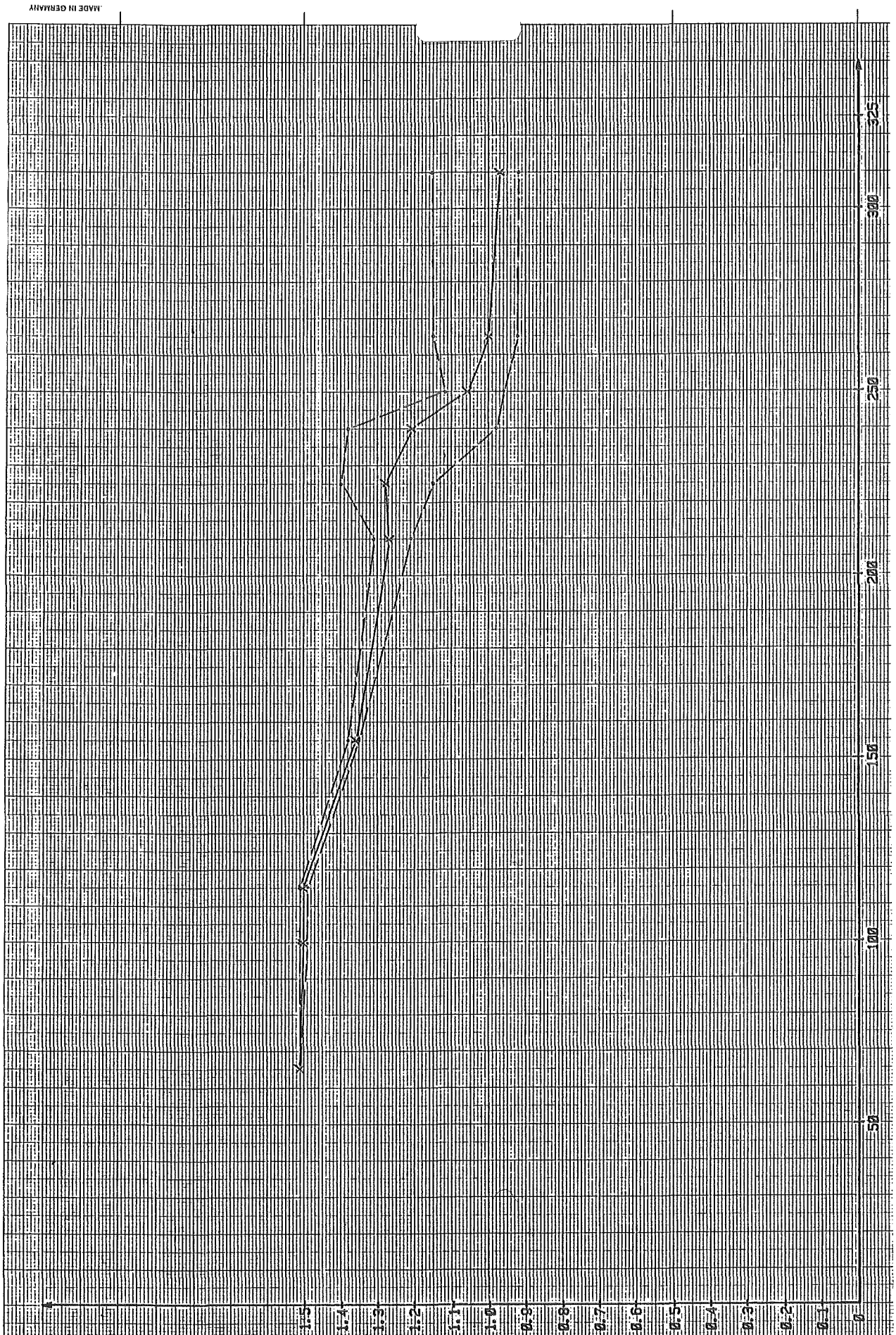

Fig. 10-B: Uranium oxide layer thickness for test ESSI-10 (---maximum or minimum value; ——mean value)

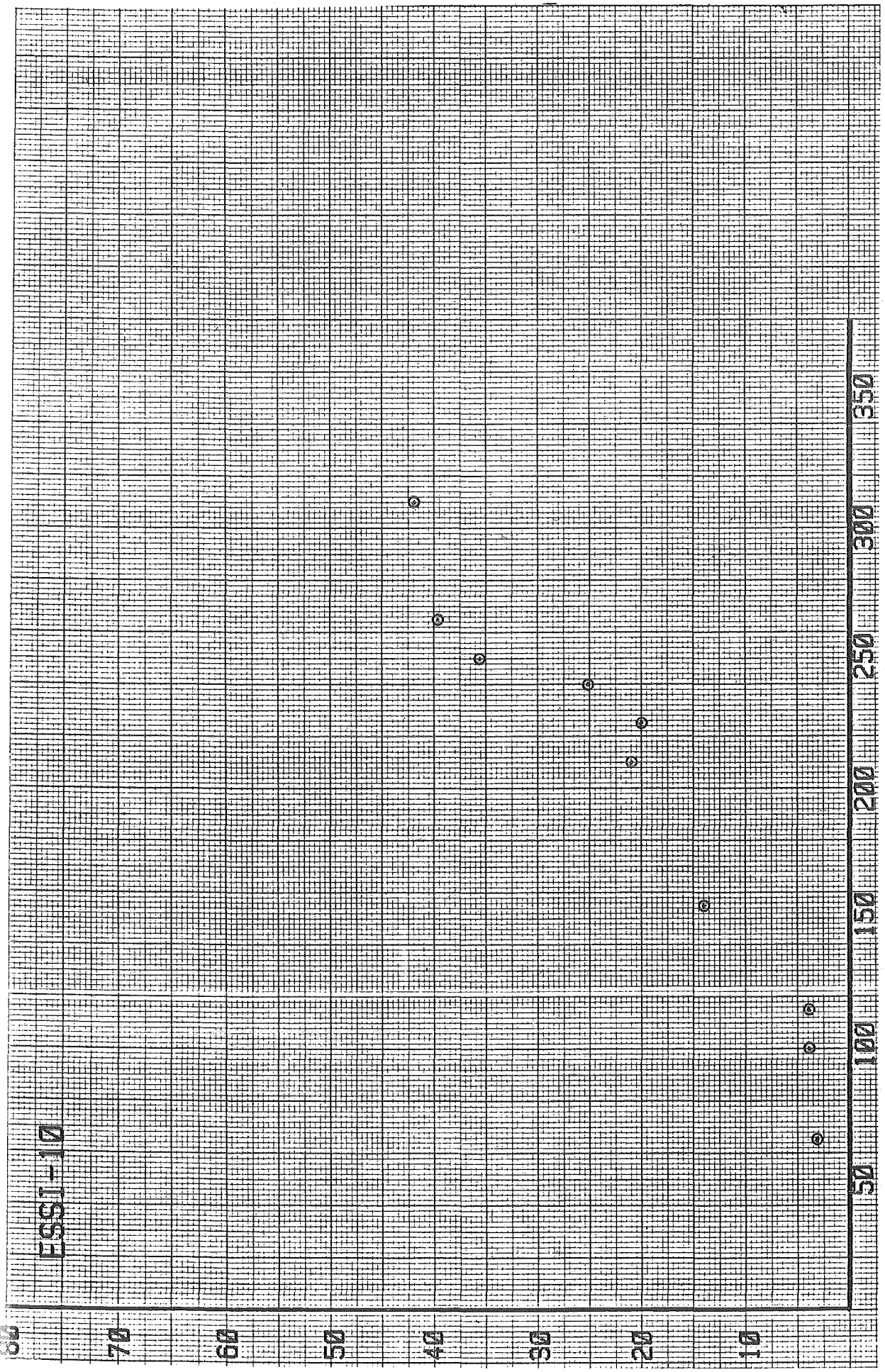

Fig.:10-C
Dissolution of the UO_2-pellet at different elevations (ESSI-10)

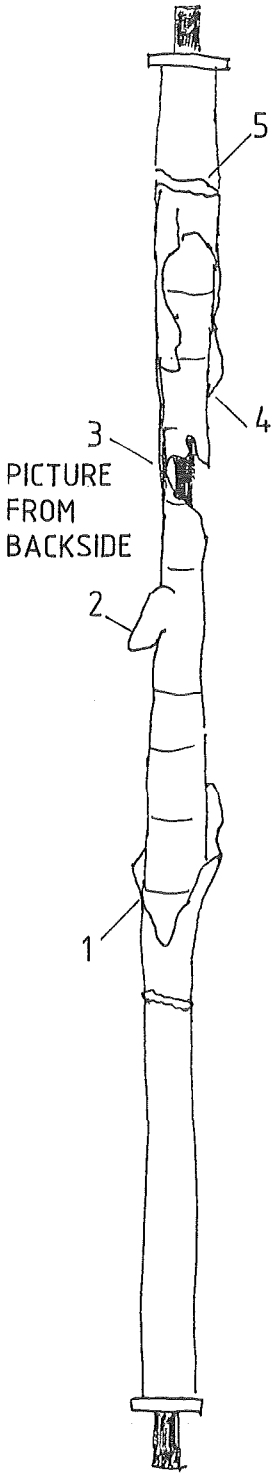

1 6x

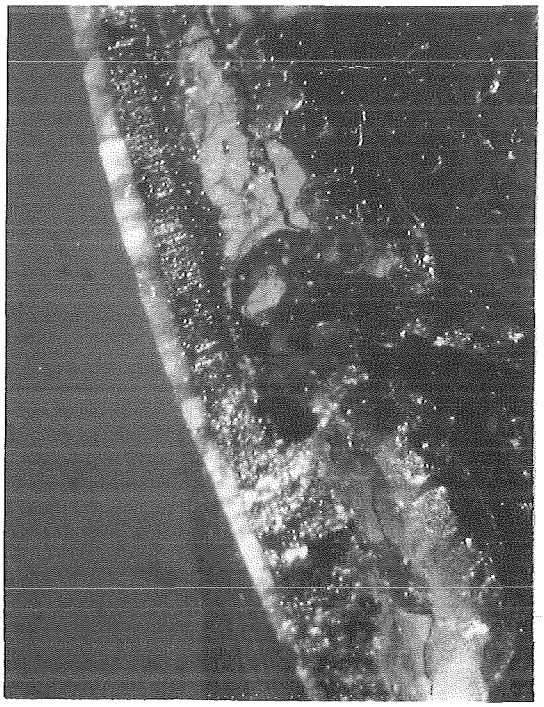

1 12x

Fig. 10-5:
LOCATIONS OF ENLARGED VIEWS OF THE FUEL ROD SIMULATOR ESSI-10

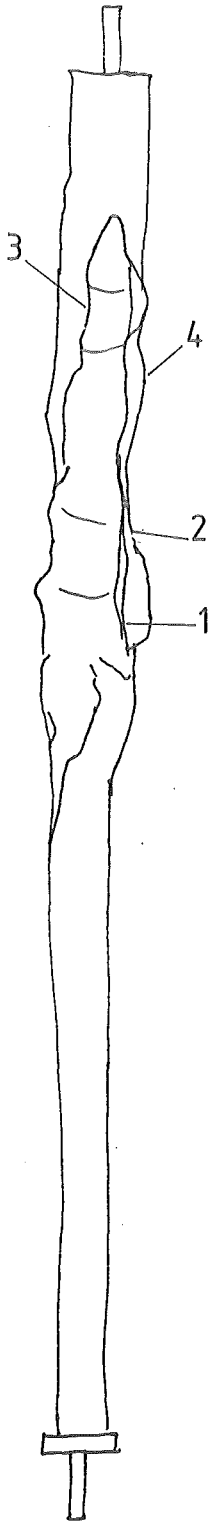

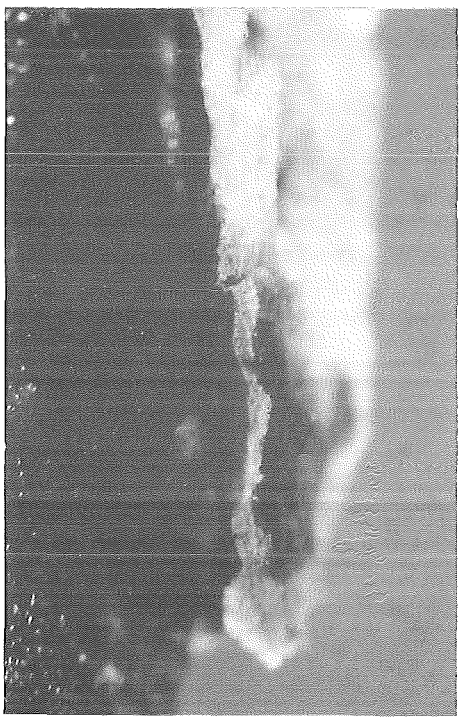

1 12x

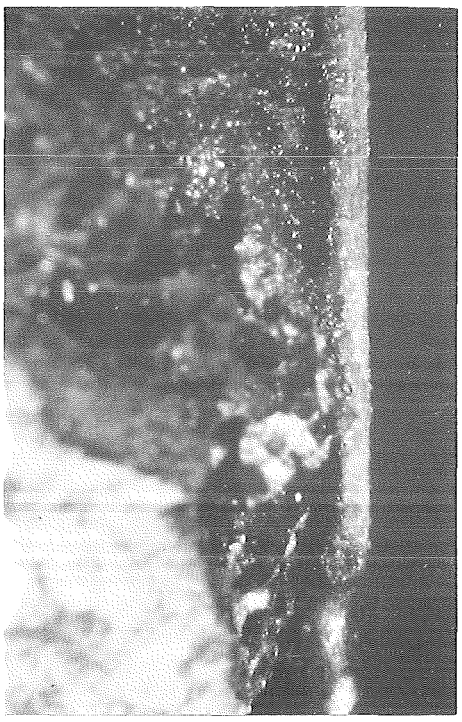

2 12x

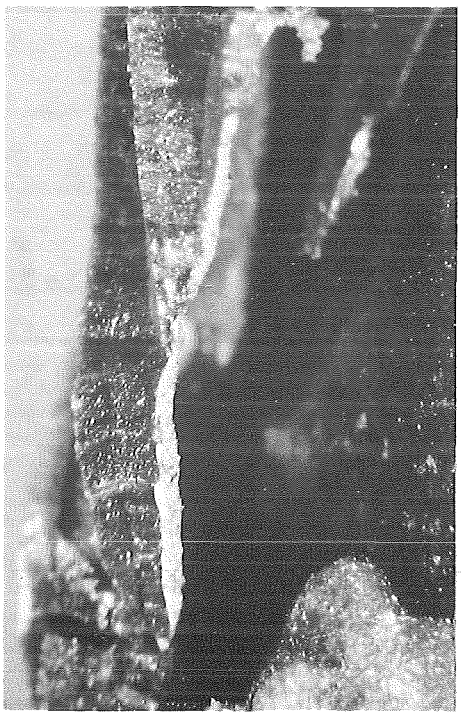

3 12x

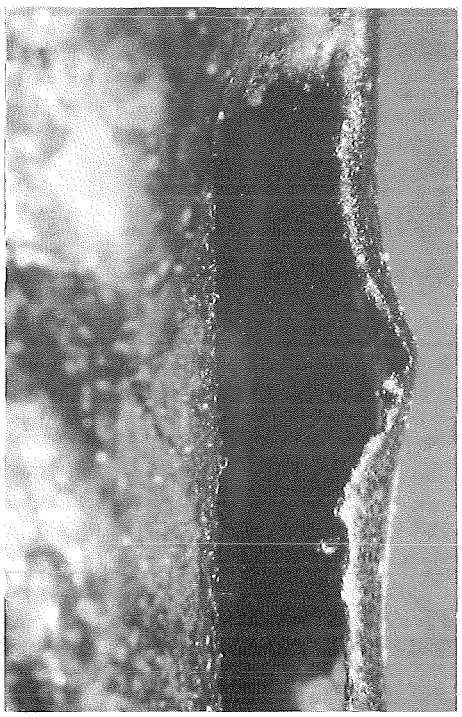

4 12x

Fig. 10-6:
ENLARGED VIEWS OF THE FUEL ROD SIMULATOR ESSI-10

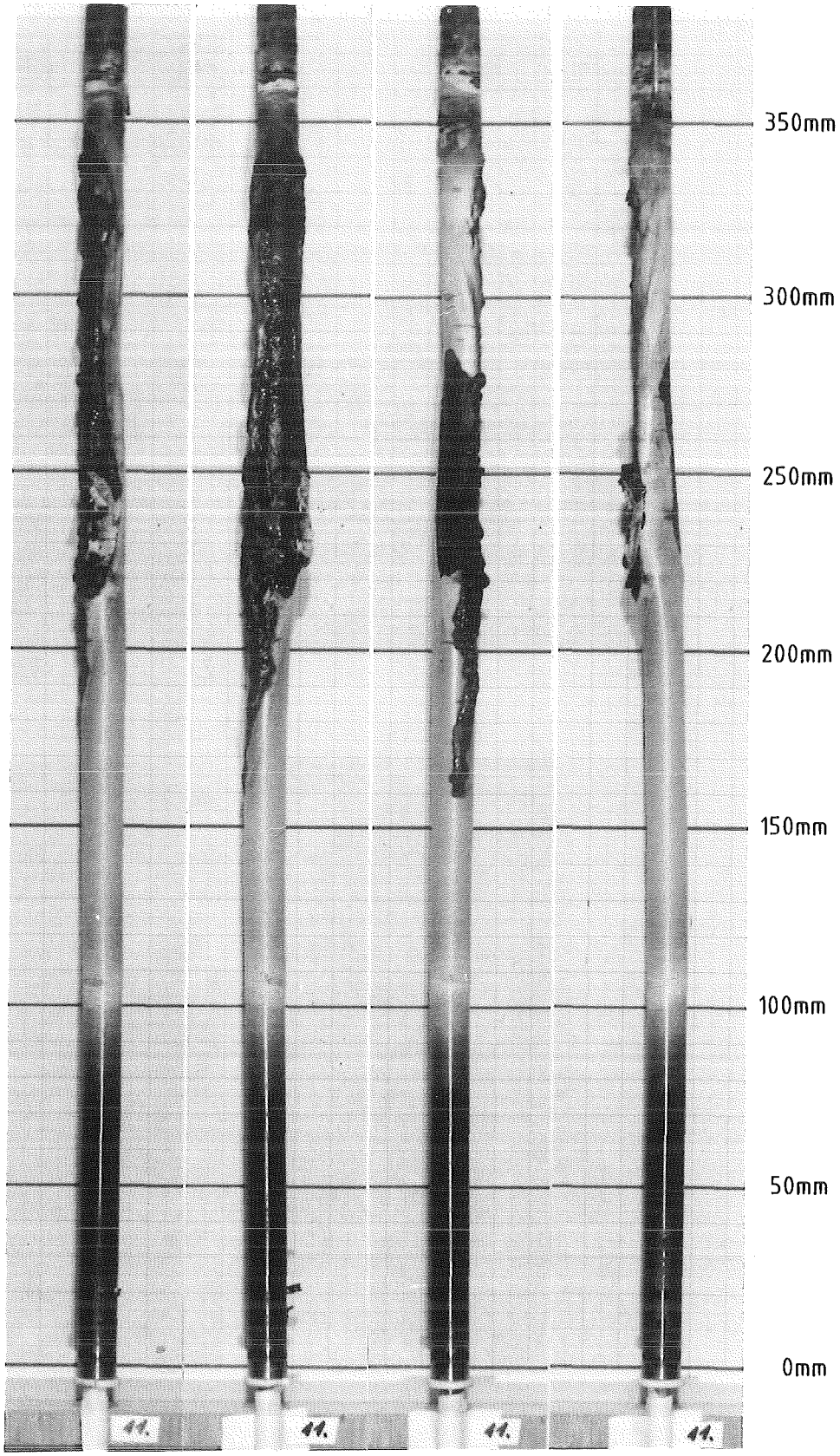

FIG. 11-1: POSTTEST APPEARANCE OF THE FUEL ROD SIMULATOR AND SCALE OF THE CROSS SECTION ELEVATIONS FOR ESSI-11

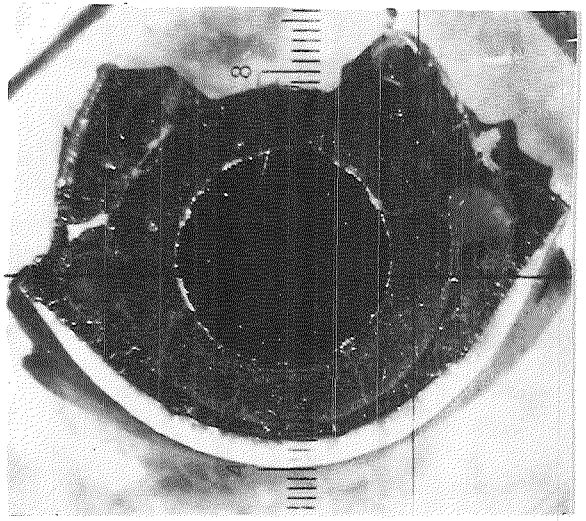

325mm

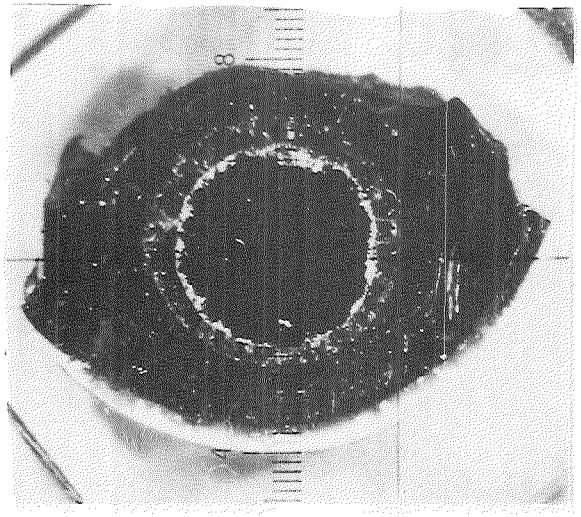

295mm

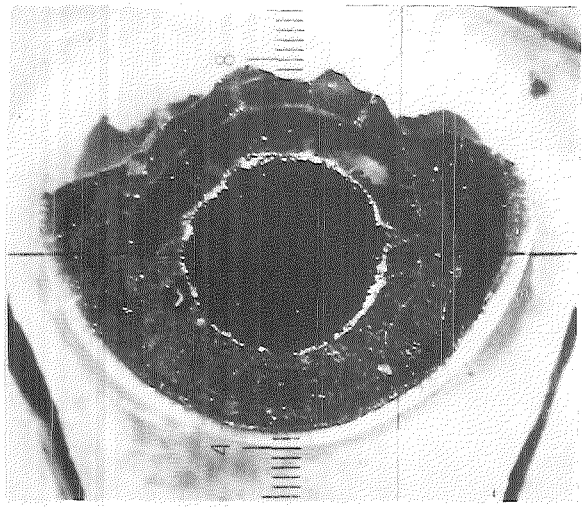

280mm

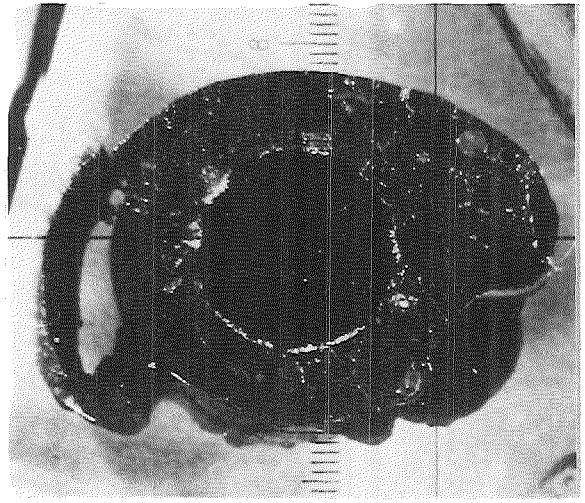

265mm

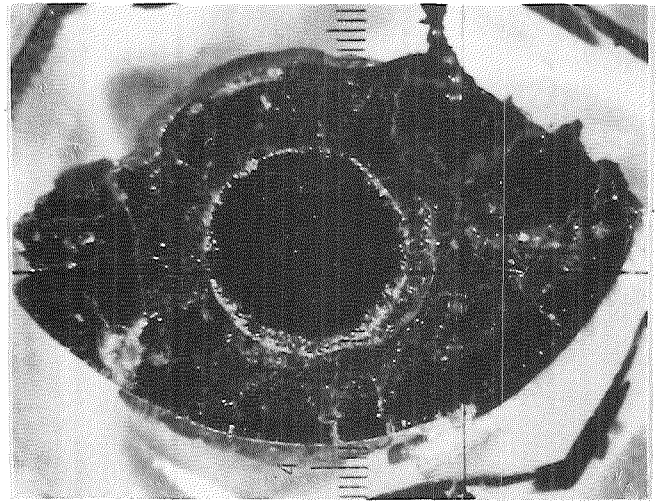

250mm

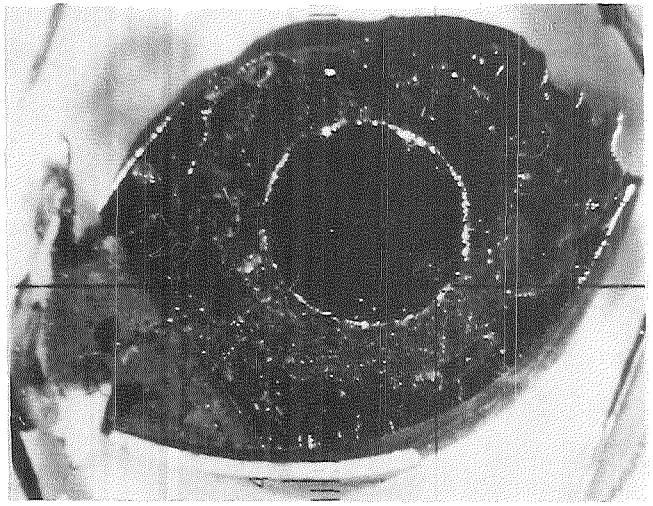

240mm

KfK

Fig. 11-2 : Cross Sections of Test ESSI-11

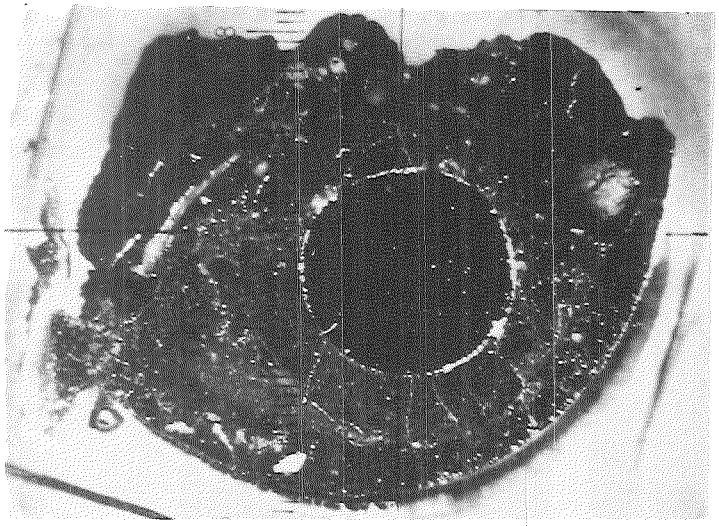

225mm

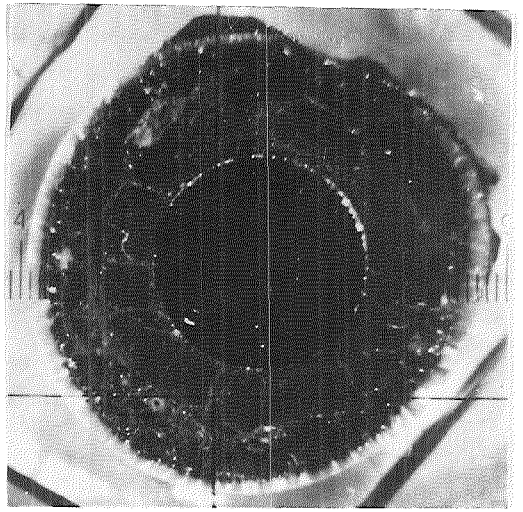

210mm

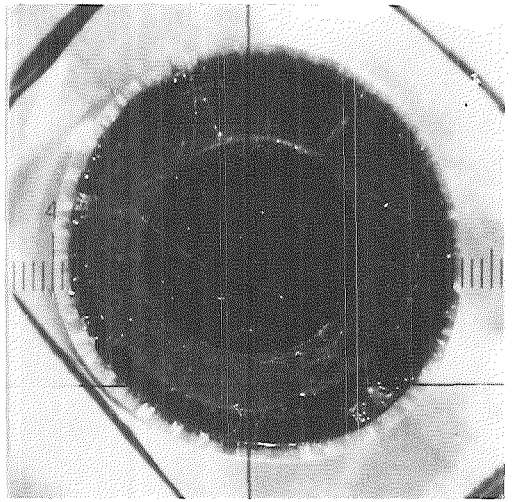

155mm

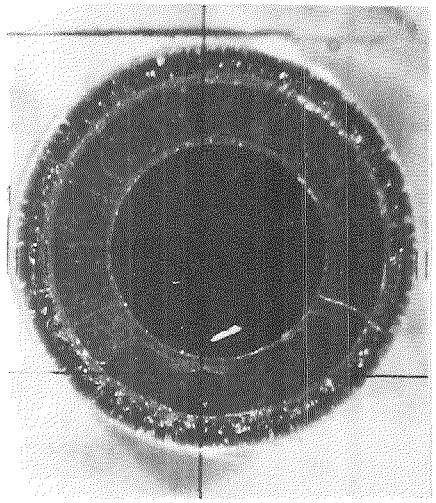

115mm

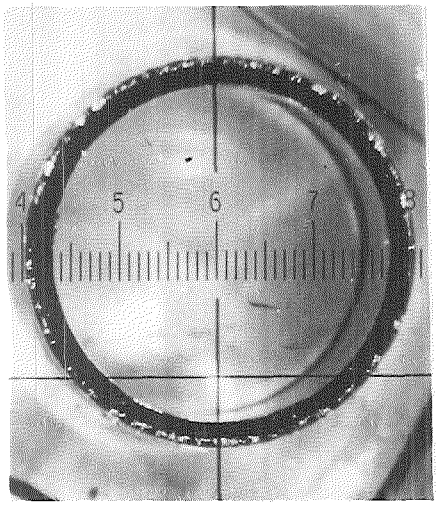

100mm

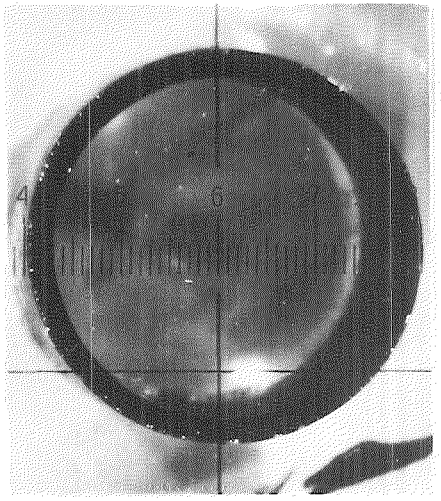

85mm

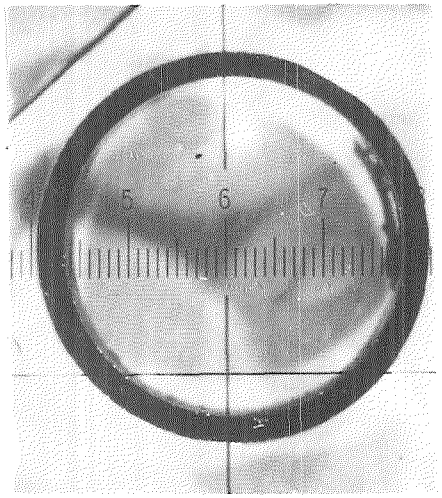

65mm

KfK

Fig. 11-3 : Cross Sections of Test ESSI-11

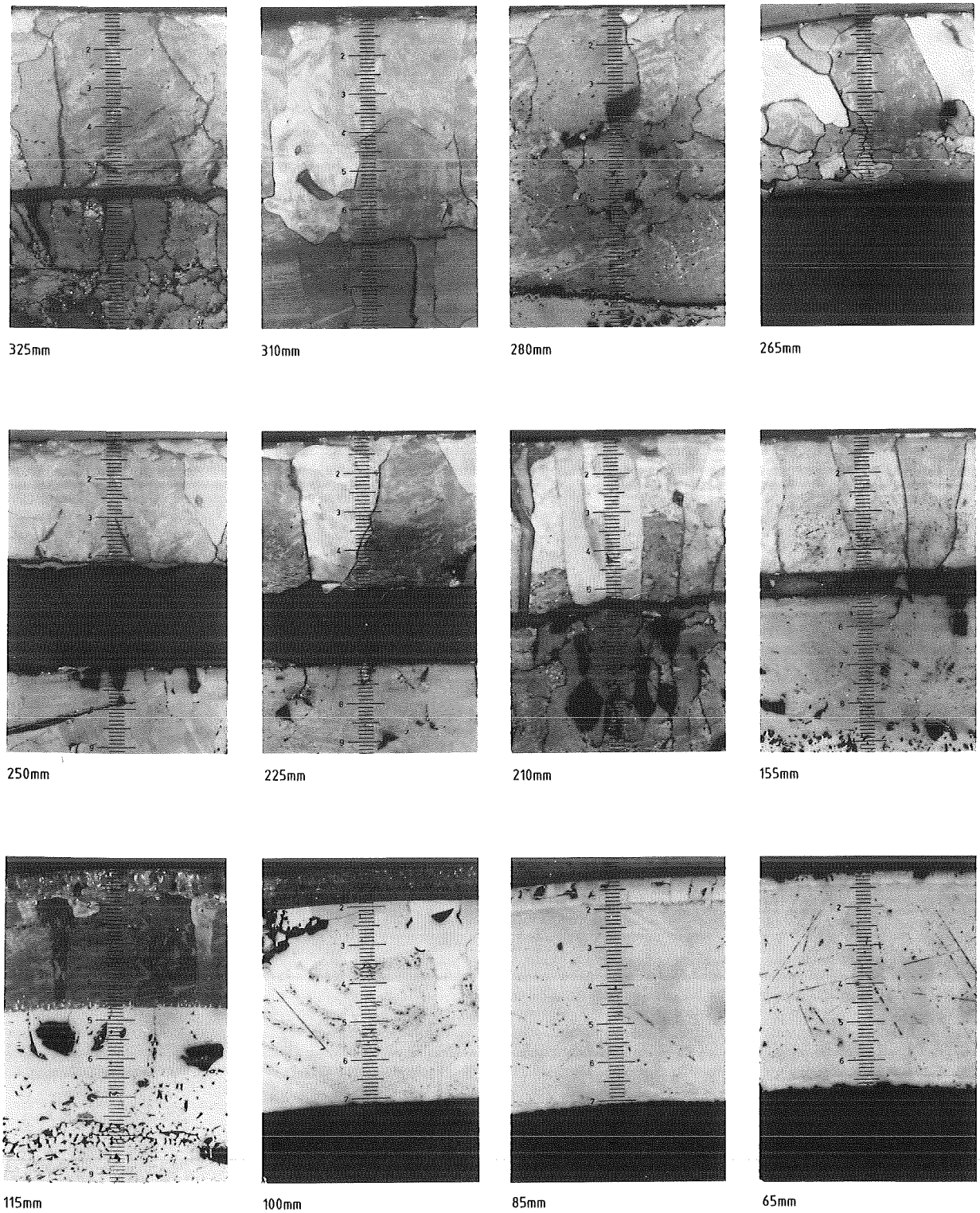

Fig. 11-4 : Enlarged View (100x) of Cross Sections From ESSI-11

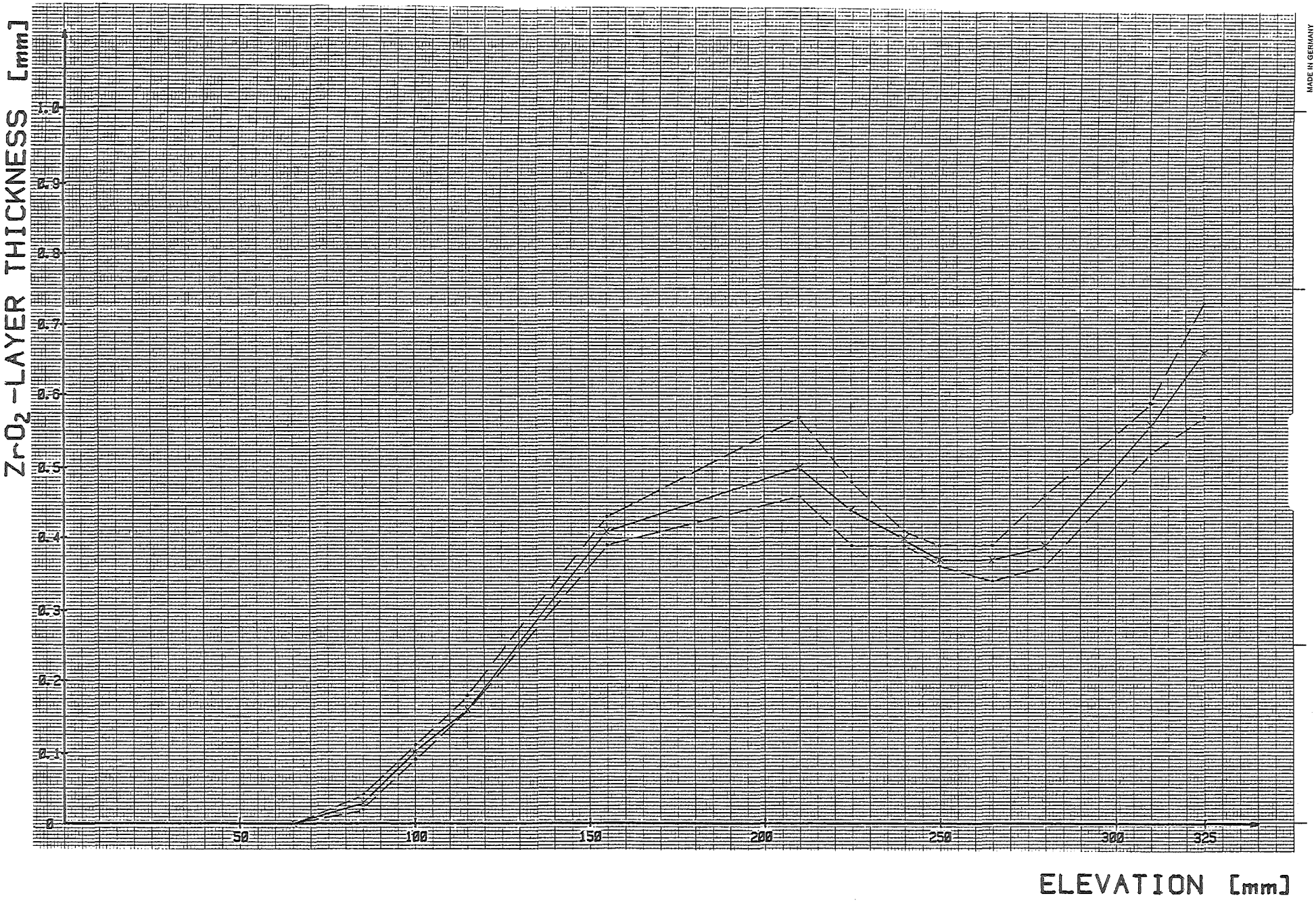

Fig.11-A: Zirconoxid layer thickness for test ESSI-11 (– – – maximum or minimum value; —— mean value)

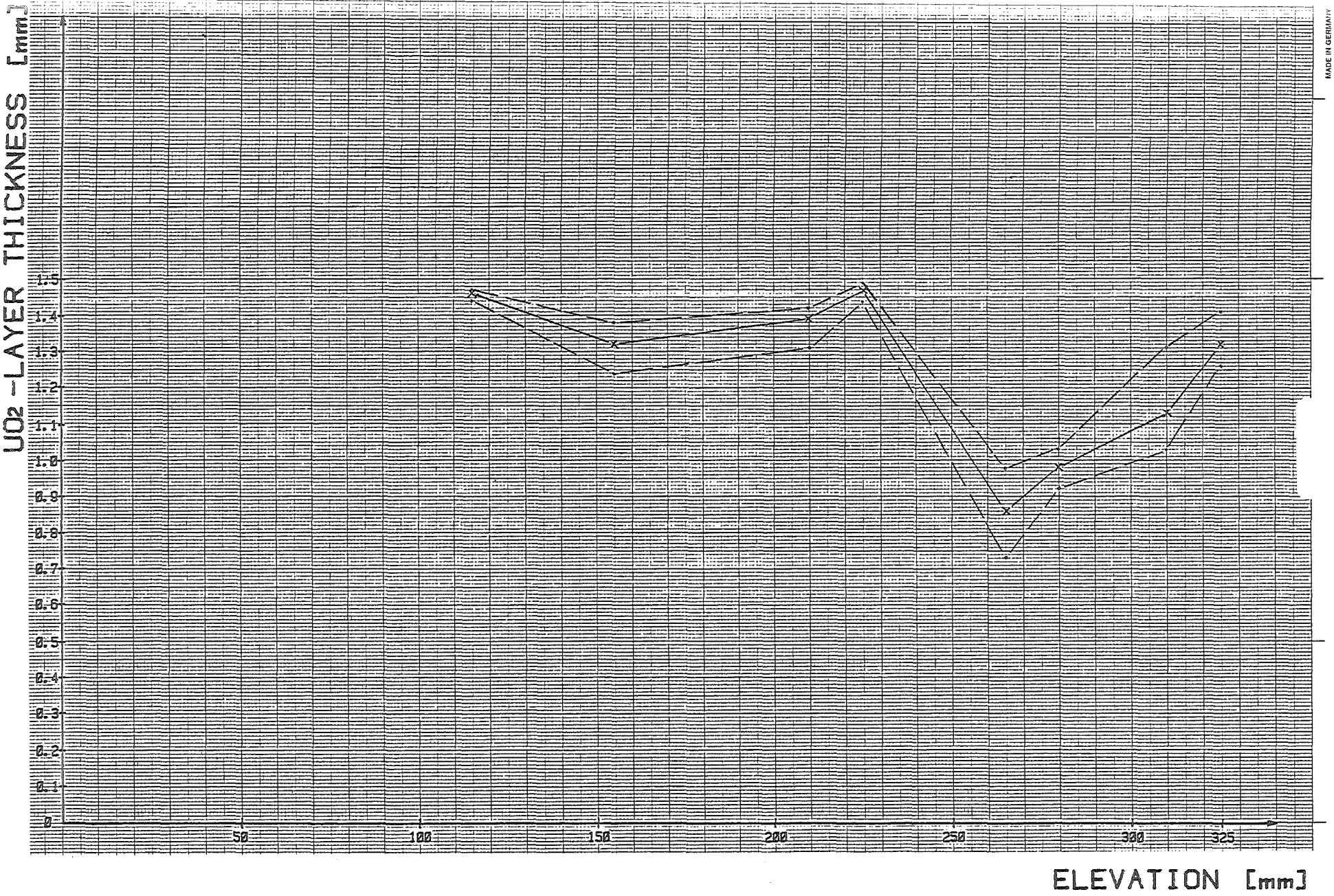

Fig. 11-B: Uranium oxide layer thickness for test ESSI- 11 (---maximum or minimum value;—— mean value)

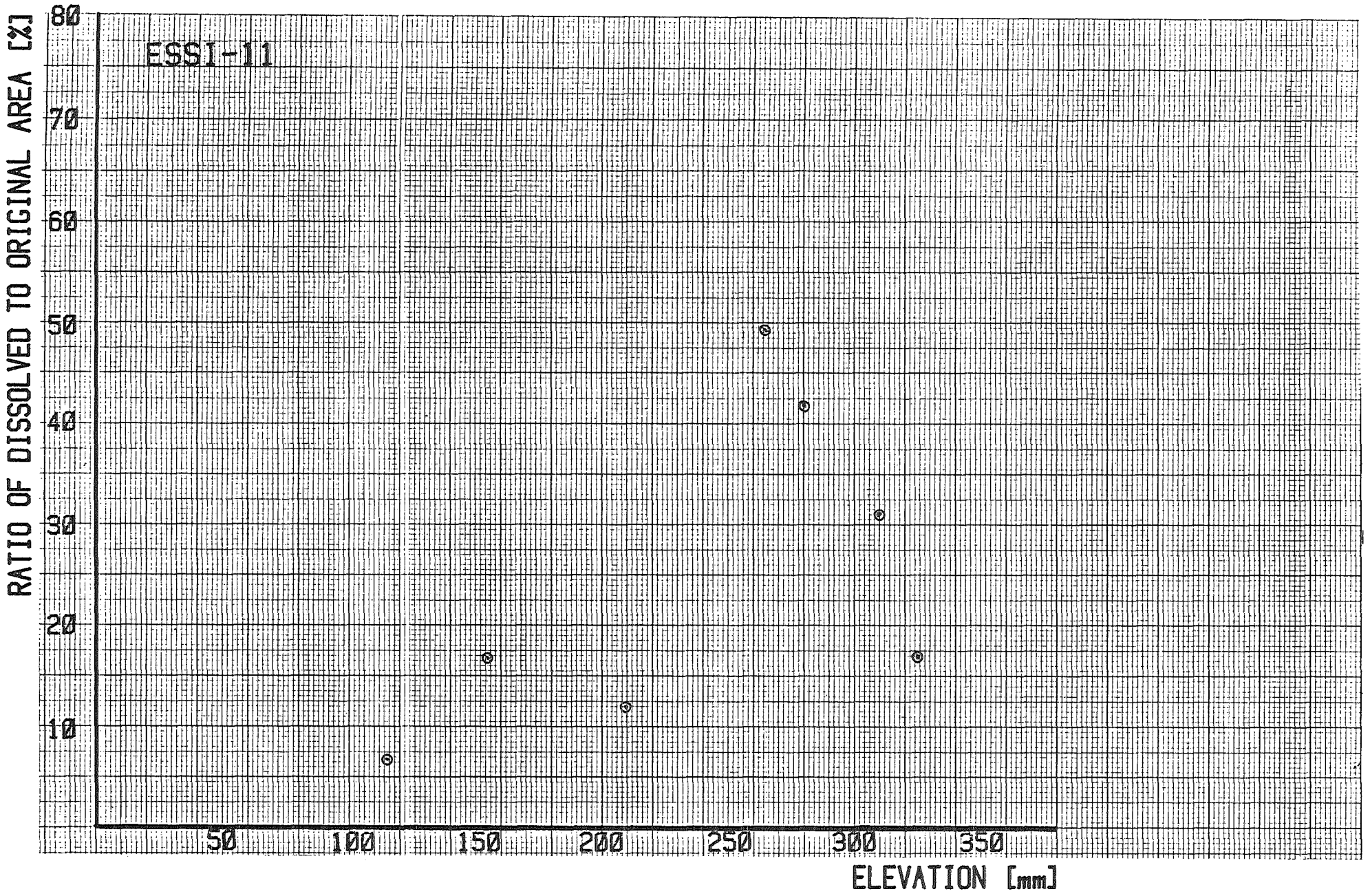

Fig.: 11-C
Dissolution of the UO_2-pellet at different elevations (ESSI-11)

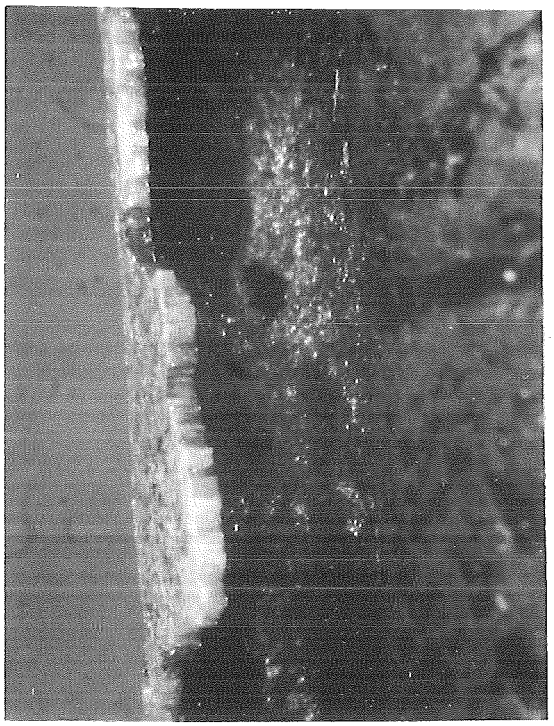

2 12x

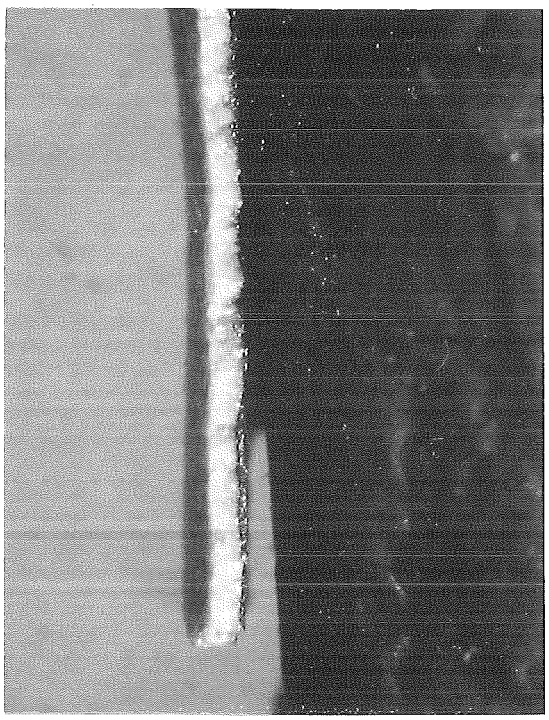

3 12x

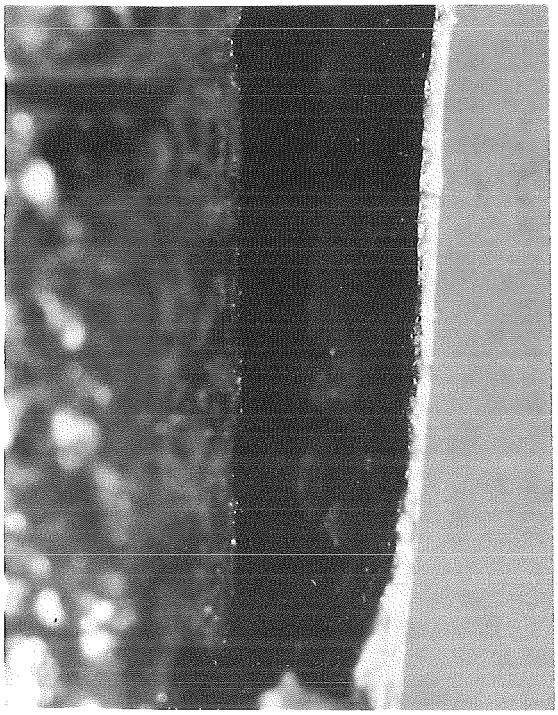

4 12x

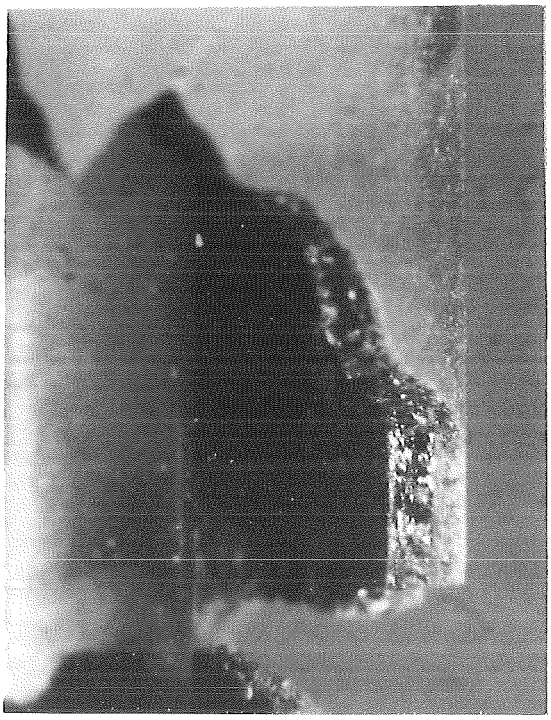

5 12x

Fig. 11-5:
LOCATIONS OF ENLARGED VIEWS OF THE FUEL ROD SIMULATOR ESSI-11

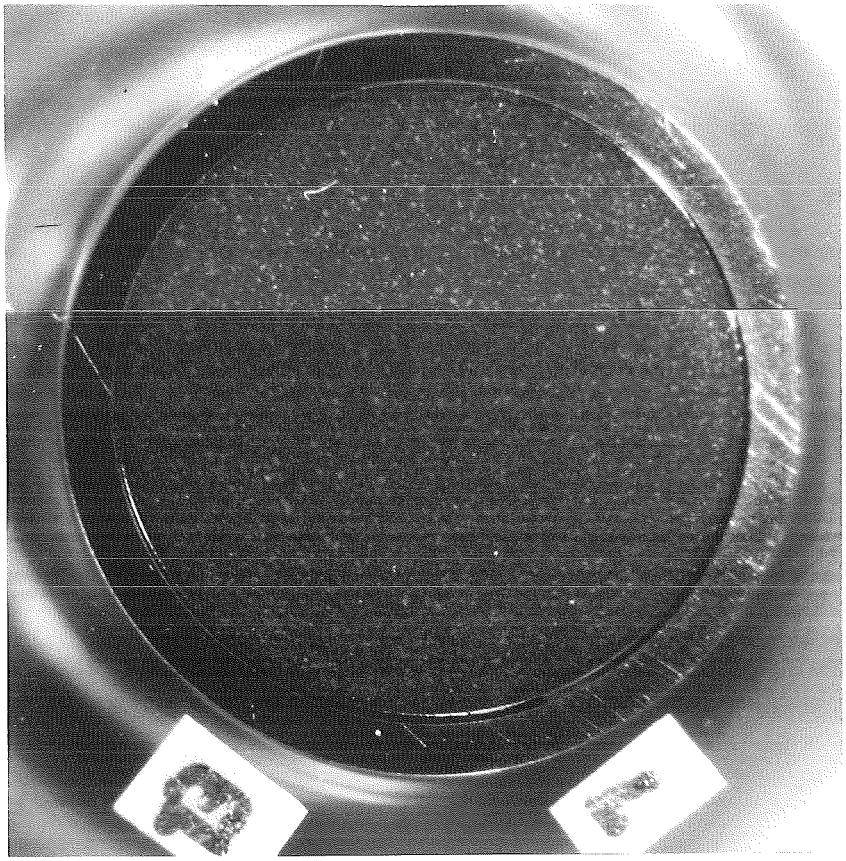

orig.
Vollpellet

Film 13

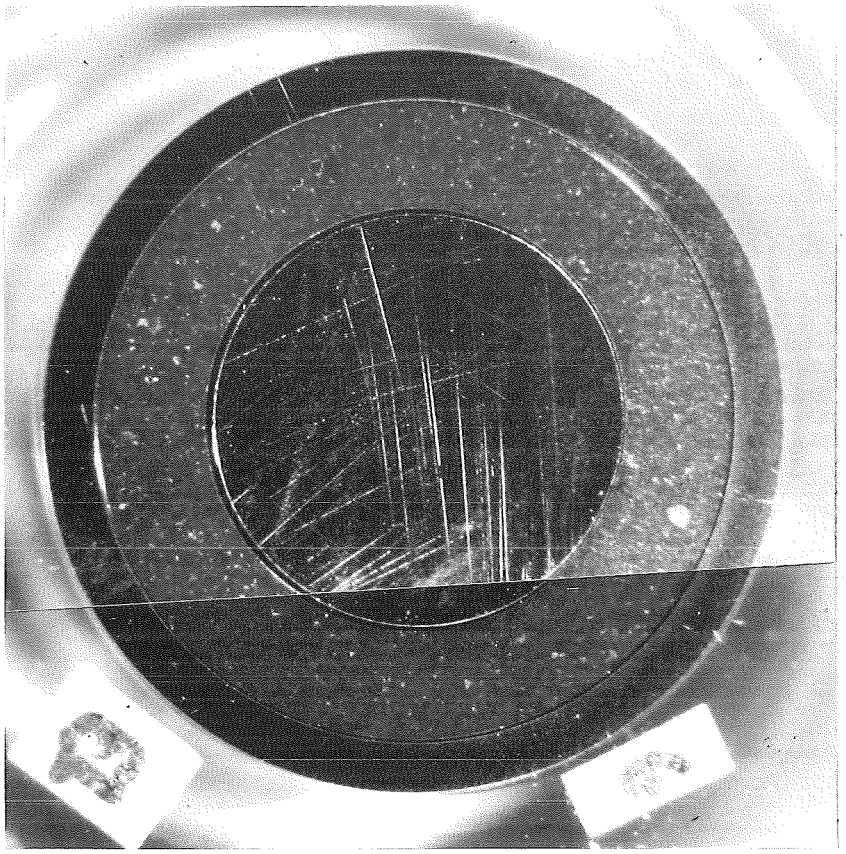

orig.
Ringpellet

Fig. 20: Cross sections of unheated solid and annular pellet.

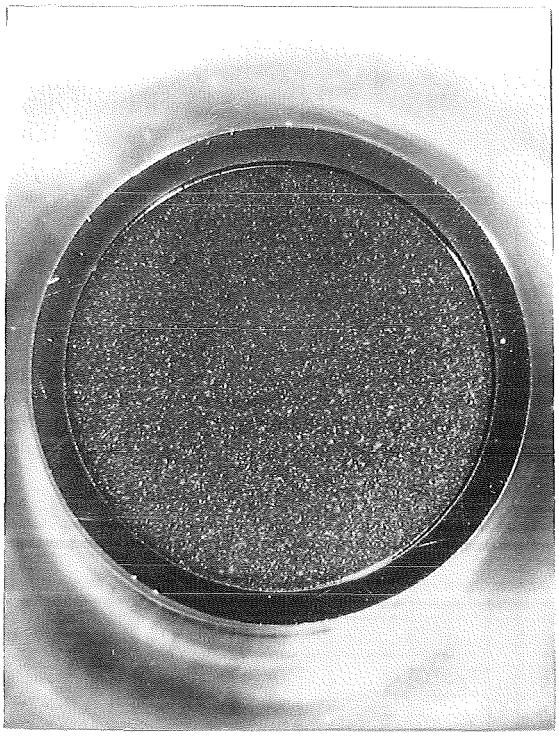

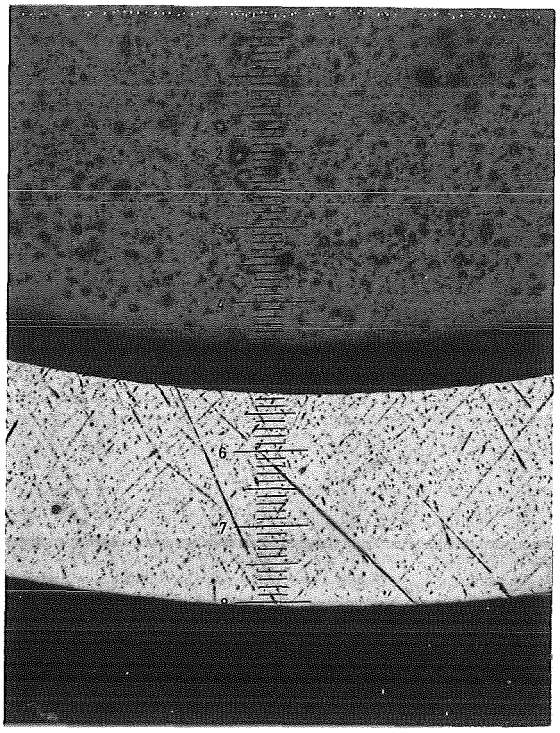

50x

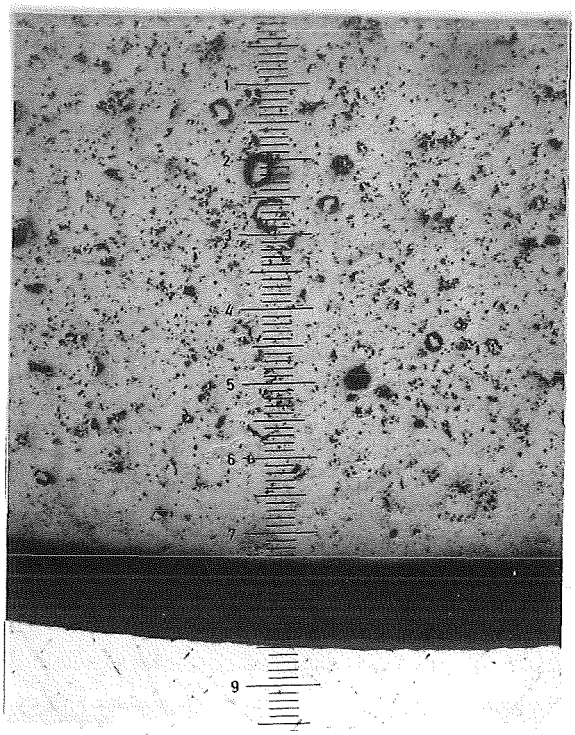

100x

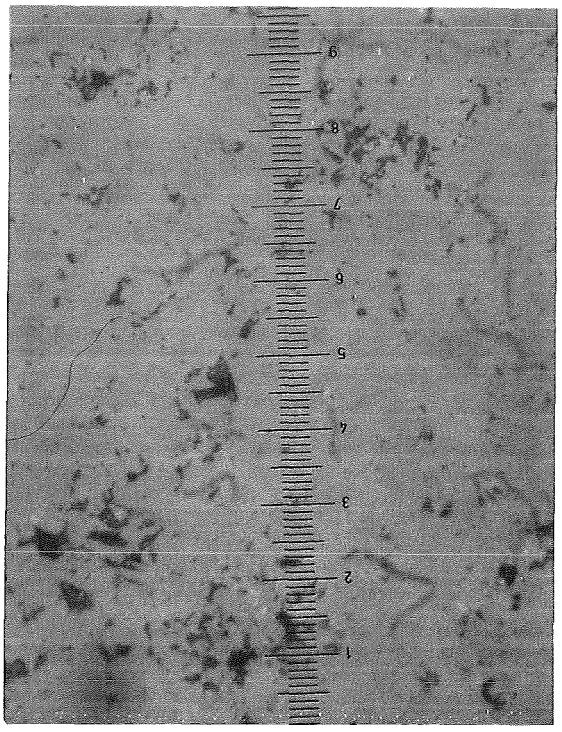

1000x

Fig. 21: Cross section of unheated annular pellet shown with different magnifications.

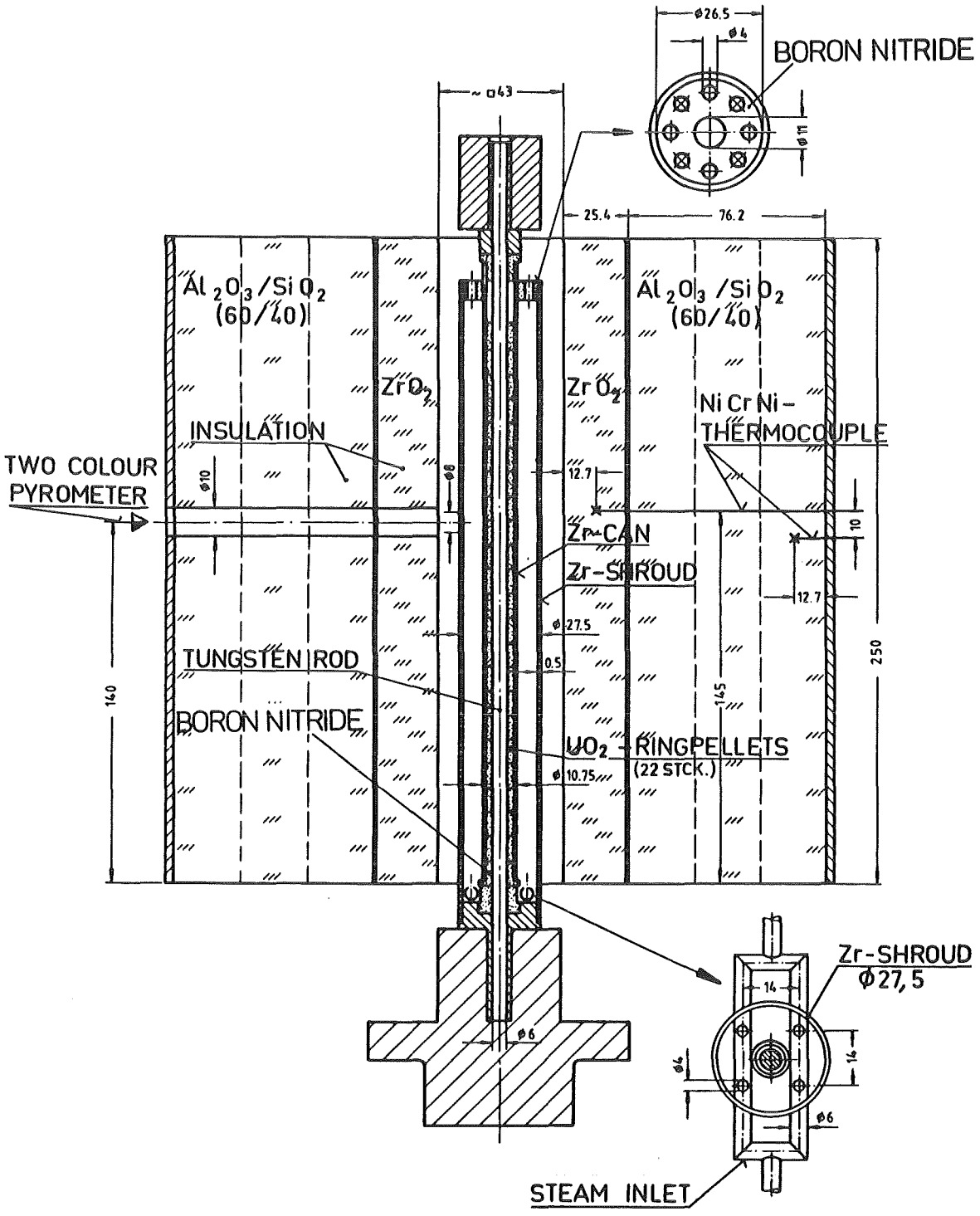

Fig. 22: Sideview of the experimental arrangement for test ESSI 1,2,3

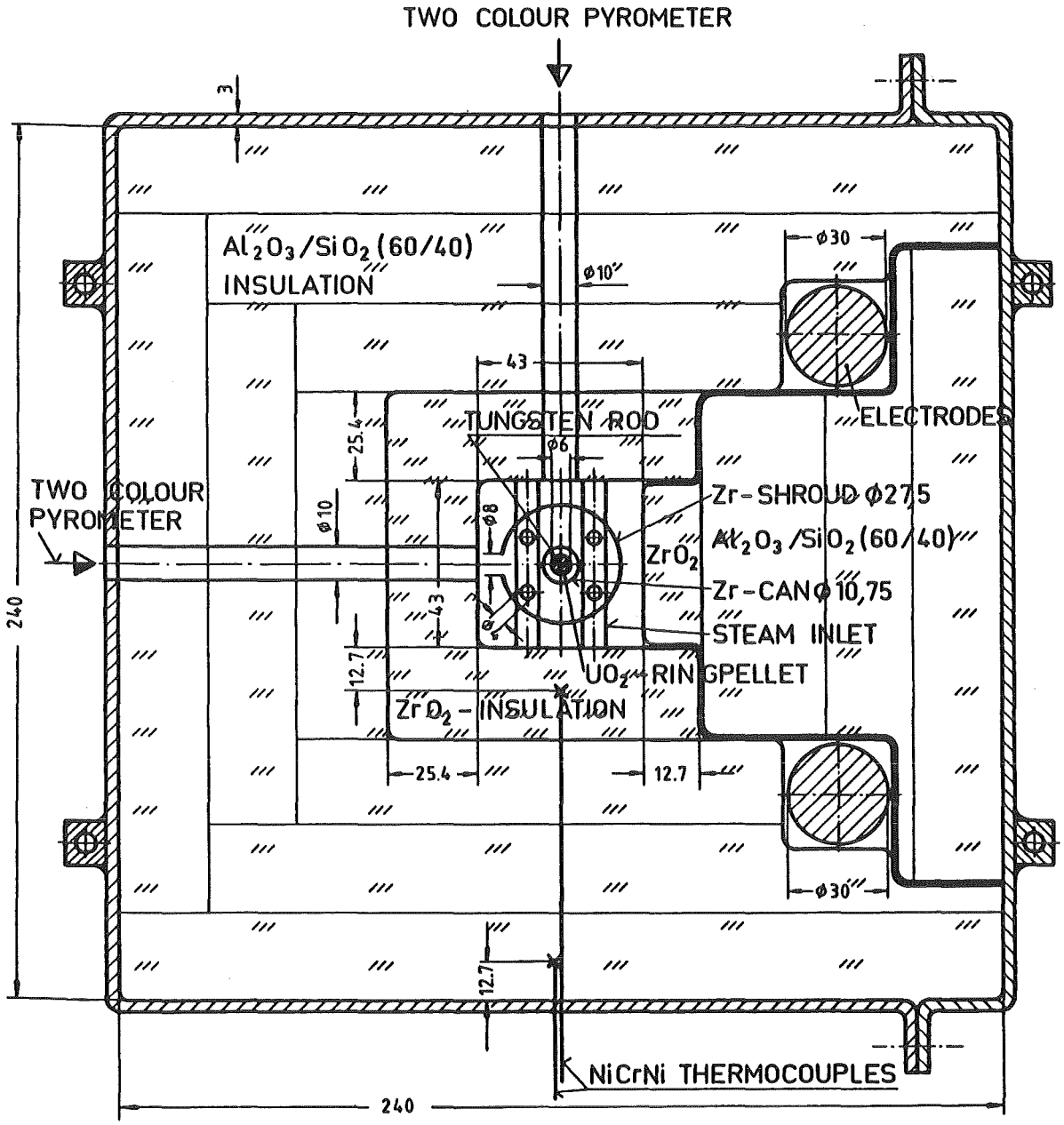

Fig. 23: Topview of the experimental arrangement for test ESSI 1,2,3

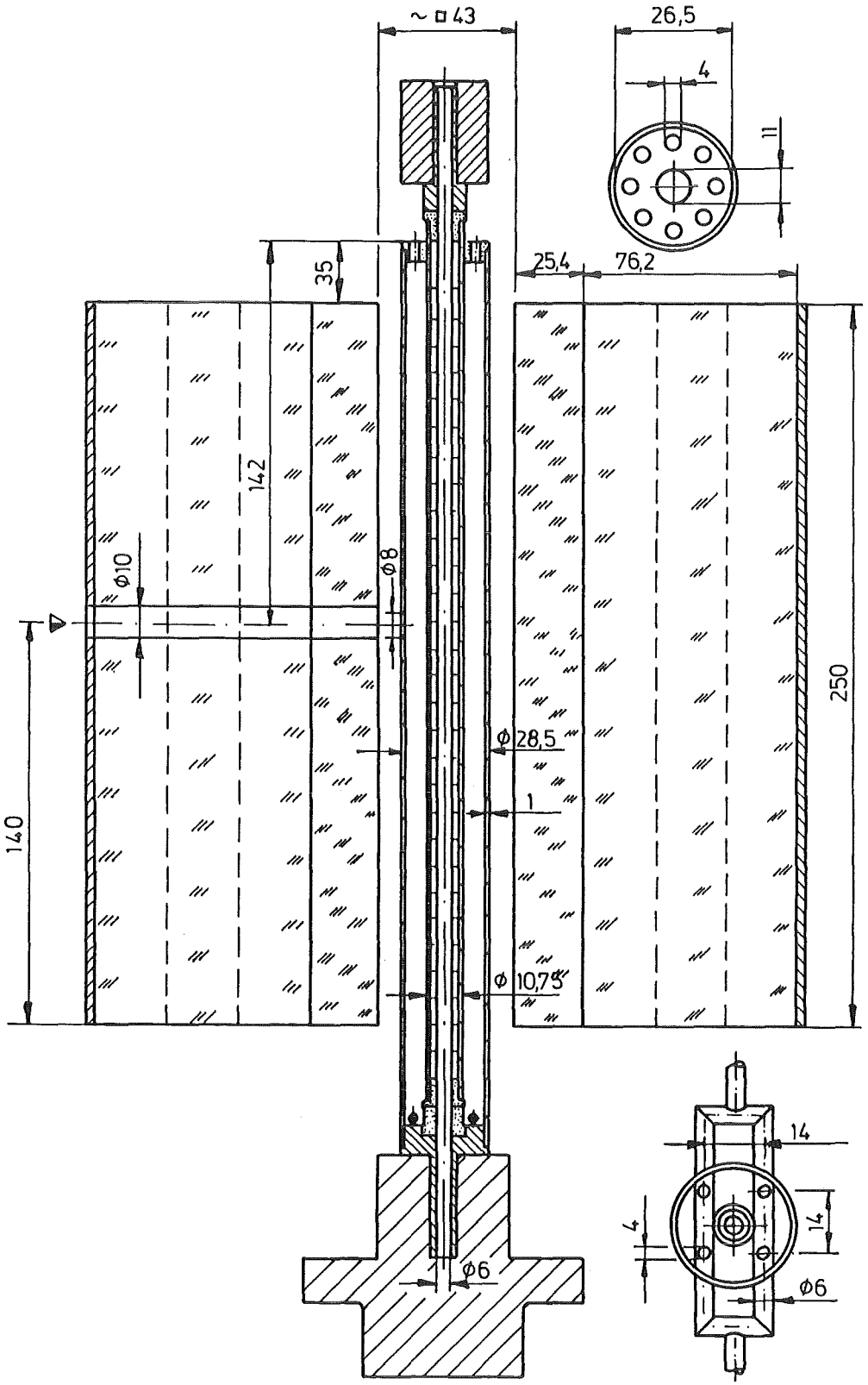

Fig. 24: Sideview of the experimental arrangements and positions of the thermocouples for test ESSI 4-8

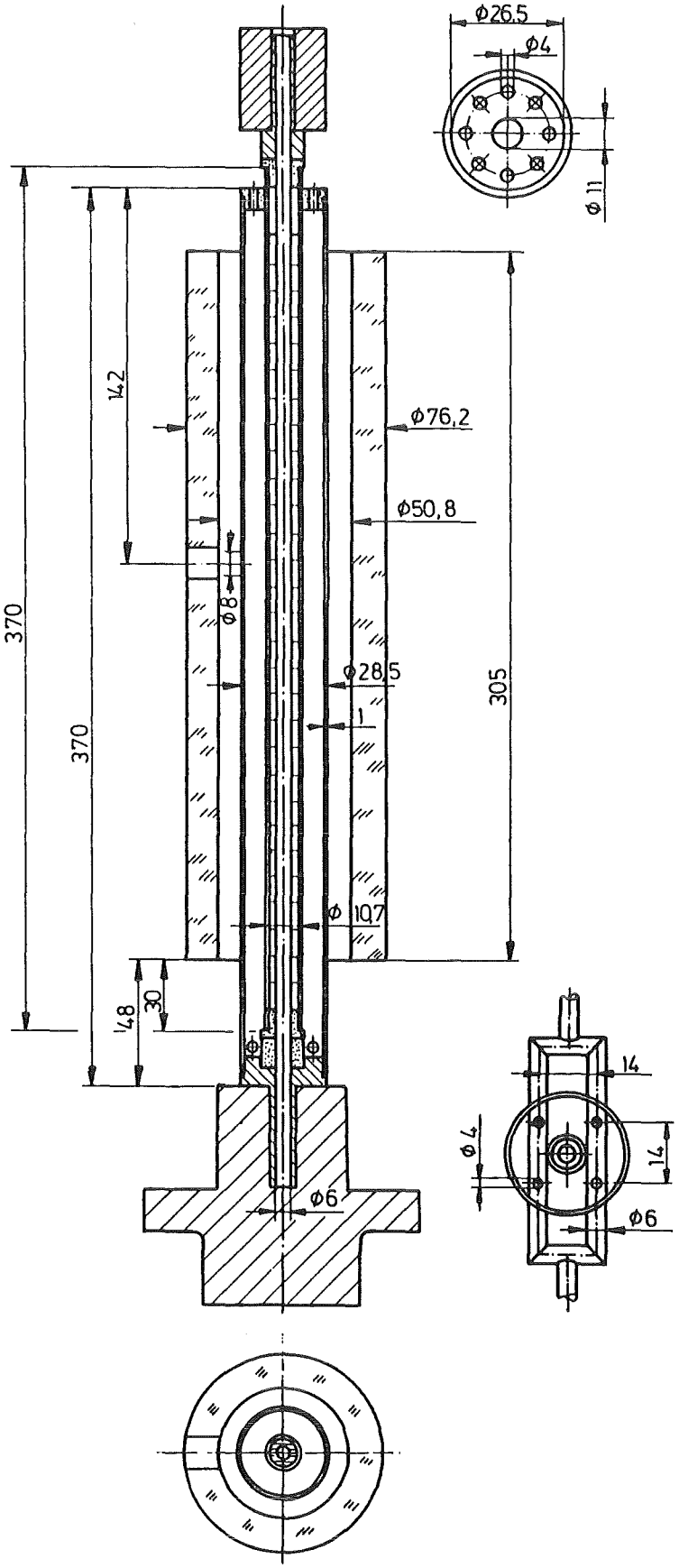

Fig. 25: Experimental arrangement and positions of the thermocouples for test ESSI 9

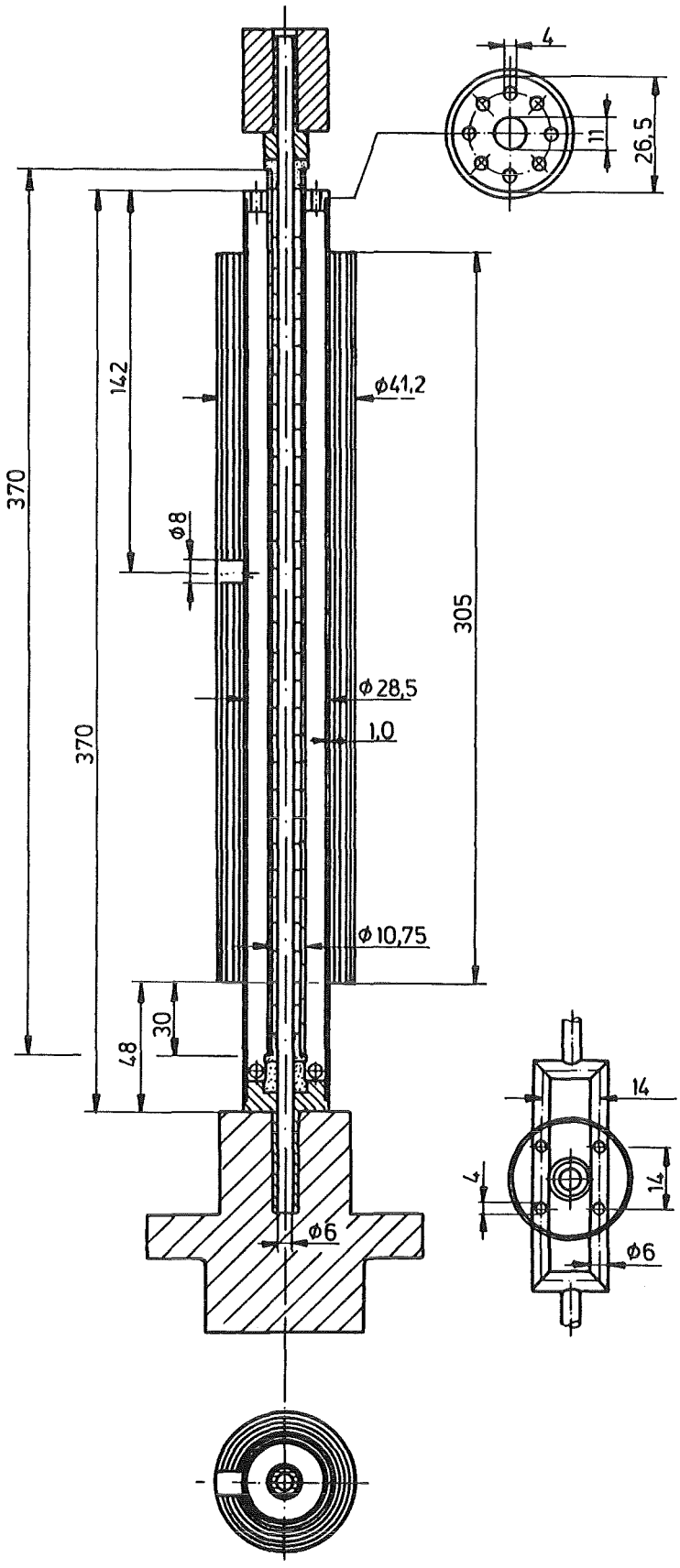

Fig. 26: Experimental arrangement and positions of the thermocouples for test ESSI 10+11